Technical Transactions

Czasopismo Techniczne

Issue 1

Volume 2018 (115)

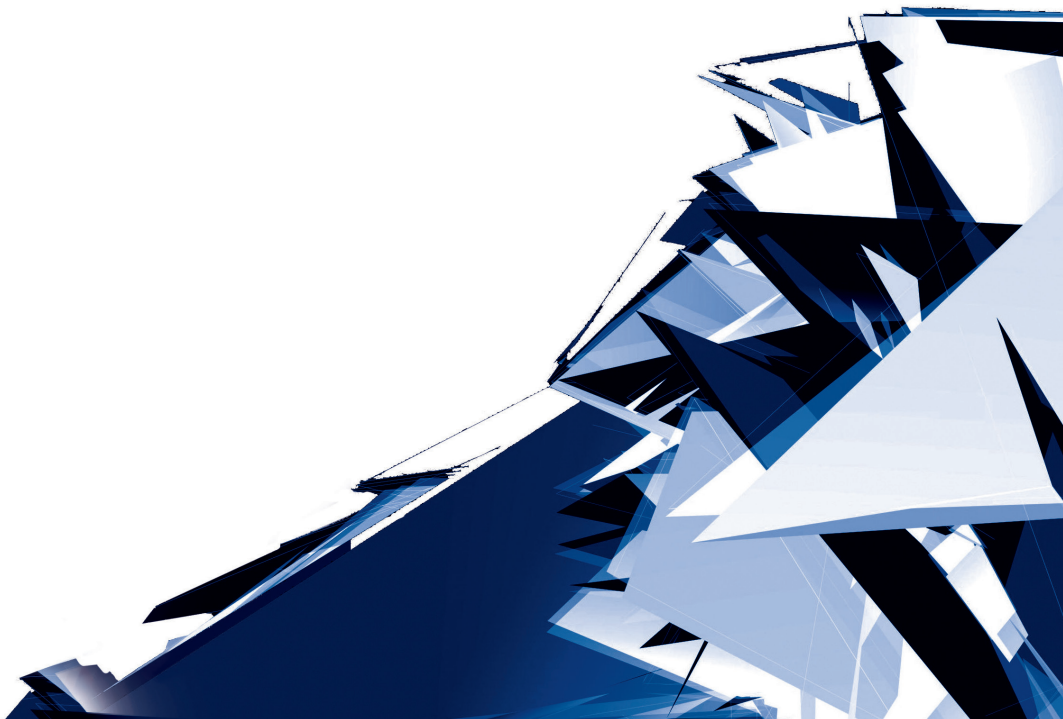

www.ejournals.eu/Czasopismo-Techniczne
www.technicaltransactions.com
www.czasopismotechniczne.pl

ISSN 0011-4561

Basic version of each Technical Transactions magazine is its online version
Pierwotną wersją każdego zeszytu Czasopisma Technicznego jest jego wersja online

Contents

ARCHITECTURE AND URBAN PLANNING

Ivor Samuels
How to kill the street without destroying the buildings 5

Karolina Dudzic-Gyurkovich
Public space and urban barriers in cracow. Analysis of the existing state 19

Michał Krupa
Revalorisation project of the 19th-century Bohaterów Monte Cassino Park in Jarosław 35

CHEMISTRY

Krzysztof S. Danel, Oskar Michalski, Zoryana Usatenko, Jerzy Sanetra, Elżbieta M. Nowak
Dicyanovinyl end-capped 9,10-bis (phenylethynyl) anthracenes for organic solar cells 47

CIVIL ENGINEERING

Małgorzata Janus-Michalska
Hyperelastic behaviour of auxetic material in tension and compression tests 61

Dariusz Starkowski
Load restraint with allsafe products. Part 1: choosing a semi-trailer – a systematic analysis 71

Rafal Szydlowski, Katarzyna Bednarz
Material and construction solutions of war shelters with the example of Hitler's main headquarters in the Wolf's Lair 87

ELECTRICAL ENGINEERING

Krzysztof Schiff
Ant colony optimisation algorithm for the facility localisation problem 103

ENVIRONMENTAL ENGINEERING

Barbara K. Wilk, Małgorzata Cimochowicz-Rybicka
Biovac® wastewater treatment plants in the mountain national parks 113

Andrzej Kotowski, Monika Nowakowska
Standards for the dimensioning and assessment of reliable operations of area drainage systems under conditions of climate change 125

Stanisław Biedugnis, Andrzej Czapczuk
The Application of the 'K-nearest neighbour' method to evaluate pressure loss in water supply lines 141

Maria Elżbieta Kowalska, Janina Zaczek-Peplinska
Examples of measuring marks used in geo-reference and the connection between classic geodetic measurements and terrestrial laser scanning 151

MECHANICS

Urszula Ferdek
The modelling and analysis of shock absorbers with stroke-dependent damping 163
Marcin Jasiewicz
The dynamic repeatability of a machine tool–holder–workpiece system 177
Patryk Różyło
Numerical analysis of crack initiation and propagation in an aluminium sample 187
Lena Krawczyk, Marlena Sołek, Łukasz Mika
Ice slurry flow in ball valves 195

TECHNICAL TRANSACTIONS 1/2018
ARCHITECTURE AND URBAN PLANNING
DOI: 10.4467/2353737XCT.18.001.7952
SUBMISSION OF THE FINAL VERSION: 18/12/2017

Ivor Samuels (ivor.samuels@googlemail.com)
AAdipl, M.Sc. ARB, MRTPI, Honorary Senior Research Fellow, Urban Morphology Research Group, School of Geography, Birmingham University

How to kill the street without destroying the buildings

Jak „zabić" ulicę bez niszczenia budynków

Abstract

A discussion of the manner in which Oxford University institutions have modified the historic street structure and its character by acquiring whole blocks or by inserting new buildings, which ignore the street context, in the pursuit of promotional advantages.

Keywords: streets, university development, Oxford, loss of character

Streszczenie

Artykuł stanowi omówienie sposobu, w jaki instytucje Uniwersytetu Oksfordzkiego zmodyfikowały historyczną strukturę ulicy i jej charakter poprzez nabycie całych bloków lub wstawienie nowych budynków, których obecność bagatelizuje kontekst uliczny w dążeniu do korzyści promocyjnych.

Słowa kluczowe: ulice, rozwój uniwersytetów, Oxford, utrata charakteru

1. Introduction

Architects trained in the 1960s were exhorted in the words of that icon of modern architecture and urbanism Le Corbusier, to kill the corridor street (*il faut tuer le rue-corridor*) [3]. In order to achieve this it was necessary to destroy all the buildings as le Corbusier (1930) so dramatically demonstrated in his Plan Voisin for Paris of 1925 where he proposed to wipe away the old city and replace it by free standing blocks in a landscape of motor roads and tree planted open space. This vision became the model for many of the post World War 2 housing projects in Europe and the United States until its validity began to be questioned before falling out of favour in Britain with the Ronan Point explosion in 1968 [6]and in the United States in the 1970s with the demolition of the Pruitt- Igoe apartments [5].

The last half century has been spent trying to reverse this approach and recover the street as the basis of urbanism in Europe and the United States [1, 4]. However, less destructive ways of destroying the street than those proposed by le Corbusier have been largely ignored in this quest to restore its importance as the prime element of the city. Recent examples in the historic city of Oxford, all the result of developments for the University of Oxford demonstrate how this has been achieved and are discussed in this article which describes four recent projects undertaken by colleges and university institutions. Two involve the acquisition and change of use of buildings while retaining intact the physical fabric and two involve inserting a free standing building into a street. The first two examples were undertaken by Pembroke and St. Hugh's Colleges, two of the independent thirty seven colleges which form the University of Oxford which functions as a federation with examinations and some teaching undertaken by central institutions. The last two cases considered, the Blavatnik School of Government and the Said Business School are both examples of privately sponsored new teaching and research facilities.

2. Pembroke College

This college of around 600 students has a central urban location and was founded in 1624. Surrounded by ancient streets it was difficult to expand by the construction of new buildings although it has managed to do this by building some new accommodation on an adjacent urban block linked to the old college by a pedestrian bridge over an existing street [5]. Another way it has expanded is by moving into adjacent old houses lining Pembroke Street running east west on the south side of the college. These dwellings are in the Central Oxford Conservation Area, which means that the fabric of the buildings is protected from major alterations. In addition to opening to the street these former row houses on narrow frontage burgage plots also had access from the narrow Beef Lane at their rear.

Having acquired the houses (according to Wikipedia in 2015 the College was reported to have an endowment of 46.9 million sterling) they were linked to the college by entrances onto Beef Lane which was then closed to public access and its entire length incorporated within its property boundaries . In the interests of restricting access to the closely controlled single college main gate, the entrances onto the street were sealed and the former houses

were entered from the rear i.e. within the boundaries of the College.. Although the doors to Pembroke Street were retained, most of them were sealed but in some cases the door handles were retained. These false front doors are easily identified by the spider webs around the door handles. Thus the structure of the old houses has been conserved and the facade of the street has been retained which fulfils the objectives of the conservation plan even though the entrances are fake. The question arises as to whether a street with no entrances can be considered a street or it is it just no more than a stage set.

3. St Hugh's College

Originally founded as a women's college in 1886 St. Hugh's college is located in a square urban block in the suburb of North Oxford one l kilometre from the city centre [9] .This is an area where the predominant form of development is large detached family houses with extensive private gardens. A number of these were initially purchased and demolished to enable the construction of new college buildings and a library. Subsequently over a number of years all the houses in the urban block of some 5.6 hectares were purchased and those which were not demolished were converted into accommodation entered from the inside of the block where a number of new buildings were constructed in the extensive rear gardens .

To access these premises a paved interior path with street lighting has been constructed. Three of the streets surrounding the urban block are therefore lined with what are single family detached houses but are in fact college buildings accessed from the rear. The only clues to their function are the metal plaques on the street side gate posts. Once again the buildings defining the street have been conserved but their function and ownership has been disguised. It is a piece of townscape, another urban stage set.

4. Blavatnik School of Government

This building, named after its sponsor, was opened in 2015 and is located on Walton Street, a radial route from the centre of Oxford which runs through a former working class and industrial extension of the old city which has been heavily gentrified in the last forty years [2].The site is adjoined by a former church in the form of a classical temple originally built in 1836 to serve the working class suburb and now converted to a night club. On the other side of the new building is an old urban house designed to face onto the street with its now exposed side elevations obviously a party walls which was never intended to be exposed.

The Blavatnik's existing neighbours were built as part of a street on the assumption their side elevations would be hidden by other buildings fronting onto the street. By setting back the new building the architects have exposed the side elevations of the existing buildings in a way to which they were never intended. This setting back has also resulted in a space along the street which is of very little use – neither shelter from the weather nor offering seating which might have justified its formation. The continuity of the street has been destroyed in order to

provide a space to view the new building. Together with the style of this building which does not seem to refer to anything in the context it suggests that the driving force for this building is a desire to market the new institution at the expense of every other consideration.

5. Said Business School

This institution, also named after its benefactor, was completed in 2001 on the former site of a railway station near the city centre in an area that has and is still undergoing considerable changes to its fabric [8]. Its front elevation facing an important entry space to the city centre has a lofty portico over a flight of steps. The elevation to the station has been carefully considered even though it has no openings at ground level. The long side elevation facing a fire station is clearly the back of house where refuse bins are collected and service deliveries arrive. The rear elevation faces north at the end of a short residential cul de sac of two storey row houses which predate the University building. It is an important pedestrian and cycle link to the railway station. The new building towers oppressively over the small houses. Trees have been planted to screen the new building but they will take time to grow and the planting of trees to hide a new building cannot be regarded as a celebration of the quality of its architecture . The new building also blocks the southern sunlight to the residential street which is a problem in the winter when sunlight in England is a precious commodity.

6. Conclusions

In all these cases the buildings have been retained but the nature of the street has been radically changed in different ways. In the first two cases the form of the street has been kept which accords with the tenets of the townscape school as set out by Gordon Cullen and his followers in the 1960s as a reaction to le Corbusier's exhortation. However these streets can be considered to represent a "landscape of deception" in that the buildings although looking like private houses accommodate other uses. Furthermore the logic of the street block has been reversed because the retained buildings are entered from their private side inside the blocks i.e. the fronts are not longer fronts .In the case of Pembroke Street the question arises as to whether a street whose doorways are obviously blocked and which do not allow movement from the public space to the private space inside the buildings can really be called a street. In both these cases a form of gated community has been created although it can be argued that they are following the typology of the monastery from which the Oxofrd collges are of course derived.

In the last two cases the structure of the street has been disrupted in different ways. The Blavatnik has destroyed the enclosure of the street in the interest of the marketing of an expensive new facility. In the last case, the Said Business School , an out of scale intrusion has destroyed the amenity of a modest residential street of no great architectural merit but which represents the investment and aspirations of a dozen families.

Finally, these cases show how a city can be progressively taken over by powerful and wealthy organisations. In this case they are public charitable institutions which behave like developers in their search for space to occupy for their own advantage and use new buildings to promote their corporate image. As a result of pursuing these objectives they are contributing to the removal of non academic uses and the conversion of the city into a monoculture … even though the buildings are retained.

References

[1] Appleyard, D., *Liveable streets*, University of California Press, Berkeley and Los Angeles 1981.
[2] Blavatnik School of Government https://www.bsg.ox.ac.uk (access: 20.10.2017).
[3] *Le Corbusier, Précisions sur un état présent de l'architecture et de l'urbanisme*, Paris, Crès, 1930.p168 . Cited in http://www.espacestemps.net/articles/espace-convexe-le-corbusier-et-le-plan-libre (access: 20.10.2017).
[4] Panerai, P. Castex, J. Depaule J.C. Samuels I. ,*Urban forms ; the death and life of the urban block*, Architectural Press, Oxford 2004.
[5] Pembroke College, https://www.pmb.ox.ac.uk (access: 20.10.2017).
[6] Pruitt-Igoe, https://www.archdaily.com/.../ad-classics-pruitt-igoe-housing-project-minoru yamasaki (access: 20.10.2017).
[7] Ronan Point, https://en.wikipedia.org/wiki/Ronan_Point (access: 20.10.2017).
[8] Said Business School, https://www.sbs.ox.ac.uk (access: 20.10.2017).
[9] St Hugh's College, http://www.st-hughs.ox.ac.uk (access: 20.10.2017).

Pembroke College

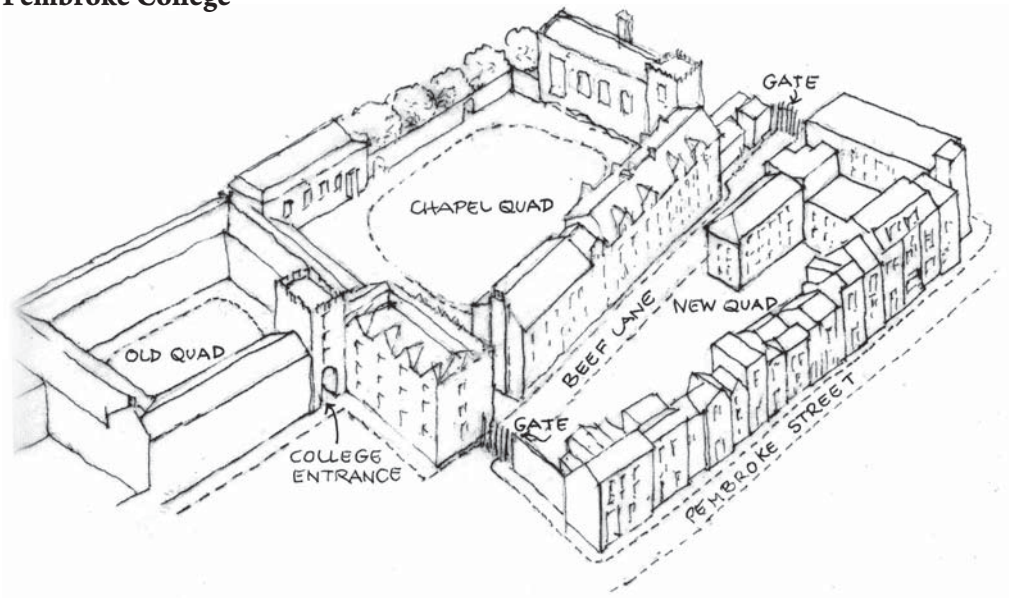

Fig. 1. Pembroke College showing the houses along Pembroke Street opening to the rear and Beef Lane now closed . Ill 1a with captions (drawing by I. Samuels)

Fig. 2. Pembroke Street houses all now part of Pembroke College and entered form the rear (photo by I. Samuels)

Fig. 3. Doors without handles on Pembroke Street (photo by I. Samuels)

Fig. 4. The locked gate to Beef Lane, now closed (photo by I. Samuels)

Fig. 5. The New Quad looking along the line of Beef Lane . On the right the backs of houses along Pembroke Street (photo by I. Samuels)

St Hugh's College

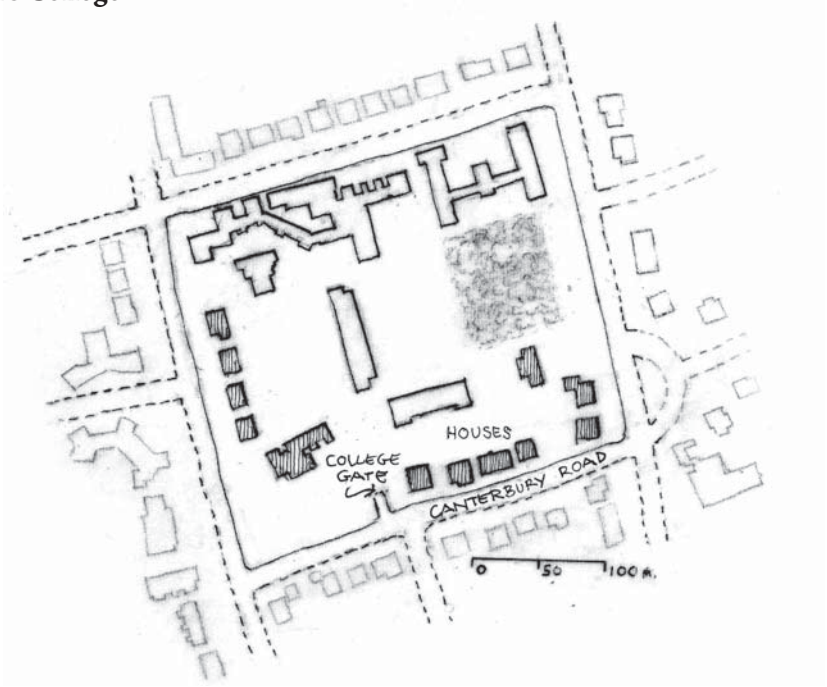

Fig. 6. Plan of the rectangular urban block owned by St Hugh's College showing new college buildings and existing houses . Ill.6a as Ill.6 with captions (drawing by I. Samuels)

Fig. 7. New buildings inside the urban block (photo by I. Samuels)

Fig. 8. Houses owned by St Hugh's College on Canterbury Road (photo by I. Samuels)

Fig. 9. Plaque indicating ownership of detached house (photo by I. Samuels)

Fig. 10. Gate leading to inside of block (photo by I. Samuels)

Fig. 11. Private internal street showing access to rear of houses on Canterbury Road (photo by I. Samuels)

Blavatnik School of Government

Fig. 12. The new space created is of little benefit - except to view the new building (photo by I. Samuels)

Fig. 13. and 14 Walton Street with the new School set back exposing the sides of neighbouring buildings (photo by I. Samuels)

Said Business School

Fig. 15. The main Business School facade facing one of the main entrystreets to Oxford . The tower is a reference to the "dreaming spires" of the University of Oxford (photo by I. Samuels)

Fig. 16. A side elevation with only service doors facing the street (photo by I. Samuels)

Fig. 17. The north elevation dominating the small scale residential street (photo by I. Samuels)

TECHNICAL TRANSACTIONS 1/2018
ARCHITECTURE AND URBAN PLANNING
DOI: 10.4467/2353737XCT.18.002.7953
SUBMISSION OF THE FINAL VERSION: 8/1/2018

Karolina Gyurkovich-Dudzic (kdudzic-gyurkovich@pk.edu.pl)
Faculty of Architecture, Cracow University of Technology

Public space and urban barriers in Cracow. Analysis of the existing state

Przestrzeń publiczna a bariery urbanistyczne w Krakowie. Analiza stanu istniejącego

Abstract

Over the last twenty years Cracow has been experiencing changes associated with the dynamic spatial development. Together with the demographic growth, mobility patterns, change as well as defining the size and volume of transport. As a result of the process, they are often transformed into the space of the city. Attractive public spaces forming logical, continuous sequences could contribute to a more harmonious, sustainable development and rehabilitation of previously neglected neighborhoods. The article will be presented in the case of the transport infrastructure. These areas will be subject to the availability of the pedestrian public space.

Keywords: urban barrier, urban composition, public space

Streszczenie

W ciągu ostatnich dwudziestu lat Kraków przeżywał zmiany związane z dynamicznym rozwojem przestrzennym – wraz ze wzrostem demograficznym, wzorami mobilności, zmianą, a także określeniem wielkości i wielkości transportu. W wyniku tego procesu są one często przekształcane w przestrzeń miasta. Atrakcyjne przestrzenie publiczne tworzące logiczne ciągłe sekwencje mogą przyczynić się do bardziej harmonijnego, zrównoważonego rozwoju i odbudowy zaniedbanych wcześniej dzielnic. Artykuł przedstawia perspektywę infrastruktury transportowej. Obszary te będą uzależnione od dostępności przestrzeni publicznej dla pieszych..

Słowa kluczowe: bariera miejska, kompozycja urbanistyczna, przestrzeń publiczna

1. Introduction

Each urban layout, besides the structures that form it, consists of uncovered areas, cut out or left in the surrounding tissue. As the research based on the history of urbanism shows, the quality of the space surrounding us depends on its geometrical configuration and on its designing principle [5, 20]. The proportion between built fabric and open spaces has been a subject of numerous researches and spatial analysis. The space syntax theory introduced by B. Hillier explores, among others, the relation between the street network and pedestrian movement, showing the importance of density and connectivity [13]. Urban density in particular in German cities has been measured in a recent paper by Angelika Krehl et.al, where some observations concerning the intensification of the city centres in terms of buildings and human activities were made [21]. According to K.Clifton et al., characterisations of the urban form often concentrate on the quantitative aspects, while the quality of the built environment depends on the humans interpretations and cannot be measured directly [6].

The perception of the city as described by Kevin Lynch in his classical work takes place mainly in the public space – the street, the square or the crossroads [22]. These elements of the urban tissue play a significant role in shaping the form of the city. As J. Clos[1] observes, "The proportion of urban areas dedicated to streets and public spaces is a crucial feature of the spatial plans of cities. Indeed, cities that have adequate street and public spaces and greater connectivity are more liveable and productive"[39]. However, the observation of a contemporary city often leads to a conclusion that well-designed, liveable open public spaces are not a common phenomenon, especially in less central locations. The quality and spatial configuration of urban design has been proven to play an important role in promoting pedestrian mobility. Recent years show a growing number of studies related to the walkability of urban environments, conditions of accessibility and pedestrian preferences [2, 29, 33]. Several conclusions can be found in the work of R. Talavera-Garcia, who states: "cities are commonly understood rather as 'multimodal spaces' (where planning should be orientated towards mobile population) than as compact developments (where planning are related to residential population). In this context, walking must not only be circumscribed to specific areas into cities, but walking should be present in places which have not been initially conceived for them" [38, p. 3–4].

Therefore, this work addresses the following questions: What is the present state of the areas adjacent to transportation routes in the city of Cracow? To what extent does the transportation route constitute an urban barrier that affects pedestrian traffic?

The general aim of this study is to provide a preliminary look into the existing state of selected areas in terms of the shape and functioning of public spaces. In the part of the paper dedicated to the case study, the Author focuses on several locations. They were chosen on the basis of criteria referring both to the location and the functions of the space. The fundamental selection principle is the location within the vicinity of car traffic routes identified in the planning documents as essential for the city and its current functioning, as well as its future

[1] Executive Director of UN-HABITAT and UN Under-Secretary-General.

development. Another condition is the location within the perimeter of the city centre or the presence of the urban tissue or defined development layouts. In the categories of the function, an important factor is the presence or documented plans of the location of public spaces or structures in the direct vicinity. In a situation where the existing or transformed transport infrastructure comes into contact with an urban structure, an examination of the relations between these elements may provide information on the currently implemented directions, tendencies, and possibilities of shaping public spaces in the city outside its strict centre.

2. Cracow. Planning Conditions at the Turn of the 21st Century

Cracow has a defined urban structure of the historical Old Town, the geometrical order and characteristic quarter layout, which is responsible for the attractiveness of the city equally with its architectural heritage. The next areas, developed in different historical periods according to the then conditions or requirements, as it is the case in most towns and cities, represent considerable diversity in terms of the architecture itself, as well as its urban disposition. During the processes of extension and growth of the city, former suburbs were becoming new districts, shifting the administrative limits further from the historically developed city centre. The last significant growth of the area took place in 1951, when under an administrative decision, Nowa Huta, designed as a separate town, and its neighbouring villages, were incorporated in the surface area of Cracow[2].

Today, the dynamic development processes of the substance of the city, as well as suburban areas, have a significant effect on its form and function, too, changing e.g. its demographic structure, population density, and space use patterns. This development – similarly to other towns and cities in Poland – takes place according to gradually prepared local plans and administrative decisions defining development conditions. As of today, resolved and valid plans cover nearly half of the area of Cracow[3]; nevertheless, at the same time, the works on resolving new plans are accompanied by quite an opposite process: filing complaints and revoking decisions. This led to a situation where in 2013, the area of the city covered with valid plans was larger than two years later, in 2015 [44]. An obvious fault of the existing planning system is the fact that the whole process is stretched over time; individual, often adjacent plans are drawn up in intervals of even several years, or simultaneously, by different external units. That may lead to a fragmentary approach and to the lack of cohesion. The situation of Cracow is not so unique against the background of the spatial planning practice in Poland in general; on the contrary, for decades now, a vast majority of towns and cities have been through the long process of drawing up and resolving fragmentary local plans.

---

2 Corrections of the limits of Nowa Huta were introduced also later, e.g. in 1986, when Węgrzynowice and Wróżenice were incorporated to it [36].

3 Since 12 April 2017 150 local plans are in force, covering 49.3% of the surface area of Cracow. Since 26 April 2017 another 170 local plans have been developed; although some of them duplicate parts of the plans which have already been resolved, as it is demonstrated on the collective map. So far, limits of administrative units demarcated in the Study have not found any reflection in the delimitation of new plans [47].

From the urban planning perspective, each selected case represents a different situation. Some of them have valid local plans that cover the area fully or partially. The examination of existing documents and studies[4] reveals that the border between plans or separate units is often drawn along main roads. That implies that the neighbouring areas surrounding transportation nodes are subject to different conditions and regulations. In terms of legal possibilities of shaping and transforming certain fragments of the city, roads can potentially constitute a barrier.

3. Systems of public spaces – accessibility

In terms of the existing public spaces, the zone of the historical urban tissue constitutes a certain pattern, in which the form of the space constitutes natural frames for social activities like walking, meeting or even being part of artistic events[5]. The concentration of services, including the growingly important tourist services, secures a constant inflow of users. Beyond the strict heart of the city, but still within the limits of the historical urban structure, the role of leading public spaces is usually played by streets with easily accessible ground floor housing service outlets. The sequential character and natural continuity in the case of historical layouts[6] are usually disturbed in areas of development reaching back to the second half of the 20th century and later [9, 12]. This phenomenon is particularly visible in places dominated by architecture erected over the last 30 years. We can still observe a growing number of fenced housing estates, where shared areas are limited to passages and access roads to individual buildings. This system of creating new structures has a negative effect on many aspects of the functioning of adjacent areas, depriving their users of convenient access to services, recreational grounds, or public transport, which may evoke social tensions and conflicts [18, 32]. Limiting physical accessibility of some areas and creating barriers implies the need to use car transport to the detriment of pedestrian and cycling traffic, which are marginalised today, especially in structures that are extensive in character [2, 10].

[4] The Study of Conditions and Directions of Spatial Development for the City of Cracow currently in force, amended in 2014 and covering the entire city, is not a formal legal document, although its provisions are valid for all drawn up plans, which theoretically should guarantee a determined level of cohesion. As the basis for further provisions, it proposes a division into 63 structural urban units, each furnished with guidelines referring to possible and recommended directions of transformations.

[5] Most of all the Old Town and Kazimierz, as well as other areas until the so-called second ring road that surrounds the city erected in the 19th century.

[6] Legible also in the oldest, social realist part of Nowa Huta.

4. Transport systems – barriers

The historical development of the city in the concentric zone model resulted in the creation of a system of ring roads, the first of which[7] encircles the city centre, repeating the course of the former city walls[8]. In the early 19th century, fortifications constituted a much undesirable barrier, hindering spatial development and the necessary reconstruction; therefore, they were disassembled, and, in the area obtained this way, a municipal park was designed, which, at the same time, constitutes a symbolic opening of the so far fortified system. Today, the first ring road of Cracow is also an important border for individual car traffic, which is much calmed within the very heart of the city, and the main traffic, also subjected to considerable limitations, takes place along its course, where routes of the public transport run, as well. Another transport line, defined as the second ring road of the city, plays an important role in the municipal transport system. It consists of streets with two carriageways and at least two, but most often three lanes in each direction. It surrounds the city built in the 19th century, as well as the old part of Podgórze, Zabłocie, and areas located to the east of the diagonal railway.

The oldest part of the route is Aleje Trzech Wieszczów, avenues built in the 1930s in the place of the liquidated ring railway line [36]. Over several decades, they became the basic route leading around the city centre. The principle of relieving the city centre and limiting the transit route on the second ring road is inscribed in a number of strategic tasks in the field of the transport system. Nevertheless, it still not implemented, because Aleje Trzech Wieszczów avenues still play the role of an access road to the complex of the main railway station and the regional coach station, which form an extensive transport and service hub located at the verge of the Old Town. Due to considerable traffic and the parameters that need to be satisfied in relation to it, the course of the second ring road can constitute an obstacle for the local pedestrian and cycling traffic, which will be examined hereinafter.

5. Analysis of selected cases

The criteria provided above are satisfied in the fullest way by areas located along the current second ring road, especially along its section located in the city centre. In a situation where the existing or transformed transport infrastructure comes into contact with an urban structure, an examination of relations between these elements may provide information on the currently implemented directions, tendencies, and possibilities of shaping public spaces in the city outside its strict centre.

---

7 As defined in the Study in force, it is formed by the sequence of streets: Straszewskiego, Podwale, Dunajewskiego, Basztowa, Westerplatte, Św. Gertrudy, and Podzamcze.

8 Similarly to the situation in e.g. Vienna, Tallinn, or Frankfurt.

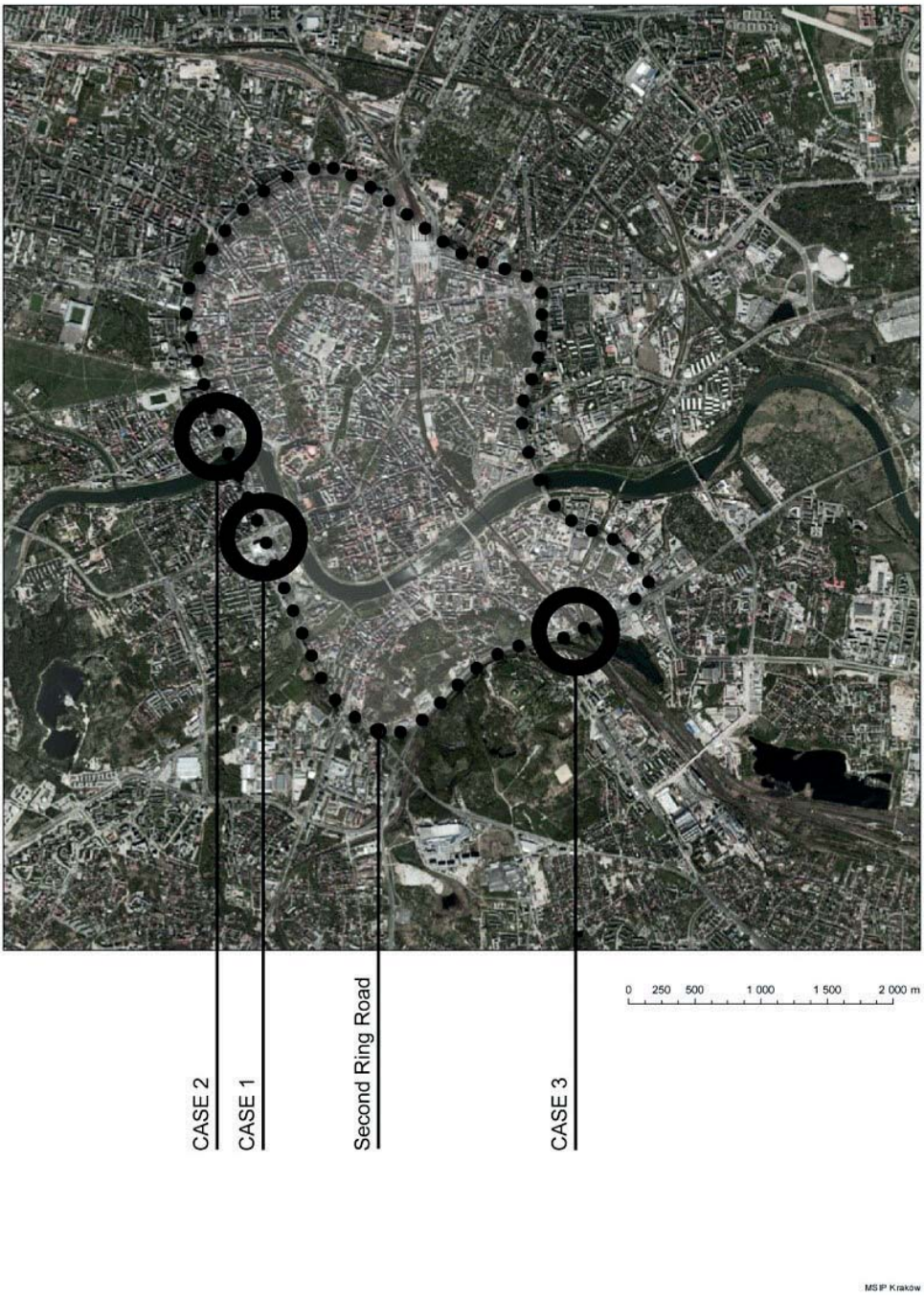

Fig. 1. The Scheme of Selected Cases
(source: Author's drawing on the basis of maps available at: [48]

Case 1

On the left bank of the Vistula, opposite the Wawel Hill in the area, which, in the Study, is defined as belonging to the city centre, there is a two-level interchange of Konopnicka street with a route that runs towards the west. Due to the heavy traffic, the Grunwaldzkie roundabout and road sections adjacent to it may constitute a barrier for the pedestrian traffic in this area. This barrier is even greater due to the fact that its effect is reinforced by the conditions of this location, in the oxbow, nearly on the very bank of the river, which, for ages, has constituted a natural limit for the development of the city. The village of Dębniki, reaching back to the medieval times, was incorporated to the administrative limits of the growing Cracow in the early 20th century, but it was the construction of the Grunwaldzki Bridge in the 1970s that finally linked both banks of the Vistula together, contributing to a considerable increase of traffic, as well. Over the last decades, this area has obtained many investments, important in the scale of the entire city. Starting from the Manggha Museum of Japanese Art and Technology, located between Konopnicka street and the Vistula boulevards, through modern hotels, to the Congress Centre erected in 2014[9], the characteristic edifice of which dominates the space, these structures fulfil the role of public utility buildings.

The public spaces that accompany them are predominantly small sections of squares, or slightly extended sidewalks. The key role in the analysed area seems to be played by the sequence of the Vistula boulevards, which, especially in the area of the Wawel castle, is an important place of recreation, leisure, entertainment, and sometimes it becomes a stage for mass events. The links, grasped in the categories of pedestrian use, between fragments of important spaces located further on from the river bank, can be defined as faint. A small number of pedestrian crossings, located predominantly within the perimeter of the main interchange, makes it difficult to cross the route in the direction of the east – west, as well as north – south. Pedestrian routes are long, and choosing them is connected with a number of inconveniences, such as the waiting time at the traffic lights, the proximity of intensive traffic, noise, exhaust fumes, no protection against atmospheric conditions, which automatically makes a pedestrian occupy the category of a worse, or less important user. The function of car traffic is executed in the form of roads of several lanes and two-level interchanges. The car traffic, predominantly transit in character[10], and public transport lines, as well as the form of the transport hub comprising exits to the tunnels and underpasses, create a real barrier, which hinders the combined functioning of fragmentary and separate spaces, or even makes it completely impossible.

---

[9] Also designed by the studio of Ingarden and Ewý. Naturally, the list of structures provided herein is not closed or complete. One should mention e.g. the building of the once luxury Forum Hotel, located on the southern bank, in the oxbow of the Vistula (designed by Janusz Ingarden, implementation 1978-1989), which for many years shaped one of the most representational skylines of the city with its dynamic form. Today, only its small part is utilised. Hotel rooms are empty, vast banquet halls on the ground floor house restaurants, fair and exhibition spaces. This informal situation is actually very favourable for the space that surrounds the hotel, which along with the nearby municipal beach constitutes a popular and attractive place.

[10] Marii Konopnickiej street is a main road according to the classification contained in the Study currently in force, which predestines it to be burdened with heavy traffic. The Grunwaldzkie roundabout is one of the key hubs of the existing road system of Cracow, as well as the one designed in the perspective of the decades to come [46].

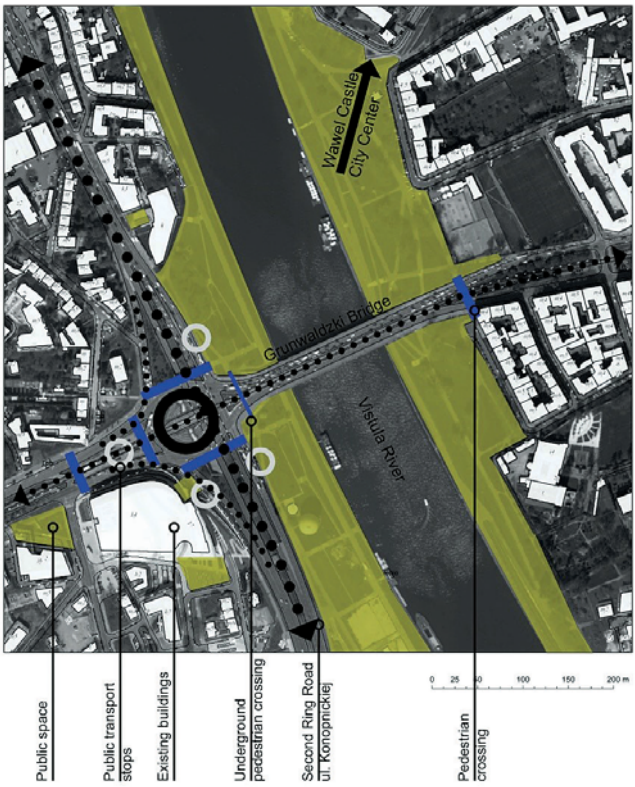

Fig. 2. The Scheme of Case 1
(source: Author's drawing on the basis of maps available at: [48]

Fig. 3. Views of the Existing State
(photos by K. Dudzic-Gyurkovich)

Case 2

Remaining in the course of the second ring road, heading towards the north, we approach the city centre. The area in which a number of important directions meet or intersect is located at the exit of the Dębnicki Bridge, on its northern side, in the place where Aleje Trzech Wieszczów avenues begin. And here, again, the part of the Vistula boulevards in the oxbow of the river, enjoying the southern exposition and the view of the Wawel Hill, should be regarded in the categories of the most vital space. The nearby square with a tourist information point[11] and a temporary coach stop decide about a close relation with the sites most often visited by tourists, located in the heart of the city. Barges moored at the river bank, housing restaurants, coffee shops and clubs, additionally improve the attractiveness of this space in the summer season. The first barrier for high social activity is the line of Zwierzyniecka and Kościuszki streets, but the role of the barrier is ascribed to them rather due to the lack of interesting, well-developed spaces on the northern side, narrow sidewalks, and temporary, chaotic kiosks and

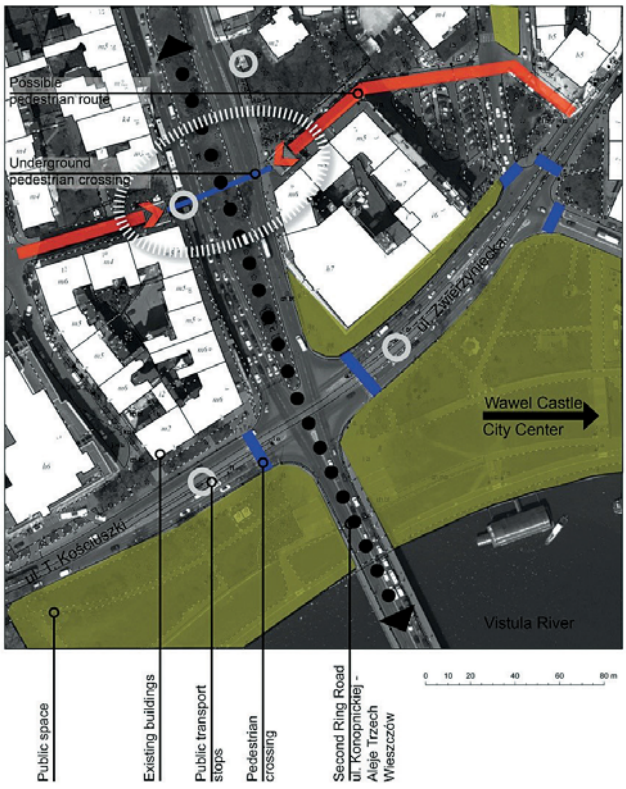

Fig. 4. The Scheme of Case 2
(source: Author's drawing on the basis of maps available at: [48]

[11] Both the square and the building embedded in the ground were designed by imb asymetria [49].

Fig. 5. Views of the Existing State
(photos by K. Dudzic-Gyurkovich)

food stalls, obscuring the potential values of the interiors[12]. Another barrier, this time closely connected with the road transport, is very noticeable. It is created by the route of the second ring road, discussed herein. On the section of ca. 700m, there is only one pedestrian crossing, and it is an underpass. It is not located within the perimeter of the interchange, but further on towards the north, and is functionally connected with the stops of public buses.

When identifying existing public structures and spaces besides the aforementioned boulevards, an observation arises that there are relatively few of them, considering the fact that they are located in the city centre; furthermore, they are not interconnected to form some legible system. Organisation of different types of traffic in its present form points to the priority of the car transport, and simultaneously the pedestrian traffic is restricted to sidewalks and passages. Arranged urban spaces in the understanding of social places, fostering staying and spending free time there, are almost exclusively located to the east from the Zygmunta Krasińskiego avenue, which determines the way of the functioning of the neighbouring spaces in the area in question.

Case 3

The southern part of the second ring road of the city runs across areas with a much less intensive development compared to the northern route, located in the city centre. Podgórze was incorporated in the administrative limits of Cracow relatively late – only in 1915. During World War II, a Ghetto was located there, and the reminiscences of those times are still visible in the oldest part of this district[13]. Structured architecture was developing along the main street in the form of a semicircle, limited from the south with the land relief, and from the north and

[12] The green walking lane of Retoryka street is finished when it reaches a makeshift car park, which today is Kossaka square, and does not find its natural continuation, e.g. in the form of pedestrian crossings, or broadened sidewalks, which could lead towards the boulevards or the city centre.

[13] These are e.g. the remains of the Ghetto wall.

the east with the course of the Vistula river and of the diagonal railway [26]. As late as until the end of the 20th century, the old Podgórze remained a district degraded to a considerable extent, developing in the shadow of the central parts of the city. Over the last years, it is possible to observe a high dynamisation of the gentrification processes, initiated and supported by new residential, cultural, and infrastructural investments [34]. Gradually, buildings and spaces are subjected to revalorisation, sometimes obtaining new functions corresponding to the changing needs of city residents, as well as tourists, who visit this area in constantly growing numbers. These phenomena are clearly visible in the historical, northern part of the district, and partially also in the post-industrial part of Zabłocie, located to the east from the railway line.

The analysed fragment is located at the border of compact quarter development, the legible limit of which is still the course of the intersecting railway lines. Along the line running to the west, there is a road[14], which constitutes a component of the aforementioned southern part of the second ring road. The location of its intersection with the route running towards the south is a very important element of the road system of the city, and in the future, it is to fulfil the role of one of the most important transfer nodes. The construction of a rail link, completing the system of the Fast Metropolitan Rail [42], has been indicated as one of the prioritised municipal strategic investments in terms of the transport system. A massive two-lane railway trestle bridge, which is at the final stage of construction, constitutes a new, aggressive landmark. Besides it, in the area in question, there is a big interchange, a road over a trestle bridge, and a small bus station. The existing buildings along Limanowskiego street[15] and on the eastern side of the tracks, as well as the greenery complex linked with the historical part of the Podgórski Cemetery[16], juxtaposed with the entire extensive infrastructure, lose their significance as elements forming the structure of the city.

Arranged urban public space is particularly difficult to identify here. It seems that Limanowskiego street, which has potentially high architectural and compositional values, does not have any continuation, or even a proper closure in the area in question. On the contrary, the closure of the view corridor could be regarded as a quite accidental one. Each of the transport routes constitutes a very clear and noticeable barrier, which can be overcome by pedestrians only within the perimeter of the interchange by means of consecutive crossings, requiring haste or waiting on small traffic islands dividing the lanes. It seems that the completion of the planned railway stops, and consequently, further extension of the transport node may only legitimise the dominance of the car transport over the pedestrian and cycling traffic. The possibility of a continuation of clearly defined, attractive open spaces has been squandered.

---

[14] Category of the main road according to the Study [46].

[15] Including a historic complex of a baroque inn, located at the corner of Limanowskiego and Powstańców Śląskich street [36]. This complex is connected with a public space planned by the city; it is not known, however, what its character is going to be [43].

[16] Partly destroyed during the World War II, and finally in the 1970s during the construction of the then Telewizyjna street, today Powstańców Śląskich street [36].

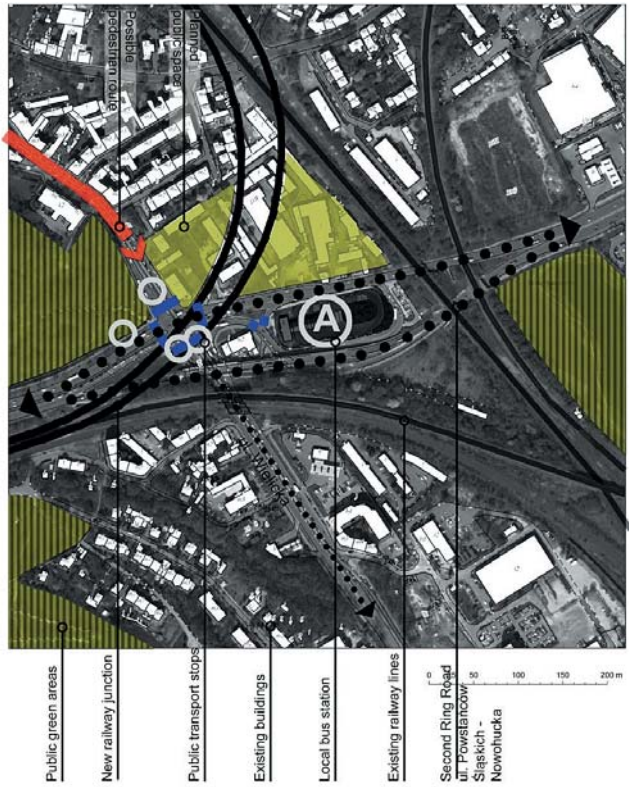

Fig. 6. The Scheme of Case 2
(source: Author's drawing on the basis of maps available at: [48]

Fig. 7. Views of the Existing State
(photos by K. Dudzic-Gyurkovich)

6. Summary

On the basis of the analysis of several selected situations where the transit car transport comes into contact with the urban tissue, several conclusions can be drawn with reference to the morphological structure, as well as to the functioning of space. In the analysed cases, transport systems dominate the areas in terms of the space they occupy, which usually exceeds the share of the public space. Roads and interchanges, junctions, acoustic screens and other elements of the infrastructure that accompany them, create powerful spatial barriers in the scale of a pedestrian, which contribute to the fragmentation of the tissue, as well legitimise and perpetuate the existing divisions. In the situations in question, transport routes usually maintain their continuity and logical course; systems of public spaces and pedestrian routes are adjusted to the conditions imposed this way. The functioning of public spaces in the direct vicinity of much frequented and well-developed roads is considerably limited by the existence of 'dead edges', by the lack of a sense of security, as well as by the accumulation of unfavourable factors, such as noise and exhaust fumes, or excessive exposition to weather conditions connected with the time of waiting for a crossing. In each of the locations discussed herein, a transport route creates a barrier in an urban scale, which, in its current form, limits the possibilities of creating sequences of public spaces, which might complete the already existing, although fragmentary, system.

Contemporary examples of projects relating to the integration of the transport infrastructure in the city, implemented globally for the last 20 years, clearly demonstrate the pursuit for attractive pedestrian spaces, which may create an integrated network comprising a considerable part of the city. Areas until recently occupied or dominated by road transport are transformed so that the pedestrian traffic and activities connected with it could be ascribed greater importance. The most radical solution, encountered e.g. in cities in America, consists in the elimination of a freeway, which constitutes a barrier, and replacing it with a local road, as well as a new arrangement of the released space taking social needs into account[17]. In Europe, where both urban systems and transport routes that accompany them have been subjected to different processes, this model does not seem to be applicable. The existence of freeways is necessary for the efficiency of the contemporary urban system, and traffic accessibility decides about the economic competitiveness to a considerable extent in the global context [19].

The relation between transport systems and the urban tissue and their mutual multi-faceted links are of a functional as well as compositional character, as the course of roads constitutes one of the most durable elements of the structure affecting the spatial disposition and form of architectural development [3, 12]. A solution, which is more and more often applied, is the aforementioned integration of transport systems and their accompanying infrastructure with the urban tissue, maintaining the previous courses of roads and their capacity[18]. As is demonstrated by numerous European and global projects, a barrier in an urbanised area, which most often is a much-frequented transport line, may be considerably

[17] This course of action was undertaken in e.g. San Francisco, Portland, and Milwaukie, and these cities became 'case studies' for many further planned and postulated projects [50].

[18] The opportunities of development of public space systems along the existing elements of the second and third ring road of Cracow are pointed out by e.g. K. Bojanowski [4].

weakened, and its unfavourable effect annulled by appropriately selected architectural measures. Many examples of such measures are to be found in e.g. Barcelona, were, for decades, there have been transformations of degraded areas performed, which also comprise the land occupied for the purposes of transport [8]. Transformations, which result in the creation of an attractive pedestrian space, are characterised by a diversified extent of interference into the barrier itself; they always bring about, however, new compositional and functional directions, enriching the space of the city and inscribing in the existing or planned systems. Strengthening the network of public spaces by means of creating new belts or nodes may become one of the tools of building the postulated cohesion of the city.

References

[1] Áuge M., *Nie-miejsca: wprowadzenie do* antropologii nowoczesności, PWN, Warszawa 2011.

[2] Banister D., *Unsustainable transport – City transport in new century*, Routlege, Oxon 2005.

[3] Bieda K., *Wpływ czynnika komunikacji na kształtowanie struktur osiedleńczych*, Zeszyty Naukowe Politechniki Krakowskiej, No. 6, 1980.

[4] Bojanowski K., *Strategia dla Krakowa – koncepcja rozwoju przestrzeni publicznych*, Wydawnictwo PK, Kraków 2013.

[5] Chmielewski J.M., *Teoria urbanistyki w projektowaniu i planowaniu miast*, Oficyna Wydawnicza Politechniki Warszawskiej, Warszawa 2001.

[6] Clifton K., Ewing R., Knaap G-J., Song Y., *Quantitative analysis of urban form: A multidisciplinary review*, Journal of Urbanism 1(1), 2008, 17–45.

[7] De Cauter, L., *The Capsular Civilization: On the City in the Age of Fear*, NAi Pub, Rotterdam 2004.

[8] Dudzic-Gyurkovich K., *Strategies of overcoming urban barriers – selected examples from Barcelona/Strategie pokonywania barier urbanistycznych – wybrane przykłady z Barcelony*, [In:] *Hybrid urban structures = Hybrydowe struktury urbanistyczne*, ed. M. Gyurkovich, Wydawnictwo PK, Kraków 2016, 107–133.

[9] Dymnicka M., *Fragmentaryzacja przestrzeni miejskiej – próby rekompozycji*, Studia Regionalne i Lokalne 9/2008, No. 33, 33–52.

[10] EEA, *Urban sprawl in Europe: the ig*No.*red challenge*, *EEA Report* No. *10/2006*, European Environment Agency, Copenhagen, 2006. https://www.eea.europa.eu /publications/eea_report_2006_10 (access: 28.07.2017).

[11] Gehl J., *Miasta dla ludzi*, Wydawnictwo RAM, Kraków 2014.

[12] Gzell S., *Miastotwórcza rola transportu w teorii urbanistyki*, Czasopismo Techniczne 1-A/2010, 5–19.

[13] Hillier B., Penn, A., Hanson, J., Grajewski, T., Xu, J., *Natural Movement – Or, Configuration And Attraction In Urban Pedestrian Movement*, Environ Plann B 20/1993 (1), 29–66.

[14] Hołuj A., *Potencjalne skutki niewłaściwych praktyk w planowaniu przestrzennym (przypadek Krakowa)*, KPZK PAN, Studia, No. 152/2013, 171–184.

[15] Jenks M., Kozak D., Takkanon P., *World Cities and Urban Form: Fragmented, Polycentric, Sustainable?*, Routlege, Oxon 2008.
[16] Kantarek A.A., *Tranzyt a spójność formy miasta*, Czasopismo Techniczne, 1-A/2010, 163–170.
[17] Kłopotowska A., *Czynnik 'obronności' we współczesnej architekturze zespołów mieszkalnych*, Budownictwo i Architektura, 6, 2010, 51–61.
[18] Kochanowska D., *Przestrzeń publiczna – kluczowy element miasta współczesnego – zintegrowana czy podzielona?*, [In:] *Problemy kształtowania przestrzeni publicznych*, eds. P. Lorens, J. Martyniuk-Pęczek, Urbanista, Gdańsk 2010, 21–35.
[19] Komisja Europejska, *Strategia na rzecz inteligentnego i zrównoważonego rozwoju sprzyjającego włączeniu społecznemu, = A European Strategy for Smart, Sustainable, and Inclusive Growth*, Komisja Europejska, Bruksela 2010, http://ec.europa.eu/eu2020/pdf/1_PL_ACT_part1_v1.pdf (access: 22.07.2017).
[20] Kostof S., *The City Assembled: The Elements of Urban Form Through History*, Thames and Hudson, London 1992.
[21] Krehl A., Siedentop S., Taubenböck H., Wurm M., *A Comprehensive View on Urban Spatial Structure: Urban Density Patterns of German City Regions*, International Journal of Geo-Information ISPRS, 5(6), 76/2016.
[22] Lynch K. *Obraz miasta*, Wydawnictwo Archivolta, Kraków 2011.
[23] Marcuse P., van Kempen R., *Of states and cities: The partitioning of urban space*, Oxford University Press, Oxford 2002.
[24] Ministerstwo Rozwoju, *Koncepcja Przestrzennego Zagospodarowania Kraju 2030*, Ministerstwo Rozwoju, Warszawa 2013, http://mr.bip.gov.pl/strategie-rozwoj-regionalny/7847_strategie. html (access: 18.07.2017).
[25] Ministerstwo Rozwoju, *Krajowa Polityka Miejska 2023*, Ministerstwo Rozwoju, Warszawa 2015, https://www.mr.gov.pl/media/10252/Krajowa_Polityka_Miejska_20-10–2015.pdf (access: 18.07.2017).
[26] Mydel R., *Rozwój urbanistyczny miasta Krakowa po drugiej wojnie światowej/Urban Development of the City of Cracow after the World War II*, Wydawnictwo i Drukarnia Secesja, Kraków 1994.
[27] OECD, *Green Growth Studies: Compact City Policies: A Comparative Assessment*. OECD Publishing, Paris 2012.
[28] OECD, *The Metropolitan Century: Understanding Urbanisation and its Consequences*, OECD Publishing, Paris 2015.
[29] Olszewski P., *Dostępność* piesza jako element jakości miejskiego transportu zbiorowego, Transport Miejski i Regionalny, 01/2008, 19–33.
[30] Pancewicz Ł., *Prywatyzacja przestrzeni publicznych*, [In:] *Problemy kształtowania przestrzeni publicznych*, eds. P. Lorens, J. Martyniuk-Pęczek, Urbanista, Gdańsk 2010, 80–91.
[31] Panerai P., Castex J., Depaule J-C., Samuels I., *Urban Forms: The Death and Life of Urban Block*, Architectural Press, Oxford 2004.
[32] Racoń-Leja K, *Bariery w kształtowaniu przestrzeni publicznej w zespołach mieszkaniowych*, Czasopismo Techniczne, 3-A/2010, 165–170.

[33] Rudnicki A., *Zrównoważona mobilność a rozwój przestrzenny miasta*, Czasopismo Techniczne, 1-A/2010, 57–74.
[34] Sarga A., *Wpływ kładki „Bernatka" na strukturę funkcjonalno-przestrzenną krakowskiego Kazimierza i Podgórza*, Przestrzeń i Forma, 2014, No. 21, 473–482.
[35] Schlossberg M., Weinstein A., Irvin K., *How Far, by Which Route and Why? A Spatial Analysis Of Pedestrian Preference*, Journal Of Urban Design, 13, No. 1/2008, 81–98.
[36] Stachowski A.H., Adamczyk E., *Encyklopedia Krakowa*, Wydawnictwo Naukowe PWN, Warszawa, Kraków 2000.
[37] Talavera-Garcia R., Soria-Lara J, *Pedestrian mobility environments: definition, evaluation and prospects*, [In:] Proceedings of the AESOP-ACSP Joint Congress, 15–19 July 2013, Dublin.
[38] Talavera-Garcia R., Soria-Lara J., *Q-PLOS, developing an alternative walking index. A method based on urban design quality*, Cities, 2015, Vol 45, 7 – 17.
[39] UN-HABITAT, *The relevance of street patterns and public space in urban areas*, United Nations Human Settlements Programme, 2013, https://unhabitat.org/the-relevance-of-street-patterns-and-public-space-in-urban-areas (access: 21.07.2017).
[40] UN-HABITAT, *Global Public Space Toolkit From Global Principles to Local Policies and Practice*, prepared by Pietro Garau, United Nations Human Settlements Programme, Nairobi 2015, https://unhabitat.org/wp-content/uploads/2015/10/ Global%20 Public %20Space%20Toolkit.pdf (access: 21.07.2017).
[41] Urząd Miasta Krakowa, Strategia Rozwoju Krakowa 2030 – *Projekt*, Kraków 2017, https://www.bip.krakow.pl/?id=47 (access: 10.07.2017).
[42] Urząd Miasta Krakowa, Katalog Inwestycji Strategicznych Układu Transportowego Krakowa, Kraków 2010, https://www.bip.krakow.pl/?dok_id=44176 (access: 10.07.2017).
[43] Urząd Miasta Krakowa, *Kierunki rozwoju i Zarządzania Terenami Zieleni w Krakowie 2017–2030 Projekt*, Wydział Kształtowania Środowiska, Kraków 2017, http:// obserwatorium.um.krakow.pl/obserwatorium/kompozycje/?config=config_ zbiorcza.json (access: 27.07.2017).
[44] Urząd Miasta Krakowa, *Raport o Stanie Miasta 2015*, Wydział Rozwoju Miasta, Kraków, 2015, https://www.bip.krakow.pl/?dok_id=79963 (accessed July 10, 2017).
[45] Urząd Miasta Krakowa, Strategia Rozwoju Krakowa, Urząd Miasta Krakowa, Kraków 2005, https://www.bip.krakow.pl/?id=47 (access: 10.07.2017).
[46] Urząd Miasta Krakowa, *STUDIUM uwarunkowań i kierunków zagospodarowania przestrzennego Miasta Krakowa – DOKUMENT UJEDNOLICONY*, Biuro Planowania Przestrzennego, Kraków 2014, https://www.bip.krakow.pl/?id=48 (access: 21.07.2017).
[47] Urząd Miasta Krakowa, https://www.bip.krakow.pl/bip_id=1&mmi=412 (access: 9.07.2017).
[48] Obserwatorium – portal Miejskiego Systemu Informacji Przestrzennej, http://msip.um.krakow.pl (access: 18.09.2017).
[49] IMB Asymetria, http://www.imbasymetria.pl/projekt, projekt,27,cort_powisle.html (access: 18.09.2017).
[50] CNU, Congress for the New Urbanism, http://cnu.org (access: 18.09.2017).

TECHNICAL TRANSACTIONS 1/2018
ARCHITECTURE AND URBAN PLANNING
DOI: 10.4467/2353737XCT.18.003.7954
SUBMISSION OF THE FINAL VERSION: 26/12/2017

Michał Krupa (michalkrupa@zeriba.pl)
Faculty of Architecture, Cracow University of Technology

Revalorisation project of the 19th-century Bohaterów Monte Cassino Park in Jarosław

Projekt rewaloryzacji XIX-wiecznego parku miejskiego im. Bohaterów Monte Cassino w Jarosławiu

Abstract

This article concerns the issue of revalorisation of the Bohaterów Monte Cassino Park in Jarosław. The park was created at the beginning of the 20th century in connection with the Industrial and Agricultural Exhibition organised there, which, in those times, was both an economic, cultural and social event. It was then that the spatial layout of the park was laid out and exhibition pavilions were erected, which, unfortunately, did not survive to the present day. However, the urban layout with its historic tree stand has been preserved. Sadly, the park is currently badly neglected, which has influenced the town authorities to agree to its revitalisation and restoration. For this purpose, a conceptual project has been prepared, and subsequently, on the basis of the former, a civil engineering design with a dendrological analysis. It should be added that, since 1992, the area has been inscribed in the voivodeship monument register, which puts it under the conservation services supervision.

Keywords: Jarosław, city park, revalorisation, revitalisation

Streszczenie

Niniejszy artykuł dotyczy rewaloryzacji parku miejskiego im. Bohaterów Monte Cassino w Jarosławiu. Park ten powstał na początku XX wieku w związku z organizowaną w mieście Wystawą Przemysłową i Rolniczą, która w owych czasach była wydarzeniem nie tylko gospodarczym, ale także kulturalnym i towarzyskim. Wówczas to wytyczono układ przestrzenny parku, a także wzniesiono pawilony wystawowe, które nie przetrwały do naszych czasów. Zachowało się natomiast samo założenie urbanistyczne z zabytkowym drzewostanem. Niestety park jest obecnie bardzo zaniedbany, co wpłynęło na decyzję władz miasta o podjęciu działań na rzecz jego rewitalizacji i rewaloryzacji. W tym celu opracowano projekt koncepcyjny i na jego podstawie projekt budowlano-wykonawczy wraz z ekspertyzą dendrologiczną. Należy przy tym dodać, że teren od 1992 roku jest wpisany do rejestru zabytków województwa, co sprawia, że jest pod kontrolą służb konserwatorskich.

Słowa kluczowe: Jarosław, park miejski, rewaloryzacja, rewitalizacja

1. Introduction

In the historic town of Jarosław, at the junction of Bandurskiego and Konfederacka streets, a vast town park covering almost 8 hectares was created in the 19th century. It was realised in connection with the Industrial and Agricultural Exhibition, organised in the year 1908, which was both an economic, cultural and social event in those times. After the exhibition, the park was used as recreational space for the inhabitants of Jarosław. However, in recent years, it has deteriorated. The local authorities of Jarosław decided to restore it to its former glory, at the same time creating a place for rest and relaxation for Jarosław residents. For this purpose, the architectonic concept of revalorisatio 3517/1, 3517/2, 3516/1, 3516/2, 3441, 3553/2, 3554/1n and revitalisation of the space was prepared in 2013, and in 2017, the civil engineering design was based on it. However, its description ought to be preceded by an outline of the history of the park, which has been inscribed in the monument register of the Podkarpackie Voivodeship since 1992 (Entry no: A-479).

2. History

As has already been mentioned above, the Bohaterów Monte Cassino Park in the town of Jarosław was founded at the beginning of the 20th century. Its development was associated with the Industrial and Agricultural Exhibition organised in the year 1908 [1].

At the turn of the 19th and 20th century, larger and smaller cities and towns frequently organised industrial-agricultural exhibitions imitating those which first appeared in England and France in the mid-18th century. Those exhibitions were intended to promote

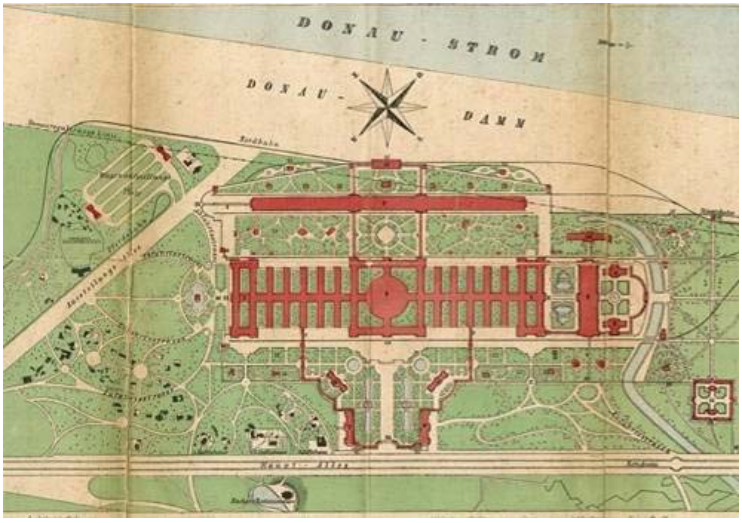

Fig. 1. Plan presenting a fragment of the World Fairgrounds in Vienna. Copy of the map (source: Archive of the Chair of History of Architecture, Urban Studies and Art, Faculty of Architecture, Cracow University of Technology WA PK, s.v.)

the achievements of a given region in the field of economy, but often education and culture, too [2]. They were also political events, which resulted in economic stimulation frequently connected to a plan of political reforms [3].

For the land of Galicia, where Jarosław is located, the models for industrial-agricultural exhibitions were found primarily in Vienna and then Lviv. The exhibition in Vienna, i.e. the Weltausstelung (the World's Fair) was organised in 1873. It is worth emphasising that entrepreneurs from Galicia were also present there [4].

Soon after the exhibition in Vienna, members of the Galician Economic Association came up with the idea of organising a similar event in Lviv. Four years later, the Association in cooperation with Włodzimierz Dzieduszycki, Prince Leon Sapieha and Ludwik Wierzbicki, supported by the Agricultural-Economic Society in Krakow, national chambers of commerce and management of industrial museums realised the plan and organised the Agricultural-

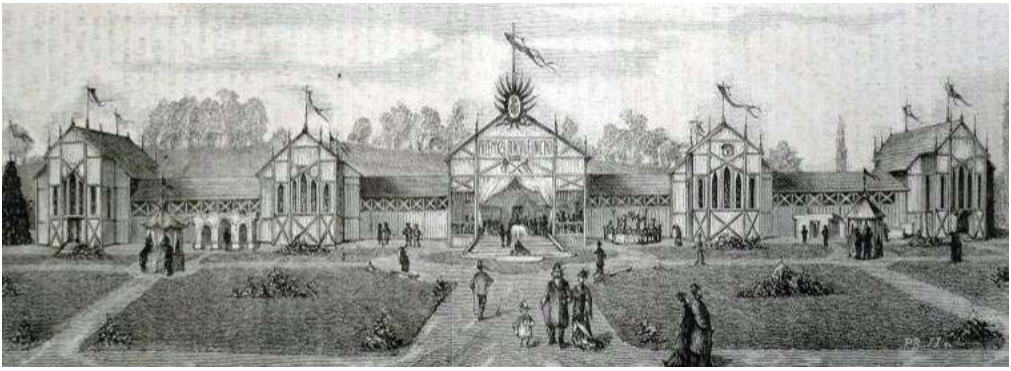

Fig. 2. Main pavilion of the Industrial-Agricultural Exhibition in Lviv on a sketch (source: Tygodnik Ilustrowany 1877)

Fig. 3. Main pavilion of the Industrial-Agricultural Exhibition in Lviv (source: Author's Archive)

Fig. 4. Main pavilion of the Industrial-Agricultural Exhibition in Lviv. View of the entrance area (source: Author's Archive)

Industrial Exhibition in Lviv. Its purpose was a review of the agricultural and industrial production in Galicia, and determining primary trends in its development [5]. The event was planned to be held in the Jabłonowski park, and particular exhibitions were situated in four pavilions. Two were specially built for the occasion, and the other two were private property [6]. The whole exhibition was divided into four sections. In each section, there was a specific group of products that were presented. Since the exhibition in Lviv turned out to be a success, other Galician cities wanted to follow in its footsteps and began to organise similar events.

Following the example of the Lviv exhibition, the idea of organising a similar event was born in Jarosław. Its author was an entrepreneur from Jarosław, a member of the League of Industrial Assistance and of the Sokoł Association - Stanisław Gurgul who, in order to organise the exhibition in Jarosław had to gain approval of the then town authorities, the authorities of neighbouring counties, as well as local landed gentry and Galician industrial milieu. At that time, Jarosław possessed all the assets indispensable to host an exhibition of a regional magnitude. Back then, the town numbered about 25 thousand inhabitants and was among the richest towns in Galicia. It had appropriate economic potential and technological infrastructure. It also boasted long commercial traditions and developed agriculture, especially in the magnate estates. The town was already well linked with Krakow and Lviv, e.g. by means of the railway line. The catering and hotel facilities in Jarosław also allowed for organising such an event as an exhibition, and hosting exhibitors and guests involved in it. However, for the exhibition to take place, a vast, empty stretch of land was needed where the organisers could build display pavilions as well as all necessary infrastructures accompanying the exhibition. For this purpose, an area was selected in the suburbs of Jarosław, known as Olszanówka, which had been used for recreational activities since 1902.

The head of the organisational committee of the exhibition was the already mentioned Stanisław Gurgul, the secretary of the agricultural committee was Józef Dąbrowski, and of

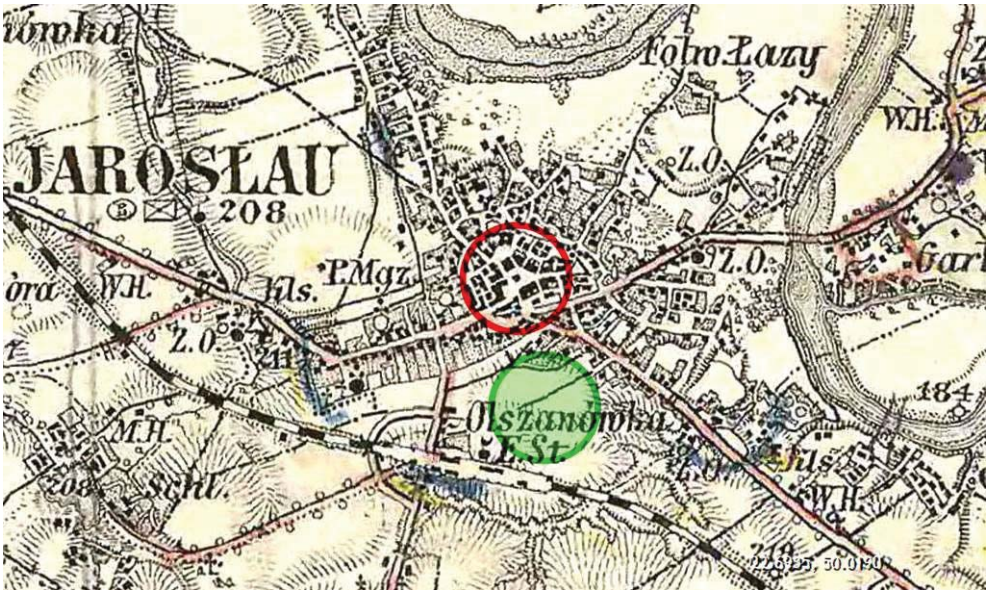

Fig. 5. Third Military Survey from the 2nd half of the 19th century depicting Jarosław. On the map red colour marks the location of the main square and green marks Olszanówka where, at the beginning of the 20th century, the town park was created (source: Archive of KHAUiSzP WA PK, s.v.)

the industrial committee Samuel Kornman. Then, the president of the exhibition itself was Witold Czartoryski from Pełkinie, and vice-presidents were – the Mayor Adolf Dietzius and Jerzy Turnau from Mikulice. The patrons of the event were prominent representatives of local landed gentry: Maria and Jerzy Czartoryski from Wiązownica, Andrzej Lubomirski from Przeworsk and Stanisław Siemieński-Lewicki from Pawłosiow. The organisers made sure that the exhibition was well advertised. For this purpose, an advertising poster was commissioned along with a large-scale promotion programme in the press by means of published announcements and advertisements.

The exhibition lasted one month; during that time craft, machines, as well as flora and fauna, were displayed in the park. Since the exhibition was also perceived as a cultural event, theatre performances, film viewings, concerts, games and other amusements were organised in the park for residents of Jarosław. In the exhibition, various commodities were presented by 240 exhibitors not only from Galicia, but also from Silesia or Greater Poland. Goods were presented according to 18 approved thematic sections. Exhibitions were organised in 29 specially prepared pavilions, which varied as far as their size and architectonic form were concerned. They were built using the funds of the exhibition committee or private investors. The committee financed, e.g. the construction of the industrial pavilion, covering the area of 1.200 m^2, which had been designed by architect Mieczysław Dobrzański. In turn, the agricultural pavilion was built according to the design by an architect from Lviv, Zygmunt Fedorski [7]. The secretary of the industrial committee, Samuel Kornman, designed the entrance gate, the theatrical and musical pavilions and the seat of the exhibition management. Unfortunately, the above-mentioned objects or

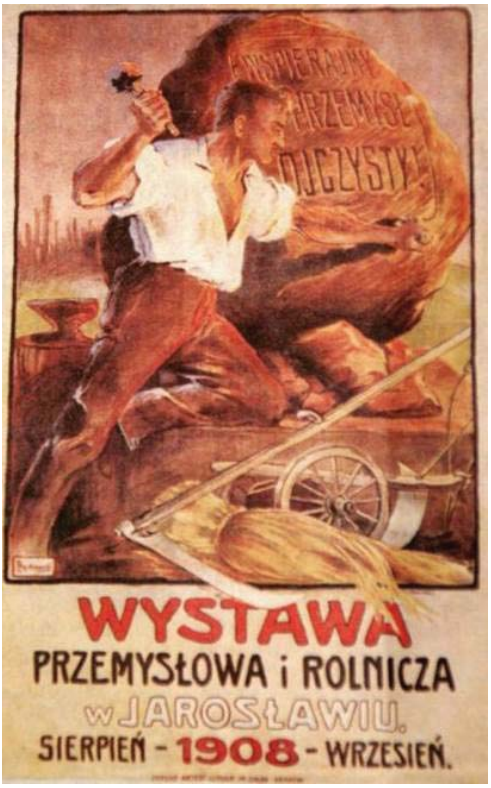

Fig. 6. Poster for the Industrial-Agricultural Exhibition in Jarosław designed by Franciszek Zajchrowski (source: Author's Archive)

architectonic features have not been preserved until today. They were destroyed in the course of World War I and II.

The exhibition turned out to be a spectacular success. It was visited by over 40 thousand people. It also ensured the promotion of the town. It was emphasised that as far as the size and perfect organisation were concerned, it rivalled national exhibitions, even though it was a local event [1].

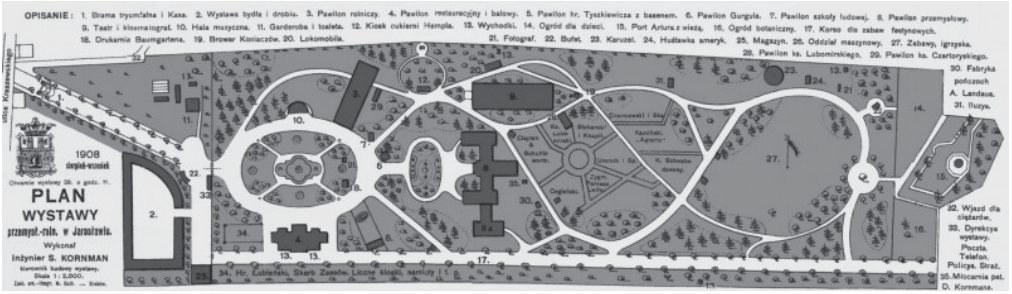

Fig. 7. Plan of the Industrial-Agricultural Exhibition in Jarosław (source: Author's Archive)

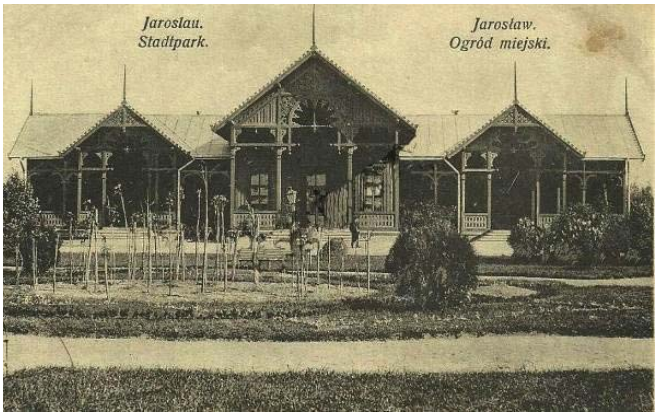

Fig. 8. View of one of the no longer existing pavilions in the Bohaterów Monte Cassino Park in Jarosław in the 1st half of the 20th century, on archive postcards (source: postcards in Author's Archive)

Fig. 9. View of the main park avenue in the 1st half of the 20th century, on an old postcard (source: postcards in Author's Archive)

Fig. 10. View of the main entrance to the park in the 1st half of the 20th century, on an old postcard (source: postcards in Author's Archive)

3. Revalorisation of the historic park

The town park, which is a legacy of the Exhibition, is currently badly neglected. In its area, there are numerous pedestrian paths with dirt surfaces, which are in poor technical condition and do not meet the currently binding standards. Architectural features in the park in the form of benches and lanterns have been vandalised, and are randomly situated instead of arranged. The entire park area is surrounded by a fence, which is varied. Fragmentarily, it is made up of historic spans of the fence from the beginning of the 20th century, while the rest of it consists of typical modern segments. The historical character of the park and its urban layout from the beginning of the 20th century have been relatively well preserved and

Fig. 11. View of one of the lawns (photo by M. Krupa, 2017)

Fig. 12. View from a distance of another lawn (photo by M. Krupa, 2017)

Fig. 13. View of a fragment of the main avenue (photo by M. Krupa, 2017)

Fig. 14. View of one of the park lanes connecting lawns (photo by M. Krupa, 2017)

Fig. 15. View of a fragment of a historic park fence (photo by M. Krupa, 2017)

are still visible. Similarly, trees are also historical. The park area borders currently on housing estates consisting of both apartment blocks and detached houses, and so is a vital place for recreation, walking and meeting among local residents, and because of its accessibility, also people living in other areas of Jarosław. Because the Bohaterów Monte Cassino Park is currently the largest recreational space in Jarosław, the town authorities decided to have it restored and revitalised.

Project work was carried out in several stages. The first stage involved preparing an inventory of the park, from the dendrological and architectonic-urban-planning point of view. The conducted inventory served as a basis for the concept created by the designing office ARCONT Robert Pelc. The concept included ordering the historic spatial layout, newly planted greenery, new architectural features in the form of benches, lanterns, fountains, information boards, deckchairs, info-kiosks, bicycle racks, rubbish bins etc. [8]. The concept, besides the investor's demands and regulations of the Local Spatial Development Plan, also had to take conservation guidelines into consideration. The designers intended to create a highly functional space for the town inhabitants, with interesting natural and educational spaces in order to increase their ecological awareness.

On the basis of the above-mentioned concept, the ZERIBA Designing Office[1] with a team of designers from the fields of dendrology, construction, electrical installations and sanitary systems prepared a detailed civil engineering project together with a Programme for tree protection – evaluation of endangered trees because of the planned investment and guidelines concerning treatment of trees during project work and execution.

The park revalorisation primarily involved the restoration of the historic communications system, which was supplemented with several modern pathways related to the current needs of users. Pedestrian and pedestrian-bicycle lanes will be made from natural, permeable gravel-clay surface. The appearance of the surface resembles the "hanse grand" surfaces, frequently applied in historic parks, but is not so expensive or difficult to maintain.

An important element of the project was the renovation and completion of the historic fence, which has been fragmentarily preserved until today. In order to achieve this, it was planned to renovate the metal and wrought-iron elements and to replace or repair the underpinning. Because the historic entrance gate to the park has not survived, and the current one does not fit in with the historic character of the place, it was redesigned according to the suggestions of the Voivodeship Monument Conservator.

Architectural features have also been selected with regard to conservation guidelines. For instance, new lanterns have been designed, black in colour and in a historical form alluding to those applied in historic park complexes. In turn, benches and park deckchairs, also maintained in the classic stylistics, will be made from wood covered with walnut shade stain varnish, and their bases will be made from cast iron and coated with black varnish. Likewise, such elements as bicycle racks, rubbish bins and information boards were chosen in such a way as to allude to the historic character of the park. Another important element is the educational garden

[1] Team: Prof. Arch. Dominika Kuśnierz-Krupa, landscape architect; Ph.D. Arch. Michał Krupa, Ph.D. Arch. Łukasz Wesołowski, M.Sc. Arch. Anna Krukowiecka-Brzęczek, landscape architects.

house, designed in the northern part of the park. It is supposed to constitute an open space, thus offering a possibility for running various educational activities in the open air and the natural surroundings.

Yet another challenge for the designers was the project of vegetation that could not overshadow historic greenery, which had previously been tidied up by cutting down self-seeders. The project highlighted the particularly valuable avenues of trees as well as individual specimen. Newly-designed plantings were divided into several groups of plants: ground covers; fragrant and nectar source plants; plants by the playground and additional vegetation. The designed botanical paths constitute a significant educational element on the way to shape pro-ecological attitudes and behaviour, both among children and adults. The paths are to enable park visitors to experience nature through direct and active contact.

Ground covers are to be planted beneath tree boughs in the form of irregular flower carpets. They include e.g. Hydrangea petiolaris; Vinca minor; Cotoneaster dammeri 'Major'; Pachysandra terminalis 'Green Carpet'; Clematis 'White Swan'; 'Parthenocissus quinqefolia'; Hedera helix. Those plants are to create educational paths called "Plant pillows". Because of their properties, they can be grown in the shade and can also replace the lawn. The "Plant pillows" pathway takes advantage of natural conditions prevailing in the park at the time and, moreover, the plants used perfectly fit in with the historic character of the place.

Fragrant and nectar source plants, in turn, are to be planted in the vicinity of the bee garden, and are to create the path called "Scents of enchanted gardens". They are to include, e.g. Heliotropium, Lavandula, Nepeta, Lathyrus odoratus, Viola, Salvia officinalis.

Special varieties of willow are designed to be planted by the playground, e.g. Salix integra, Salix purpura 'Nana', Salix purpura 'Pendula', which are to allow children to create labyrinths from willow osiers, and thus learn while playing.

Besides greenery related to intended educational paths, other plantings have been planned in the park in order to add to the existing vegetation. That aim has been achieved by using plants, such as e.g.: Rhododendron, Philadelphus, Magnolia, Syringa, Mahonia, Calycanthus, Buddleia davidii, Frangula alnus, Pyracantha coccinea, Cornus mas, Tilia cordata and Hydrangea paniculata [9–11].

In conclusion, it should be remembered that the fundamental idea of the designers while creating the project of the park was related to making it available to the largest possible number of users of different ages. Inhabitants of Jarosław, both older and younger, are to find in the park a place for rest, leisure, but also education through entertainment. The park is to be a safe haven, where one can spend free time away from the hustle and bustle of the city. Such elements of the project as the educational garden house, the bee garden or the natural playground are meant to give visitors an opportunity for active recreation combined with education, e.g. via observing nature through a telescope designed in the western part of the park. In turn, specially selected plants are to allow for contemplation and relaxation among flowers, bushes and trees with diverse textures, colours and aromas. Such a project solution meets the requirements of the inhabitants and the authorities of Jarosław in their strife for modernising the recreational urban space within the broadly understood standards of the 21st century.

Fig. 16. Visualisations of the project of the town park in Jarosław. View of the leisure laws (Prep. by Zeriba Designing Office, 2017)

Fig. 17. Visualisations of the project of the town park in Jarosław. View of a fountain (Prep. by Zeriba Designing Office, 2017)

Fig. 18. Visualisations of the project of the town park in Jarosław. View of the pedestrian path (Prep. by Zeriba Designing Office, 2017)

Fig. 19. Visualisations of the project of the town park in Jarosław. View of the educational garden house (Prep. by Zeriba Designing Office, 2017)

Fig. 20. Visualisations of the project of the town park in Jarosław. View of the bee garden (Prep. by Zeriba Designing Office, 2017)

Fig. 21. Visualisations of the project of the town park in Jarosław. View of a fountain (Prep. by Zeriba Designing Office, 2017)

References

[1] Kostka-Bieńkowska Z., *On 100th anniversary of the Industrial and Agricultural Exhibition in Jarosław,* [in:] MC Archive in Jarosław, s.v., internet access: http://www.jaroslaw.pl/nasze-wydawnictwa/id84_13_4,W-setna-rocznice-Wystawy-Przemyslowej-i-Rolniczej-w-Jaroslawiu.html (access: 21.09.2017).

[2] Meus K., *Z dziejów Wadowic Austriackich: wystawa Rolniczo-Przemysłowa w 1907 roku*, Wadoviana: Przegląd Historyczno-Kulturalny 14/2011.

[3] Komorowski J., *Postawa ziemian galicyjskich wobec przemysłu – wystawa przemysłowo-rolnicza w Jaworowie w 1907 r.*, Studia z Historii Społeczno-Gospodarczej, Vol. VII, 2010.

[4] Dzieduszycki W., *Wystawa powszechna w Wiedniu 1873*, Publ. Księgarnia i Skład Nut Gubrynowicza i Schmidta (Lwów), Lviv 1872, p. 5 and Pemsel J., *Die Wiener Weltausstellung von 1873. Das gründerzeitliche Wien am Wendepunkt*, Publ. Böhlau, Wiedeń 1989.

[5] Łopuszański T.J., *Pamiętnik C. K. Galicyjskiego Towarzystwa Gospodarskiego: 1845–1894*, Publ. Galician Economic Association, Lviv 1894, s.v. and K. Karolczak, *Dzieduszyccy. Dzieje rodu. Linia poturzycko-zarzecka*, Krakow 2001.

[6] *Catalogue of the National Industrial and Agricultural Exhibition* (from September 6 to October 4), Lviv 1877, s.v.

[7] Łoza S., *Architekci i budowniczowie w Polsce*, Publ. Budownictwo i Architektura, Warszawa 1954.

[8] ARCONT Designing Office Robert Pelc, *The concept of revitalising the Bohaterów Monte Cassino Park in Jarosław,* ts, Rzeszów 2013, [in:] MC Archive in Jarosław.

[9] Pelc R., *The concept of revitalising the Bohaterów Monte Cassino Park in Jarosław*, ts, Rzeszów 2013.

[10] Bobek W., *Programme for tree protection – evaluation of endangered trees because of the planned investment and guidelines concerning treatment of trees during project work and execution*, ts, Krakow 2017.

[11] Zeriba Designing Office, *Detailed civil engineering project of revitalization of the Bohaterów Monte Cassino Park in Jarosław*, ts, Krakow 2017.

TECHNICAL TRANSACTIONS 1/2018
CHEMISTRY
DOI: 10.4467/2353737XCT.18.004.7955
SUBMISSION OF THE FINAL VERSION: 4/1/2018

Krzysztof S. Danel (rrdanelk@cyf-kr.edu.pl)
Oskar Michalski
Institute of Chemistry, Agricultural University
Zoryana Usatenko
Jerzy Sanetra
Institute of Physics, Cracow University of Technology
Elżbieta M. Nowak
Faculty of Materials Science and Ceramics, AGH University of Science and Technology

Dicyanovinyl end-capped 9,10-bis (phenylethynyl) anthracenes for organic solar cells

9,10-bis (fenyloetynolo) antraceny z peryferyjnymi grupami dicyjanowinylowymi dla ogniw słonecznych

Abstract

A series of 9,10-bis(phenylethynyl)anthracene dicyanovinyl end-capped derivatives have been used in bulk heterojunction (BHJ) photovoltaic cells prepared by the solution process. The compounds were excessively decorated with moieties enhancing solubility to avoid spontaneous crystallisations in the blends. The topology of the dyes is of the acceptor-donor-acceptor (A-D-A) type. The quantum chemical calculations were done at the B3LYP/6-31G(d) level of theory and HOMO-LUMO levels were calculated. The solar cells' configuration was as follows: ITO/PEDOT:PSS/P3HT(P3OT)dyes/Al and parameters characterising them, open-circuit voltage (Voc), short-circuit current density (Jsc), fill factor (FF) and power conversion efficiency (PCE) are presented. Anthracene based A-D-A molecules showed photovoltaic activity with an average power conversion efficiencies (PCE) of 2.7%.

Keywords: anthracene, BPEA, solar cells, donor-acceptor systems, bulk-heterojunction cells

Streszczenie

Zsyntetyzowano grupę związków na osnowie 9,10-bis(fenyloetynylo)antracenu z peryferyjnymi grupami eletrono-akceptorowymi typu dicyjanowinylenu. Związki zmodyfikowano grupami funkcyjnymi zwiększającymi ich rozpuszczalność i utrudniającymi krystalizację. Przygotowano komórki fotowoltaiczne o strukturze objętościowej metodą wirową. Obliczenia kwantowo-chemiczne przeprowadzono przy funkcjonale B3LYP na poziomie 6-31G(d) i wyliczono energię poziomów elektronowych HOMO-LUMO. Opisane ogniwa scharakteryzowano podając następujące parametry: sprawność urządzenia (PCE), współczynnik wypełnienia (FF), napięcie rozwarcia (Voc) i prąd zwarcia (Jsc). Skonstruowane urządzenie o konfiguracji: ITO/PEDOT:PSS/P3HT(P3OT)barwnik/Al osiągnęło sprawność 2.7%.

Słowa kluczowe: antracen, BPEA, ogniwa słoneczne, układy donorowo-akceptorowe, komórki objętościowe

1. Introduction

The beauty of the anthracene 1 (Fig. 1) molecule has been attracting the attention of the scientific community since many years. Its intrinsic reactivity at positions 9- and 10- gives the possibility to create a lot of compounds possessing many unique properties. The crystal of anthracene placed between two electrodes by Pope *at al.* as a source of light [1, 2] triggered extensive research, which gave rise to a huge number of publications concerning this molecule [3–9]. The high quantum yield and simple modification of the anthracene skeleton makes it an attractive object for different applications in many fields. Because of the electron-rich properties and the large π-conjugation system, anthracene can be substituted at the aforementioned positions with many different functionalised blocks in order to give a variety of compounds with interesting properties. For example, 9,10-bis(phenylethynyl) anthracene (BPEA) **2**, which exhibits an exceptionally high fluorescent quantum yield and excellent chemiluminescent performance, has been synthesised [10–15].

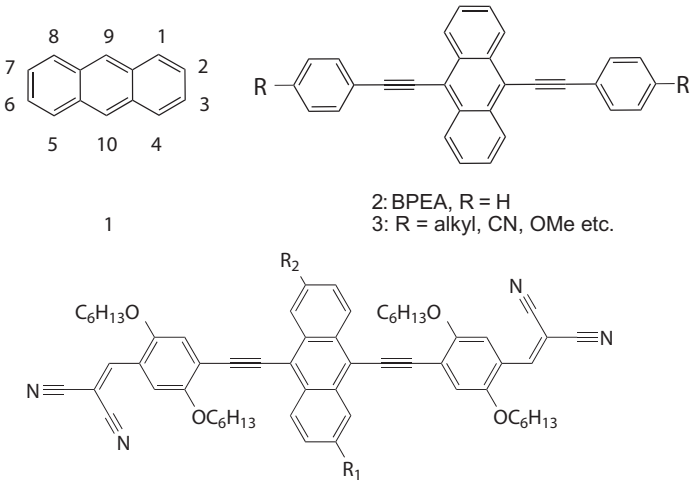

Fig. 1. Anthracene derivatives

Derivatives of BPEA **3** have been applied in the investigation of Langmuir Blodgett mono- and multilayer arrays [16–18], as well as good molecular probes, to study translational and rotational motions in diverse media, such as organic glasses and polymers [19–21]. Besides, they have been used for the synthesis of luminescent liquid crystals [22], sensors [23, 24], organic semiconductors [25, 26], useful fluorescent dyes for DNA labelling [27] and for the production of organic light-emitting diodes (OLEDs) [28, 29]. The combination of anthracene with strong acceptors to form an acceptor-donor-acceptor (A-D-A) system seems also to be an opportunity to enhance its optoelectronic properties and apply it in the dye-sensitised solar cells.

Up to now, the well-known A-D-A systems include different architectures of oligothiophenes, indolo[3,2-*b*]indoles, fluorenes and tetrathiafulvalenes end-capped with acceptors, as it was shown in a series of papers [30–33]. The potential of that type of molecules is connected with their ambipolar character, and due to the efficient transport of the charge carriers from the donor to the acceptor, which is reached by intramolecular charge transfer (ICT). Besides, acetylene-based materials were exploited extensively in organic photovoltaics (OPVs) [34], because of their electron-withdrawing character and a rigid, rod-like structure. Moreover, the availability of efficient synthetic protocols allows modifying the specific structural features: the π-conjugation length and the core functionalisation with proper chromophores. These can exert influence on the charge carrier mobility and photon/light harvesting, and leads to the improvement of short circuit current density and fill factor. Some time ago, we prepared strongly fluorescent BPEA dicyanovinyl (DCV) end-capped derivatives 4 as candidates for red light emitting devices, Fig. 1 [35]. However, substantial losses during the deposition process affected the good performance of the diodes. In the present study, we explore the compounds 4 as potential candidates for solar cells and the spin-coating is the method of choice to deposit them onto the ITO electrode, which helps to solve the stability problem of the chromophores. The preliminary study of photovoltaic performance revealed that anthracene-based A-D-A molecules exhibit photovoltaic activity with average power conversion efficiencies (PCE) of 2.7% (Table 2).

2. Experimental

2.1. Chemistry

The topology of the dyes in this study is as follows: the centre is an electron-rich anthracene core, decorated with two π-extended arms end-capped with electron accepting (EA) groups and four alkoxy groups to increase solubility. Their synthesis has been described in detail earlier [35, 36]; here is a short recollection of the synthetic path, Fig. 2:

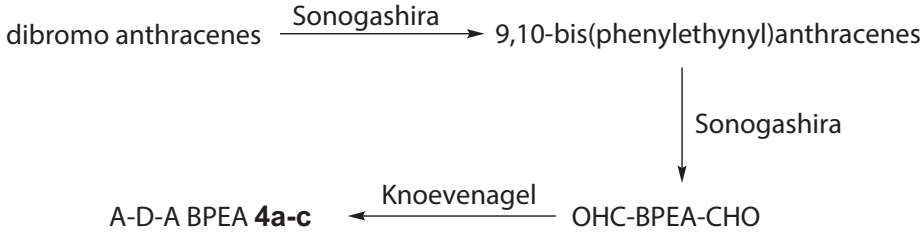

Fig. 2. Synthetic route to A-D-A BPEAs 4a-c

The A-D-A BPEA 4a-c were prepared in three consecutive steps from dibromoantracenes to deliver BPEA dialdehydes followed by Knoevenagel condensation of the latter with malodinitrile.

2.2. Calculation procedures

Density Functional Theory (DFT) calculations of the fused A–D–A system were performed using Gaussian 03 at the B3LYP/6-31G(d) level of theory [37]. Full geometry optimisation confirmed that the lowest energy conformers of 4a-c are totally flat.

Table 1. Frontier orbital levels of arylethynylanthracenes 4a-c

Molecule		Basis set	HOMO	LUMO	Bandgap, eV	Substituents
4a	F[a]	6-31G(2d,p)	–5.27	–3.21	2.06	$R_1 = R_2 = H$, Alk = C_6H_{13}
4a	F	6-31G(d)	–5.29	–3.23	2.06	
4a	S[b]	6-31G(d)	**–5.38**	**–3.33**	**2.05**	$R_1 = R_2 = H$, Alk=CH_3
4b	F	6-31G(d)	–5.31	–3.22	2.09	R_1 = *t*-Bu, R_2 =H, Alk = C_6H_{13}
4b	S	6-31G(d)	**–5.35**	**–3.30**	**2.05**	$R_1 = CH_3$, R_2 =H, Alk = CH_3
4c	S	6-31G(d)	**–5.31**	**–3.27**	**2.04**	$R_1 = R_2 = CH_3$, Alk = CH_3
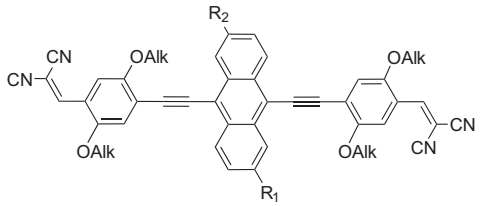						

[a] full structure, [b] simplified structure

The acetylene spacers are long enough to prevent a steric hindrance between alkoxy groups and the anthracene moiety that could disturb the planarity of the molecule. As hexyl and *t*-butyl groups do not influence the geometry of the backbone, they were replaced by methyl groups in order to simplify the calculations. In two cases (4a and 4b), hexyl and *t*-butyl moieties were included in optimised structures for comparison purposes. As it is possible to see from the data in Table 1, the structure simplification has been justified because

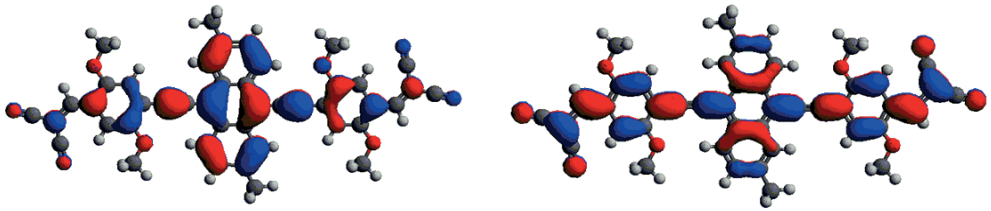

HOMO LUMO

Fig. 3. Plots of the HOMO and LUMO density of the states of 4c calculated at the B3LYP/6-31G (d) level

of meaningless differences in energy level values. For all the discussed compounds, HOMO is essentially located on the anthracene core. The LUMO density of states is mainly delocalised along the longest axis of the BPEA backbone and within the DCV acceptor framework, Fig. 3.

It is easy to notice a slight dependence of both the HOMO and LUMO levels on the substitution of anthracene core with methyl groups. These slightly electron-donating substituents raise the HOMO and LUMO energy ($-5.38 < -5.35 < -5.31$; $-3.33 < -3.30 < -3.27$). Alkoxy groups also contribute to this substantially. Similar trends have been observed for the series of 9,10-disubstituted anthracenes 3 reported in the paper of Linker *et al.* [38]. The calculated energies for HOMO and LUMO are −5.31 eV and −3.27 eV in 4c, respectively. The HOMO–LUMO gap in 4c was estimated to be 2.04 eV. The band-gap estimated from the long wavelength absorption edge gives a similar value of 2.02 eV.

2.3. Absorption and fluorescence

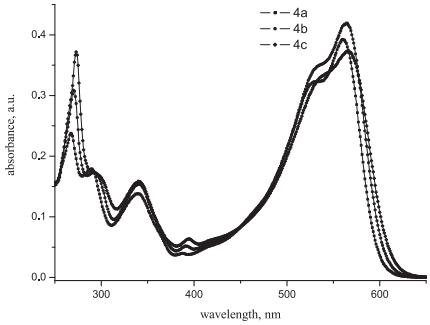

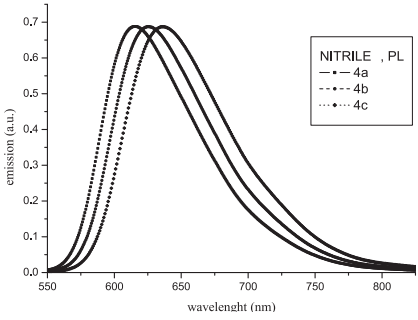

(a) $\lambda_{max\ abs}$ [nm] 4a: 556; 4b: 560; 4c: 564 (b) $\lambda_{max\ em}$ [nm] 4a: 616; 4b: 626; 4c: 636

Fig. 4. Absorption (a) and emission (b) spectra of 4a, 4b, 4c (λ_{ex}=405 nm)

The basic spectroscopic characterisation of BPEA dicyanovinyl (DCV) end-capped derivatives, i.e. their optical absorption and fluorescence spectra, can be derived from Fig. 4. The absorption spectrum exhibits two distinct bands in the CH_2Cl_2 solution, Fig. 4a. The absorption bands are similar to that of unsubstituted BPEA in the low energy region [15, 39]. The most prominent band associated with ICT transfer is centred around 560 nm. The band at the shorter wavelength region results from localised π–π^* transitions. The photoluminescence (PL) spectra of the compounds exhibiting featureless emission are also shown in Fig. 4b. They are slightly dependent on alkyl substitution and they are batochromically shifted from 616 to 636 nm, respectively.

2.4. Device preparation

The current–voltage (I–V) characteristics of the devices were measured using the Keithley 2400 sourcemeter. The devices were illuminated with a light intensity of 1.3 mW/cm^2. The thicknesses of layers were determined by spectroscopic ellipsometry. In the present work, the

Woollam Spectroscopic Ellipsometer (SE) with dedicated software has been used. The multilayer model was fitted to the following layer arrangements: glass / ITO / PEDOT: PSS / active layer /Al. This required the application of various models and sophisticated experimental procedures [40–43]. First of all, the parameters associated with the substrate, which is a glass coated with ITO, were set out using the Cauchy model. Then, the n and k parameters, as well as the thickness of the ITO (glass / ITO), were determined by means of the Drude model with the generic oscillator describing semiconducting properties. The latter-mentioned model was also employed to conduct separate measurements and to perform the calculations of n and k for: (a) poly-(styrenesulfonate) (PEDOT: PSS); (b) mixtures of poly(3-hexylthiophene-2,5-diyl (P3HT) and a synthesised compound; (c) 3-buthylthiophene (P3OT) and a synthesised compound. They were all prepared on a glass substrate. The designated values of n and k for the above listed compounds were subsequently used to determine the parameters of the thin layers of PEDOT: PSS on an ITO substrate (glass / ITO / PEDOT: PSS). Finally, the layer of P3HT and a synthesised compound, as well as the layer of P3OT and a synthesised compound, were applied on this substrate (glass / ITO / PEDOT: PSS). The tests finished with ellipsometric measurements and the thickness of the active layer was determined using dielectric functions of bulk heterojunction (BHJ) by applying the effective medium approximation model (for the results, see Table 2).

2.5. Preparation of photovoltaic cells

Photovoltaic cells were fabricated on ITO-covered glass slides (15 mm x 15 mm), which were cleaned in an ultrasonic bath using organic solvents. Next, ITO was covered with a PEDOT:PSS thin film (thickness about 100 nm) by spin-coating at 6000 rpm for 30 s and left for 30 min in a vacuum heater at 120 °C. After 30 min, the mixture of BPEA derivatives 4 and thiophenes (dissolved in chloroform) was spun over (at 2000 rpm for 30 s) the PEDOT:PSS thin film in order to obtain the active layer (about 100 nm). Next, the devices were left for 30 min in a vacuum heater at 60 °C. After that, the samples were introduced into a high vacuum chamber (10^{-6} mbar) in order to deposit Al contacts (100 nm) by thermal evaporation. The active surface of the samples was 12 mm^2.

3. Results and discussion

The BPEA compounds (4a, 4b, 4c) were measured as components of the active layer in bulk heterojunction (BHJ) photovoltaic (PV) cells. Two kinds of solar cells were prepared and characterised based on active layers consisting of blends of P3HT or P3OT and BPEA (weight ratio 2:1, 1:1 or 1:2), Fig. 5a, where P3HT and P3OT play the role of a donor.

Consequently, the energy levels of the acceptors were chosen in such a way that caused the division of an exciton. When comparing HOMO and LUMO levels of our compounds and thiophenes, it is not possible to foresee unequivocally which pair of the compounds will have good photovoltaic properties. One has to also take into account problems caused by the

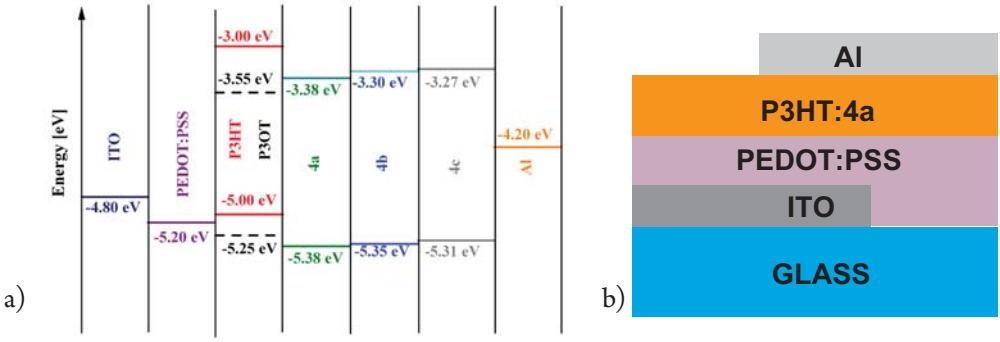

Fig. 5. a) Schematic diagram of HOMO/LUMO energy levels of donors: P3HT, P3OT and acceptors: 4a, 4b, 4c, b) a typical solar cell in this study

spatial arrangement of the chemical structures. The compounds mentioned were analysed in blends containing P3HT and P3OT.

The photovoltaic experiments were done for non-encapsulated devices. The fabricated BHJ PV cells consist of electrodes, Fig. 5b: aluminium acts as a cathode (collecting electrons) and ITO applied as the anode for the purpose of collecting holes, PEDOT:PSS used as a hole transporting material (HTM) and anode buffer layer and active layers. As donors in devices two poly(3-alkylthiophene)s were tested, that is, regioregular P3HT and P3OT. According to the estimated value of orbital energy levels (Table 1), it seems that both P3HT and P3OT could act as electron donors as compared to BPEA compounds (4a, 4b, 4c).

Table 2. Characteristics of devices in the configuration ITO/PEDOT:PSS/P3HT:4a/Al and ITO/PEDOT:PSS/P3OT:4a(4b,4c)/All under light illumination (1.3 mW/cm^2)

Active layer (weight ratio)	Thickness [nm]	U_{oc} [V]	J_{sc} [μA/cm^2]	FF	PCE [%]
4a:P3HT (1:1)	112	0.554	102	0.143	0.61
4a:P3HT (2:1)	98,4	0.651	76.7	0.060	0.417
4a:P3OT (1:2)	121	0.501	92.4	0.225	0.793
4a:P3OT (1:1)	106	0.406	112	0.190	0.659
4b:P3OT (1:2)	101	0.498	137	0.172	0.896
4b:P3OT (1:1)	119	0.680	58.1	0.105	0.315
4c:P3OT (1:2)	123	0.295	351	0.236	1.85
4c:P3OT (1:1)	99.1	0.321	415	0.274	2.77
4c:P3OT (2:1)	89.4	0.236	364	0.326	2.13

a)

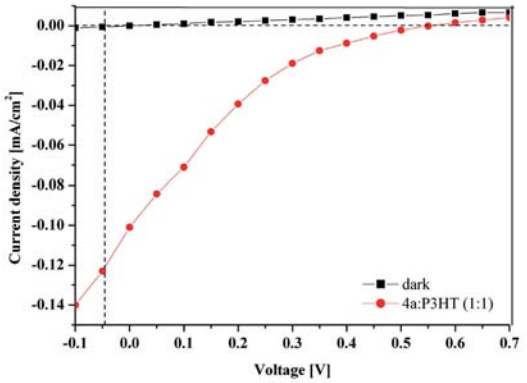

b)

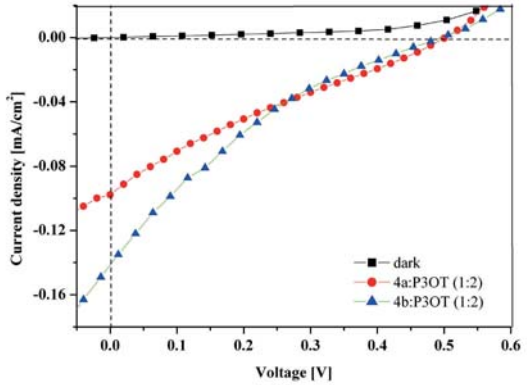

c)

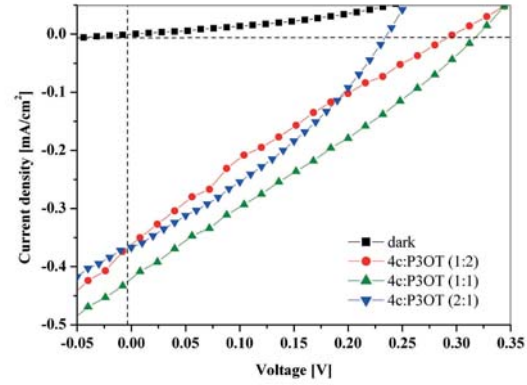

Fig. 6. Comparison of the dark and illuminated current density versus voltage characteristics for device a) ITO/PEDOT:PSS/P3HT:4a/Al, b)ITO:PEDOT:PSS/P3OT:4a(4b)/Al and c) ITO:PEDOT:PSS/P3OT:4c/Al

Table 2 shows that compound 4c is more compatible with P3OT in photovoltaic structures. Better results are shown by those that contain more polythiophene. This is connected with an easier conduction along the polymer chain. On the other hand, the blend of 4c with polythiophene (weight ratio 1:1) presents better photovoltaic parameters (Table 2) if combined with P3OT than with P3HT.

Considering the data presented in Table 2, one can conclude that the increase of compound 4a content in the active layer with P3HT from 1:1 to 2:1 results in a reduction in the value of the current density and the power conversion efficiency, but it causes a slight increase in the open circuit voltage.

Taking into account the effect of poly(3-alkylthiophene) on device performance, a higher value of both J_{sc} and open-circuit voltage was observed for P3OT given a higher value of PCE, except for 4b:P3OT (1:2). In the case of device with 4c, the higher J_{sc} and PCE showed the cell with P3OT. The best PCE of about 2.77 % was exhibited a device with 4c:P3OT (weight ratio 1:1). The value of PCE is significantly lower compared to BHJ PV cell based on P3HT and typical acceptor [6]-phenyl-C61 butyric acid methyl ester (PCBM) [44–47]. Comparing the results, it can be said that the higher PCE value was obtained for the device with the active layer consisting of 4c and P3OT in relation to cell containing 4a or 4b and P3OT. In the case of 4c, the PV parameters were strongly dependant on the weight ratios of components.

Figure 6 displays the representative dark and illuminated current density versus voltage (J–V) characteristic for a device based on 4a, 4b and 4c mixed with P3HT or P3OT. The photovoltaic parameters: open-circuit voltage (V_{oc}), current density (J_{sc}), fill factor (FF) and power conversion efficiency (PCE) are gathered in Table 2.

4. Conclusions

The study revealed pronounced effects of the chemical structure on the optical properties of the investigated compounds. They absorbed light in the range from 250 to 600 nm. The maximum absorption band is cantered around 570 nm and moves slightly batochromically because of anthracene core substitution. The emission maxima move from 610 to 640 nm, respectively. The energy band gap is about 2 eV for all structures: 4a, 4b and 4c. The presented structures, based on photovoltaic tests, can be treated as n-type semiconductors with HOMO level between -5.31, -5.35 and -5.38 eV. Three compounds were studied for their photovoltaic effect. They were analysed in blends containing P3HT and P3OT. Better results are exhibited by those that contain more polythiophene. The best efficiency (2.77%) is seen in photovoltaic cell based on the 4c blended with P3OT (1:1 weight ratio). This can either be explained in terms of a better uptake of charge carriers by 4c, or it could also well be the mutual spatial arrangement of the molecules to support this point of view. It is known that anthracene based-oligomers possess greater structural symmetry, which may enhance supramolecular organisation in BHJ blends [48]. The comparison of HOMO-LUMO energy levels (see Fig. 5) clearly shows which of the produced photovoltaic cells will demonstrate the greatest efficiency. The electron donors are, of course, P3HT and P3OT thiophene polymers.

P3OT energy levels with a 4c compound provide the easiest possibility of separating charges as well as their transportation and delivery to the electrodes without losses associated with placing them in one molecule. When analysing the photovoltaic properties of 4c: P3OT for the weight ratios of 2:1, 1:1 and 1:2, one can see that the easiest conduction of holes in the device occurs for the weight ratio of 1:1. It, in turn, gives the highest efficiency of converting light to electric energy. In summary, 9,10-bis(phenylethynyl)anthracene, BPEA, extensively modified with electron donating and accepting groups, seems to be quite suitable as a material for optoelectronic applications.

KD and OM would like to thank for the financial support from the basic funding of the University of Agriculture in Krakow DS-3711/ICh/17.

References

[1] Pope M., Kallmann H.P, Magnante P., *Electroluminescence in Organic Crystals*, J. Chem. Phys. 38, 1963, 2042–2046.

[2] Helfrich W., Schneider W.G., *Recombination Radiation in Anthracene Crystals*, Phys. Rev. Lett. 14, 1965, 229–231.

[3] Nasu K., Nakagawa T., Nomura H., Lin C.-J., Cheng C.-H., Tseng M.-R., Yasuda T., Adachi C., *A highly luminescent spiro-anthracenone-based organic light-emitting diode exhibiting thermally activated delayed fluorescence*, Chem. Commun. 49, 2013, 10385–10387.

[4] Wan W., Du H., Wang J., Le Y., Jiang H., Chen H., Zhu S., Hao J.A., *Novel blue luminescent materials for organic light-emitting diodes based on C9-fluorenyl anthracenes*, Dyes Pigm. 96, 2013, 642–652.

[5] Zhang P., Dou W., Ju Z., Yang L., Tang X., Liu W., Wu Y., *A 9,9′-bianthracene-cored molecule enjoying twisted intramolecular charge transfer to enhance radiative-excitons generation for highly efficient deep-blue OLEDs*, Org. Electron. 14, 2013, 915–925.

[6] Wang J.-J., Hu T.-L., Bu X.-H., *Cadmium(ii) and zinc(ii) metal-organic frameworks with anthracene-based dicarboxylic ligands: Solvothermal synthesis, crystal structures, and luminescent properties*, CrystEngComm. 13, 2011, 5152–5161.

[7] Zhu M., Wang Q., Gu Y., Cao X., Zhong C., Ma D., Qin J., Yang C., *Efficient deep-blue emitters comprised of an anthracene core and terminal bifunctional groups for nondoped electroluminescence*, J. Mater. Chem. 21, 2011, 6409–6415.

[8] Zhang J., Xu B., Chen J., Ma S., Dong Y., Wang I., Li B., Ye L., Tian *W., An organic luminescent molecule: What will happen when the "butterflies" come together?*, Adv. Mater. 26, 2014, 739–745.

[9] Ye S., Chen J., Di C.-A., Liu Y., Lu K., Wu W., Du C., Liu Y., Shuai Z., Yu G., *Phenyl-substituted fluorene-dimer cored anthracene derivatives: Highly fluorescent and stable materials for high performance organic blue- and white-light-emitting diodes*, J. Mater. Chem. 20, 2010, 3186–3194.

[10] Li B., Miao W., Cheng L., *Synthesis and fluorescence properties of 9,10-bis(phenylethynyl) anthracences*, Dyes Pigm. 43, 1999, 161–165.
[11] Kilså K., Macpherson A.N., Gillbro T., Mårtensson J., Albinsson B., *Control of electron transfer in supramolecular systems*, Spectrochim. Acta, Part A 57, 2001, 2213–2227.
[12] Kawai T., Sasakia T., Irie M., *A photoresponsive laser dye containing photochromic dithienylethene units*, Chem. Commun., 2001, 711–712.
[13] Kilså K., Kajanus J., Macpherson A.N., Mårtensson J., Albinsson B., *Bridge-Dependent Electron Transfer in Porphyrin-Based Donor-Bridge-Acceptor Systems*, J. Am. Chem. Soc. 123, 2001, 3069–3080.
[14] Ribierre J.C., Ruseckas A., Cavaye H., Barcena H.S., Burn P.L., Samuel I.D.W., *Photophysical Properties of 9,10-Disubstituted Anthracene Derivatives in Solution and Films*, J. Phys. Chem. A 115, 2011, 7401–7405.
[15] Levitus M., Garcia-Garibay M.A., *Polarized Electronic Spectroscopy and Photophysical Properties of 9,10-Bis(phenylethynyl)anthracene*, J. Phys. Chem. A 104, 2000, 8632–8637.
[16] Angelova A., Ionov R., *Monolayer and Spectroscopic Studies of an Amphiphilic (Phenylethynyl)anthracene Probe in Pure and Mixed Films with Charged and Neutral Lipids*, Langmuir 15, 1999, 7199–7207.
[17] Angelov B., Angelova A., Ionov R., *An Amino-Substituted Phenylethynyl-anthracene Probe Shows a Sensitivity to Changes in the Lipid Monolayer Curvature of Nonlamellar Lipid/Water Phases*, J. Phys. Chem. B 104, 2000, 9140–9148.
[18] Lübtow M., Helmers I., Stepanenko V., Albuquerque R.Q., Marder T.B., Fernández G., *Self-Assembly of 9,10-Bis(phenylethynyl) Anthracene (BPEA) Derivatives: Influence of p–p and Hydrogen-Bonding Interactions on Aggregate Morphology and Self-Assembly Mechanism*, Chem. Eur. J. 23, 2017, 6198–6205.
[19] Wang C.-Y., Ediger M.D., *Enhanced Translational Diffusion of 9,10-Bis(phenylethynyl) anthracene (BPEA) in Polystyrene*, Macromolecules 30, 1997, 4770–4771.
[20] Deppe D.D., Dhinojwala A., Torkelson J.M., *Small Molecule Probe Diffusion in Thin Polymer Films Near the Glass Transition: A Novel Approach Using Fluorescence Nonradiative Energy Transfer*, Macromolecules 29, 1996, 3898–3908.
[21] Wisnudel M.B., Torkelson J.M., *Small-Molecule Probe Diffusion in Polymer Solutions: Studies by Taylor Dispersion and Phosphorescence Quenching*, Macromolecules 29, 1996, 6193–6207.
[22] Giménez R., Pinol M., Serrano J. L., *Luminescent Liquid Crystals Derived from 9,10-Bis(Phenylethynyl)anthracene*, Chem. Mater. 16, 2004, 1377–1383.
[23] Xiao D., Xian Y., Liu L., Gu Z., Wen B., *Organic nanoparticle of 9,10-Bis(phenylethynyl) anthracene: a novel electrochemiluminescence emitter for sensory detection of amines*, New J. Chem. 37, 2013, 1–3.
[24] Ponnu A., Anslyn E.V., *A fluorescence-based cyclodextrin sensor to detect nitroaromatic explosives*, Supramol. Chem. 22, 2010, 65–71.
[25] Kim S.-O., Lee M.W., Jang S.H., Park S.M., Park J. W., Park M.-H., Kang S.H., Kim Y.-H., Song C.K., Kwon S.K., *Organic semiconductor based on phenylethynyl end-capped anthracene*, Thin Solid Films 519, 2011, 7998–8002.

[26] Li Y., Ji D., Liu J., Yao Y., Fu X., Zhu W., Xu Ch., Dong H., Li J., Hu W., *Quick Fabrication of Large-area Organic Semiconductor Single Crystal Arrays with a Rapid Annealing Self-Solution-Shearing Method*, Sci. Rep. 5, 2015, 13195,1–9.
[27] Malakhov A.D., Skorobogatyi M.V., Prokhorenko I.A., Gontarev S.V., Kozhich D.T., Stetsenko A.D., Stepanova I.A., Shenkarev Z.O., Berlin Y.A., Korshun V.A., *1-(Phenylethynyl) pyrene and 9,10-Bis(phenylethynyl)anthracene, Useful Fluorescent Dyes for DNA Labeling: Excimer Formation and Energy Transfer*, Eur. J. Org. Chem., 2004, 1298–1307.
[28] Fatemi D.J., Murata H., Merritt C.D., Kafafi Z.H., *Highly Fluorescent Molecular Organic Composites for Light-Emitting Diodes*, Synth. Met. 85, 1997, 1225–1228.
[29] Huang J., Su J.-H., Tian H., *The development of anthracene derivatives for organic light-emitting diodes*, J. Mater. Chem. 22, 2012, 10977–10989.
[30] Fitzner R., Mena-Osteritz E., Walzer K., Pfeiffer M., Bäuerle P., *A–D–A-Type Oligothiophenes for Small Molecule Organic Solar Cells: Extending the π-System by Introduction of Ring-Locked Double Bonds*, Adv. Funct. Mater. 25, 2015, 1845–1856.
[31] Lai Y.-Y., Yeh J.-M., Tsai C.-E., Cheng Y.-J., *Synthesis, Molecular and Photovoltaic Properties of an Indolo[3,2-b]indole- Based Acceptor–Donor–Acceptor Small Molecule*, Eur. J. Org. Chem., 2013, 5076–5084.
[32] Sahu D., Padhy H., Patra D., Yin J.-F., Hsu Y.-C., Lin J. T., Lu K.-L., Wei K.-H., Lin H.-C., *Synthesis and applications of novel acceptoredonoreacceptor organic dyes with dithienopyrrole- and fluorene-cores for dye-sensitized solar cells*, Tetrahedron 67, 2011, 303–311.
[33] Kuropatov V., Klementieva S., Fukin G., Mitin A., Ketkov S., Budnikova Y., Cherkasov V., Abakumov G., *Novel method for the synthesis of functionalized tetrathiafulvalenes, an acceptoredonoreacceptor molecule comprising of two o-quinone moieties linked by a TTF bridge*, Tetrahedron 66, 2010, 7605–7611.
[34] Silvestri F., Marrocchi A., *Acetylene-Based Materials in Organic Photovoltaics*, Int. J. Mol. Sci. 11, 2010, 1471–1508.
[35] Danel K., Lin J.T., *Novel red-light-emitting 9,10-bis(phenylethynyl)anthracenes*, Arkivoc (i), 2002, 12–18.
[36] Danel K., Ozga K., Kityk I.V., *Circularly light-induced electrogyration in the arylethynyl derivatives incorporated within the oligoetheracrylate photopolymer matrices*, Chem. Phys. 313, 2005, 33–38.
[37] Frisch M.J., Trucks G.W., Schlegel H.B. et al., *Gaussian 03: Revision E.01*, Gaussian Inc., Wallingford CT 2004.
[38] Fudickar W., Linker T., *Why Triple Bonds Protect Acenes from Oxidation and Decomposition*, J. Am. Chem. Soc. 134, 2012, 15071–15082.
[39] Yucel B., Meral K., Ekinci D., Uzunoğlu G.Y., Tüzün N.S., Özbey S., Kazak C., Ozdemir Y., Sanli B., Kayık G., Dağdeviren M., *Synthesis and characterization of solution processable 6,11-dialkynyl substituted indeno[1,2-b]anthracenes*, Dyes Pigm. 100, 2014, 104–117.
[40] Pettersson L.A.A., Ghosh S., Inganas O., *Optical anisotropy in thin films of poly (3,4-ethylenedioxythiophene)–poly(4-styrenesulfonate)*, Org. Electron. 3, 2002, 143–148.
[41] Fujiwara H., *Spectroscopic Ellipsometry: Principles and Applications*, John Wiley&Sons, Ltd . 2007.

[42] Feller L., Bearinger J.P., Wu L., Hubbell J. A., Textor M., Tosatti S., *Micropatterning of gold substrates based on poly(propylene sulfide-bl-ethylene glycol), (PPS–PEG) background passivation and the molecular-assembly patterning by lift-off (MAPL) technique*, Surf. Sci. 602, 2008, 2305–2310.
[43] Woollam J. A., *Co. Inc.CopleteEASE™ Data Analysis Manual*, Lincon 2009.
[44] Bujak P., Kulszewicz-Bajer I., Zagorska M., Maurel V., Wielgus I., Pron A., *Polymers for Electronics and Spintronics*, Chem. Soc. Rev. 42, 2013, 8895–8999.
[45] Bijak K., Sek D., Siwy M., Grucela-Zajac M., Janeczek H., Wiacek M., Malecki G., Schab-Balcerzak E., *Spectral, electrochemical and thermal characteristics of glass forming hydrazine derivatives*, Opt. Mater. 37, 2014, 498–510.
[46] Kung Y.-C., Hsiao S.-H., *Novel luminescent and electrochromic polyhydrazides and polyoxadiazoles bearing pyrenylamine moieties*, Polym. Chem. 2, 2011, 1720–1727.
[47] Grigoras M., Vacareanu L., Ivan T., Catargiu A.M., *Photophysical properties of isoelectronic oligomers with vinylene, imine, azine and ethynylene spacers bearing triphenylamine and carbazole end-groups*, Dyes Pigm. 98, 2013, 71–81.
[48] Mishra A., Bäuerle P., *Small Molecule Organic Semiconductors on the Move: Promises for Future Solar Energy Technology*, Angew. Chem. Int. Ed. 51, 2012, 2020–2067.

TECHNICAL TRANSACTIONS 1/2018
CIVIL ENGINEERING
DOI: 10.4467/2353737XCT.18.005.7956
SUBMISSION OF THE FINAL VERSION: 29/12/2017

Małgorzata Janus-Michalska (mjanus-michalska@pk.edu.pl)
Institute of Structural Mechanics, Faculty of Civil Engineering, Cracow University of Technology

Hyperelastic behaviour of auxetic material in tension and compression tests

Hypersprężystość materiałów auksetycznych na przykładzie testu jednoosiowego rozciągania i ściskania

Abstract

This paper presents the numerical simulation of uniaxial tension and compression tests for negative Poisson's ratio materials subjected to large strains. Numerical calculations are performed for the determination of the material characteristics of auxetic periodic lattices. The finite element method (FEM) coupled with 2D periodic homogenisation technique is used. The results show the existence of large variations in strain-stress plots, which can be achieved by changing the lattice geometry parameters.

Keywords: auxetic microstructure, hyperelasticity, material characteristics

Streszczenie

W artykule przedstawiono numeryczne symulacje testów jednoosiowego rozciągania i ściskania dla materiałów o ujemnym współczynniku Poissona w zakresie dużych odkształceń. Celem wyznaczenia charakterystyk materiałowych wykonano obliczenia numeryczne dla materiałów auksetycznych o strukturze periodycznej. Zastosowano metodę elementów skończonych połączoną z teorią homogenizacji. Wyniki wskazują na dużą różnorodność otrzymanych ścieżek naprężenie-odkształcenie uzyskanych przez zmianę parametrów geometrycznych struktury materiału.

Słowa kluczowe: mikrostruktura auksetyczna, hypersprężystość, charakterystyka materiałowa

1. Introduction

Materials with cellular microstructure are used in a variety of structural applications due to the enhancements they offer with regard to many mechanical properties. Contrary to ordinary materials, in which work is restricted to a linear elastic regime, cellulars reveal nonlinear elastic behaviour and deformability in the range of large strains. Among cellular microstructures are special lattices which produce negative Poisson's ratio materials, these are called auxetics. Such materials reveal counterintuitive behaviour. These materials are of particular interest due to their improved properties such as fracture toughness, shear resistance, indentation resistance, elastic energy absorption and energy damping. Auxetics possess a wide range of applications in innovative smart structures and composite materials. They are used in the aerospace and automotive industries.

The development of the concept of auxeticity dates from the first publication by Lakes in 1987 and the fabrication of micromorphous polethylene with a negative Poissons ratio. In 1988, Gibson realised the auxetic effect for silicone rubber and aluminium honeycombs. In 2004, Yang formulated the basis for molecular design within the field of nanotechnology. Great contribution to the development of auxetic materials was made by Alderson [1], who manufactured, tested and found potential applications of cellular solids, polymers and composites. A recent extensive review on the properties of auxetic materials compared with positive ratio materials was provided in an article published in 2011 in Nature Materials [8] by Greaves, Greer, Lakes & Rouxel.

For cellular materials, a variety of microstructures were developed to achieve auxetic behaviour. A re-entrant honeycomb structure was first used by Gibson and Kolpakov. The auxetic effect in foam and re-entrant honeycombs lies in the unfolding of re-entrant cells when they are stretched. Symmetries represented by non-chiral structures were proposed by Lakes, Theocaris, Smith and Gaspar. Chiral microstructures were proposed by Prall, Lakes and Grima. In chiral structures, the auxetic effect is achieved through the unwrapping of the ligaments around the circular nodes.

Cellulars reveal strongly nonlinear behaviour within the elastic range. A micromechanics framework for the development of continuum-level constitutive models for the large-strain deformation of porous isotropic hyper-elastic materials is given by Danielsson, Parks & Boyce [3], and Horgan [10] for non-compressible materials. Murphy formulated a strain energy function for nonlinear compressible isotropic materials. An alternative approach was introduced by Ogden [9] who modelled compressible materials by using strain energy functions based on polynomial functions of the principal stretches. Anisotropic hyper-elastic materials form a narrow group among constitutive models which describe elastic behaviour. An energetic approach to the analysis of anisotropic hyper-elastic materials is proposed by Vegori et al., [18]. According to work by Dłużewski [6], the explicit form of a constitutive equation for anisotropic nonlinear materials for Cauchy stress has not yet been formulated. When the material undergoes finite deformation, the material properties are strongly dependent on the deformation and the effective material properties have to be calculated for

each deformation state (Vegori, [18]). Therefore, it is possible for instantaneous stiffness in uniaxial strain test.

The mechanical properties of cellular solids are controlled by both constituent materials and cell topologies. The cell topologies can function as either load-bearing structures or flexible structures. If a cellular solid is used for a structural purpose, it should be stiff, otherwise, it should be compliant. The design of stiffness is possible through the selection of material and cell topologies.

To obtain effective properties of cellular material, classical homogenisation theory can be used (Nemat & Naser, [16]). The hyper-elastic behaviour of cellular structures at small strain was described by Janus-Michalska [11]. The concept of obtaining effective material properties using a numerical homogenisation procedure under finite deformation is given by Nakshatrala et al. (2013).

In the present paper, effective material characteristics, tangent Young moduli functions and Poisson's ratio functions are calculated for a set of cellular microstructures in tension-compression tests. The influence of geometric microstructural parameters on effective material properties is tested.

2. Micromechanical modelling of auxetic material

Microstructured auxetic material is modelled using a beam structure with the 2D re-entrant lattice shown in Fig. 2a. The properties of an equivalent continuum can be obtained through homogenisation. The classical theory of continuum is sufficient for this microstructured body. The following procedure given by Nemat-Naser's [16] with representative unit cell of the geometric parameters shown in Fig. 1b is studied.

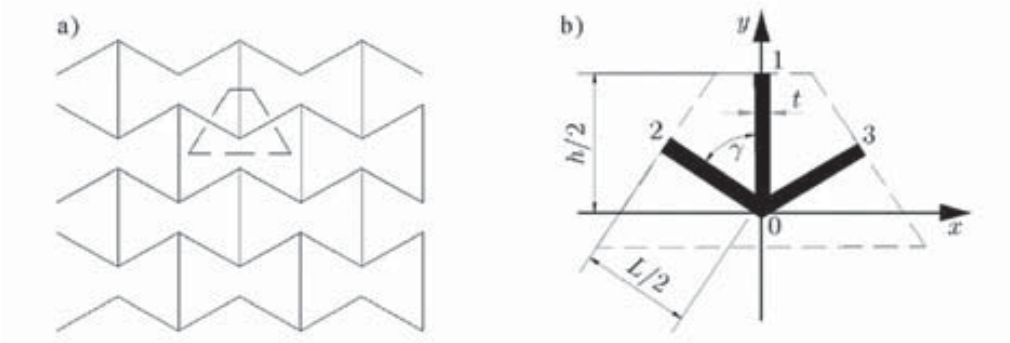

Fig. 1. a) Auxetic structure; b) representative unit cell

Analytical homogenisation was used for cellular materials with typical symmetries by Janus-Michalska [12, 13]. For auxetic structures, numerical homogenisation was used to obtain the material constants for small strain regime [11].

The deformation of the cell model can then be solved numerically as a boundary value problem and the macroscopic stress-strain response can be extracted. Details on the cell model, boundary conditions and the calculation of the macroscopic properties and framework are described in works [11–13].

3. Strain dependent Poisson's function

The Poisson's ratio is defined for infinitesimal strain. The measure was first introduced by Simeon Dennis Poisson (1787–1840). The definition is as follows: $\nu_{12} = {}^{-\varepsilon_2}\!/_{\varepsilon_1}$

where: 1 – denotes the direction of stretching, 2 – denotes the perpendicular direction.

For highly nonlinear elastic materials, the definition is extended to a strain dependent Poisson's function. This is analogous to the definition of a tangent Young modulus. For auxetic materials, Poisson's ratio is usually highly strain dependent, moreover, the Poison's ratio can be negative only over the certain strain range.

4. Parametric study

Materials of several geometric configurations are considered. The geometric parameters are collected in Table 1, the structures are shown in Fig. 2.

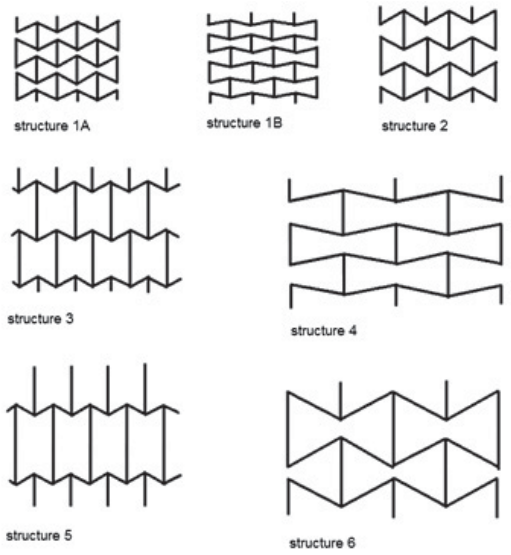

Fig. 2. Geometrical configurations of auxetic structures

Table 1. Microstructural geometric parameters

Structure	L [mm]	H [mm]	γ [°]	t [mm]
1A	1.50	1.65	60	0.15
1B	1.50	1.50	80	0.15
2	1.50	2.00	60	0.15
3	1.50	3.00	80	0.15
4	3.00	1.40	80	0.15
5	1.50	3.00	60	0.15
6	3.00	4.00	60	0.15

Material skeleton with the following material data: E_s=10*GPa*, v_s=0,3,${}^{S}R_m$=10*MPa* is adopted, where: E_s, v_s -elastic constants, ${}^{S}R_m$ - rupture modulus.

Computations were carried out in the ABAQUS system with the use of Timoshenko beam elements.

5. Results

Tension-compression tests were carried out for each microstructured material in the X and Y directions. Material characteristics are given in Fig. 3 and Fig. 4. Stress-strain plots ends for rupture of skeleton material for tension and contact of skeleton beams for compression.

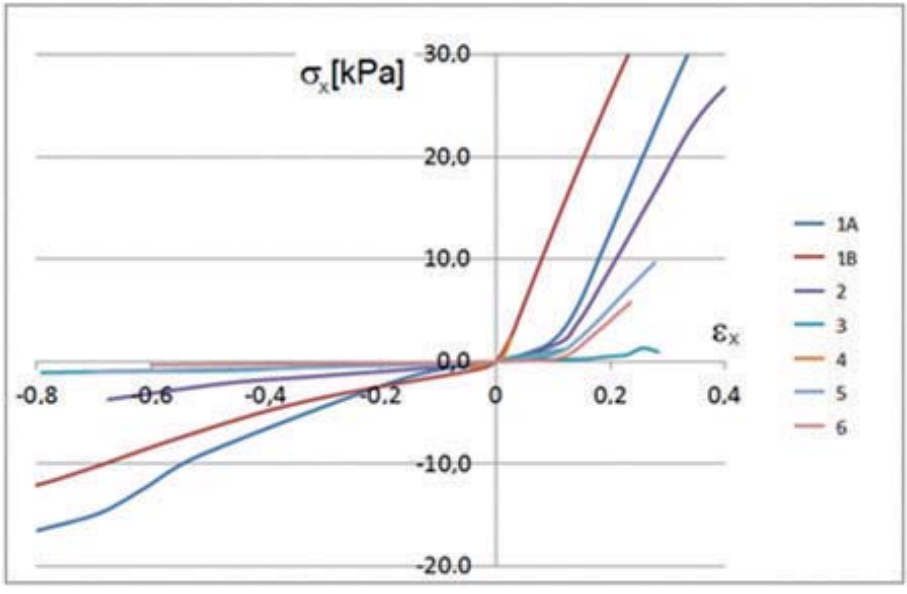

Fig. 3. Material characteristics for tension-compression in the X direction

It can be observed that in the test in the X direction, the stiffness decreases under compression and increases under extension. This results from microstructural deformation effects. The increasing of equivalent material stiffness is related to the extension of beams in the microstructure, which is governed by tensional stiffness. The decreasing of the equivalent material stiffness is related to the deflection of the beams in the microstructure – this is governed by flexural stiffness. The relationship between stiffness and the H, L and γ parameters is clearly visible. For increasing parameters, the tensional stiffness decreases, whereas the compression stiffness increases.

In the test in the X direction, the stiffness increases under compression and decreases under extension. The relation between of stiffness and he H, L and γ is not clearly visible.

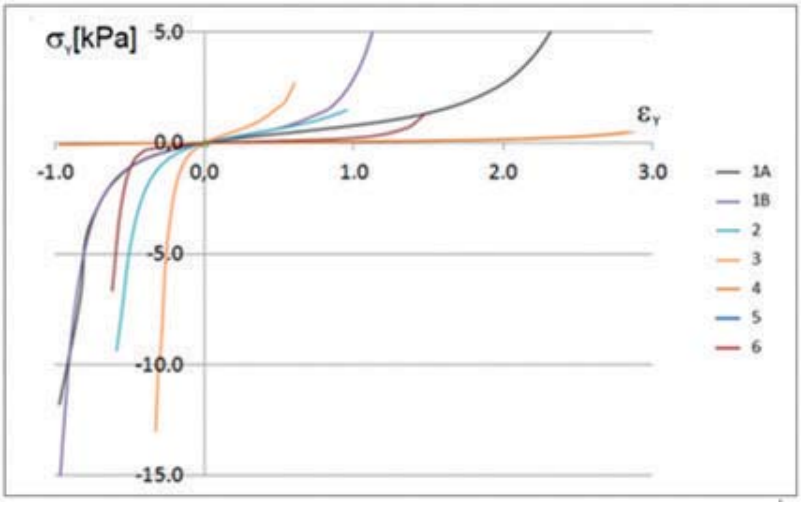

Fig. 4. Material characteristics for tension-compression in the Y direction

A variety of equivalent material properties calculated for infinitesimal strain state can be obtained due to changes of geometrical parameters and skeleton material constants. For the chosen structures the equivalent Young moduli and Poisson's ratios are collected in Table 2.

Table 2. Equivalent material constants

Structure	E_X [kPa]	E_Y [kPa]	ν_{XY}	ν_{YX}
1A	13.53	3.62	-15.21	-0.481
1B	46.18	1.29	-5.058	-0.142
2	6.27	1.941	-1.718	-0.532
3	20.90	2.808	-2.289	-0.307
4	20.07	0.058	-17.708	-0.053
5	3.67	3.407	-0.9823	-0.912
6	0.783	0.2402	-1.786	-0.547

For large strains, plots of the functions of tangent elastic moduli are presented in Figs 5 and 6.

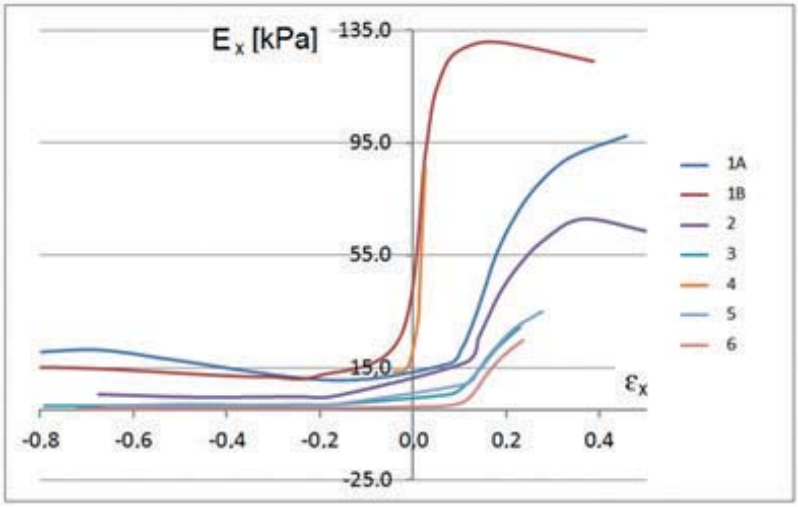

Fig. 5. Plots of elastic modulus E_X for microstructured equivalent continua

The relation between the elastic modulus E_X and the parameters H, L and γ is clear. For increasing parameters, the tangent elastic modulus E_X decreases. The relation between the elastic modulus E_Y and the parameters H, L and γ is not visible.

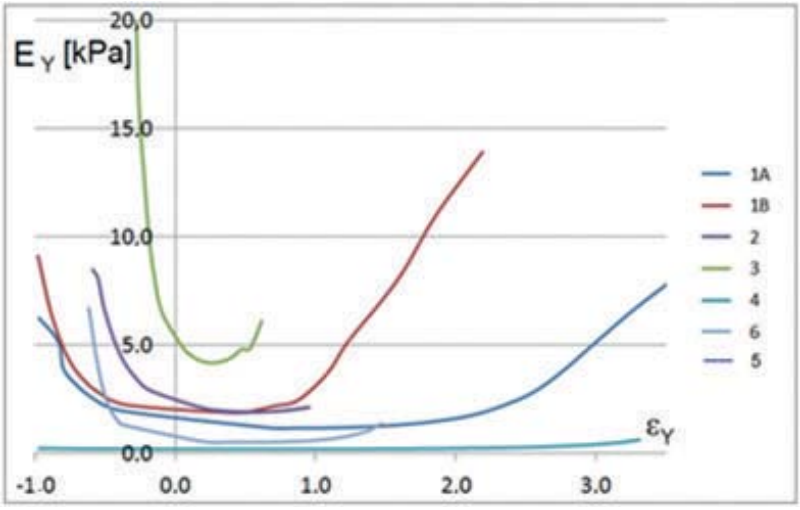

Fig. 6. Plots of elastic modulus E_Y for microstructured equivalent continua

Plots of the functions of Poisson's ratio are presented in Figs 7 a & b and Fig. 8.

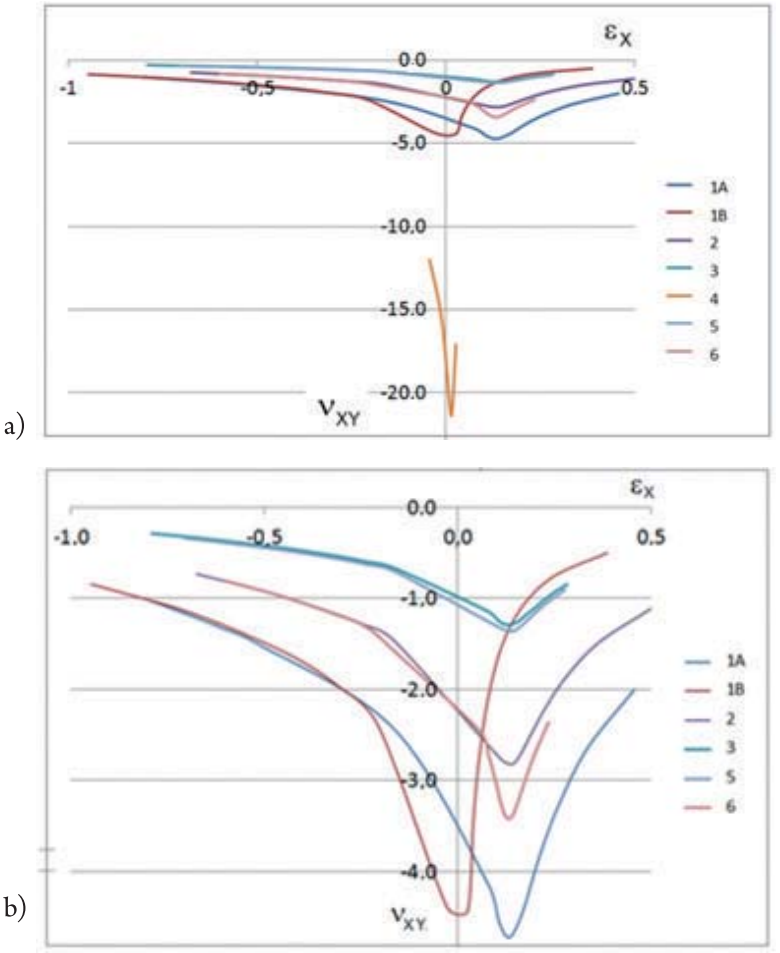

Fig. 7. Plots of function of elastic Poisson's ratio for the tension-compression tests in the *X* direction

The plot for Structure 4 in Fig. 7a gives exceptionally high values of the Poisson's ratio function with relation to other structures. Other plots are presented in Fig. 7b to precisely show their changeability. It is worth noting that for tension-compression tests in the *X* direction in the whole range of strains, the Poisson's ratio functions remain negative.

For tension-compression tests in the *Y* direction, the plot for Structure 3 in Fig. 7a gives exceptionally high and positive values of Poisson's ratio function. Other plots are presented in Fig. 8b to precisely show their changeability. It is worth noting that Poisson's ratio functions can have negative or positive values.

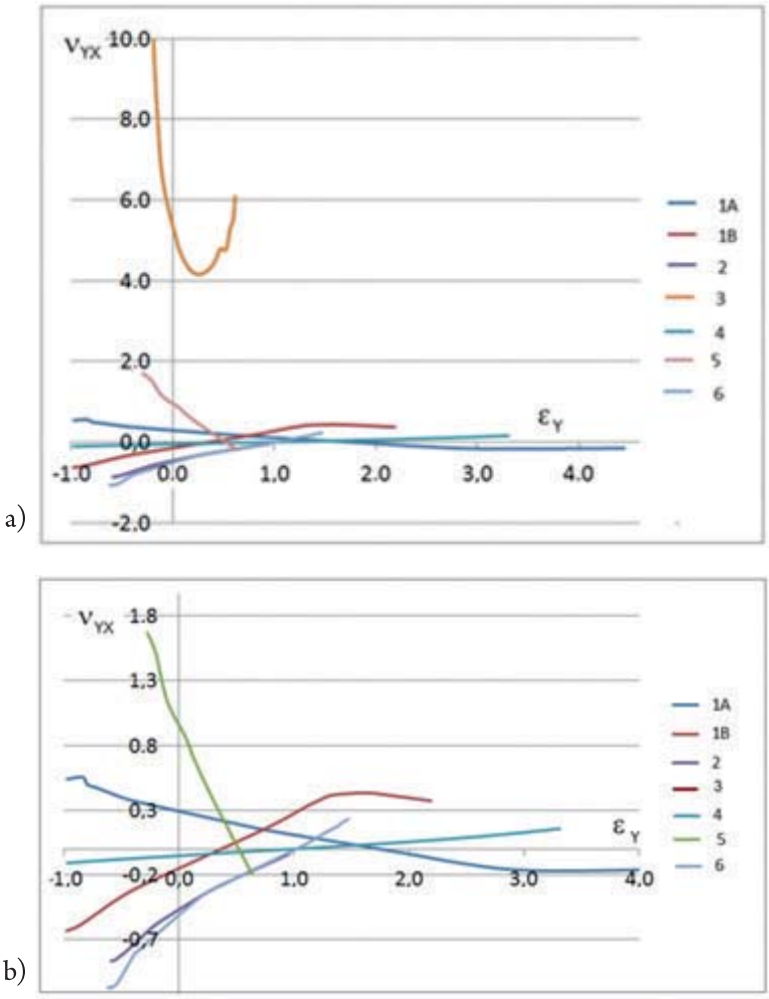

Fig. 8. Plots of function of elastic Poisson's ratio for the tension-compression test in the *X* direction

6. Conclusions

The tested class of microstructered cellulars shows that the behaviour of materials with the auxetic beam microstructure is significantly nonlinear. The paths of material characteristics are dependent on the tension-compression direction and on the material and geometric microstructural parameters. An attempt to assess the type of dependence is made.

Poisson's ratio and tangent stiffness Young moduli functions are introduced to visualise the effect of the influence of large strain deformation; it shows the ability of modelling microstructures to achieve the required properties.

References

[1] Alderson A., Alderson K.L., *Auxetic materials*, Proceedings of the Institution of Mechanical Engineers, Part G, Journal of Aerospace Engineering – Special Issue Paper, 2007, 565–575.

[2] Alderson K.L., Alderson A., Evans K.E., *The Interpretation of the Strain–dependent Poisson's Ratio in Auxetic Polyethylene*, J. Strain Anal., 1998, 32, 201– 212.

[3] Danielsson M., Parks D., Boyce M.C., *Constitutive modelling of porous hyperelastic materials*, Mechanics of Materials, 2004, 36, 347–358.

[4] Darijani H., Naghdabadi R., *Hyperelastic materials behavior modeling using consistent strain energy density functions*, Acta Mechanica, 2010, 213, 235–254.

[5] Dirrenberger J., Forest S., Jeulin D., Colin C., *Homogenization of periodic auxetic materials*, Procedia Engineering 10, 2011, 1847–1852.

[6] Dłużewski P., *Anisotropic Hyperelasticity Based Upon General Strain Measures*, Journal of Elasticity, 60, 2000, 119–129.

[7] Federico S., Grillo A., Imatani S., Giaquinta G., Herzog W., *An energetic approach to the analysis of anisotropic hyperelastic materials*, International Journal of Engineering Science, 46, 2008, 164–181.

[8] Greaves G.N., Greer A.L., Lakes R.S., Rouxel T., *Poisson's ratio and modern materials*, Modern Materials, Published online, review article, 24 October 2011, DOI: 10.1038 NMAT 3134.

[9] Holzeapfel G.A., *Nonlinear Solid Mechanics, A Continuum Approach for Engineering*, Technical University, Graz, Austria 2000.

[10] Horgan C., *The remarkable Gent constitutive model for hyperelastic materials*, International Journal of Non–Linear Mechanics, 68, 2015, 9–16.

[11] Janus-Michalska M., *Hyperelastic behavior of cellular structures based on micromechanical modeling at small strain*, Archives of Mechanics, Issue 1, Vol. 63, Warszawa 2011, 3–24.

[12] Janus-Michalska M., *Micromechanical Model of Auxetic Cellular Materials*, Issue 4, Vol. 47, Journal of Theoretical and Applied Mechanics, 2009, 5–22.

[13] Janus-Michalska M., *Effective Model Describing Elastic Behaviour of Cellular Materials*, Archives of Metallurgy and Materials, Vol. 50/3, 2005, 595–608.

[14] Kumar R.S., McDowell D.L., *Generalized Continuum Modelling of 2–D periodic Cellular Solids*, Int. Journal of Solids and Structures, 41, 7299–7422.

[15] Murphy G.J., *Strain Energy Functions for a Poisson Power Law Function in Simple Tension of Compressible Hyperelastic Materials*, Journal of Elasticity, 60, 2000, 151–164.

[16] Nemat-Maser S., Hori M., *Micromechanics*, 2nd Edition, Elsevier, 1999.

[17] Smith C.W., Wootton R.J., Evans K.E., *Interpretation of experimental data for Poisson's ratio of highly nonlinear materials energy density functions*, Acta Mechanica, 213, 2010, 235–254.

[18] Vegori L., Destrade M., McGarry P., Ogden R., *On anisotropic elasticity and questions concerning its Finite Element implementation*, Computational Mechanics, 52, 2013, 1185–1197.

[19] Wang F., Sigmund O., Jensen J.S., *Design of materials with prescribed nonlinear properties*, Journal of mechanics and Physics of Solids, 69, 2014, 156–174.

TECHNICAL TRANSACTIONS 1/2018
CIVIL ENGINEERING
DOI: 10.4467/2353737XCT.18.006.7957
SUBMISSION OF THE FINAL VERSION: 28/12/2017

Dariusz Starkowski (dariusz.starkowski@wsl.com.pl)
Chair of Logistics Bases, Poznan School of Logistics

Load restraint with allsafe products. Part 1: choosing a semi-trailer – a systematic analysis

Wykorzystanie metod zabezpieczenia ładunków przedsiębiorstwa allsafe. Część 1: analiza systemowa doboru naczepy ciężarowej

Abstract

The appropriate selection of a semi-trailer in food transport is one of the most significant factors related to management in transport companies. Two parts of the paper present research and analytical issues concerning this subject matter (second part available in: TT 2/2018). The description of this logistics problem is initiated with the proper planning of the road transport process, from consignor to recipient. Furthermore, the choice of a modern vehicle and loading system is based on the transportation of fresh strawberries. The first part of the article discusses current legal provisions existing in the European Union and Poland that concern the transport of perishable products. Moreover, the paper presents community law that concerns load restraint, and the choice of a vehicle, which is done by means of weighted-average methodology.

Keywords: road transport, provisions of law, transport centre, legislative directive, transport operation, load-carrying semi-trailer

Streszczenie

Problem optymalnego doboru odpowiedniej naczepy ciężarowej do przewozu towaru żywnościowego jest jednym z najważniejszych elementów prawidłowego zarządzania przedsiębiorstwem transportowych. Problematykę badawczą i analityczną przedstawiono w dwóch częściach referatu (część druga dostępna w numerze TT 2/2018). Przedstawiono ten ważny problem logistyczny, zaczynając od prawidłowego zaplanowania procesu transportowego rozpoczynającego się u nadawcy, a kończącego u odbiorcy pod kątem i na przykładzie wyboru nowoczesnego pojazdu drogowego i systemu ładunkowego na przykładzie przewozu truskawki świeżej. W części pierwszej szczegółowo przedstawiono obecną sytuację przepisów prawnych obowiązujących w Unii Europejskiej oraz w Polsce związanej z transportem artykułów łatwopsujących. Szeroko zaprezentowano wspólnotowe przepisy prawne dotyczące prawidłowego zabezpieczenia ładunku oraz dokonano wyboru pojazdu drogowego metodą wagową (ważoną) do transportu wybranego ładunku.

Słowa kluczowe: transport drogowy, przepisy prawne, środek transportowy, dyrektywa, operacja transportowa, naczepa ciężarowa

1. Introduction

The provision of transport services has recently undergone dynamic growth that accompanies an enormous increase in the exchange of goods on national and international level. Transport constitutes a primary activity, carried out in the context of a range of logistic services. As for food transport, it is exceptionally difficult both for the carrier and the organizer of the transport operation. Many factors can work to the detriment of the load, such as changing conditions during transport, wrong choice of vehicles or faults in their construction, and lastly, improper packaging and securing of the load. The loss of food caused by inadequate transport conditions reaches 30% – this entails financial losses. The first part of the article describes present legal provisions of the European Union and Poland in detail. When it comes to the planning of transport operations, a number of measures connected with the load need to be integrated and logistically synchronized. Firstly, an appropriate vehicle needs to be selected at the planning stage, with consideration to rules and methods of appropriate selection. Planning and putting those plans into action determine safe load delivery that should be carried out in accordance with individual terms of contract.

2. Material and scientific research method

This article addresses a part of the problem of road vehicle selection – this is dependent upon: the type of load; conditions required by the consignor, in accordance with ATP treaty that establishes standards for international transport of perishable goods; the agreement on the international carriage of perishable foodstuffs; the special equipment to be used for a given scenario [1]. The aim of the article is to select an appropriate semi-trailer for the carriage of strawberries, taking into account technical parameters related to active and passive safety systems. The selection of a means of transport may performed in several ways (inductive method, observation method). A method of comparative analysis was chosen in order to evaluate a proper vehicle, and in turn, help the carrier to choose a vehicle that would enable full performance of the transportation task, at the lowest possible costs, and in compliance with legal regulations. A weighted-average methodology is a comparative method chosen for the purpose of this article. Determining significant requirements connected with the transport order and defining the importance of a given requirement is essential in making the appropriate selection of a vehicle. A further step is to determine the technical features of the main and additional vehicle parameters and their evaluation. It is significant *to conduct effective* evaluation of particular parameters and compare the main technical parameters of selected vehicles. In this case, two vehicles are compared, and the following parameters are treated as criteria [8]**:**

- compliance with legal requirements;
- compliance with cargo shipping requirements;
- meeting requirements connected with the maximum payload and volume capacity of a vehicle;

- assessment of loading- handling capacity and load protection against damage or theft;
- assessment of vehicle traction possibilities with respect to planned routes;
- vehicle evaluation in terms of active and passive safety;
- meeting requirements concerning vehicle and cargo supervision on the route.

Levels of relevance (weight) are defined in points: scale from 0–10:

10 – necessary;
8 – very important;
6 – important;
4 – advisable;
2 – less important;
0 – unimportant.

Standard deviation, taking the values of:

1 – in accordance with the requirements;
0.7 – minor deviation;
0.5 – average deviation;
0.3 – divergence;
0 – significant divergence.

Furthermore, a summary table containing technical features of means of transport was established (0–10 scale).

The more satisfactory the technical conditions were, the higher the *score* was attributed to the vehicle. Subsequently, points were multiplied by weights and the results were divided by the sum of all weights.

I. The following parameters were adopted as technical comparative requirements:

- external parameter characteristics of semi-trailers;
- evaluation of traffic safety parameters and loading systems of the vehicles (technical characteristics).

II. Final choice of a vehicle (semi-trailer) with the use of weighted average – comparative method [8].

Weighted average – average value of technical parameters with weights assigned in such a way that elements with a higher unit value have a greater impact on the average value. The type of load and conditions set forth by a consignor are the main criteria taken into account. If all the weights are the same (all elements are of equal relevance), then the weighted average equals the arithmetic average.

Weighted average formula:

$$Śr\ \text{weighted avarage} = \frac{\sum_{i=1}^{n} \text{value}_i \cdot \text{weight}_i}{\sum_{i=1}^{n} \text{weight}_i}$$

$\sum_{i=1}^{n} \text{value}_i \cdot \text{weight}_i$ - Priority

$\sum_{i=1}^{n} \text{weight}_i$ - Conventional standard deviation

The total of points achieved by a vehicle/the total of priority points (possible to achieve) = weighted average.

Research was complemented by a substantive analysis that covers, inter alia, research relating to whether use of a given type of vehicle should be avoided due to its specific character. Therefore, there may be a need to change the conditions or reduce certain requirements that are not met – these changes could be achieved through adaptation or conversion of the routes, change in volume of load units, or taking measures that increase the utility and safety of the vehicle in question.

As for optimal storage conditions for fresh strawberries, the parameters are [1]:

- temperature conditions: temperature in loading area 0–1 [°C],
- atmospheric composition: humidity of the air 90–95 [%].

The means of transport and technology used during transport operations needs to meet specific requirements. Research analysis related to cold-storage vehicles need to meet the conditions of ATP (the Agreement on the International Carriage of Perishable Foodstuffs and on the Special Equipment to be used for such Carriage) [1]. Taking into account temperature and air humidity, a vehicle cooler should guarantee the proper storage and technical conditions (including physical, sanitary, bio-chemical and economic conditions). Considering standards of perishable food transport included in ATP, analysed transport operation requires 'B' class cooler vehicles equipped with cooling devices that maintain a temperature of +12 and -10 [°C] in a loading area, or 'C' class vehicles equipped with cooling devices that maintain a temperature of +12 [°C] and -20 [°C]. Currently, 'C' class vehicles are used most often, due to their broad range of maintained temperatures.

Further analysis of means of transport that are used for the carriage of strawberries will focus on two modern means labelled as FRC, in accordance with ATP (the Agreement on the International Carriage of Perishable Foodstuffs and on the Special Equipment to be used for such Carriage). These means of transport are heavily insulated class 'C' chiller trailers – FRC refers to [7]:

F – means of transport (chiller trailer)
R – heavy insulation (K coefficient k=0.4 W/(m^{2}K))
C – class C, cooler vehicle equipped with devices maintaining temperature +12[°C] and -20[°C] inclusive

Road vehicles analysed in the research process should meet additional technical requirements stipulated in regulations [14]:

1) Vehicle should provide any desired, practically constant temperature and air humidity, in conformity with the standards.
2) Airtight cargo area to prevent food from spoilage.
3) Water resistant, corrosion-proof and durable floor in cargo area.
4) Floor and walls of cargo area made of easy to clean materials that meet all hygiene requirements.

5) Watertight floor pan.
6) Vehicles used for food transport need to be cleaned and disinfected.
7) Loading area with no sharp edges or angles for rapid cleaning and disinfection.
8) Driver's compartment separated from cargo area.
9) Separate temperature zones allow the transport of different food products.

2.1. Research resources

Comparative research was based on the example of two modern semi-trailers:

1. Schmitz Cargobull semi-trailer TRIAXIAL FERROPLAST Type SKO 24/L- 13.4 FP 60 COOL (Table 1) [2, 3].
2. Krone Cool Liner cooling semi-trailer with double floor system by allsafe ATD II (Table 2) [5, 6].

The aim of the analysis of technical features is to check whether the trailers meet the requirements to perform the transport of strawberries. Particular attention will be paid to parameters that influence the technical capacities of vehicles used in transport of palletised strawberries. Additionally, road safety systems, driver's comfort, technical condition standards, modern systems of load securing, work economy, load safety and handling capacities will be described (Figs 1&2) [2–5].

Fig. 1. Volvo FH 4x2 420 and Schmitz Cargobull cooling semi-trailer

Table 1. Technical data of Schmitz Cargobull semi-trailer

Technical data	
King pin load: 12,000 [kg]	Inner height: 2,650 [mm]
Axle load: 27,000 [kg]	External length: 13,550 [mm]
Allowable gross weight.: 39,000 [kg]	External width: 2,600 [mm]
Tare weight with cooling unit and tank : 8,500 [kg]	Total height without load: 4,000 [mm]
Internal length: 13,310 [mm]	Loading capacity: 87.45 [m^3]
Internal width: 2,470 [mm]	Wheelbase: 7,875 [mm]

Fig. 2. Mercedes TGX 6x2 480 and Krone Cool Liner cooling semi-trailer with ATD II system

Fig. 3. Dimensions of Krone Cool Liner cooling semi-trailer with ATD II system

Table 2. Technical data of Krone Cool Liner semi-trailer with ATD II system

Technical data	
King pin load : 12,000 [kg]	Internal height: 2,650 [mm]
Axle load: 27,000 [kg]	External length: 13,550 [mm]
Allowable gross weight .: 39,000 [kg]	External width: 2,600 [mm]
Tare weight with cooling unit and tank : 8,500 [kg]	Total height without load: 4,000 [mm]
Internal length: 13,310 [mm]	Loading capacity: 87.45 [m^3]
Internal width: 2,470 [mm]	Wheelbase: 7,875 [mm]

2.2. Legal regulations concerning transport operation

Here follows the basic regulations referring to the transportation of goods and food in the European Union:

a) Regulation (EC) No 1071/2009 of the European Parliament and of the council of 21 October 2009 came into force on 4 December 2009 and became obligatory on 4 December 2011 – this established common rules concerning the conditions to be complied with to pursue the occupation of road transport operator. Regulation (EC) No 1071/2009 of the European Parliament and of the council regulates basic issues concerning undertakings that relate to requirements such as [10]:
   - establishing a transport manager in an undertaking;
   - having a head office of the establishment;
   - having authorization to pursue the occupation of a road transport operator (this is the same for all EU member states);
   - maintaining a good reputation;
   - having appropriate financial standing;
   - having rules concerning obtaining, suspension and withdrawal of licence.

b) Regulation (EC) No 1072/2009 of the European Parliament and of the council of 21 October 2009 on common rules for access to the international road haulage market, came into force as Regulation1071/2009 on 4 December 2009 and started to be obligatory on 4 December 2011. Regulation (EC) No 1072/2009 regulates issues concerning [10]:
   - member states licence to carry out international road transport;
   - driver's certificate for non-resident hauliers;
   - cabotage operations.

c) Regulation (EC) No 561/2006 of the European Parliament and of the Council of 15 March 2006 on the harmonisation of certain social legislation relating to road transport is a basic EU act that concerns driver's working and rest time [9].

d) Act of 16 April 2004 on driver's working time (Journal of Laws of 2004, No 92, item 879 as amended) regulates the system of drivers' working time [9].

e) The International Consignment Note on the international road haulage of goods was signed in Geneva in 1956. It was then ratified by Poland in 1962 when Poland became a party in international trade along with many other European countries. This note introduced and regulated requirements concerning road haulage and transport documentation. The application of the mentioned rules pertains solely to paid services in the international road haulage of goods carried out by professional road hauliers who have obtained appropriate authorisation in their countries [9].

f) International treaty on the carriage of perishable foodstuffs and on the special equipment to be used for such carriage. ATP (the agreement on the international carriage of perishable foodstuffs and on the special equipment to be used for such carriage) is a document of an extensive and complex structure concerning the implementation of transport requirements with reference to goods that demand controlled temperature. The agreement is valid from 1970 and it was adopted and

signed by Poland in 1984. It consists of 20 articles listed in 4 chapters and 3 appendices. The last amendment of the agreement took place in 2011 and includes [7]:

- types of perishable foodstuffs,
- temperatures required during transport,
- special conditions that vehicles need to meet to perform the transport of the mentioned products,
- required vehicle tests and signatures.

The treaty sets forth two main goals:

- maintaining quality and improving conditions of the transport of perishable foodstuffs, especially in international trade,
- contributing to growth in trade of the mentioned products.

Vehicles intended for the carriage of perishable goods should fulfil the requirements stipulated in the ATP agreement that concern [13]:

- heating equipment which is capable of raising the inside temperature of the empty body to + 12 [°C], and maintaining it for not less than 12 hours at;
- mechanical refrigeration which is capable of lowering the temperature inside the body from +12 [°C] to 0°C, from +12 [°C] to -10 [°C], and from +12 [°C] to -20 [°C];
- insulation equipment.

At the stage of transport *planning*, the transport manager should be acquainted with the range of temperatures that each product requires as this influences the choice of one of four vehicle groups that are accepted by the ATP agreement:

- mechanical refrigeration equipment,
- non-mechanical refrigeration equipment,
- heating equipment,
- insulation equipment.

2.3. Characteristics of legal provisions concerning the securing of loads

The system of legal regulations that refer to road transport is undergoing constant changes. Provisions are continuously being updated due to sustained progress in automotive technology. Much attention is paid to issues connected with transport safety and methods of securing loads. If restrained properly, loads should not displace or overturn, which would affect the safety of all traffic participants. A moving load may damage other cargo in the body or the body itself, it may constitute a danger for people or a serious obstruction to the traffic flow.

2.3.1. International provisions of law

a) Directive 2014/47/EU of the European Parliament and of the council of 3 April 2014 on the technical roadside inspection of the roadworthiness of commercial

vehicles circulating in the EU and repealing Directive 2000/30/EC, together with the international guidelines concerning safe load clamping on roads International Commission on Technology IRU (CIT) IRU_CIT-2014 version 01'. The aim of the guidelines is to provide information and instructions on loading/unloading, and the securing of loads for every participant of a transport chain, including consigners, carriers and freight forwarders. The instructions may be useful for controlling bodies and judicatory, or serve as a basis for organising vocational courses for drivers and carriers such as the Certificate of Professional Competence for drivers and the Certificate of Professional Competence for road hauliers. The guidelines provide a reference work of safe and effective load securing in all situations that may appear during a typical transport operation. These regulations should be treated as common ground for practical usage and the enforcement of load fixing. The document promotes safe ways of load restraint in the road transport of goods; moreover, it gives useful tips and information on how to achieve a safe level of load clamping in accordance with legal requirements and standards EN 12195-1:2010. Additional indications may shed the light on vital requirements to be complied with in reference to specific types of loads but should not aim at creating new requirements or limitations. Standard EN 12195-1:2010 contains more details useful for road hauliers such as 'Load Affixing Sets on Road Vehicles. Safety, Part 1:Calculation of Lashing Forces'.

b) German industry standards VDI
The standards describe ways of securing loads in detail, depending on its type. Standard VDI 2700 describes basic forces that influence the load, rules of cargo placement and practical tips on load clamping. Standard VDI 2701 refers to required clamping elements and standard VDI 2702 provides specifies rules concerning the choice of clamping elements. VDI standards are abundant with concrete examples and pictures that present how to clamp a load and secure it in a proper way, for example: huge glass panes, steel pipes, etc. [7].

c) Characteristics of standard PN – EN 12195 – 2 : 2010
This standard was introduced to assure compliance with basic safety regulations that relate to lashing strap traps used in Europe. Standard PN –EN 12195-2 'Load Clamping. Safety, Part 2: Lashing Straps' describes requirements concerning lashing straps for trucks and trailers, ships, railway wagons, and combinations of these [12].

2.3.2. National regulations

a) Law on road traffic
The Traffic Code regulates issues connected with load lashing in Poland. Moreover, a significant document that relates to load lashing is act of 20 June 1997, amended by an act 29 October 2010 r. on the amendment of the act on Road Traffic and other acts (Journal of Laws of 30 November 2010 No 225, item.1466).

b) Polish legislature introduced the Regulation of the Minister of Infrastructure and Construction on 6 May 2016, which amends the regulation on technical requirements,

as well as the scope of the necessary equipment, introducing the description of clamping points. Currently international road carrier association in Poland (ZMPD) translated "International guidelines referring to safe load lashing in road transport" which are unfortunately only guidelines, not regulations.

c) Transport Law

Pursuant to Article 65, Paragraph 1 of Transport Law the carrier shall be liable for the loss, partial loss, or damage of the consignment, occurring between the acceptance of the consignment, for handling and its delivery, as well as for late delivery. The liability of the carrier is not dependent upon fault, but rather on accepted risk. To hold the carrier liable on the basis of Article 65, four obligatory regulations were introduced [7]:

- Damage needs to take the form of loss, partial loss or damage;
- Damage takes place under the care of the carrier;
- A direct causal link between the occurring circumstances and the damage has to exist;
- A person entitled to compensation needs to perform so-called 'acts of diligence'.

Damage is the basic premise for a carrier's liability, which may take the form of loss, partial-damage or breakage. Loss of a load takes place when a carrier can't release the consignment to the receiver when the transportation deadline has expired. Partial load damage takes place when, at the moment of load release, there are losses in the form or decreases to weight, measures or number of units in comparison to the moment of its acceptance for transport. Damage of a parcel occurs when its market value is reduced, or its usability is decreased, due to quality changes. Such damage may be the result of mechanical factors (breakage, crushing, indentation), external factors (soaking, freezing, rust), biological or chemical changes (decay, fermentation, mould) [11].

3. Research results

Research of technical parameters and the basic requirements of the examined vehicles are presented in Table 3.

Adding together all points awarded to the researched semi-trailers across the separate groups of criteria, the following results were obtained:

- Schmitz Cargobull semi-trailer TRIAXIAL FERROPLAST Type SKO 24/L- 13.4 FP 60 COOL – 159 points;
- Krone Cool Liner cooling semi-trailer with double floor system by allsafe ATD II – **192 points.**

Taking into consideration the technical characteristics and results obtained according to the weighted average method, the Krone Cool Liner cooling semi-trailer, with double floor system by allsafe ATD II would be the most satisfactory choice for the transportation of strawberries [6].

Table 3. Results of road vehicle choice by the use the weighted average method

The method of weighted average was used in order to choose optimal means of transport on the basis of technical criteria										
No.	Requested technical parameters and basic requirements				Technical parameters and basic requirements for vehicles			Technical parameters and basic requirements for vehicles		
	Details	Unit of measurment	Figures or established requirements	Relevance	Volvo FH 4x2 Schmitz Cargobull cooling semi-trailer			Man TGX 6X2 Krone Cool Liner cooling semi-trailer (ATD II) Krone – box liner 40'		
					Figures or features	Standard deviation	Weight points	Figures or features	Standard deviation	Weight points
1	allowable gross vehicle mass	KG	42,000	9	4,000 kg	1	9	4,000 kg	1	9
2	tare weight	KG	18,000	8	14,845 kg	1	5	16,865 kg	1	9
3	authorised maximum load for a trailer	KG	32,000	9	31,040 kg	1	8	31,090 kg	1	9
4	authorised maximum load for a semi-trailer truck	KG	26,000	7	25,155 kg	0.7	7	25,250 kg	1	8
5	external dimensions of cooling semi-trailer (length/width/ height) [mm]	MM	13,600/2,600/40oo	6	13,600/2,600/4,008	0.7	6	13,550/2,600/4,000	1	6
6	internal dimensions of cooling semi-trailer (length/width/ height]	MM	13,400/2,500/2,650	8	13,315/2,460/2,650	0.7	8	13,310/2,470/2,650	1	8
7	double-deck loading	Y/N	Y	10	N(optional)	0.7	5	Y	1	10
8	maximum amount of pallet units	Pcs.	66	5	33	0.7	5	66	1	10

Table 3. Continuation

The method of weighted average was used in order to choose optimal means of transport on the basis of technical criteria										
No.	Requested technical parameters and basic requirements				Technical parameters and basic requirements for vehicles			Technical parameters and basic requirements for vehicles		
	Details	Unit of measurment	Figures or established requirements	Relevance	Volvo FH 4x2 Schmitz Cargobull cooling semi-trailer			Man TGX 6X2 Krone Cool Liner cooling semi-trailer (ATD II) Krone – box liner 40'		
					Figures or features	Standard deviation	Weight points	Figures or features	Standard deviation	Weight points
9	king pin load	KG	12,000	5	11,500 kg	0.5	5	12,000 kg	1	6
10	load securing systems	Y/N	Y	10	Y	0.7	7	Y	1	7
11	telematics systems (internal load monitoring)	Y/N	Y	10	Y	1	8	Y	0.7	8
12	ATP-FRC Certificate	Y/N	Y	10	Y	0.3	6	Y	0.5	6
13	loading platform in semitrailer	Y/N	Y	7	Y	1	7	Y	1	7
14	support lashing for intermodal transport	Y/N	Y	8	Y	0.7	8	Y	1	8
15	centre dividing insulated wall	Y/N	Y	9	Y	1	9	Y	1	9
16	load securing tracks in a side wall	Y/N	Y	6	Y	1	6	Y	1	6
17	load securing longitudinal and transverse tracks in side walls	Y/N	Y	10	Y	1	10	Y	1	10
18	additional all-around kick strip	Y/N	Y	8	N (OPTIONAL)	1	5	Y	1	8
19	ABS+ASR	Y/N	Y	8	Y	1	5	Y	1	5

Table 3. Continuation

The method of weighted average was used in order to choose optimal means of transport on the basis of technical criteria										
No.	Requested technical parameters and basic requirements				Technical parameters and basic requirements for vehicles			Technical parameters and basic requirements for vehicles		
	Details	Unit of measurment	Figures or established requirements	Relevance	Volvo FH 4x2 Schmitz Cargobull cooling semi-trailer			Man TGX 6X2 Krone Cool Liner cooling semi-trailer (ATD II) Krone – box liner 40'		
					Figures or features	Standard deviation	Weight points	Figures or features	Standard deviation	Weight points
20	aerodynamic system of semi-trailer	Y/N	Y	8	Y	0.6	8	Y	0.6	8
21	EBS with tilt stabilisation system RSP	Y/N	Y	8	Y	1	8	Y	1	8
22	automatic axle load measurement	Y/N	Y	10	Y	0.7	10	Y	0.7	10
23	telescopic locking bars on rubber feet	Y/N	Y	7	N (OPTIONAL)	0.5	5	Y	0.5	7
24	automatic safety locks	Y/N	Y	10	N (OPTIONAL)	1	5	Y	1	10
	TOTAL						159 points			**192 POINTS**
	$\sum_{i=1}^{n} \text{mean}_i$						0.81			0.97

4. Conclusions

The present legal situation concerning rules of transport operations and methods of load securing during transportation is governed by Polish and EU laws. The priority is to provide protection for people engaged in loading, unloading and transport, and also other traffic participants, pedestrians, the load itself and the vehicle. Loading and unloading should be performed by trained staff who are aware of the possible dangers. The analysis revealed that the Krone Cool Liner cooling semi-trailer with a double floor system by allsafe ATD II is the optimal choice – **192 points** (evaluation of competitive vehicle – 159 points). Loading capacities of semi-trailer and modern systems connected with load securing were the most decisive factors. Usage of double floor system ATD II by allsafe with adjustable height, allows the loading of sixty-six pallets at one time (the task required the usage of 64 pallets), whereas in the case of the Schmitz Cargobull semi-trailer TRIAXIAL FERROPLAST Type SKO 24/L- 13.4 FP 60 COOL, due to its low load capacity, there would be a need to use another set, or organize another transport – this would increase costs. Apart from economic factors, safety parameters also influenced the result (EBS and RSP in Krone) together with an additional load securing 'pallet stop' that allows reducing or avoiding the use of bars (or other security systems), thus reducing the load pressure on the front wall – this simplifies and shortens loading time. In the second part of the article, the weighted average method was used in the analysis of the safety systems of three producers. The rules of proper load placement and securing during transportation was discussed together with safety systems aimed at reducing the risk for the driver, the environment and other road traffic participants

References

[1] Konwencja ATP – umowa międzynarodowa dotycząca przewozu szybko psujących się towarów żywnościowych i o specjalnych środkach transportu przeznaczonych do tych przewozów [ATP – the agreement on the international carriage of perishable foodstuffs and on the special equipment to be used for such carriage].

[2] Instrukcja obsługi pojazdów Volvo Cars Group., 2017 [Operating manual of Volvo Cars Group Distributors].

[3] Instrukcja obsługi naczep Schmitz Cargobull AG., 2017 [Operating manual of Schmitz Cargobull].

[4] Instrukcja obsługi pojazdów Mercedes., 2017 [Operating manual of Mercedes].

[5] Instrukcja obsługi naczep chłodniczych Krone Cool Liner., 2017 [Operating manual of Krone Cool Liner].

[6] Materiały techniczno-handlowe przedsiębiorstwa allsafe., 2017 [Technical – sales material of allsafe].

[7] Starkowski D., Bieńczak K., Zwierzycki W., *Samochodowy Transport Krajowy i Międzynarodowy. Kompendium Wiedzy Praktycznej, TOM 5*, Poznań 2012.

[8] Starkowski D., *Zasady i metody doboru środka transportowego podczas planowania operacji transportowej przy pomocy analizy ważonej (wagowej) część 3*, Czasopismo TTS – Technika Transportu Szynowego, No. 12/2015.
[9] Starkowski D., *Bezpieczeństwo ładunków w transporcie drogowym. Zasady i metody zabezpieczania ładunków w transporcie drogowym – charakterystyka przepisów prawnych. Monografia*, Konferencja w ramach trzecie kongresu Polskiej Izby Opakowań, Warszawa-Poznań 2016.
[10] Starkowski D,. *Zasady wykonywania zawodu przewoźnika drogowego według nowych rozporządzeń unijnych nr 1071/2009 i nr 1072/2009*, Materiały konferencyjne z seminarium szkoleniowe dla Doradców DGSA nt. "Wszystko co ważne w transporcie drogowym towarów niebezpiecznych. ADR 2013 już wkrótce", Kraków 27–28.10.2012.
[11] Starkowski D., Bieńczak K ., Zwierzycki W., *Samochodowy transport krajowy i międzynarodowy. Kompendium wiedzy praktycznej TOM 3. Środowisko Pracy kierowcy. Logistyka*, Wydanie I, Poznań 2012.
[12] Starkowski,.D, Bieńczak K., Zwierzycki W., *Samochodowy transport krajowy i międzynarodowy. Kompendium wiedzy praktycznej. TOM 1. Zabezpieczenia ładunków oraz zagadnienia techniczno-eksploatacyjne w transporcie drogowym*, Poznań 2010.
[13] Zwierzycki W., Bieńczak K., *Pojazdy chłodnicze w transporcie żywności*, Poznań 2006.
[14] Kwaśniowski S., *Pojazdy izotermiczne i chłodnicze*, Wrocław 1997.

TECHNICAL TRANSACTIONS 1/2018
CIVIL ENGINEERING
DOI: 10.4467/2353737XCT.18.007.7958
SUBMISSION OF THE FINAL VERSION: 5/1/2018

Rafal Szydlowski (rszydlowski@pk.edu.pl)
IMBS, Faculty of Civil Engineering, Cracow University of Technology
Katarzyna Bednarz
Student at Cracow University of Technology

Material and construction solutions of war shelters with the example of Hitler's main headquarters in the Wolf's Lair

Rozwiązania materiałowo-konstrukcyjne schronów wojennych na przykładzie kwatery głównej Hitlera w Wilczym Szańcu

Abstract

The technology of erecting war shelters has been evolving over the centuries alongside the development of technology and building-oriented requirements. Many papers have been published on this subject in recent times. The ruins of the Wolf's Lair war fortress prompted the authors to write this work with a slightly different emphasis than the previous papers. In addition to a brief history of the objects, the work presents the design guidelines used in their construction and describes the construction solutions applied. In addition, where appropriate, the advantages and disadvantages of these construction solutions from an engineering point of view are highlighted.

Keywords: concrete building , war shelter, Wolf's Lair

Streszczenie

Technologia wznoszenia schronów wojennych ewaluowała na przestrzeni wieków wraz z rozwojem techniki i stawianych obiektom wymagań. Pozostałości po twierdzy wojennej Wilczy Szaniec skłoniły autorów do napisania tej pracy – o nieco odmiennym charakterze niż dotychczasowe. Prócz krótkiej historii obiektów w pracy przedstawiono ówczesne wytyczne wykorzystane w konstruowaniu obiektów oraz opisano zastosowane rozwiązania konstrukcyjne. Dodatkowo opatrzono je stosownym komentarzem inżynierskim.

Słowa kluczowe: budownictwo betonowe, schron wojenny, Wilczy Szaniec

1. History, location and military significance of Wolf's Lair

During World War II, a dozen or so fixed headquarters of the occupying forces were established in Europe, serving as command centres for the war front. They were usually found in the mountains and in areas surrounded by lakes and marshes; they were always near the fronts in areas difficult to penetrate. On the whole, they were powerful, massive reinforced-concrete buildings and bunkers. The most famous and most frequently discussed military quarters is Wolf's Lair, located in the Kętrzyn Forest in Masuria (near the former border with the Soviet Union – Fig. 1). The construction of Wolf's Lair was entrusted to the 'Todt' organisation, which under the guise of building the 'Askarnia' chemical plants, began construction work in the autumn of 1940. The construction and extension of the fortress can be divided into three stages: 1940–1941, 1942–1943 and 1944.

Fig. 1. Location of Wolf's Lair [1]

The works started with the modernisation of the railway station in Kętrzyn, the construction of a large platform, railway sidings and utility infrastructure. The forest road to Kwidy (Queden) was paved and the road to Kętrzyn was asphalted. The lifetime of Wolf's Lair was planned for the Blitzkrieg led against the Soviet Union, which was scheduled to start at the beginning of May 1941. At the time of Hitler's arrival at Wolf's Lair (24.06.1941), the quarters consisted of eight single-storey, terrestrial concrete bunkers and several wooden and masonry buildings. Some of these were equipped with metal doors and shutters (in case of an air attack) and rubber seals (in case of a gas alarm).

In the summer of 1942, as a consequence of the prolonged war with the Soviet Union, the 2nd stage of construction commenced. Due to the growing number of persons occupying the quarters, wooden barracks were mostly built – these housed office and residential areas. Due to the risk of air raids, some of these were strengthened with reinforced concrete.

In April 1944, due to the approaching eastern front, the third phase of the extension commenced in Wolf's Lair. Some of the existing concrete buildings were strengthened at that time: Hitler's shelter, the guesthouse (No. 6), two teleprinter terminals. Other shelters were constructed from scratch: for Goring (No. 16), for Martin Bormann (No. 11) and for public use (No. 26). The above-mentioned objects were created on the principle of double walls and ceilings, between which, there was 700 mm of space filled with basalt grit or gravel. In the event of bombing, these would absorb the shock. The complex of facilities built in the years 1940-44 occupied an area of 250 hectares. In total, there were about 200 objects of different sizes and uses, including 7 heavy anti- aircraft shelters, dozens of masonry and concrete buildings and dozens of wooden buildings.

In October 1944, the Red Army troops reached the eastern borders of East Prussia. It could be assumed that its next target would be, above all, Wolf's Lair. For this reason, on 20 November 1944, the headquarters were transferred to Zossen, near Berlin. Two days later, on 22 November 1944, Field Marshal W. Keitel issued an order to blow up Wolf's Lair. The bombing of the shelters and barracks under the code name 'Inslsprung' was performed on the night of January 24th, 1945. These were the strongest explosions that shook the immediate surroundings. The large concrete blocks flew 20–30 meters. According to witnesses, shocks caused ice to crack in the nearby lakes. Polish sappers calculated that about eight tons of tritium had to be used to blow up one heavy shelter. The ruins of the blown-up bunkers, as well as many undamaged, lighter buildings, can now be seen in the state they were left in that January night in 1945. They only carry traces of time, and they perfectly present the construction solutions used.

2. Contemporary guidelines and regulations for the construction of bunkers

The technology of building shelters has evolved over the years. Further technological developments have been patented and systematised over time. The formation of the fortification zone, the placement of individual objects and their method of elevation have been the subject of scientific papers, textbooks and finally, standards.

The elaboration of detailed guidelines and norms for the construction of fortification objects was preceded by a number of trials and error attempts using different materials, technologies and construction systems.

The development of artillery, and in particular the use of threaded barrels, increased the range of guns, and new explosives increased artillery fire power. Forts have been erected using materials known for centuries – brick structures were surrounded by earthen ramparts and brick embankments. At the end of the nineteenth century, a few gun-resistant domes appeared on shelter ceilings these were cast from steel. However, steel is an expensive material, and although the casting technique of large cast iron and steel castings was developed a long time ago, the transportation and assembly of multi-ton domes has given rise to many problems, especially since the forts were often erected in terrains that were difficult to access.

A major milestone in the development of fortification was the development of Portland cement production technology in 1880. As a result of this, concrete allowed the mould to get

any shape and significantly increased the resistance of objects to artillery fire in relation to brick and earth buildings. For comparison, the resistance to an explosion provided by a 300 mm concrete layer on the ceiling of a shelter corresponded to the resistance offered by a 2 m thick earth embankment. As a result of the explosion of a 155 mm demolition grenade, a concrete funnel with a depth of 0.6 m and a diameter of 2 m is formed.

France led the way in the field of the theory of fortification. Here, field tests of the construction and firing tests (Fig. 2) were carried out. The first norms shaping the formula of the concrete mixture were created here.

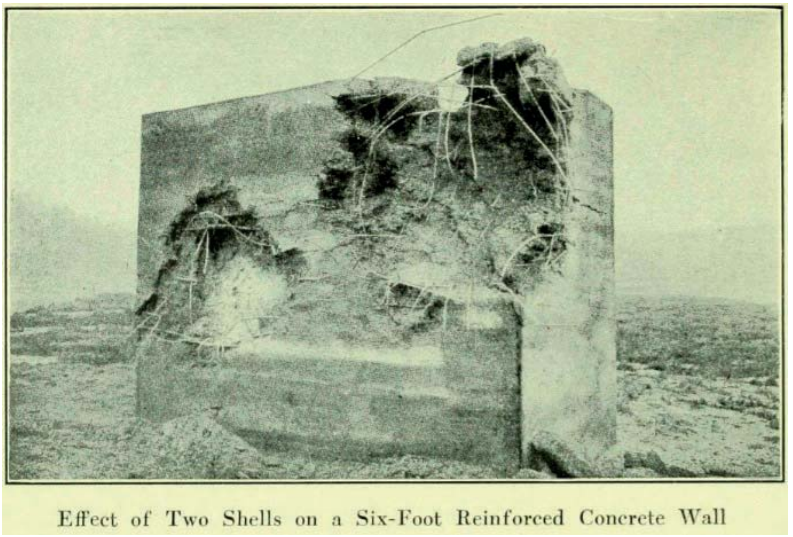

Fig. 2. Polygon test on a 1830 mm (6 ft) thick reinforced-concrete wall [2]

The French General Staff claimed that the construction of the mighty and extensive fortifications of the Maginot Line would protect their country from the greatest threat – the German army. This was the reason why the French focused on improving the building technology. Other European countries followed them, including Germany and Belgium. Table 1 shows the composition of the concrete mix used in the aforementioned countries for the construction of war buildings published in the paper [3]. In later years, the composition of concrete mixtures underwent changes due to technical progress and the development of construction techniques. Changes resulting from the geological structure of aggregates obtained locally from sources near to the construction were also introduced.

In the early nineteen-twenties and early nineteen-thirties of the twentieth century, strength and resistance standards of field fortification facilities were established. These classifications were mainly based on the determination of the resistance of walls and ceilings to the firing of demolition ammunition of a given calibre. Important data derived from the French guidelines for the classification of combat shelters is given in Table 2; this data was used by many countries at that time. The measure necessary for the classification of fortification objects was the reinforced-concrete penetration parameter. The relationship between the necessary

thickness of the wall or the reinforced-concrete ceiling and the resistance to artillery fire is described by the following formula [4]:

$$S = \frac{10 \times \text{shell caliber}}{2} \text{ [mm]}$$

This should be interpreted as follows: a 200 mm diameter pierced a 1 m reinforced-concrete wall or ceiling. Standards and classifications relating to resistance to fire provided the required construction parameters according to the object element.

The classification of the resistance of fortification objects was developed in nineteen-thirties Germany. This classification had four levels: A – resistance to direct artillery fire of a 520 mm calibre shell and the strike of an aerial bomb of up to 1000 kg; B – fire with a shell of 220 mm calibre and a single hit with a 500 kg bomb or 300 mm calibre shell; C – fire with shells of up to 105 mm; D – protection against shattering and fire from light artillery guns. The original classification was extended in 1938 (Table 3).

It should also be emphasised that it is essential to estimate the necessary expenditure for the construction of the fortification facilities. In the German literature of World War II, there was a list of the necessary quantities of materials and labour for the construction of

Table 1. Composition of the concrete mixture and the amount of steel used to construct fortifications in European countries in the early nineteen-twenties and early nineteen-thirties [3]

Material	Germany	Belgium	France
cement [kg/ m^3]	275	400	400
sand [m^3/ m^3]	0.40	0.40	0.30
aggregate (broken stone) [m^3/ m^3]	0.90	0.90	0.90
reinforcement [kg/m^3]	80-120	70	80

commonly erected, 5×5 m reinforced-concrete passive bunkers for one or two infantry units. The requirements and quantity of materials for such a shelter are given in Table 4, and requirements relating to the necessary construction personnel are provided in Table 5.

Although the layouts shown in the tables are relatively large, the construction of such shelters or whole lines of defence was several times cheaper than the development of weapons needed to break them. It was calculated that the construction of such a bunker was 2-5 times cheaper than the cost of the ammunition needed to destroy it. The durability and indestructibility of the shelters were of paramount importance from the perspective of military strategy – neither financial nor human resources were spared on their construction.

Table 2. French classification of combat shelters [4]

Shell diameter	380—420 mm		305—380 mm		210—305 mm		150 mm	
	plain concrete	reinforced concrete	plain concrete	reinforced concrete	plain concrete	reinforced concrete	plain concrete	reinforced concrete
front walls [m]	3.0–3.5	2.5–3.0	2.5–3.0	1.75–2.5	2.0	1.5	1.5	1.2
ceiling slab (with span of 3–4 m) [m]	2.5	2.5–3.0	1.75	2.1–2.5	1.3	1.5	1.0	1.1

3. Main construction principles

In the early nineteen-twenties and early nineteen-thirties engineers have set some rules regarding the erection and maintenance of fortification objects. Technological advances, World War I experiments and field laboratories, and numerous field trials have contributed to the formulation of several important (obvious in today's construction) conclusions. It was noted that:

Table 3. German classification of the resistance of fortification objects to artillery fire from 1938 [4]

Resistance class	Thickness of external walls [m]	Ceiling slab thickness [m]	Thickness of internal walls [m]
A	3.5	3.5≤	1
A1	2.5	2.2	1
B-neu	2	2	0.8
B	1.5	1.5	0.8
B1	1	0.8–1	0.8
C	0.5–0.6	0.5	0.5
D	0.3	0.3	0.3

Table 4. Quantity of materials needed to construct German 5×5 m concrete passive bunkers, [4]

Material	Unit	Quantity
gravel	m^3	38
sand	m^3	38
cement	t	26.5

Table 4. continuation

Material	Unit	Quantity
reinforcing bars of 8-10 mm diameter	m	825
	t	0.51
reinforcing bars of 15-20 mm diameter	m	1600
	t	3.95
connecting wire of 1 mm diameter	kg	70
200 mm 'I' beam (length of 4.2 m)	piece	16
lintel of 200 mm 'I' beam (length of 1.2 m)	piece	4
f25 mm threaded rod (length of 1.2 m)	piece	12
f25 mm threaded rod (length of 0.5 m)	piece	4
shuttering boards	m^2	120
squared and round timber	m	305
steel smooth nails	kg	25

Table 5. Building personnel needed to construct German 5×5 m concrete passive bunkers [4]

Task	Occupation	Number of workers
timbering	carpenters	12 + foreman
reinforcing	steel fitters	8 + foreman
ground works and casting	other workers	24-40 + foreman

- As a material, plain concrete probably protects against the explosion of an artillery shell but, due to its low deformability and elasticity, it splits and cracks not only as a result of fire but also as a result of thermal stress, especially during frost.
- There is a necessity to perform dilatation when erecting retaining walls, earthworks and other long-length structures.
- Plain concrete during explosion poses an enormous threat to people inside the shelter, where heavy debris from walls and ceilings is torn off from the inner surface and wounds and buries people. Initially, this was attempted to be resolved by strengthening the vaults from the bottom with corrugated steel sheeting; however, it was more effective to pour the ceilings on a composite structure of steel T-beams arranged at short distances with separators between them in the form of a filler steel plate.
- A better solution for the construction of bunkers is the construction of a monolithic block rather than a construction made from prefabricated elements which, as a result of shock and vibration, are subject to delamination and faster destruction.
- The foundation slab is necessary in construction because the people who are in the shelter are most threatened by missiles which are coming up from ground (i.e. those

that hit the ground near the object). Because of their explosive force, they penetrate the ground deeply and reach below the walls and into the inside of the shelter.
- The cubature of the object plays a big role. Bunkers of too small dimensions turn over due to the force of the explosion, or are pressed into the ground.
- The use of reinforced concrete proved to be a breakthrough in the construction of fortification objects exposed to artillery fire or aerial bombardment. Smooth rods with a diameter of 10–20 mm were used for reinforcement. Reinforced concrete had greater strength than non-reinforced concrete, and at the same time, it had a high degree of deformability and made it difficult for fragments of concrete to peel off and for the construction to disintegrate. Thus, before the First World War, it became the basic material for the construction of fortification buildings.

4. Functional layout and bunker design

The bunkers that were created at the turn of 1940–1941 were quite inconspicuous. The structural assumptions of these objects were based on the pre-war defence standards of fortification construction, quickly verified by the development of aviation. Their 1.0–1.5 m thick walls and two-meter ceilings were supposed to protect against the explosion of 500 kilogram bombs. Several small rooms in their interior provide the minimum of space for work and sleep. The bunkers were equipped with sanitary installations and electricity. In 1943, the effectiveness of bombing by the British and American aviation considerably increased. Their reach grew so much that they began to attack targets in places which had so far been deemed safe, including East Prussia. The threat of an air attack on Hitler's main headquarter – Wolfschanze, began to be possible. In mid-1943, Hitler decided to expand the facilities of the headquarters. It was decided to reinforce the existing shelters by enclosing them with reinforced-concrete armour resistant to direct impacts of even the largest 10-ton bombs which the Allies were in possession of.

The final construction was different from the shelters which had been built prior to the expansion of 1943. They had much larger dimensions, the height exceeded 10 m (Fig. 3), and the thickness of their ceilings reached 8 m. The work connected with the reinforcement of the existing bunkers mainly constituted their enclosure with reinforced-concrete coats which increased their resistance to bombardment. Between the reinforced-concrete armour coats, a layer of grit with a thickness of 0.7 m was used. Fat concrete (at least 600 kg of cement in a cubic meter) and a significant amount of reinforcing steel were used for the construction of the coat. The shelter layout on the example of the Special Communications Bunker is shown in Figure 4 and its vertical cross-section, in Figure 5. The entrances were at the ends of arterial corridors running through the entire width of the shelter. From there, there were corridors leading to small, internal spaces deprived of windows and with a height of 2.0–2.1 m. Entrances to the internal corridor were equipped with gas-tight armoured doors. At the top of some of the bunkers, anti-aircraft defence posts were placed. Much attention was paid to camouflaging objects. The outer walls were covered by a camouflage mix of sea grass, chips and cement. On the roofs, basins were filled with earth were formed and cultivated.

Fig. 3. View of the heavy bunker of Martin Bormann's Shelters in Wolf's Lair (own photo)

5. Construction of ceilings in bunkers

The construction of the ceilings in the fortification buildings evolved along with the resistance needs resulting from the development of artillery or warfare techniques. Initially, these were costly steel domes which were not very resistant to bomb attacks and were buried in earth, brick or concrete vaults, and later secured with corrugated steel

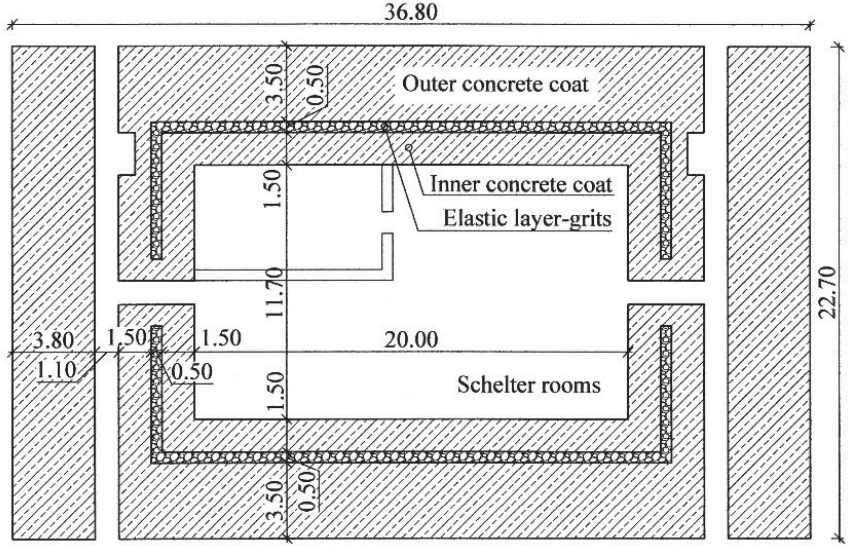

Fig. 4. Plan of the Special Communications Bunker with outer concrete coat [4]

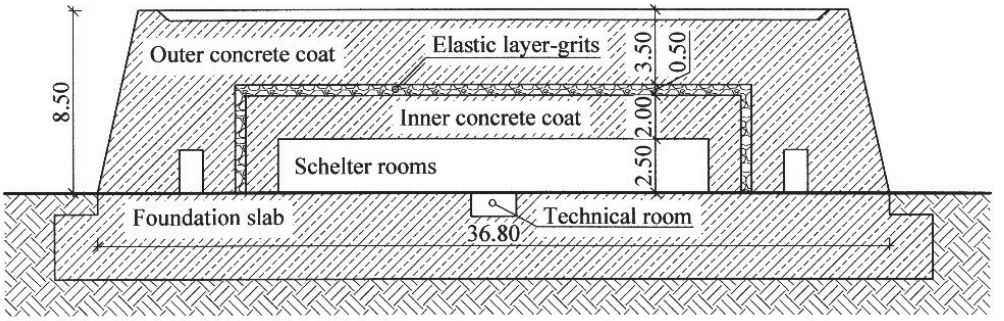

Fig. 5. Vertical section of the Special Communications Bunker with outer concrete coat [4]

sheeting. If necessary, the roofs evolved to concrete and later, reinforced concrete cast on steel beams or whole reinforced concrete cast in a traditional wooden formwork. Below are some ceiling solutions used in Wolf's Lair.

5.1. Concrete and reinforced-concrete ceilings on steel beams

After many less successful attempts, the concrete ceiling on the steel beams became such an effective solution that it became an important element of fortification architecture for many years. Steel 'I' beams were laid parallel at intervals of 0.4–0.7 m and the filling between them was several-millimetre-thick steel sheets based on lower footers (Fig. 6). Steel beams constituted both a self-supporting formwork required for the concreting stage as well as reinforcement of the lower zone of the slab ensuring its bending resistance. Such a solution allowed the pouring of a slab with a thickness of up to 2 m without additional support (Fig. 7a). A tight steel coating protected against breakage of concrete elements from the bottom during fire or explosions. The maximum span of the ceiling was 7.20 m. Initially, a concrete slab was cast on a steel structure. With the development of reinforced concrete, a spatial net was used to provide horizontal reinforcement in both directions and in the vertical direction (Fig. 7b) thus giving the composite slab.

a)  b) 

Fig. 6. a)Composite slab on steel beams cross-section, b) the view of the slab in good condition (own photos)

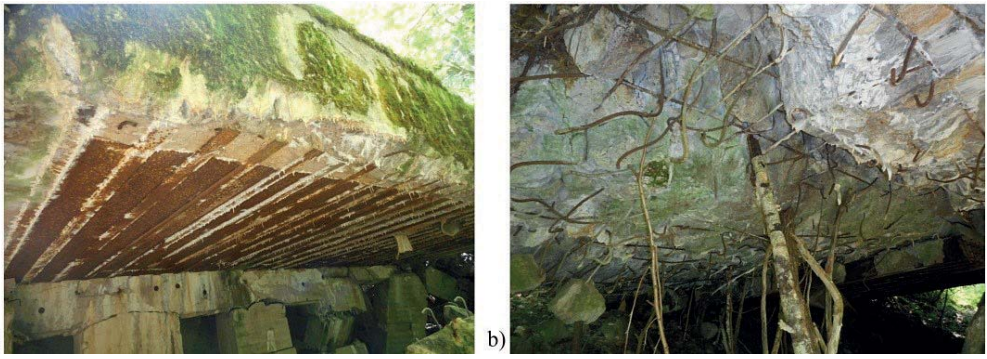

Fig. 7. a) View of a thick slab on steel beams b) and dense steel reinforcement (own photos)

5.2. Reinforced concrete ceiling in wooden formwork or on corrugated steel sheeting

After the dissemination of reinforced concrete and appreciating its advantages, today's reinforced concrete slabs are commonly used in wooden formwork. Such ceilings were constructed in small defensive structures. Their spans did not exceed 5 m. Wooden formworks – often in fragments – have been left visible in the interiors of buildings until today (Fig. 8). A better type of formwork was corrugated steel sheeting used as permanent formwork. The use of plates from the underside provided additional air tightness and limited the fall of concrete fragments.

Fig. 8. View of left fragment of wooden formwork (own photo)

5.3. Ceiling constructed on pre-tensioned concrete beams – the first application of prestressed concrete on Polish land

Another solution in the construction of ceilings was casting the slab on pre-tensioned concrete beams. The modern form of reinforced concrete was actively used in the construction industry in the 1930s. This was the so-called technology of active reinforcement where preliminary compressive stresses were applied to the concrete, acting against tensile stresses extending from external loads. The initial stress system is introduced by tensioning wires of low-relaxation steel, which are able to maintain tensions for a long time. Throughout the

lifetime of the structure, through the adherence of the wires to the concrete (pre-tensioned concrete), or through additional anchorage at the heads of the element (post-tensioned concrete), the tensioned tendons act on the concrete element with the force with which they have been tensed. The force from the tendon, through its eccentric application in relation to the centre of gravity of the element, causes an inverse state of bending stresses generated by the external loads.

T-section pre-tensioned prestressed beams were already used in the thirties to make ceilings with a span of several dozen metres – this was necessary for the protection of high volume armour (e.g. U-Boats). Due to the considerable advantage of prestressed concrete structures in terms of bearing capacity relative to other solutions, they have also begun to be used in smaller but strategically significant command centres. This is undoubtedly the first application of prestressed concrete on Polish land in the Wolf's Lair complex.

During the second stage of the modernisation of the fortress, pre-tensioned concrete beams were delivered from Cologne and used to reinforce lightweight brick buildings (Fig. 9). Beams with an inverted T-shape had a maximum span of 12 m and a height of 0.45 m. Available for research study by the authors, the sections of the beams were prestressed with 82 wires with a diameter of 2.5 mm, placed in the lower footer with a width of 0.25 m and 8 wires in the upper section of the web. Figure 10a shows the cross section of the beam inverted by 180 degrees relative to the position of mounting into the ceiling, and Figure 10b is the cross section of the ceiling. The composite slab had different thicknesses depending on the span and the required load capacity for a given building. Height of the beams was in the range from 450 mm to the total height of about 1.2 m. Depending on the expected load on the slab and its span, different spacings of beams were used. With more prestressing required, the beams were laid for contact (Fig. 11a), one next to the other. With smaller spans and slab thicknesses, the beams were parted and the space between them was supplemented with shuttering boards placed on the lower footers (Fig. 11b and c).

Fig. 9. View of the slab with pre-tensioned beams and concrete topping

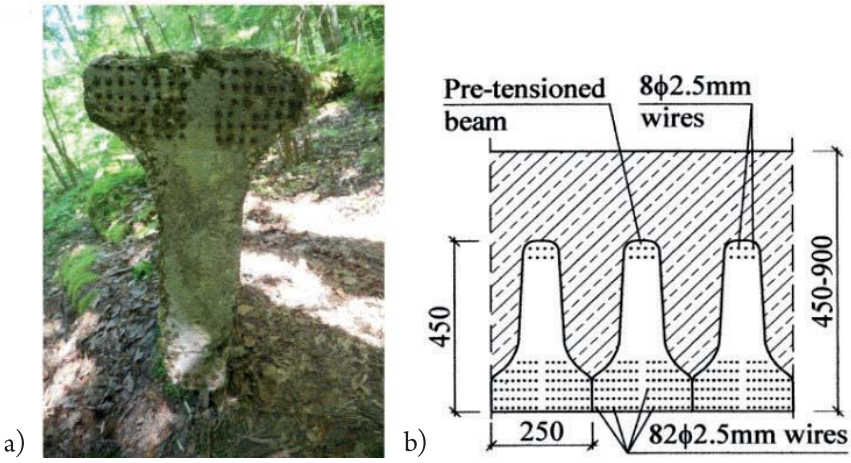

Fig. 10. a) View of pre-tensioned beam cross section (own photo), b) slab cross-section

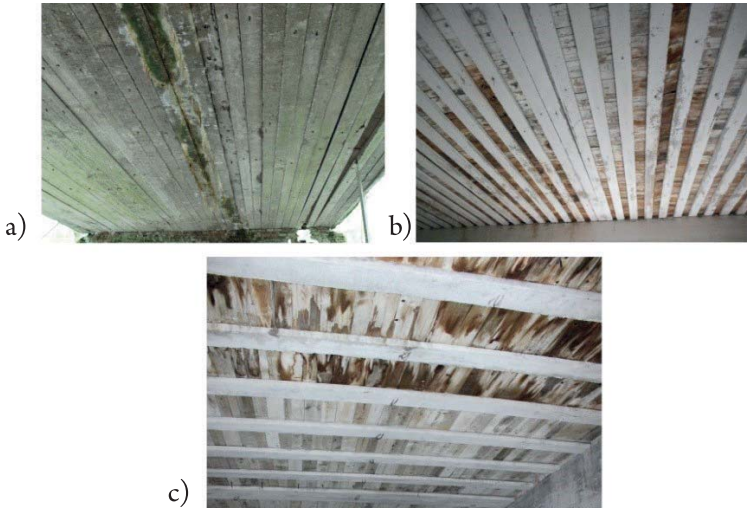

Fig. 11. a) Different spacing of pre-tensioned beams depending on slab load and span: for contact, b, c) spaced with shuttering boards (own photos)

6. The current conservation status of objects

Most of the heavy concrete shelters in the Wolf's Lair fortress were either completely or partially blown up. At a distance of about 25 km northeast, there is the Mamerki fortress with many similar shelters, but these are intact. The condition of the concrete objects in Mamerki is almost perfect (Fig. 12a). The steel elements of the ceilings actually show signs of corrosion, but the condition of the concrete is satisfactory. The technology used in the construction of the facilities was adequate and thus, the objects have survived intact for almost 80 years.

The nature of the ruins of the blown-up shelters shows the strength of the structure and also the difficulty and huge investment cost of their destruction mentioned in Section 2.

a)  b) 

Fig. 12. a) Building of electric transformers in Mamerki, b) view of separated but entirely preserved wall of heavy bunkers (own photos)

Fig. 13. Concrete wall blocks of heavy bunkers (own photos)

a) 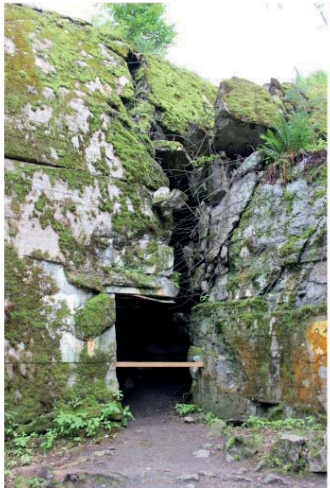 b) 

Fig. 14. View of the importance of reinforcement in ensuring ductility and compactness of concrete structures (own photos)

Many of the walls of the bunkers have survived almost completely or with few cracks (Fig. 12b), despite being subjected to strong explosions. Solid concrete walls often rest on great concrete blocks (Fig. 13). The number of explosives needed to separate them and shift them to great distances was impressive. Figure 14 shows the role of reinforcement in structural resistance to explosions. Fragments of walls were actually moved several dozen centimetres but were not separated. In Figure 14b, this is particularly noticeable, the surface of the fraction on the left fragment corresponds exactly to the surface on the right-hand fragment. This demonstrates the fragmentation and elongation of the concrete reinforcing bars. Such ductility of reinforced concrete structures is certainly achieved by the use of smooth rods that lose more adhesion over longer distances than ribbed rods and thus offer greater elongation. This example shows the advantage of smooth reinforcement over ribbed in explosion-prone objects and the need for reinforcement of high ductility.

It is also worth to note the durability and resistance of composite ceilings to explosions, which in many cases have been preserved as a homogenous form or large sections of composite slab. The strength of the bond (especially for reinforced concrete slabs) was achieved by using steel beams and spatial internal reinforcement.

7. Conclusions

Undoubtedly, many of the technologies we use today, such as mobile telephony, internet, GPS etc. were created for the needs of the army and later popularised for civilian purposes. Also, the first computer was invented and built to speed up the calculation of ballistic missile routes (ballistic curves). Although it is hard to say that concrete construction has been invented for military purposes, it is safe to say that the two world wars have significantly contributed to its development and improvement. Today's reinforced concrete and its existing construction products are not much older than 100 years. However, many buildings have not survived from the early years of use of reinforced concrete, and those that have been preserved are often in poor condition. The condition of the objects not damaged by explosions in Mamerki and fragments of constructions in Wolf's Lair show, however, the advancement of concrete technology and appropriate construction solutions as long as 80 years ago. The materials and solutions used in the construction of military fortifications were certainly helpful, and should continue to be so, in understanding and properly forming concrete structures – especially massive structures.

References

[1] https://www.awesomestories.com
[2] Henderson E., *Germany's fighting machine*, Indianapolis 1914.
[3] Biesiekierski K., Kleczke K., Rewieński M., *Fortyfikacje polowe*, Warszawa 1929.
[4] Szymański J., Szymańska M., *W krainie wielkich bunkrów*, Łódź 2009.
[5] Dragun M., *Wilczy Szaniec. Była wojenna kwatera Adolfa Hitlera*, Algraf S.C., Biskupiec 2015.

TECHNICAL TRANSACTIONS 1/2018
ELECTRICAL ENGINEERING
DOI: 10.4467/2353737XCT.18.008.7959
SUBMISSION OF THE FINAL VERSION: 2/1/2018

Krzysztof Schiff (kschiff@pk.edu.pl)
Department of Automatic Control and Information Technology, Faculty of Electrical Engineering, Cracow University of Technology

Ant colony optimisation algorithm for the facility localisation problem

Algorytm mrówkowy dla problemu lokalizacji punktów obsługi

Abstract

This article describes a new ant colony optimisation algorithm for the facility localisation problem with a new heuristic pattern proposed by the author, which consists of three parts: the function of the average cost of client servicing; the total minimum cost of servicing from a site, which is selected and included into the solution; the function of improving the cost of already serviced clients. In this comparison, simulations were presented, and two parameters were observed: the number of sites and the cost of client servicing. The new algorithm allowed to improve the solution in both of these parameters.

Keywords: facility localisation problem, ant colony optimisation, heuristic algorithm

Streszczenie

W artykule przedstawiono algorytm mrówkowy dla problemu lokalizacji fabryk z nową zaproponowaną heurystyką wyboru obiektów i został on porównany z innym znanym już z literatury przedmiotu algorytmem mrówkowym. Nowa heurystyka wyboru została wyrażona jako iloraz trzech funkcji pożądania wyboru, to jest funkcji określającej średni koszt obsługi klientów poprzez włączaną lokalizację do rozwiązania, funkcję określająca całkowitą minimalną sumę obsługiwania klientów z włączanej do rozwiązania lokalizacji oraz funkcję określająca maksymalną minimalizację kosztów obsługiwania klientów poprzez włączaną lokalizację, gdy ci klienci są już obsługiwani przez lokalizacje wybrane do rozwiązania. W artykule przedstawiono wyniki przeprowadzonych testów pod kątem uzyskania jak najmniejszej liczby lokalizacji i jak najmniejszego kosztu obsługiwania klientów w funkcji rozmiaru problemu i natężenia obsługiwania klientów z danej lokalizacji.

Słowa kluczowe: problem lokalizacji punków obsługi, algorytm mrówkowy, heurystyka

1. Introduction

The facility localisation problem is the most important logistic problem. It is a very important decision for managers to consider where to locate new facilities, such as retailers, warehouses or factories. This optimisation problem is the problem of locating p facilities relative to a set of customers in such a manner that the sum of the shortest demand weighted distance between the customers and the facilities is minimised. It is shown by Kariv and Hakimi (1979) that the facility placement problem is NP-hard. Exact methods take a lot of time in order to reach solutions [8, 9]; therefore, most often, heuristic methods are used to solve this problem [4, 6, 7, 10–13] and, among them, meta-heuristics algorithms, such as genetic algorithms [1, 14–16, 19, 20] or ant colony algorithms [2, 3, 5, 17, 18].

The facility localisation problem consists of a set of customers N where $N = \{1, 2, ... n\}$ and a set of potential sites for the facilities M where $M = \{1, 2, ..., m\}$. It is assumed that the cost of transporting the w_i units of product from a facility j to the customer i is cij; for each $i \in N$ and $j \in M$, there is no fixed cost for locating at a particular site and there is no capacity constraint on the demand supplied by the facility. The problem is to choose p of the m sites where a facility will be located in such a way that the total transportation cost is minimised.

A mathematical formulation of the problem is as follows:

$$\text{Min} \sum_{i=1}^{n} \sum_{i=1}^{n} c_{ij} x_{ij} \tag{1.1}$$

$$\sum_{i=1}^{n} x_{ij} = 1 \tag{1.2}$$

$$\sum_{i=1}^{m} y_j = p \tag{1.3}$$

$$x_{ij} \leq y_j \, \forall i \in n, \forall j \in M \tag{1.4}$$

$$x_{ij}, y_j \{0,1\} \forall i \in N, \forall j \in M \tag{1.5}$$

where p – the number of facilities,
y – the site for the facility to be located at
$y_{j=1}$ if a facility is located at site j, otherwise y j =0 $\forall$ $j \in M$
and x_{ij} =1 if customer i is serviced by a facility at site j, otherwise xij =0 $\forall$ $i \in N, j \in M$.

Constraints 1.2 guarantee that each customer is assigned to a facility. Constraints 1.3 ensure that p sites are chosen. Constraints 1.4 guarantee that a customer selects a site only from those that are chosen. Constraints 1.5 force the variables to be an integer.

2. Structure of the ACO algorithm

In ant algorithms, a colony of artificial ants is looking for a good quality solution to the problem. A pseudo-code of the ACO procedure is presents as algorithm 1. Each ant constructs

an entire solution. In order to construct a solution, each ant uses common information, which is deposited is sites; this means a set of sites selected and included in the solution.

Each ant selects a new site j with probability *pj* using the pheromone trail τ_j and the attractiveness *nj* of the move (2.1). These to parameters can be intensified by power expressed by coefficients α and β. The neighbourhood *NHi* of the already selected sites *Si* consists of sites, which can be added to the already selected sites *Si*. *NHi = M- Si –Vex*, where *Vex* are sites, which cannot be included into set *Si,* since they service only those customers who are serviced from sites already selected and included in the set *Si*.

$$p_j = \begin{cases} \dfrac{\tau_j^{\alpha} n_j^{\beta}}{\sum j \in N_i \tau_j^{\alpha} \mu_j^{\beta}}, & for\ j \in NH_i \\ 0 & for\ j \notin NH_i \end{cases} \tag{2.1}$$

Algorithm 1

ACO algorithm

```
while (exist cycle)
begin
while (exist any ant, which has not worked)
begin
while (a solution has not been completed)
begin
choose a next site to be added to the already selected sites Si with a probability pj
update NHi – a neighbourhood of the set Si
end
update a best solution if a better solution has been found
end
update a global best solution if a better solution has been found
update a pheromone trails τ(i) = τ(i) + Δτ
end
```

After a solution has been found, each ant deposits a pheromone with a quantity $\Delta\tau$ on all sites, which constitute the solution, in accordance with the pattern (2.2). Thus, those sites, which were included in the solution, have received an additional quantity of the pheromone and can be chosen to a solution with a higher probability than other sites.

$$\tau = \tau + \Delta\tau \tag{2.2}$$

The quantity of the deposited pheromones $\Delta\tau$ is expressed by formula 2.3, where: z – the current solution, z_{best} – the best solution.

$$\Delta\tau = f(Q) = \frac{1}{1 + \dfrac{Z_{best} - Z}{Z_{best}}} \tag{2.3}$$

Thus, those sites, which were included in the solution, have received an additional quantity of pheromones and can be selected afterwards with a higher probability than other objects.

An evaporation mechanism is incorporated into the ant algorithms in order to avoid too rapid a convergence to a suboptimal solution. The intensity of evaporation is controlled by the parameter ρ. The quantity of a pheromone on each object is updated at the end of each cycle in accordance with the pattern:

$$\tau=\rho\tau,\ \rho\in(o,1] \tag{2.4}$$

3. Improved Hybrid ACO algorithm

The algorithm presented in this paper, called the Improved Hybrid ACO algorithm (IHACO), is a modified version of the ant algorithm described in [5], which would be called the Hybrid ACO algorithm (HACO). The new algorithm is called the Improved Hybrid ACO algorithm since a desirability function is presented in a new form in comparison with the Hybrid ACO algorithm. In both of these algorithms, site j is selected to be in set S_i with probability

$$p(j)=\frac{\tau(j)n(j)}{\sum k\in NH_i\left(\tau(k)n(k)\right)},NH_i\in M \tag{3.1}$$

where:

NH_i – a neighbourhood of the set S_i

$NH_i = M\text{-}S_i - V_{ex}$

V_{ex} – these are sites, which cannot be included into the set S_i since they service customers who are serviced from sites already included in set Si

$\tau(j)$ – the quantity of pheromone deposited on site j,

$n(j)$ – the desirability of selecting site j.

In both algorithms, a following site that should be added to a partial solution is selected with a probability that depends on the pheromone trail, heuristic information and transition rule. The m differences between the elaborated algorithm and the algorithm, which is presented in paper [5], concern the heuristic information. The heuristic pattern, which has been presented in paper [5], is described by

$$n(j)=\frac{c}{\sum_{j=1}^{n} w_j},j\in NH_i \tag{3.2}$$

and a new heuristic formula presented in this paper by $n(j)=n1(j)n2(j)n3(j)$; this is the main contribution presented in this paper, where

$$n1(j)=\frac{nc}{\sum_{j=1}^{n} w_j},j\in NH_i \tag{3.3}$$

$$n2(j)=\sum_{j=1}^{n}\left(w_{\max}-w_{jk}\right), j\in NH_i, k\in N_n, N_n=N-N_s \tag{3.4}$$

$$n3(j)=\sum_{j=1}^{n}\left(w_{jk}-w_{ik}\right), i\in S_i, k\in N_S, j\in NH_i \tag{3.5}$$

where:
nc – the number of customers, which can be potentially serviced from site j
w_{max} – the maximal cost taken from all costs of customer servicing
w_{ij} – the cost of servicing customer j from site i
N_n – customers not yet serviced by any site already included into the set Si
N_s – customers serviced by sites already included into the set Si
S_i – already selected sites

The desirability function $n(j)$ of selecting site j consists of: $n1(j)$ – this is the inverse of the cost attributable to client servicing from site j, $n2(j)$ – this allows to choose site j at a minimum cost for all clients who are serviced from site j and who are not serviced already, $n3(j)$ – this allow to choose site j, which can lower the cost of servicing clients who are already serviced by sites included in solution S_i. The quantity of pheromone $\Delta\tau$ is deposited by ants during one cycle of the algorithm on all sites of the set S_i

$$\Delta\tau=\frac{1}{1-\frac{c_{best}-c}{c_{best}}} \tag{3.6}$$

where:
c_{best} – the minimum global cost of customer servicing from all cycles,
c – the actual cost of customers from the current cycle.

4. Results of experiments

The first is the HACO algorithm, which was described in [5], and the second is the IHACO algorithm, which is described in this paper and presents a new desirability function. The two main parameters of the facility placement problem under observation are: the average cost and the average number of localisation sites, which were received as a result of 50 measures. The number of cycles, the number of ants and the evaporation rate were taken from experience of dealing with ant algorithms, and under the conducted investigation, these parameters are not so important since we will see that the quality of the solution of the IHACO algorithm is better than the HACO algorithm. The number of cycles and the number of ants cause time constraints, so under these time constraints, the IHACO algorithm provides a better solution than the HACO algorithm. When we change the value of the evaporation rate, we cannot see any relevant influence on the obtained solutions, so these results were omitted and were not shown here. In this paper, only the most important results of experiments were shown.

During the first experiment, both algorithms were studied for a bipartite graph with 100x100 vertices and for different graph densities q, which were generated randomly. One set

of the vertices represents clients and the second set of vertices represents the potential sites. The weight assigned to the edge represents the cost of servicing. Any edge links a client with a site. These graphs with a density q belong to the particular group of graphs, since each edge exists with probability q and each vertex has an almost equal degree, meaning that it almost has an equal number of edges. The graph density q is a model of the proportion of all clients, which can be serviced by a site, so these proportions are equal for all sites.

The average costs for the 50 measures were presented in Table 1 and in Figure 1. The average number of localisation sites for the 50 measures was presented in Table 2 and in Figure 2.

These algorithms operate with the following parameters: the evaporation rate was set to $r = 0.995$, the number of ants was set to $lm = 30$ and the number of cycles was set to $lc = 100$.

Table 1. Average minimum cost of localisation for $\boldsymbol{n} = 100$, $\boldsymbol{lc} = 100$, lm = 30, $\boldsymbol{r} = 0.995$

q	0.1	0.3	0.5	0.7	0.9
HACO	2251.62	1852.19	1788.58	1800.06	2161.2
IHACO	1880.48	1672.22	1660.11	1714.59	2088.8

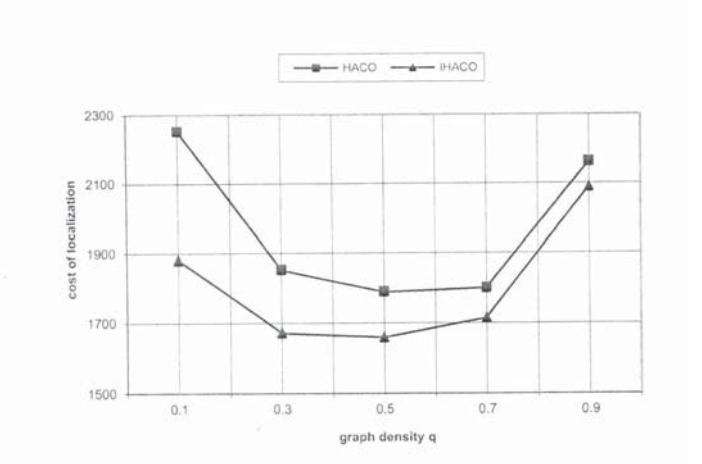

Fig. 1. Average minimum cost of localisation for $n = 100$, $lc = 100$, $lm = 30$, $r = 0.995$

Table 2. Average number of localisation sites $\boldsymbol{n} = 100$, $\boldsymbol{lc} = 100$, $\boldsymbol{lm} = 30$, $\boldsymbol{r} = 0.995$

q	0.1	0.3	0.5	0.7	0.9
HACO	26.98	11.74	7.2	4.95	3
IHACO	25.42	11.04	6.98	4.88	3

During the second experiment, both algorithms were studied for a constant graph density $q = 0.5$ and for a different graph size $n = \{50, 100, 150, 200, 250\}$. The average costs for the 50 measures were presented in Table 3 and in Figure 3.

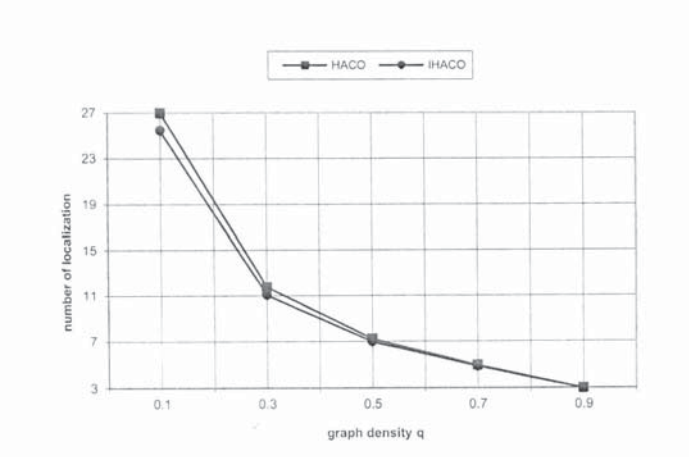

Fig. 2. Average number of localisation sites $n = 100$, $lc = 100$, $lm = 30$, $r = 0.995$.

The average number of localisation sites for the 50 measures was presented in Table 4 and in Figure 4.

These algorithms operate with the following parameters: the evaporation rate was set to $r = 0.995$, the number of ants was set to $lm = 30$ and the number of cycles was set to $lc = 100$.

Table 3. Average minimum cost of localisation for $q = 0{,}5$, $lc = 100$, $lm = 30$, $r = 0.995$.

n	50	100	150	200	250
HACO	925.48	1788.58	2635.98	3405.41	4232.29
IHACO	834.4	1660.11	2490.35	3303.22	4118.43

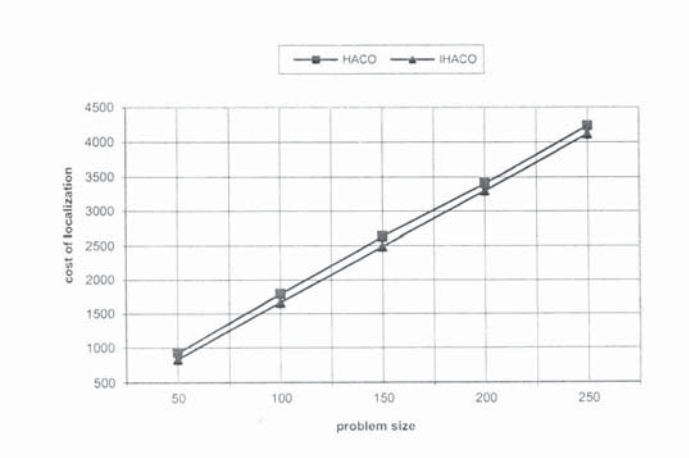

Fig. 3. Average minimum cost of localisation for $q = 0{,}5$, $lc = 100$, $lm = 30$, $r = 0.995$.

There is an improvement in the quality of the solution when the IHACO algorithm is used instead of the HACO algorithm, since there are lower average numbers of localisation sites and costs for the investigated graph density $q = \{0.1, 0.3, 0.5, 0.7, 0.9\}$ and the size of the problem $n = \{50, 100, 150, 200, 250\}$.

Table 4. Average number of localisation sites for $q = 0{,}5$, $lc = 100$, $lm = 30$, $r = 0.995$.

n	50	100	150	200	250
HACO	5.93	7.2	7.97	8.57	8.99
IHACO	5.87	6.98	7.73	8.39	8.65

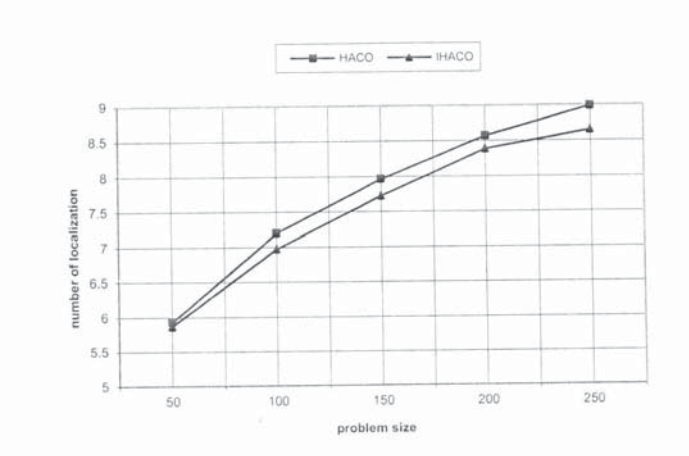

Fig. 4. Average number of localisation sites $q = 0{,}5$, $lc = 100$, $lm = 30$, $r = 0.995$

5. Conclusion

This paper presents a new ant algorithm and, primarily, a new desirability function in the probabilistic formula of site selection. This improvement makes the algorithm more efficient in searching for localisation sites at a minimum cost. Ants in the new elaborated algorithm take into consideration not only new unselected sites from set M, which service as many customers as possible from set N at a minimum cost, but also the already serviced costumers from set N, which can be serviced by these new sites from the M at a lower cost. This strategy makes this new elaborated ant algorithm more efficient than others in searching for a minimum number of facility sites at a minimum cost.

References

[1] Pasricha R., Wadhwa V., *Optimizing facility location problem using genetic algorithm, comparison between ACO algorithms for the set covering problem,* International Journal of Computer Science and Telecommunication, Vol. 2, Issue 3, 2011, 13–15.

[2] Varnamkhasti M.J., *Overview of algorithms for solving the p-median facility location problems, comparison between ACO algorithms,* Advanced studies in biology, Vol. 4, No. 2, 2012, 49–55.

[3] Lessing L., Dumitrescu I., Stutze T., *A comparison between ACO algorithms for the set covering problem,* LNCS, Vol. 3172, 2004, 1–12.

[4] Lghoseiri K., Ghannadpour S.F., *An efficient heuristic method for capacitated p-median problem,* International Journal of Management Science, Vol. 4, 2009, No. 1, 72–80.

[5] Crawford B., Soto R., Momfroy E., Paredes F., Palma W., *A hybrid Ant algorithm for the set covering problem,* International Journal of the Physical Sciences, Vol. 6/19, 2011, 4667–4673.

[6] Antomoshkin A.N., Kazakovtsev L.A., *Random search algorithm for the p-median problem,* Informatica, Vol. 37, 2013, 267–278.

[7] Sevkli M., Mamedsaidov R., Camci F., *A novel discrete particle swarm optimization for p-median problem,* Journal of King Saud University – Engineering Sciences, Vol. 26, 2014, 11–19.

[8] Balas E., Carrera M.C., *A dynamic subgradient-based branch-and-bound procedure for set covering,* Operations Research, Vol. 44/6, 1996, 875–890.

[9] Fisher M.L., Kedia P., *Optimal solution of set covering/partitioning problems using dual heuristics,* Management Science, Vol. 36/6, 1990, 674–688.

[10] Chvatal V., *A greedy heuristic for the set-covering problem,* Oper. Research, Vol. 4/3, 1979, 233–235.

[11] Lan G., Depuy G.W., *On the effectiveness of incorporating randomness into a multi-star -heuristic with application to the set covering problem,* Computer Industrial Engineer., Vol. 51, No. 3, 2006, 362–374.

[12] Cerias S., Nobili P., Sassano A., *A Lagrangian-based heuristic for large-scale set covering problems,* Mathematical Programming, Vol. 81, 1998, 215–228.

[13] Caprara A., Fischetti M., Toth P., *A heuristic method for the set covering problem,* Operations Research, Vol. 47/5, 1999, 730–743.

[14] Chiou Y., Lan L.W., *Genetic clustering algorithms,* European Journal of Operational Research, Vol. 2, No. 132, 2001, 413–427.

[15] Bozkaya B., Zhang J., Erkut E., *An efficient genetic algorithm for the p-median problem,* in Facility Location: Applications and Theory Operations Research, Berlin, Springer, 2002, 179–205.

[16] Alp O., ErkutE., Drezner Z., *An efficient genetic algorithm for the p-median problem,* Annals of Operations Research, Vol. 122, 2003, 21–42.

[17] Lessing L., Dumitrescu I., Stutzle T., *A comparison between ACO algorithms for the set covering problem*, [in:] *Ant Colony Optimization and Swarm Intelligence*, LNCS, Vol. 3172, Springer Verlag, Berlin, 2004, 1–12.
[18] Crawford B., Castro C., *Integrating look ahead and post processing procedures with ACO for solving set partitioning and covering problems*, [in:] *Proc. of the 8th international conference on Artificial Intelligence and Soft Computing*, Springer–Verlag, Berlin, Heidelberg, 2006, 1082–1090.
[19] Lim A., Hu Z., *A fixed-length subset genetic algorithm for the p-median problem*, LNCS, Vol. 2724, Springer Verlag, Berlin, 2003, 1596–1597.
[20] Lorena A.N., Furtado J.C., *A Constructive genetic algorithm for clustering problems*, Evolutionary Computation, Vol. 3, No. 9, 2001, 309–328.

TECHNICAL TRANSACTIONS 1/2018
ENVIRONMENTAL ENGINERING
DOI: 10.4467/2353737XCT.18.009.7960
SUBMISSION OF THE FINAL VERSION: 2/1/2018

Barbara K. Wilk (barbara.k.wilk@gmail.com)
Department of Water and Wastewater technology, Faculty of Civil and Enviromental Engineering, Gdańsk University of Technology

Małgorzata Cimochowicz-Rybicka
Institute of Water Supply and Environmental Protection, Cracow University of Technology

BIOVAC® WASTEWATER TREATMENT PLANTS IN THE MOUNTAIN NATIONAL PARKS

OCZYSZCZALNIE ŚCIEKÓW TYPU BIOVAC® NA TERENACH GÓRSKICH PARKÓW NARODOWYCH

Abstract

This paper presents characteristics of the Biovac® wastewater treatment plants operating in the mountain areas of the Polish national parks (NP): Tatrzanski NP and Babiogórski NP as well as in the West Spitsbergen NP. On the basis of the laboratory tests performed on raw sewage and the final effluent the efficiency of the wastewater treatment plants was evaluated. It was found that high COD values and rather high COD / BOD5 ratios were observed in the raw sewage during an off-peak tourist season. The research has also shown that the Biovac® treatment plants (SBR technology) showed a high level of removal of pollutants from sewage discharged from mountain hostels.

Keywords: sewage treatment, SBR, mountain hostels

Streszczenie

W pracy dokonano charakterystyki wybranych oczyszczalni ścieków typu Biovac®, pracujących na terenach górskich parków narodowych: Tatrzańskiego, Babiogórskiego oraz Zachodniego Spitsbergenu. Na podstawie wykonanych oznaczeń analitycznych ścieków surowych oraz oczyszczonych dokonano oceny efektywności pracy oczyszczalni. Na podstawie wyników badań stwierdzono, że w okresie niskiego ruchu turystycznego w ściekach surowych występują: wysokie wartości wskaźnika ChZT oraz niekorzystny stosunek wartości ChZT/BZT5. Badania wykazały ponadto, że oczyszczalnie typu Biovac®, pracujące w oparciu o technologię SBR, wykazują dużą efektywność usuwania zanieczyszczeń ze ścieków pochodzących ze schronisk górskich.

Słowa kluczowe: oczyszczanie ścieków, SBR, schroniska górskie

1. Introduction

In the mountain national parks, a rapid development of tourism has been observed accompanied by the expansion of the tourist infrastructure [1]. As a result, the mountain hostels generate many different types of waste, including domestic sewage. The sewage generated at national park hostels usually has high concentrations of pollutants due to the rather strict water saving policy enforced in such buildings. The sewage, if not discharged to a wastewater treatment plant, is dumped into the mountain streams or disposed into the ground by a drainage system [2]. It is obvious that poorly treated sewage can be harmful for water [3-4] and land ecosystems in the neighbouring area.

Sewage volumes and pollution loads discharged from such hostels change seasonally, and the specific mountain climate can adversely affect the biological treatment processes. Therefore, wastewater treatment plants must not only work in a very efficient way, but also their operation and maintenance should be trouble free [2–5]. It should also be emphasised that such treatment facilities should have a long-term guarantee of failure-free operation due to the often difficult access to the treatment site. Moreover, the total dimensions of the equipment should be relatively small due to frequent area restrictions. Choosing the proper modern sewage treatment system that would work well both at the tourist peak season and off-season has become a challenge and a problem for engineers [5].

The Biovac® treatment plants (based on SBR technology) may be a good example of wastewater treatment plants that treat sewage from mountain hostels. These have been in operation in two Polish national parks (NP): Tatrzański NP and Babiogórski NP as well as in the West Spitsbergen NP.

Sewage characteristics

The volume and quality of sewage generated in the mountain hostels show a substantial variability on an annual and daily basis [4–8]. The greatest hydraulic stresses for the treatment plant occur during the peak tourist seasons – summer and winter holidays. According to the research conducted by Świerczok and others in 1994 [5], the Samotnia wastewater treatment plant in Karpacz received twelve times more sewage during the peak tourist season than during the off-peak period (1.2 m^3/d compared to 15.1 m^3/d). The above relationship has been also confirmed by Kaczor and others [4], who analysed the sewage volume discharged from the Chochołowska mountain hostel in 2009–2011 (9.0 m^3/d – 58.5 m^3/d, respectively).

The pollution load discharged with sewage from mountain hostels changes due to the seasonal nature of the tourism. According to the literature reports [4–10], the values of BOD_5, COD and pH during the peak tourist season in mountain trails are very close to those found in typical household sewage. By contrast, the values of the total suspended solids (TSS) and total nitrogen (TN) are slightly higher than typical levels, while the values of the total phosphorus (TP) are lower.

Of course, the off-season values of COD, BOD_5, TN and TP are significantly lower than those observed in the peak season. It should be noted that a significant decrease in the organic carbon content in sewage is observed, and consequently, an unfavourable COD/BOD_5 ratio. This negatively affects the treatment processes taking place in biological reactors and can

result in, for example, high COD values in the effluent; it may also disturb other treatment processes, such as phosphorus removal and biological denitrification. An unfavourable COD / BOD_5 ratio in sewage is due to a low water consumption in mountain hostels and a large amount of fats discharged from different restaurants located there [9-14]. It should also be mentioned that daily fluctuations in the sewage volume and the daily changes of pollutant concentrations in raw sewage are more diverse than during the peak tourist season.

Biovac® wastewater treatment plant description

Biovac® technology is based on the activated sludge process taking place in sequencing batch reactors (SBR). SBR technology [9], as an activated sludge option, is used mainly at small municipal wastewater treatment plants and at small domestic applications. The flow chart of the Biovac® wastewater treatment plant is presented below:

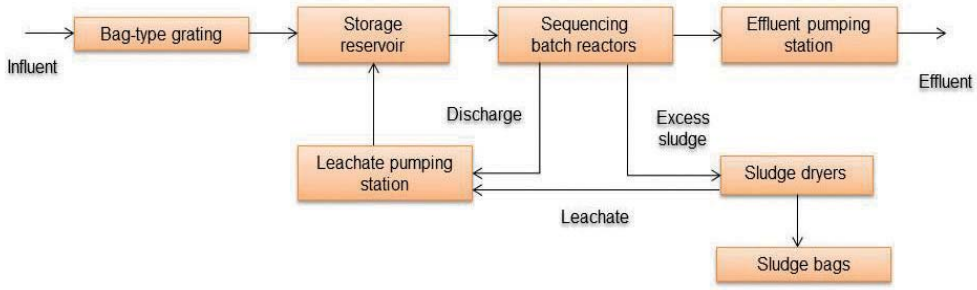

Fig. 1. Flow chart of the Biovac® wastewater treatment plant [10]

Primary treatment

The mechanical (primary) sewage treatment is a stage where solids are removed from sewage. Biovac® plants usually employ basket screens and bag screens, although occasionally fine screens, sieves or screenings and grit separators (combined in a single unit) are used for larger wastewater treatment plants. The basket screen is a coarse screen made of stainless steel. This device is placed directly by the inlet in manholes or pumping stations to which wastewater is carried by pipe. It is guided by rails and has electric or hand hoist. Floating solids of a particular size are caught in the filtering compartment. The basket moves along the rails in vertical direction [10]. After being pulled out of the tank, the basket turns to a position that guarantees automatic unloading of screenings. The separated solids/screenings are transported to a storage tank or to a filter press via a gutter. The bag screen (Fig. 2) is mounted in front of the retention tank. The bag is made of plastic fibres and removes solids of a particular diameter. Similar bags can also be found in agriculture as a packing material for agricultural crops.

The vertical retention tank (Fig. 2) equalises the sewage flow/composition and serves as a buffer during large flow fluctuations. The tank houses submersible pumps that pump sewage to the SBRs.

The pumps transport sewage from the retention tank to the SBR reactors where the cyclic treatment process is carried out. The SBR cycle is comprised of the following phases: filling

Fig. 2. Biovac® wastewater treatment plant at West Spitsbergen a) bag screen , b) retention tank [10]

the reactor with sewage; biological treatment; separation of activated sludge from the effluent; partial effluent discharge; removal of excess sludge; finally, an idle phase. During the treatment process, organic substances and nitrogen and phosphorus compounds are removed from the sewage. The typical durations of the phases in the SBR cycle used in the Biovac® wastewater treatment plants are shown in Table 1. These can be changed by the plant operator.

Table 1. Biovac® treatment process parameters [10]

Phase	**1. Fill**	**2. Nitrification**	**3. Mixing**	**4. Idle**
Time (min.)	5	180	0.17	4
Phase	**5. Denitrification**	**6. Settling**	**7. Sludge removal**	**8. Effluent discharge**
Time (min.)	40	100	0.5	25

The reactors are equipped with aeration systems that ensure the simultaneous aeration and mixing of the reactor volume (provided by disc diffusers). Compressed air is supplied using blowers. Two independent reactors are connected by a drainage system and a valve system; in this way, it is possible to transfer the activated sludge from one reactor that has finished its operation to another one that is starting.

Sludge processing

Excess sludge is directed to an aerobic stabilisation tank in which a cyclic aeration takes place via disc diffusers and a blower. After aerobic stabilisation, sludge becomes a stable product that can be stored without risk of odour. The stabilisation process also results in the partial or complete removal of pathogenic microorganisms [10–13]. The stabilised sludge is discharged to the dewatering units and subsequently dried in sludge dryers (Fig. 3).

Sludge presses or centrifuges are used for the mechanical dewatering of sludge at larger wastewater treatment plants. Centrifuges (working in a batch or in continuous mode) separate the solids from the liquid with gravitational and centrifugal forces while filter presses, squeeze water out of the sludge [14–16].

Fig. 3. Sludge processing at the Biovac® wastewater treatment plant [10]

The wastewater treatment plant at West Spitsbergen (Polish Polar Station)

In August 2001, the Biovac® wastewater treatment plant with a capacity of 10 m^3/d was launched at Spitsbergen. The new wastewater treatment plant replaced the rotating biological contactors (RBC), which had been in operation there since 1985 [10]. The following diagram shows the current sewage treatment technology.

The SBR-type treatment plant at Spitsbergen treats mostly domestic sewage comprising toilet waste, food waste, surfactants, toilet paper, fats and detergents. The sewage composition shows high levels of phosphorus, nitrogen, and the presence of coliforms. The sewage composition is also influenced by the chemical laboratory located at the station where various types of chemical analyses are carried out over the year (mainly chemical analyzes of surface waters and rainwater) [10].

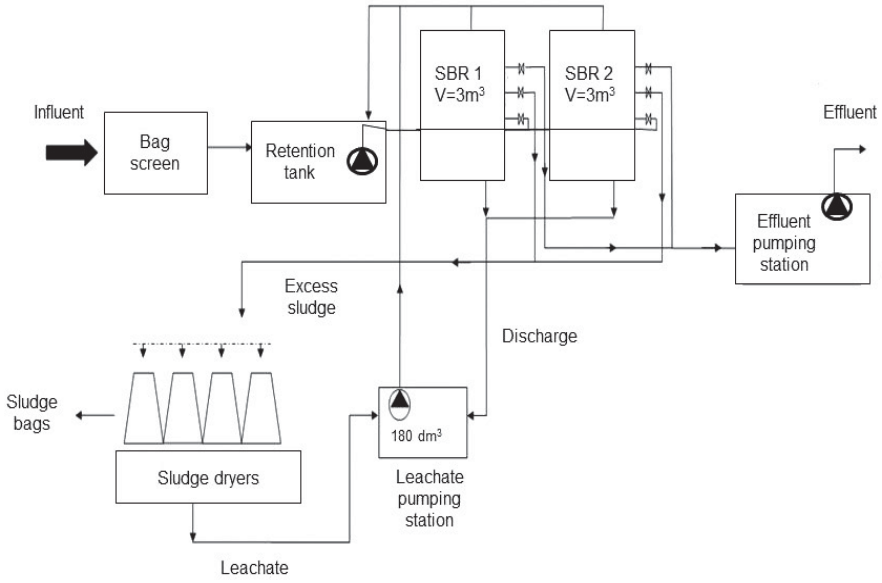

Fig. 4. Flow chart of the West Spitsbergen wastewater treatment plant [10]

Wastewater treatment plant at the Murowaniec mountain refuge

According to the work of Siwek J. et al. [2], the Murowaniec hostel discharged large amounts of NH_4^+ and PO_4^- to the Sucha Woda creek in the years 2008-2009 (the highest concentrations were reported during the summer holidays). Since a new wastewater treatment plant started its operation in 2011, the situation has significantly improved [2]. Figure 5 shows a flow chart of the new Murowaniec wastewater treatment plant.

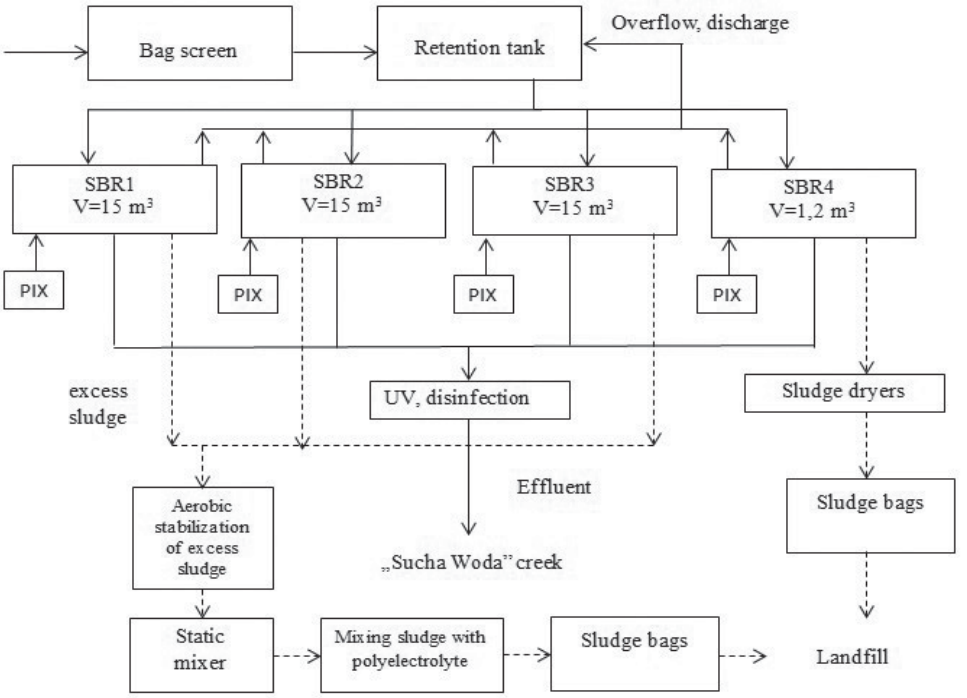

Fig. 5. Flow chart of the Murowaniec wastewater treatment plant [10]

The plant treats domestic sewage. The hostel has 116 beds and a restaurant. The wastewater treatment plant effluent is discharged into the Sucha Woda creek (13 + 800 km of the Cicha Woda creek).

Wastewater treatment plant at the Dolina 5 Stawów mountain refuge

Until 2010, the Dolina 5 Stawow hostel did not have a wastewater treatment plant. Raw sewage was discharged to the Litwor's gully and then to the Roztoka creek [2]. According to Siwek J. et al., the pollution accumulated over many years in crust of the Litwor's gully will continue to affect surrounding water ecosystems for a long time. Since 2010, the sewage from the Dolina 5 Stawów hostel has been treated by the Biovac® wastewater treatment plant. The process flow of the plant is shown below.

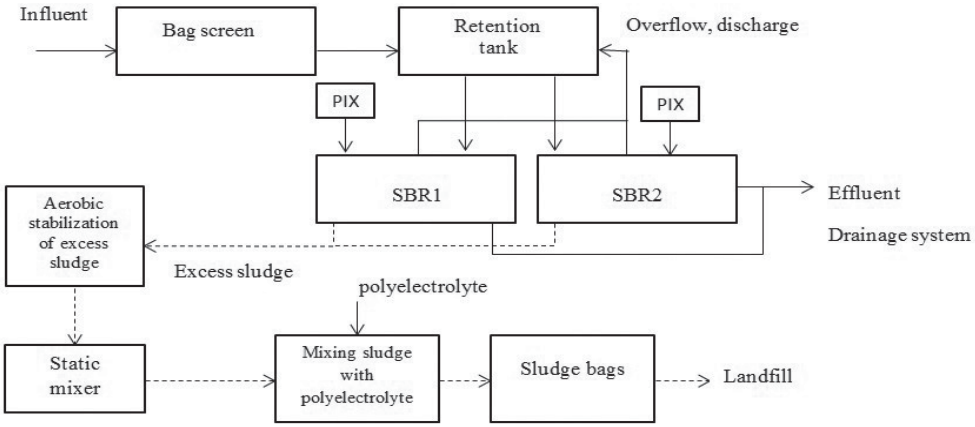

Fig. 6. Flow chart of the Dolina 5 Stawów wastewater treatment plant [10]

The plant treats domestic sewage. The mountain refuge has 67 beds and a restaurant.

Wastewater treatment plant at the Markowe Szczawiny

The Biovac® wastewater treatment plant has been treating sewage from the hostel at Markowe Szczawiny since 1995. Figure 7 shows a flow chart of the current treatment process.

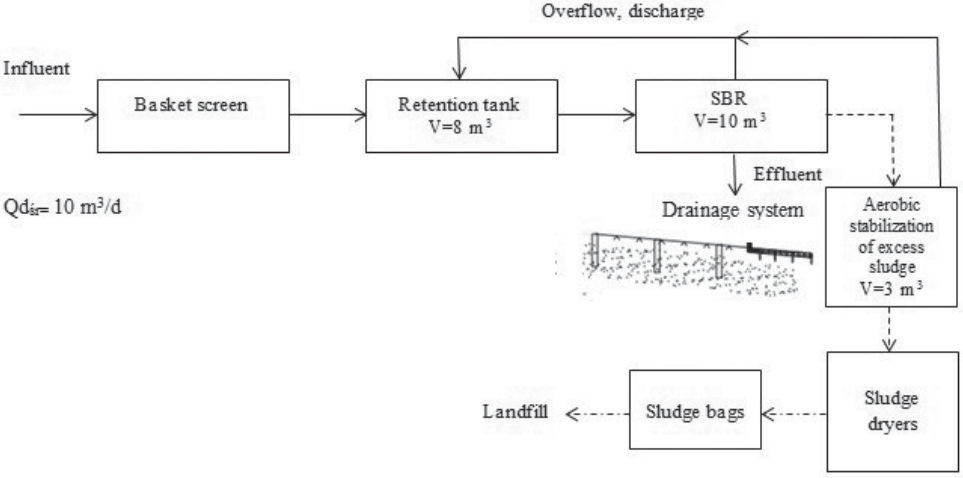

Fig. 7. Flow chart of the Markowe Szczawiny wastewater treatment plant [10]

The plant treats domestic sewage. The hostel has 72 beds and a restaurant.

2. Materials and Methods

The main goal of the research was to determine the efficiency of the Biovac® wastewater treatment plants located in the mountainous areas of national parks at: West Spitsbergen with

a capacity of 10 m^3/d (Spitsbergen NP); the Murowaniec hostel with a capacity of 35 m^3/d (Tatra NP); the Dolina 5 Stawów hostel of a capacity of 10 m^3 /d (Tatra NP); the Markowe Szczawiny hostel (Babiogórski NP). Two sewage quality parameters were analysed – BOD_5 and COD. Based on their values, the efficiency of the biological treatment process was determined. All samples were taken in an off-season period.

Wastewater treatment plants located at the Murowaniec mountain refuge, the Dolina 5 Stawów mountain refuge and the Markowe Szczawiny mountain refuge

The characteristics of the raw sewage and the plant effluent were determined on the basis of time-proportional composite samples collected daily. The analyses were carried out by the certified laboratory in October 2016 (Murowaniec and Markowe Szczawiny hostels) and in November 2016 (Dolina 5 Stawow hostel). The raw sewage samples were collected from raw sewage sampling tanks, while the effluent samples were taken from the effluent sampling tanks. COD tests were carried out according to PN-ISO 6060:2006, while BOD_5 were performed according to PN EN 1899-1:2002 and PN-EN ISO 5814:2013 – 04E.

Wastewater treatment plant at West Spitsbergen

All samples were taken in the end of September. Raw sewage samples were collected downstream from the bag screen while the effluent samples were collected at the point of the effluent discharge from the treatment plant. The sewage samples were kept frozen for a week at the polar station. The samples were then transferred to a freezer located on a ship where they were kept in the dark for seven days. The BOD_5 measurements for raw sewage and the effluent (made in 2009) remained in the range of 0–400 mg O_2/dm^3 and 0–40 mg O_2/dm^3, respectively. The samples were stored and stirred for five days at 20°C in a thermostat cabinet. After this period, the BOD_5 value was read using the Oxi Top Control; this method provides a manometric, mercury-free BOD_5 measurement. COD was analysed using the bichromatic method with couvettes. The measuring range for both raw sewage and the effluent was 100–1500 mg/dm^3, the reaction time was 2 h and the process temperature in thermostat was 148°C.

3. Results and analysis

According to the studies, the average COD values in raw sewage at the wastewater treatment plants were as follows: Markowe Szczawiny, 3790 mg/dm^3; Murowaniec, 920 mg/dm^3; Dolina 5 Stawów, 1298 mg/dm^3; West Spitsbergen, 2301 mg/dm^3. The values were much higher than those found in typical domestic sewage.

The following average values of COD were observed in the effluent: Markowe Szczawiny, 106 mg/dm^3; Murowaniec, 77 mg/dm^3; Dolina 5 Stawów, 58 mg/dm^3; West Spitsbergen, 1288 mg/dm^3. The average COD removal efficiency was as follows: Markowe Szczawiny, 97%; Murowaniec, 92%; Dolina 5 Stawów, 95%; West Spitsbergen, 44%.

The average BOD_5 concentrations in raw sewage at mountain hostels were as follows: Markowe Szczawiny, 1500 mg/dm^3; Murowaniec, 310 mg/dm^3; Dolina 5 Stawów, 337 mg/dm^3;

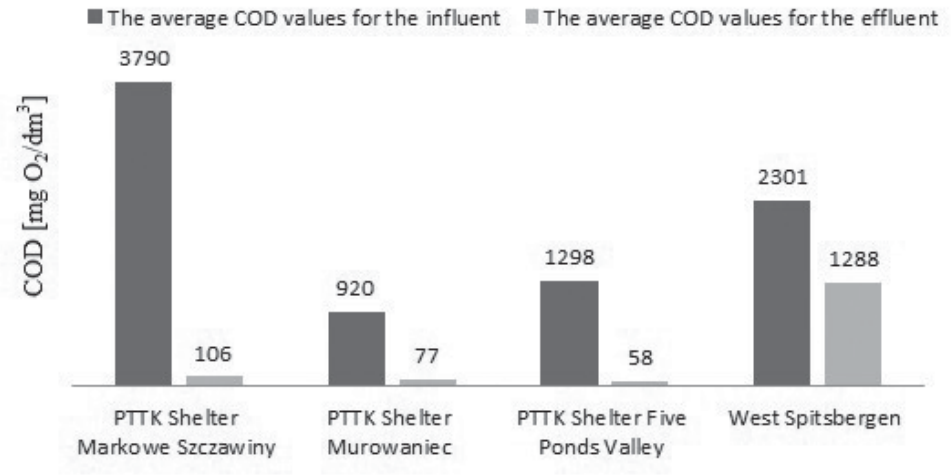

Fig. 8. COD in raw sewage and the effluent from the wastewater treatment plants located in the mountain hostels

the BOD concentrations in raw sewage from the Spitsbergen Polar Station were not determined since the samples were diluted before the BOD_5 analysis to match the expected content of organic compounds subject to biochemical oxidation. However, the dilution ratio turned out to be wrong since the BOD values were significantly higher than expected. Due to the fact that only a limited amount of the raw sewage was available, the BOD_5 analysis could not be repeated.

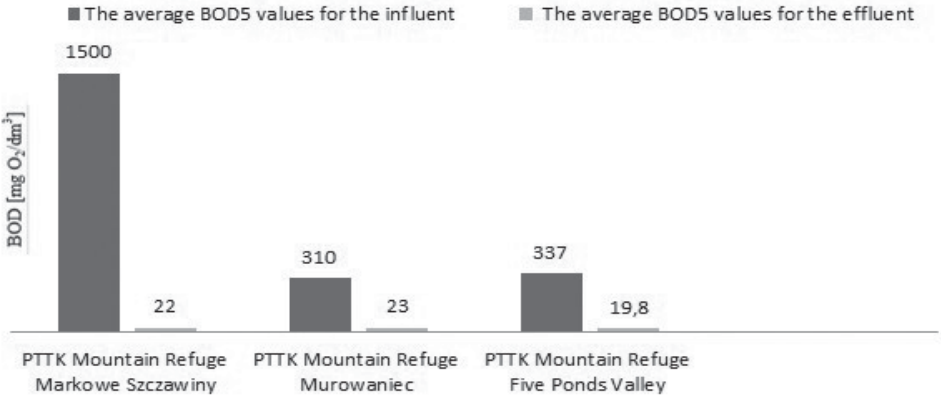

Fig. 9. BOD_5 in the raw sewage and in the effluent from the mountain hostels

The average BOD_5 concentrations in the effluent from the wastewater treatment plants were as follows: Markowe Szczawiny, 22 mg/dm^3; Murowaniec, 23 mg/dm^3; Dolina 5 Stawów, 19.8 mg/dm^3; a Polish polar station at West Spitsbergen, 500 mg/dm^3.

The average BOD_5 removal was: Markowe Szczawiny, 79%; Murowaniec, 92%; Dolina 5 Stawów, 96%.

Both raw sewage and the effluent samples were collected during an off-season period. Rather high values of the COD/BOD_5 ratio were observed in raw sewage – these were: 2.5 for Markowe Szczawiny; 2.9 for Murowaniec; 3.5 for Dolina 5 Stawów; 4.6 for West Spitsbergen. According to the literature, sewage may be successfully treated with activated sludge when the COD/BOD_5 values are less than or equal to 2.2 [4]. Such high values of COD as those observed during the research study are mostly due to the fact that the hostels impose a strict water-saving regime. The value of this parameter is also influenced by the restaurant's activity (high fat content) and the kitchen sink grinders used in most hostels.

4. Conclusion

On the basis of the study, the following conclusions have been made:

- the average BOD_5 reduction observed at sewage treatment plants located in the Polish national parks was very high and ranged from 94 % to 99 %;
- the average COD_{Cr} reduction observed at sewage treatment plants located in the Polish national parks ranged from 92% to 97%, and confirmed a very high level of efficiency of the tested sewage treatment plants;
- unfortunately, the lack of the accurate BOD_5 values in the effluent from the Spitsbergen sewage treatment plant makes it impossible to assess the efficiency of the biological treatment process. It is possible, however, to determine that the sewage treatment plan is not working correctly. This is because effluent BOD_5 average values were 500 mgO_2/dm^3 .The average COD removal at this plant was low and reached only 44%. The reasons behind such a poor performance of the sewage treatment plant included the specific climate of West Spitsbergen, and incorrect procedures of sampling and sample storage before analysis;
- raw sewage samples collected off-season showed high COD/BOD_5 ratios, this can seriously disrupt the biological treatment of sewage using activated sludge.

References

[1] Myga-Piątek U., Jankowski G., *Tourism impact on the national environment and cultural landscape. Analysis of chosen examples of highlands*, Problemy Ekologii Krajobrazu, XXV/2009, 27–38.

[2] Siwek J. P., Biernacki W., *Wpływ* ścieków odprowadzanych ze schronisk turystycznych na stężenie związków biogennych w potokach – odbiornikach tych ścieków na terenie Tatrzańskiego Parku *Narodowego (lata 2008–2009)*, Gospodarka Wodna, 7/2016, 201–209.

[3] Wilk B., *Ultrafiltration membranes made of: polyaniline, ionic liquid and cellulose*, Technical Transactions, 1-Ś/2016, 171–187.

[4] Kaczor G., Bergel T., Bugajski P., Pijanowski J., *Aspects of Sewage Disposal from Tourist Facilities in National Parks and Other Protected Areas*, Polish Journal of Environmental Studies, 24(1)/2015, 107–114.
[5] Świerczok R., Łukawska R., Włodyga J., *Oczyszczanie ścieków z obiektów turystycznych na przykładzie schroniska „Samotnia" w Karpaczu*, Ochrona Środowiska, 1(56)/1995, 41–43.
[6] Mucha Z, Mucha M., *Zastosowanie reaktorów z osadem czynnym o działaniu cyklicznym w gminnych oczyszczalniach ścieków*, Rynek Instalacyjny, 12/2016, 75–78.
[7] Weissenbacher N., Mayr E., Niederberger T., Aschauer C., Lebersorger S., Steinbacher G., Haberl R., *Alpine infrastructure in Central Europe: integral evaluation of wastewater treatment systems at mountain refuges*, Water Science & Technology – WST, 57.12/2008, 2017–2022.
[8] Maunoir S., Philip H., Rambaud A., *Small wastewater treatment plants in mountain areas: combination of septic tank and biological filter*, Water Science & Technology, 56(10)/2007, 65–71.
[9] Mucha Z., Wójcik W, *Investment costs of small wastewater treatment plants with SBR reactors in Poland*, Ekonomia i Środowisko, 1(52)/2015, 124–130.
[10] "Bionor" informational materials, Kielce 2017, http://www.bionor.pl (access: 07.2017).
[11] Al-Rekabi W.S., Qiang H., Qiang W.W., *Review on sequencing batch reactors*, Pakistan Journal of Nutrition RG Impact & Description, 6(1)/2007, 11–9
[12] Govindassamy V., Raman S., Sundararajan T., *Influence of Nitrogen Residue on the Performance of Sequencing Batch Reactor (SBR) in Wastewater Treatment – A Review*, International Journal of Environmental Monitoring and Protection, 1(3)/2016, 1–16.
[13] Anielak A. M., *Unconventional methods of biogenic substance removal in sequencing batch reactors*, Gaz, woda i technika sanitarna, 2/2006, 23–27.
[14] Dionisi D., Rashed A.A.,Majumder A., *A new method to calculate the periodic steady state of sequencing batch reactors for biological wastewater treatment: Model development and applications*, Journal of Environmental Chemical Engineering, 4 (3)/2016, 3665–3680.
[15] Marzec M., Jóźwiakowski K., Gizińska M., Pytka A. *Problems of operation and effects of pollution removal in wastewater treatment plants such Biovac®*, Gaz, Woda i Technika Sanitarna, 2/2012, 85–87.
[16] Fudala-Ksiazek S., Luczkiewicz A., Kulbat E., Jankowska K., Czerwionka K., Quant B., Olanczuk-Neyman K., *Combined treatment of landfill leachates with wastewater in a sequencing batch reactor (SBR)*, In: Gidarakos E., Cossu R., Stegmann R. (Eds.), Crete 2010 – 2nd International Conference on "Hazardous and Industrial Waste Management", 5–8 October, 457–459.

TECHNICAL TRANSACTIONS 1/2018
ENVIRONMENTAL ENGINERING
DOI: 10.4467/2353737XCT.18.010.7961
SUBMISSION OF THE FINAL VERSION: 5/1/2018

Andrzej Kotowski (andrzej.kotowski@pwr.edu.pl)
Monika Nowakowska (monika.nowakowska@pwr.edu.pl)
Department of Water and Sewage, Faculty of Environmental Engineering, Wrocław University of Science and Technology

Standards for the dimensioning and assessment of reliable operations of area drainage systems under conditions of climate change

Standardy wymiarowania i oceny niezawodności działania systemów odwodnień terenów w warunkach zmian klimatu

Abstract

Contemporary area drainage dimensioning standards are presented in this paper. Hazards for drainage systems arising from climate changes are discussed and trends of changes in the precipitation structure are presented using the example of data obtained from Wrocław. The need for changes within precipitation scenarios is indicated for modelling overflow in channels and a research methodology and assessment criteria of the degree of reliability of the drainage system are proposed. Results are presented of an analysis of the operation of the rainwater drainage system in the Gaj and Tarnogaj housing estates in Wrocław – these were conducted using a calibrated hydrodynamic model in SWMM software. It was proved that the examined system does not meet the standards of PN-EN 752:2008, DWA-A 118:2006 and Merkblatt no. 4.3/3:2009 with regard to instances of flooding from channels and that adaptation to climate change is required.

Keywords: urban hydrology, storm water drainage, dimensioning, modelling, overflow, flooding from channels

Streszczenie

Przedstawiono współczesne standardy wymiarowania odwodnień terenów. Omówiono zagrożenia dla systemów kanalizacyjnych wynikające ze zmian klimatu i zaprezentowano trendy zmian w strukturze opadów, na przykładzie danych z Wrocławia. Wskazano na potrzebę zmiany scenariuszy opadów do modelowania nadpiętrzeń w kanałach oraz zaproponowano metodykę badań i kryteria ocen stopnia niezawodności kanalizacji. Przedstawiono wyniki analizy działania kanalizacji deszczowej na osiedlach Gaj i Tarnogaj we Wrocławiu, przeprowadzonej na skalibrowanym modelu hydrodynamicznym w programie SWMM. Wykazano, że badany system nie spełnienia standardów PN-EN 752:2008, DWA-A 118:2006 i Merkblatt Nr. 4.3/3:2009 odnośnie wylewów z kanałów i wymaga dostosowania do zmian klimatu.

Słowa kluczowe: hydrologia miejska, kanalizacja deszczowa, wymiarowanie, modelowanie, nadpiętrzenia, wylewy z kanałów

1. Introduction

In Poland, like in other countries in Europe and in the world, changes to the climate are observable – these manifest themselves in, for example, the growing intensity of precipitations and the frequency of the occurrence of extreme events such as urban floods in the form of flooding from channels [1]. The reason for climate warming (the so-called greenhouse effect caused by, among other factors, the emission of steam and CO_2 to the atmosphere) has not been completely identified and still remains a matter of disagreement. Unquestionably still, the observed increase in air temperature significantly affects the circulation of water in the hydrological cycle: vaporisation – condensation – precipitation. According to the report by the Intergovernmental Panel on Climate Change (IPCC: 2007) [2], in the period 1960-2005 alone, the average annual temperature increase was 0.74°C. As a result, over the period 1901-2010, the levels of seas and oceans rose by an average of 0.19 m (IPCC: 2014) [3]. According to forecasts based on the global climate model, the air temperature may rise by anything from 1.7°C to as much as 4.4 °C this century, and each degree of temperature increase is expected to be accompanied by a global growth in precipitation intensity by approximately 7% [4]. In central European countries, for instance, catastrophic flooding will occur more frequently than once every 50 years on average [5].

Floods threaten most Polish cities which are located in river valleys (river floods) and in the coastal zone (storm floods). On the other hand, local area flooding (urban floods) may occur everywhere, most often as a result of sudden convective precipitation, a long-lasing front or low-pressure rainfall. This is exacerbated by a large density of urban development and a large sealed surface area – this leads to a significant limitation in rainfall water infiltration to the ground. Hazards and losses generated by urban floods are manifested by local flooding from rain channels or combined sewers (flooding of streets, estates and basements – Fig. 1), as a consequence of, among other factors, an inadequate flow capacity and a lack of retention in the existing drainage systems [6].

Fig. 1. Urban floods [6]

A considerable proportion of rainfall water drainage systems built in Poland after World War II have been dimensioned with methods that are unsuitable in the present day (MGN and MSN), using the out-dated Błaszczyk formula for rain intensity (based on precipitation from

the turn of the 19th and 20th centuries), which makes them unlikely to fulfil the requirements of the most recent standard PN-EN 752:2008 [7] with regard to acceptable frequency of flooding from channels, especially in the future. This generates a need to examine the degree of hydraulic reliability of systems which have been dimensioned in such a manner in hydrodynamic modelling and undertake the appropriate remedial actions, such as those suggested in this paper.

2. Contemporary dimensioning standards for urbanised area drainage

The risk of the occurrence of phenomena with unfavourable consequences is defined as a combination of the probability of occurrence and measurement of their adverse effects. Under conditions of climatic change, anticipating the risk of hazards from flooding from channels is vital for rational water management in cities. It especially applies to the basis for dimensioning drainage systems for urbanised areas, i.e. rainwater drainage or combined drainage [6, 8]. According to the Act of 12 September 2002 on standardisation, Polish (PN) and international standards (EN and ISO) should be regarded, as compare to current technical design guidelines (WTP) or published results of the most recent research works (e.g. with regard to drainage system dimensioning methods). The present legal condition puts a greater responsibility on the designers, including the obligation to design safely, i.e. in accordance with the art of construction resulting from the best available technical knowledge: BAT – *Best Available Techniques*; BMP – *Best Management Practices*; LID – *Law Impact Development*; ZWT – *Principles of Technical Knowledge*.

It is, however, not possible to ensure fully reliable area-drainage operations owing to the stochastic nature of precipitation. We can only aim to dimension them safely, i.e. adjust the systems to accept the maximum forecasted rainfall water streams, with frequency of incidence equal to the acceptable frequency of the occurrence of flooding onto the area surface. This also applies to future drainage basin loads resulting from precipitation exacerbated by climate change. The Polish standard PN-EN 752:2008 limits the acceptable frequency of flooding from the drainage system to rare frequencies of incidence (Table 1). Thus, this is a type of 'social

Table 1. Frequencies of calculated rain and acceptable frequencies of flooding from channels according to PN-EN 752:2008

Location	Frequencies of:	
	precipitation	floodings
	[1 in *C* years]	
rural areas	1 per 1	1 per 10
residential areas	1 per 2	1 per 20
city centres, services and industrial areas	1 per 5	1 per 30
underground transport facilities, passages and crossings under streets, etc.	1 per 10	1 per 50

contract' for obligatory compliance. On the other hand, for drainage system dimensioning, it accepts the adoption of smaller values of the calculated frequencies of precipitation; however, no overload may then occur in the operation of the systems, e.g. work under pressure. This generates a need to select channels for incomplete filling, i.e. with a flow capacity reserve in case of less frequent rains. According to PN-EN 752:2008 the recommended frequency of calculated rain is a facultative.

However, determination of the relationship between the frequency of calculated rain and the frequency of flooding is not possible, especially when the drainage system is only at the design stage. Reliability of operation of drainage systems may thus be examined only by means of hydrodynamic modelling. To determine the degree of reliability of the drainage system, the DWA-A 118:2006 [9] guidelines are of help by introducing the notion of frequency of overflow under the ground level for verifying calculations by means of modelling. As a result, it is possible to determine the overload condition which is closest to potentially flooding occurring later (Table 2).

Table 2. Acceptable frequencies of overflow for verifying calculations of the newly designed or modernised drainage systems according to DWA-A 118:2006

Location	**Frequency of overflows [1 in *C* years]**
rural areas	1 per 2
residential areas	1 per 3
city centres, services and industrial areas	less frequently than 1 per 5
underground transport facilities, passages and crossings under streets, etc.	less frequently than 1 per 10

The idea of complete water drainage of urbanised areas is presently being abandoned in Europe, i.e. carrying away all rainfall waters (rain and thaw waters) to rain drainage or combined drainage systems in favour of draining only water originating from contaminated sealed surfaces (after initial treatment). In accordance with the principle of sustainable development, proper water management in urbanised areas should mainly consist of the management of as much a volume of 'clean' rainfall waters as possible, so as to decrease and delay surface water run-off to receivers, and prevent reduction in the levels of underground waters in cities. This is achieved with the use of retention, infiltration and evapotranspiration processes, in such structures as: storage-infiltration reservoirs, natural terrain basins or the recently promoted so-called green roofs [10-13]. At the same time, excessive sealing of area surfaces should generally be avoided, for example, openwork sealing should be used. When dimensioning new rain channels, their minimum diameter should be increased from the presently required D_{min} = 0.30 m to 0.40 m – according to work [6]. Similarly, it becomes necessary to increase the number of street inlets for rainfall, and thus reduce their spacing from the presently recommended ≤ 30 m to ≤ 20 m – depending on the road class and longitudinal and transverse slopes of the roadway – on the basis of research by Edel & Suligowski [14]. These and other remedies shall prove effective in the future.

3. Trends of changes in the frequency of occurrence of intensive precipitation

Drainage systems reliability tests, recommended by standard PN-EN 752 from 2008 are rarely conducted in Poland – these are even required by the law according to the Regulation of the Minister of Environment of 2014 with regard to the verification of the frequency of the operation of storm overflows (in cities with RLM>100000). The reason for this failure to conduct the reliability tests stems mainly from the absence of relevant input databases (monitoring of precipitation and flows in the network) and an insufficient methodological basis for the tests. Therefore, it is of worth to improve the tools for the mathematical modelling of area drainage systems on the basis of local databases obtained through monitoring [15, 16].

Referring to precipitation as reference precipitation for the design and modelling of the operation of area drainage – according to contemporary standards PN-EN752:2008 (Table 1) and DWA-A118:2006 (Table 2), growth is forecast in their intensity in the future as a result of climate changes. The basis for the assessment of the future hazards is thus the selection of appropriate scenarios – relating to the frequency of precipitation with regard to the present patterns, such as: IDF (*Intensity-Duration Frequency*) or DDF (*Depth-Duration Frequency*). Probability models of maximum precipitation are applied here, e.g. the Bogdanowicz – Stachý model, which was established on the basis of Polish national rain measurements for 20 IMGW meteorological stations in the period 1960-1990 [17]:

$$h_{max} = 1.42t^{0.33} + \alpha(R, t)\cdot(-\ln p)^{0.584} \quad (1)$$

where:
h_{max} – maximum precipitation amount (mm);
t – rain duration: $t \in [5; 4320]$ (min);
p – probability of precipitation elevation: $p = 1/C \in (0; 0.5]$ (-);
α – scale parameter dependent on the region of Poland (R) and rainfall duration (t).

In Poland, due to climatic warming, the structure of regional precipitation is projected to substantially change for the period 2071-2100, taking the years 1951-2009 as the starting measurement period – according to the monograph [18]. These changes will manifest themselves, among other ways, in the fact that short (single) intensive rainfall will be subject to rearrangement into longer episodes that may even last a few days with the total amount of precipitation being much higher than before. Because of the systematic increase in air temperature, more extreme rainfall phenomena will occur in the future – this will cause even greater economic and social losses than now. Since drainage systems are usually built with the life perspective of a minimum of 50-100 years, consideration for these forecasts is vital today in order to safely dimension such systems for the future [6].

Considering the present state of knowledge about change of precipitation trends until 2100, should be made by correcting intensity curves (IDF) – for the present frequency of incidence, or changing the frequency of incidence of precipitation in the future – for the present intensities (Table 1 & 2) [19–21]. Staufer et al. [21] suggested adjustment in the

frequency of precipitation currently adopted for the verification of overflow and flooding according to standard DWA-A118:2006 – this is presented in Table 3.

Table 3. Adjustments to DWA-A118:2006 with regard to precipitation scenarios for the identification of future drainage system overload according to Merkblatt No. 4.3/3:2009

Location	Frequency of precipitation for simulation of:	
	overflow	flooding
	[once every *C* years]	
rural areas	3 instead of 2	50 instead of 10
residential areas	5 instead of 3	100 instead of 20
city centres, services and industrial areas	10 instead of 5	100 instead of 30

For instance, for residential areas, Staufer et al. suggested a precipitation scenario of $C = 5$ years (instead of $C = 3$ years according to Table 2) for verification of the presence of future overflow, and a precipitation scenario of $C = 100$ years to provide an acceptable frequency of flooding once every 20 years (according to Table 1). Based on this, the Land Office for Bavaria Environment issued a recommendation (Merkblatt no. 4.3/3:2009 [22]) with regard to changes in the frequency of precipitation for the identification of future overloads in the drainage system (Table 3).

Further research concerning scenarios of growing precipitation intensity in the future is necessary [23–25]. For instance, in the work [25], in order to examine local trends of changes in the frequency of the occurrence of intensive precipitation in Wrocław, the analysis covered precipitation amounts time series from the last five decades (1960-2009), in 16-time intervals of duration $t \in [5, 4320]$ in minutes. The data came from IMGW-PIB Wrocław-Strachowice meteorological station. To conduct the tests, a local probabilistic model of maximum precipitation was used [26, 27]:

$$h_{\max}(t,p) = -4.58 + 7.41t^{0.242} + \left(97.1t^{0.0222} - 98.7\right)\left(-\ln p\right)^{0.809} \tag{2}$$

on the basis of which, threshold values of the ranges of the precipitation levels were calculated for the frequency of incidence: from once a year to once every 10 years. The maximum measured ranges of precipitation levels were then grouped into 4 classes of frequency of incidence with precipitation elevation, i.e.: $C \geq 1$ ($p \leq 1$), $C \geq 2$ ($p \leq 0.5$), $C \geq 5$ ($p \leq 0.2$) and $C \geq 10$ years ($p \leq 0.1$). The examined trends of changes, described by linear regression, are specified in Table 4.

It seems from the conducted studies that a growing trend occurred in the period 1960–2009 in the amount of precipitation in 4 classes of the designed frequencies. Growth trends determined for the frequency of the occurrence of precipitation $C \geq 5$ years and $C \geq 10$ years (Table 4, Fig. 2) are statistically reliable.

Table 4. Trends of changes in maximum precipitation amount in Wrocław in the period 1960–2009

Frequency of precipitation	Number of items of data	*a*	*b*	Value of test F	Level of significance, %
$C \geq 1$ year	804	33.0	0.0534	1.05	69
$C \geq 2$ years	397	37.7	0.0986	1.31	75
$C \geq 5$ years	198	37.3	0.323	5.43	98
$C \geq 10$ years	108	38.2	0.524	6.63	99

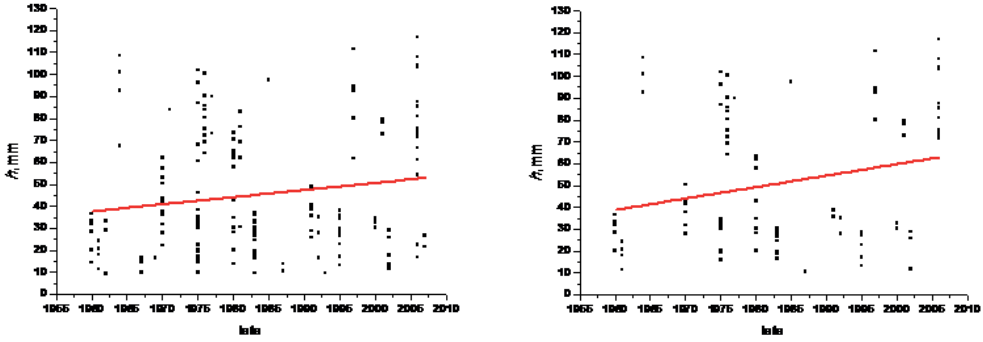

Fig. 2. Trends of changes in the range of precipitation levels for the frequency of incidence $C \geq 5$ years (on the left) and $C \geq 10$ years (on the right) in Wrocław in the period 1960–2009

The growth trends of changes in the frequency of the occurrence of intensive precipitation as observed in Wrocław are confirmed in monograph [18], where, on the basis of the climate model of Europe HadRM3-PRECIS and SRES A2 and B2 scenarios, likely precipitation intensity changes in Poland were determined for the time period 2071–2100, starting from the similar measurement period of 1951–2009. This suggests a need for changes in the frequency of precipitation, which is currently adopted as reference precipitation for the dimensioning and verification of drainage system overloads in Poland which are induced by climate change.

With calibrated hydrodynamic models of area drainage systems, in order to accommodate their expansion or modernisation, the frequency of precipitation should be changed in DWA-A118:2006 to simulate the incidence of overflow, so as to ensure that they reflect the likely overload of the channels in the future. Specifically, it is suggested to check overflows for the present rains with frequencies of incidence: $C = 3, 5, 10$ years (dependent upon the type of land development) – according to the recommendations of Merkblatt no. 4.3/3:2009 provided in Table 3. Supplementing these recommendations – for underground transport facilities, passages and crossings under streets, etc., due to the effects of hazards, it is recommended to adopt $C \geq 50$ years according to [6].

Assuming a similar reasoning logic, in the case of no possibility to simulation of flooding from rain channels, eg in the of designing new drainage systems, the frequencies of rain (recommended by PN-EN 752:2008), should be increased accordingly – to the preserve in the future the acceptable frequency of incidence of flooding from channels. Proposed changes in PN-EN 752:2008 for facultative use are specified in Table 5, on the basis of paper [6].

Table 5. The proposed changes to PN-EN 752:2008 with regard to the frequencies of calculated rain in the case of no possibility to simulate flooding from channels [6]

Location	Frequencies of precipitation
	[1 in *C* years]
rural areas	2 instead of 1
residential areas	5 instead of 2
city centres, services and industrial areas	10 instead of 5
underground transport facilities, passages and crossings under streets, etc.	50 instead of 10

4. Standards for the testing and assessment of the reliability of drainage systems

The first stage in the identification of overloads of channels in the future should be the simulation of the operation of the existing or the newly-designed drainage system with regard to overflow. For instance, for urban drainage areas in the vicinity of residential buildings (total area $F > 2$ km^2), in accordance with the previous recommendations of DWA-A118:2006 (Table 2), it was recommended to load rain channels with precipitation with a frequency of incidence of $C = 3$ years and a duration at least twice as long as the time of flow in the network. Currently, according to Merkblatt no. 4.3/3:2009 (Table 3), it is recommended that simulations should relate to future drainage system load scenarios. For residential drainage areas, these are today's precipitations with the frequency of incidence of $C = 5$ years for the verification of overflow and $C = 100$ years to provide an acceptable frequency of floodings in the future according to PN-EN 752:2008 (Table 1). After assessment of the results of such simulations, a need may be observed for system adaptation in accordance with the forecasted growth of rainfall water runoff in streams in the future.

Reference parameters to demonstrate the need to adjust a given drainage system to climate changes may be, for example, the degree of flooding (*DF*) and the specific flood volume (*SFV*) [28]. *DF* ratio is the ratio of the number of wells flooded to the land surface level (N_f) to the general number of wells (N) of a given system or its mutually related parts:

$$DF = \sum N_f / \sum N \tag{3}$$

SFV ratio (in m^3/ha) results from the calculated volume of flooding from channels V (in m^3) in relation to the sealed surface (F_s) of a given basin (in ha):

$$SFV = \sum V / \sum F_s \tag{4}$$

Threshold values of *DF* and *SFV* ratios should be individually agreed for a given system. For example, results of the assessment of the reliable operation of three drainage systems in North Rhine-Westphalia are specified in the work [28]. The examined drainage basins were located inside urban areas or city centres. To simulate overflow and flooding, precipitation with a frequency of incidence of C = 5 years and extreme precipitation with a frequency of C = 100 years has been adopted as the load of the channels. Based on this, threshold values were determined: DF = 0.33 and SFV = 13 m^3/ha. Above of those values, systems already require of modernization. In the event of local system overloads being identified (according to the scenarios from Table 3), further risk analysis is necessary [29]. This can be made on the basis of GIS and/or in-situ assessments [30], and in the case of observing extensive overloads, additional simulation of the system operation becomes necessary in combination with a digital land model. A detailed analysis of the simulation results allows not only the marking out of flood land boundaries, but also specifying the depth of water, stream speed and water flow volume.

The suitability of the presented reliability testing methodology has been verified in the conditions of Wrocław in works [31–33]. For instance, the PhD thesis [33] presents an assessment of the degree of reliable operation of the rainwater drainage system in the Gaj and Tarnogaj housing estates in Wrocław. The research was conducted on a calibrated hydrodynamic model in SWMM software for conditions of the present precipitation load and for the forecast load growth in the future. The channelled drainage area is 1.04 km^2 (Fig. 3).

Fig. 3. Rainwater catchment area orthophoto map of the Gaj and Tarnogaj housing estates in Wrocław

The total length of the catalogued rain channels was 17.730 m, and the number of wells was 509. Seventy-five partial drainage basins were separated in the model ($F_{i,average}$ = 1.39 ha, at $F_{i,\min}$ = 0.22 ha and $F_{i,\max}$ = 5.34 ha). Using the analysis of clusters by the Ward method and

the so-called box charts, the partial drainage basin hydraulic width (W_i) was determined from formula [33]:

$$W_i = 1.6\sqrt{F_i} \tag{5}$$

where:
F_i – partial drainage basin area, m^2.

Calibrated on front and low-pressure precipitation, and then validated on convective precipitation, the hydrodynamic model of the examined drainage system had the following parameters: rain channel roughness coefficient (n) was 0.020 s/m$^{1/3}$; sealed drainage basin surface roughness coefficient was 0.020 s/m$^{1/3}$, non-sealed surface roughness coefficient was 0.30 s/m$^{1/3}$; field retention height (h) on sealed areas was 2.0 mm, and on non-sealed areas it was 5.0 mm. The agreed infiltration parameters in the Horton model are: initial infiltration intensity, 90 mm/h; final infiltration intensity, 10 mm/h; recession constant, 4 1/h; ground total drying time, 7 d. The scheme of the examined drainage network, created in SWMM software, is presented in Fig. 4.

Fig. 4. Scheme of the examined rainwater drainage basin drainage system in SWMM software

Two convective precipitations were used as the drainage basin's load [33]:

- type II Euler method with the frequency of incidence in Wrocław of C = 3 years for the simulation of the present drainage basin's supply conditions (according to Table 2);
- the real rain, a heavy rain scenario with the frequency of incidence in Wrocław of C = 5 years for simulation of the drainage basin's supply conditions in the future

Real precipitation with an intensity of 34 mm/h was registered on 19.07.2015 on an R05 rain meter, at a distance of 620 m from the centre of gravity of the examined drainage basin (Fig. 5). It was assumed that point overflooding, with a volume of over 200 m^3, can create potential hazards. For example, assuming that water is dammed up to the level of roadway

curbs (0.15 m), the range of flooding would then cover a surface area of 37 m x 37 m = 1369 m^2 (i.e. approx. 10% $F_{i,average}$ = 1.39 ha). For drainage basin load with a model precipitation of C = 3 years, the presence of 4 critical nodes was observed in the examined network with flooding above 200 m^3 (Fig. 5). On the basis of Formula (3), the value of indicator DF = 0.16 was calculated (as the ratio of the number of flooded wells N_f = 79 to the total number of wells N = 509). However, the specific flood volume according to Formula (4) is SFV = 19 m^3/ha (for ΣV = 1171 m^3 and drainage basin sealed surface F_s = 61.5 ha). The calculated value of SFV > 13 m^3/ha, according to the quoted Siekmann & Pinnekampf criteria [28], indicates no fulfilment of the requirement of standards PN-EN 752:2008 and DWA-A 118:2006 by the studied drainage system, and thus the need for its adaptation to the effects of climate change that are already happening.

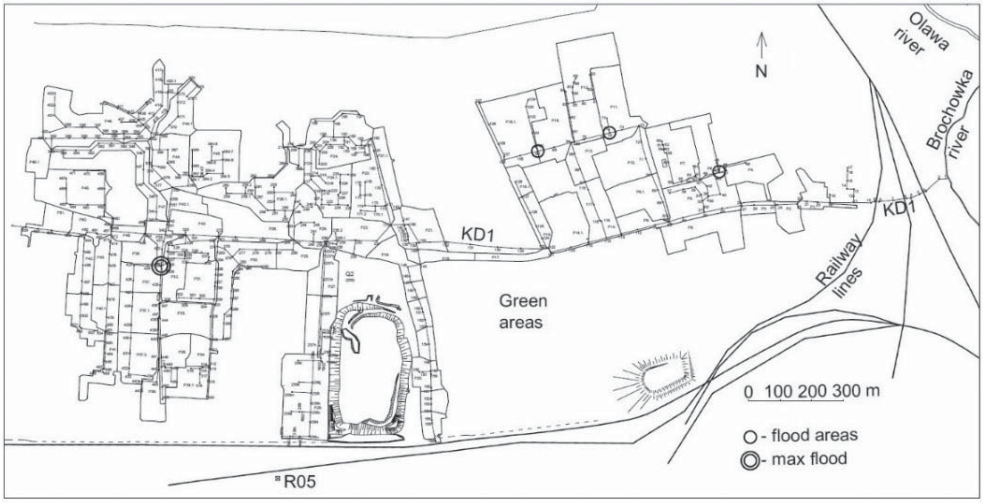

Fig. 5. Location of flooding from channels for Euler type II model precipitation of C = 3 years

In the second stage of the research concerning the drainage basin's supply conditions in the future, i.e. during simulation of the drainage basin's load with precipitation of C = 5 years, floodings were already observed in 8 network nodes. Degree of flooding was DF = 87/509 = 0.17, and the specific flood volume SFV = 2641/61.5 = 42.9 m^3/ha. Figure 6 presents the KD1 collector profile during the occurrence of maximum overflow and flooding: on two-thirds of the length of the collector, rainwater flows under pressure, and on one-third of the length, there are critical points where the level of water reaches the ground level (like for the model precipitation).

As in model precipitation of C = 3 years, in the case of real precipitation of C = 5 years, the value of the indicator SFV > 13 m^3/ha indicated no fulfilment by the studied drainage system of the requirements of standards PN-EN 752:2008 and Merkblatt no. 4.3/3:2009, i.e. the need for its adaptation to climate changes in the future. Thus, there was no need to simulate the operation of the examined system of C = 100 years.

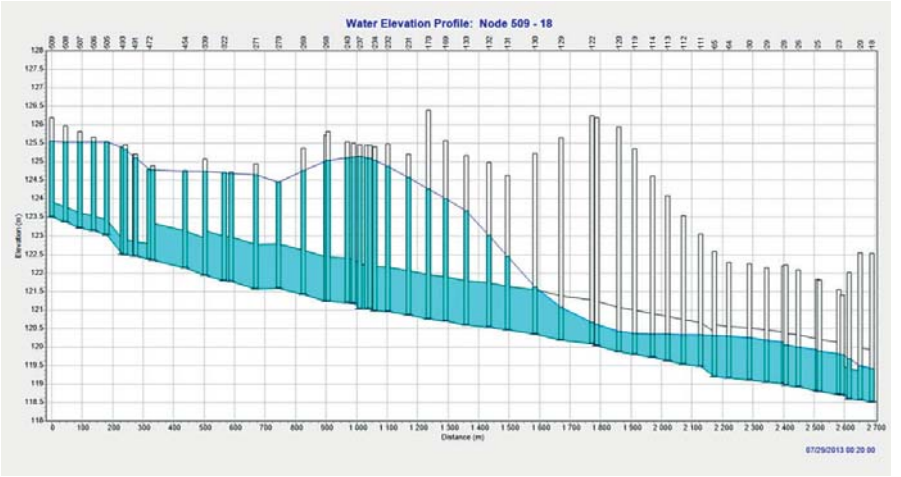

Fig. 6. Collector profile at the time of the largest overflow during precipitation of C = 5 years

5. Summary and final conclusions

Hazards for drainage systems are triggered both by climatic factors (growth in air temperature and precipitation intensity) and non-climatic factors. Environmental transformations of today's cities under the effect of urbanisation and industrialisation cause changes in water balance. Therefore, climate change is affected by a number of processes, such as business operations and the occupancy of new areas for development, including those particularly sensitive to the effects of climate changes, (e.g. flood areas). The proportion of impermeable surfaces is also growing in areas that are already developed.

The paper presents contemporary dimensioning standards of area drainage systems. Hazards for drainage systems arising from climate change have been discussed. Trends of changes in the precipitation structure have been presented on the example of data from Wrocław. The need for changes in precipitation scenarios has been indicated for modelling overflow in channels and a research methodology and assessment criteria have been proposed to assess the degree of reliability of the drainage system. Sample results of the analysis of the operation of the rainwater drainage system in the Gaj and Tarnogaj housing estates in Wrocław have been presented – this analysis was conducted on a calibrated hydrodynamic model in SWMM software. The degree of flooding and the specific flood volume have been used as the assessment criteria for system overload. It has been proved that the examined system does not meet the PN-EN 752:2008, DWA-A 118:2006 and Merkblatt no. 4.3/3:2009 standards and requires adaptation to climate changes.

To sum up, it should be emphasised that with the today's dimensioning of newly built drainage systems (and the modernisation of existing systems), it becomes necessary to take the forecast climate changes into consideration in the future. Therefore, safe dimensioning methods of rainwater drainage networks and structures should be used (MMN, according to [6]) and their operational reliability should be examined using hydrodynamic modelling.

The identification of potential system overloads already justifies the need to prepare new remedial actions for example, those consisting of the modernisation of the drainage infrastructure, such as the construction of relief channels and storage-infiltration reservoirs, and the raising of roadside curbs or the embanking of specific areas [6, 10–14, 23, 34].

This work has been completed as part of the statutory activity of the Department of Environmental Engineering, Wrocław University of Science and Technology, financed from the funds of the Ministry of Science and Higher Education in the period 2016–2017.

References

[1] Ministerstwo Środowiska, *Projekt VI Raportu Rządowego oraz Raportu dwuletniego dla Konferencji Stron Ramowej Konwencji NZ w sprawie zmian klimatu*, Warszawa 2013.
[2] IPCC: *The Physical Science Basis*, Cambridge University Press, 2007.
[3] IPCC: *Impacts, Adaptation, and Vulnerability*, Cambridge University Press, 2014.
[4] Landerink G., Van Meijgaard E., *Increase in hourly precipitation extremes beyond expectations from temperature changes*, Nature Geosci, 2008, No. 1, 511–514.
[5] Kundzewicz Z. W., *Zmiany ryzyka powodziowego w Europie*, Symposium Paris – Orlean 28–30.03.2012, 11–20.
[6] Kotowski A., *Podstawy bezpiecznego wymiarowania odwodnień terenów, Sieci kanalizacyjne* (Tom I); *Obiekty specjalne* (Tom II), Wydawnictwo Seidel-Przywecki (Edition II), Warzsawa 2015.
[7] PN-EN 752:2008: Drain and sewer systems outside buildings.
[8] Kotowski A., *Kwantyfikacja problemu zmian klimatu w projektowaniu infrastruktury wodno-kanalizacyjnej miast*, Wydawnictwo Politechniki Lubelskiej, Lublin 2014, 177–189.
[9] Arbeitsblatt ATV-A118:2006: *Hydraulische Bemessung und Nachweis von Entwässerungs-systemen*, DWA, Hennef 2006.
[10] Geiger W., Dreiseitl H., *Nowe sposoby odprowadzania wód deszczowych*, Wydawnictwo Projprzem-EKO, Bydgoszcz 1999.
[11] Bolt A., Burszta-Adamiak K., Gudelis-Taraszkiewicz K., Suligowski Z., Tuszyńska A., *Kanalizacja. Projektowanie, wykonanie, eksploatacja*, Wydawnictwo Seidel-Przywecki, Warszawa 2012.
[12] Królikowska J., Królikowski A., *Wody opadowe. Odprowadzanie, zagospodarowanie, podczyszczanie i wykorzystanie*, Wydawnictwo Seidel-Przywecki, Warszawa 2012.
[13] Królikowska J., Królikowski A., Żaba T., *Kanalizacja. Podstawy projektowania, wykonawstwa i eksploatacji*, Wydawnictwo Politechniki Krakowskiej, Kraków 2015.
[14] Edel R., Suligowski Z., *Wpływ parametrów wpustów deszczowych na sprawność odwodnienia powierzchniowego dróg i ulic*, Wydawnictwo Politechniki Gdańskiej, Gdańsk 2004.
[15] Nowakowska M., Kaźmierczak B., Wartalska K., Kotowski A., *Budowa modelu hydrodynamicznego skanalizowanej zlewni deszczowej we Wrocławiu*, GWiTS 2017, No. 4, 189–195.

[16] Nowakowska M., Kotowski A., *Metodyka i zasady modelowania odwodnień terenów zurbanizowanych*, Oficyna Wydawnicza Politechniki Wrocławskiej, Wrocław 2017.
[17] Bogdanowicz E., Stachý J., *Maksymalne opady deszczu w Polsce. Charakterystyki projektowe*, Materiały badawcze, Seria: Hydrologia i Oceanologia, No. 23, IMGW, Warszawa 1998.
[18] Pińskwar I., *Projekcje zmian w ekstremach opadowych w Polsce*, Wydawnictwo Komitetu Gospodarki Wodnej PAN, No. 32, Warszawa 2010.
[19] Willems P., Revision of urban drainage design rules based on extrapolation of design rainfall statistics, 12th Int. Conf. on Urban Drainage, Porto Alegre, 11–16 September 2011.
[20] Larsen A.N., Gregorsen I.B., Christensen O.B., Linde J.J., Mikkelsen P.S., *Potential future increase in extreme one-hour precipitation events over Europe due to climate change,* Water Science Technology 2009, Vol. 60, 2205–2216.
[21] Staufer P., Leckebusch G., Pinnekamp J., *Die Ermittlung der relevanten Niederschlags-charakteristik für die Siedlungsentwässerung im Klimawandel. Korrespondenz Abwasser*, Abfall 2010 (Jg. 57), No. 12.
[22] Merkblatt Nr. 4.3/3, *Bemessung von Misch- und Regenwasserkanälen*, Teil 1: *Klimawandel und möglicher Anpassungsbedarf*, Bayerischen Landesamtes für Umwelt (Referat 66) 2009.
[23] Dąbrowski W., Dąbrowska B., *Przewidywany wpływ zmian klimatu na dysfunkcję systemów odprowadzania ścieków*, GWiTS 2012, No. 1, 17–20.
[24] Kotowski A., *Prognozowane skutki ocieplenia klimatu w modelowaniu przeciążeń systemów kanalizacyjnych w Polsce*, GWiTS 2013, No. 5, 201–205.
[25] Kaźmierczak B., Kotowski A., *The influence of precipitation intensity growth on the urban drainage systems designing*, Theoretical and Applied Climatol. 2014, Vol. 118, No. 1, 285–296.
[26] Kotowski A., Kaźmierczak B., Dancewicz A., *Modelowanie opadów do wymiarowania kanalizacji*, Wydawnictwo KILiW PAN, Studia z zakresu Inżynierii, No. 68, Warsaw 2010.
[27] Kotowski A., Kaźmierczak B., *Probabilistic models of maximum precipitation for designing sewerage*, Journal of Hydrometeorology 2013, Vol. 14, No. 6, 1958–1965.
[28] Siekmann M., Pinnekamp J., Indicator based strategy to adapt urban drainage systems in regard to the consequences caused by climate change, 12th Int. Conf. on Urban Drainage, Porto Alegre, 11–16 September 2011.
[29] Schmitt T. G., *Risikomanagement statt Sicherheitsversprechen,* Korrespondenz Abwasser, Abfall 2011, No. 1, 40–49.
[30] Zawilski M., *Niestandardowe wykorzystanie GIS w modernizacji systemów kanalizacyjnych*, GWiTS 2009, No. 6, 34–36.
[31] Kaźmierczak B., Kotowski A., *Weryfikacja przepustowości kanalizacji deszczowej w modelowaniu hydrodynamicznym*, Oficyna Wydawnicza Politechniki Wrocławskiej, Wrocław 2012.
[32] Kotowski A., Kaźmierczak B., Nowakowska M., *Analiza obciążenia systemu odwadniania terenu w przypadku prognozowanego zwiększenia częstości i intensywności deszczów z powodu zmian klimatycznych*, Ochrona Środowiska 2013, Vol. 35, No. 1, 25–32.

[33] Nowakowska M., *Identyfikacja parametrów hydrologicznych i hydraulicznych zlewni miejskiej w modelowaniu hydrodynamicznym SWMM*, PhD dissertation. Faculty of Environmental Engineering Wrocław University of Technology, Wrocław 2016.
[34] Licznar P., *Wymiarowanie zbiorników retencyjnych ścieków deszczowych na podstawie syntetycznych szeregów czasowych opadów deszczu*, Ochrona Środowiska 2013, Vol. 35, No. 2, 27–32.

TECHNICAL TRANSACTIONS 1/2018
ENVIRONMENTAL ENGINERING
DOI: 10.4467/2353737XCT.18.011.7962
SUBMISSION OF THE FINAL VERSION: 5/1/2018

Stanisław Biedugnis (stanislaw.biedugnis@pw.edu.pl)
The Main Fire Service School, Warsaw

Andrzej Czapczuk (andrzej.czapczuk@fbitasbud.pl)
F.B.I. TASBUD S.A., Science and Research Division, Warsaw

The application of the '*K*-nearest neighbour' method to evaluate pressure loss in water supply lines

Zastosowanie metody *K*-najbliższych sąsiadów do oceny strat ciśnienia w przewodach wodociągowych

Abstract

Water supply systems are complex engineering structures; certainly, the most important part is the water distribution network. The design of this element requires calculations and many analyses to arrive at the best solution. The main task of the calculation is to determine the flow rates through pipes, to determine pressure losses, height of tanks, pressure required in the supply pumping station, pressure levels in the individual nodes of the network. Correct execution of the calculations requires careful evaluation of the results obtained and accuracy in the solutions applied. The issue of controlling the results of calculations is difficult to present in algorithmic form as these are mainly based on the experience and knowledge of the designer. Classes of decisions describing the problems of pressure loss in the pipework were established in order to evaluate the results of calculations. Numerical experiments were carried out in this paper to show how the '*K*-nearest neighbour' method can be used to evaluate pressure loss in water pipes.

Keywords: water distribution system, hydraulic calculations, evaluate of pressure loss, *K*-nearest neighbour method

Streszczenie

Systemy zaopatrzenia w wodę są skomplikowanymi układami obiektów inżynierskich, które pełnią różnorodną rolę w funkcjonowaniu całości. Najważniejszym elementem jest z pewnością system dystrybucji wody. W zawiązku z powyższym projektowanie systemów dystrybucji wymaga przeprowadzenia obliczeń oraz wielu analiz mających na celu doprowadzenie do najlepszego rozwiązania. Podstawowym celem obliczeń jest wyznaczenie natężeń przepływów przez przewody, określenie strat ciśnienia, wysokości zbiorników, wymaganego ciśnienia na zasilaniu oraz ciśnienia w poszczególnych węzłach sieci. Poprawne zrealizowanie obliczeń wymaga wnikliwej oceny uzyskanych wyników oraz poprawności zastosowanych rozwiązań. Zagadnienia kontroli rezultatów obliczeń trudno jest ująć w postaci algorytmicznej, gdyż oparte są głównie na doświadczeniu i wiedzy projektanta. Do oceny wyników obliczeń zdefiniowano klasy decyzyjne opisujące problemy związane ze stratami ciśnienia w przewodach. W pracy przeprowadzono eksperymenty numeryczne pokazujące, w jaki sposób może być zastosowana metoda *K*-najbliższych sąsiadów do oceny strat ciśnienia w przewodach wodociągowych.

Słowa kluczowe: system dystrybucji wody, obliczenia hydrauliczne, ocena strat ciśnienia, metoda *K*-najbliższych sąsiadów

1. Introduction

Water supply systems are complex engineering structures; certainly, the most important part is the water distribution network. This is dictated by high construction costs as well as the complex processes of operation and renovation. The design of this element requires calculations and many analyses to arrive at the best solution. The main task of the calculation is to determine the flow rates through pipes, to determine pressure losses, height of tanks, pressure required in the supply pumping station, pressure levels in the individual nodes of the network.

For many years, computer technology has been used for the calculation of hydraulic water distribution systems [1, 2]. Such computer programs appeared in the second half of the 20th. century [3, 4]; however, they were relatively difficult to handle and required a lot of input work – they are now equipped with many functions [5, 6]. Despite significant advances in computer technology for calculating water distribution systems, the procedures that are used still have a predetermined course. Implementing such calculations requires the designer to take a number of decisions that affect both technical and economic parameters; however, other factors, such as reliability [7–10] and safety in relation to water supply systems, are often taken into account [11]. This requires careful assessment of the results obtained and accuracy in the solutions applied. Methods involving artificial intelligence or non-parametric regression can be a great support in the implementation of this kind of task as it can be difficult to handle with regard to devising the required algorithms.

In the literature, there are numerous examples of artificial intelligence methods being used to evaluate the results of analyses of water distribution systems [12–16]. This paper discusses the possibility of using the '*K*-nearest neighbour' method to evaluate pressure loss in water supply lines.

2. Methodology for estimating pressure loss in water supply lines

The evaluation of pressure losses can be difficult because identical values of Δh_l, depending on conditions, may be considered to be high, within the optimum range, or relatively low. For example, Fig. 1 shows a case in which equal values of Δh_l for segments of different lengths, can be classified in one of the three categories above.

The basic decisive factor for pressure loss is the diameter of the pipeline, which is selected on the basis of speed. However, you can specify other parameters that affect pressure loss and are not related to velocity. The first of these is the length L of the pipe section, while the second is the coefficient of absolute roughness k.

When evaluating pressure losses, it is firstly necessary to determine whether Δh_l is correct for a given condition; if it is too low or too high, the reason for that situation should be determined. A review of results for individual sections, especially in the case of large water distribution systems, can be tedious, time consuming, and confusing. The causes of pressure losses that would require correction, or the introduction of specific operating instructions, such as periodic pipe rinsing, are quite varied. For the purposes of this paper, four classes

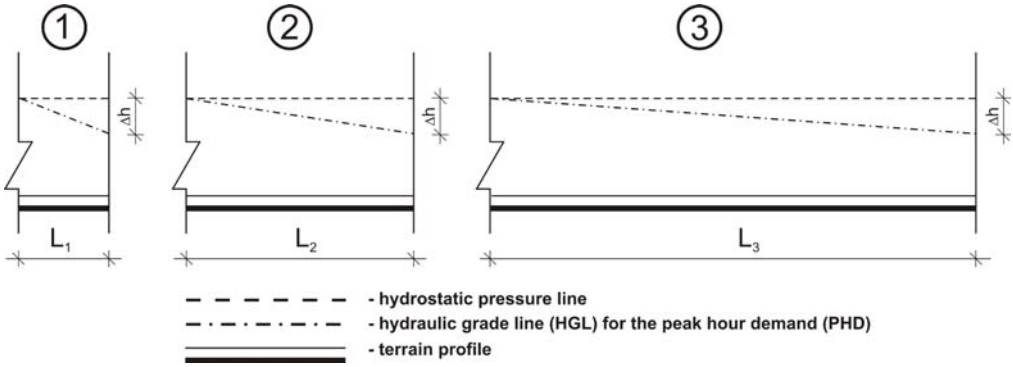

Fig. 1. Evaluation of pressure losses on sections of various lengths *L*

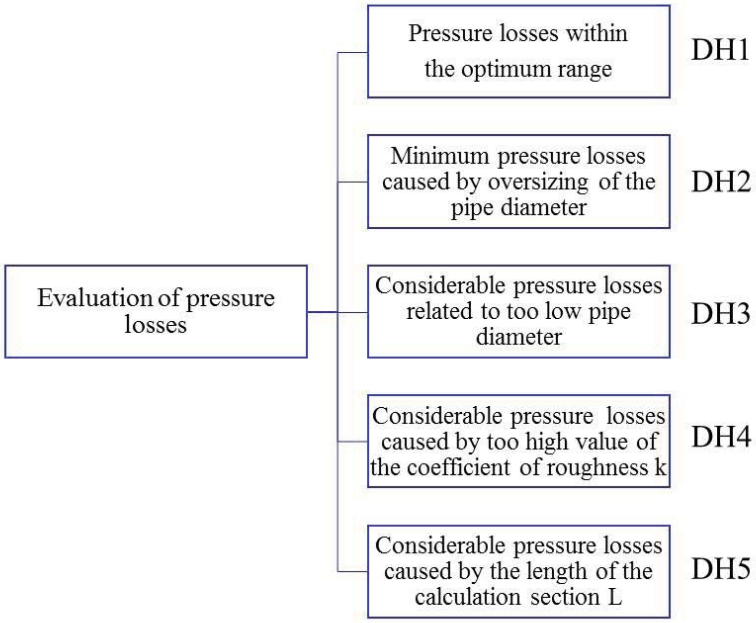

Fig. 2. Classes for the assessment of pressure losses in pipelines of water distribution systems

have been identified; these describe the causes of incorrect assumptions *vis-à-vis* Δh_l pressure losses. One further class corresponds to the range of appropriate values. Classes described with labels DH1–DH5 are shown in Fig. 2 [12].

Defining the DH1 class corresponding to the range of correct values of pressure losses on a computational section, takes into account not only flow velocity and diameter but also the length of the section and the coefficient of absolute irregularity *k*.

No proposal was found in the available literature, which would clearly define the optimal range of pressure losses Δh_l in the section.

There are no proposals in the literature that would specifically define the optimal pressure loss range Δh_l in the section. However, proposals and instructions for maximally permissible, unit pipeline pressure drops are available; these are determined in relation to the diameter [16] or flow rate along the section [18]. Depending on the diameter, the following unit values for maximum pressure losses, conditioned by the need to maintain their respective flow rates, [16] are given:

- 15–20 ‰ for the pipework with diameters DN100–DN250 mm
- 15 ‰ for busbar with diameters up to DN500 mm
- 5 ‰ for pipework with diameters greater than DN500 mm

The limit values, as a function of the flow rate for a flat area, are given in Table 1.

Table 1. Permissible unit pressure loss for flat land, depending on the flow rate [18]

Stream (dm^3/s)	**Pressure-drop in the pipelines** (‰)
0.1–72	10
72–480	5
480–4000	3.5

It seems, however, that the permissible unit pressure loss as a function of the diameter of the pipework or flow rate is insufficient when assessing pressure losses. The computer system should also detect situations in which the pressure losses are low or definitely too high. This paper assumes that the range of permissible pressure losses described in the DH1 class occurs when the following conditions are met:

- the flow rate is higher than 0.5 m/s;
- the flow velocity for individual diameters does not exceed the recommended values for the individual diameters;
- the roughness coefficient does not exceed the upper limit of resistance, assumed on the basis that $k = 1.5$ mm;
- pressure losses resulting from the length of the calculation of section L will not cause the pressure line to fall below the value required for a 4-storey building, i.e. the pressure line will not fall below 25.5 m, assuming that the losses resulting from the absolute roughness coefficient k are normal. The starting pressure is assumed to be 40 m; therefore, the pressure loss cannot exceed 14.5 m. This condition is required in order to ensure the required pressure, while keeping the pressure as low as possible.

The DH2 class describes the situation where low pressure losses are caused by oversized pipework or by restricted flow at the ends of the water supply network, where the flow rate is less than 0.5 m/s.

The DH3 class is characterised by a pressure loss which is due to too small a diameter in the pipeline. The flow rate exceeds the recommended values for individual diameters. The value of the roughness coefficient is below the upper limit of $k = 1.5$ mm.

The DH4 class describes conditions in which pressure losses are dictated by a high value of the absolute coefficient *k*, above the *k* limit of 1.5 mm.

The DH5 class refers to a situation in which the primary cause of pressure loss in the pipeline – below the required value –is the pressure loss associated with the calculated length of a particular section of the line. In the case where calculations of long water transits or mains are taken into account as a single, computational section, this variant signals the need for zoning of the system. This length is different each time, depending on the pipe diameter, flow rate and roughness.

The above classes will be assigned to individual computational sections of the water distribution system, using the '*K*-nearest neighbour' method.

Using the *K*-nearest neighbour approach requires a set of teaching examples containing arguments or variables and classes corresponding to them. Teaching examples, in the form of calculation results for sections of the water distribution system, were prepared using EPANET software and EXCEL spreadsheets. Pressure losses over the length of the section are calculated according to the Darcy-Weisbach formula.

PE100 polyethylene pipelines of the SDR17 series (PN-EN 12201-2:2011) were used for the calculations.

Hydraulic calculations were made using the following assumptions:

- internal diameters of pipelines D_w were used in the calculations;
- the minimum cable diameter was DN110;
- the maximum cable diameter was DN630;
- the following roughness coefficients were assumed: $k = 0.01; 0.1; 0.5; 1.0; 1.5; 2.0$ mm;
- the maximum calculated length of the sections was 3000 m.

The teaching examples relate to individual sections of the water supply network and were developed in such a way that they could be used to assess pressure losses in classes DH1–DH5. In order to induce the decision tree, the problem domain is defined with the following attributes:

- the length of the computational line L
- calculation flow on the Q_m section
- the absolute roughness coefficient of the pipework on a given section k
- linear pressure losses on the computational section Δh_1

All teaching examples were described by the DH1–DH5 label indicating that they belonged to a specific class characterising pressure losses. Tutorials are saved as an Excel spreadsheet file, where each row corresponds to learning examples and the columns correspond to attributes. A collection of 17019 teaching examples was formed – these represented all the DH1-DH5 classes described above.

3. The *K*-nearest neighbour method

A non-parametric regression algorithm was used for forecasting the value of random variable values and for classification. The task was to classify a new object into a positive or

a negative group based on what it is adjacent to. An important parameter in this method is the value of *K*, which is the number of teaching examples in the nearest neighbourhood. A new value for introduction into the space was sought on the basis of the value of those *K* neighbours closest. In the case of classification, the method takes into account the value of most of the examples in the neighbourhood, i.e. it sets the value of the new example by voting.

Choosing a neighbourhood, in other words choosing the value of the *K* parameter, is essential. With this method, this parameter is decisive with regards to the accuracy of the prediction. At a low *K* value there is a high variability of prediction, while at a high *K* value, there may be a significant, systematic shift of prediction values. On the basis of the analyses, the *K* value must be chosen to minimise the likelihood of misclassification. The *K*-nearest neighbour method proposes an optimal *K* value based on the cross-check method [20].

The Euclidean Mara is most often used to evaluate the distance between the points describing the training examples:

$$D(x,p) == \sqrt{(x-p)^2} \tag{1}$$

where:

x – is a new case to be classified,

p – is one of the training cases.

Application of the *K*-nearest neighbour method to evaluate pressure losses in water-supply lines

Calculations for water pipes were made using the **EPANET** programme. Pressure losses were then calculated along individually calculated sections using a spreadsheet; a suitable DH class was then assigned to each section. Calculations were made using different coefficients of roughness k and the lengths of the sectors calculated. This step was dictated by the fact that the variability of attributes across the whole possible range needed to be taken into account in the examples. Some of the hydraulic calculations were deliberately misplaced; however, these examples were described by the appropriate DH classes so that the expert system could identify the cause of the pressure losses. 12,754 teaching examples were obtained.

Based on the set of teaching examples, the *K*-nearest neighbour method was graded using different neighbourhood values.

Detailed classification results are included in the matrix of confusion [20]. This is a square matrix, in which information as to which classes individual examples actually belong, are in rows and information as to how they were classified by the classifier are in columns. The diagonal contains examples that are categorised as correct while those located beyond the diagonal are classified as incorrect. At the same time, examples beyond the diagonal indicate the classes to which they were classified, albeit incorrectly.

Tables 1 and 3 show the teaching outcomes of the *K*-nearest neighbour for neighbourhood $K = 1$ and *K*-5. The Euclidean measure was used to calculate the distance between teaching examples. Tables 2 and 4 summarise the classification of examples for $K = 1$ and *K*-5.

Table 2. Matrix of confusion for the nearest neighbourhood method for $K = 1$

	DH3	DH5	DH2	DH1	DH4
DH3	1296	141	43	0	7
DH5	96	855	0	20	0
DH2	42	0	971	0	7
DH1	0	31	0	556	0
DH1	6	2	13	5	164

Table 3. Summary of classification results for $K = 1$

	Total	Accurate	Invalid	Relevant (%)	Invalid (%)
DH3	1440	1296	144	90.00000	10.00000
DH5	1029	855	174	83.09038	16.90962
DH2	1027	971	56	94.54722	5.45278
DH1	581	556	25	95.69707	4.30293
DH1	178	164	14	92.13483	7.86517

Table 4. Matrix of confusion for the nearest neighbourhood method for $K = 1$

	DH3	DH5	DH2	DH1	DH4
DH3	1300	118	60	0	9
DH5	116	831	0	24	0
DH2	54	0	959	0	7
DH1	0	13	0	574	0
DH1	7	2	14	7	160

Table 5. Summary of classification results for $K = 5$

	Total	Accurate	Invalid	Relevant (%)	Invalid (%)
DH3	1477	1300	177	88.01625	11.98375
DH5	964	831	133	86.20332	13.79668
DH2	1033	959	74	92.83640	7.16360
DH1	605	574	31	94.87603	5.12397
DH1	176	160	16	90.90909	9.09091

4. Summary and Conclusions

The results obtained by the *K*-nearest neighbour method for neighbourhoods $K = 1$ and $K = 5$ are comparable. They differ in the accuracy of the classification for individual classes. In general, however, classification errors for both *K* values are quite high. The results obtained, along with previous experiments with other artificial intelligence methods, especially with the decision tree induction method, show that the *K*-neighbour approach is a much worse solution than induction or artificial neural networks.

References

[1] Biedugnis S., *Metody informatyczne w wodociągach i kanalizacji*, Oficyna Wydawnicza Politechniki Warszawskiej, Warszawa 1998.

[2] Rossman L.A., *EPANET 2 User's manual, EPA/600/R-00/057*, National Risk Management Research Laboratory, U.S. Environmental Protection Agency, Cincinnati, OH, USA 2000.

[3] Epp R., Fowler A.G., *Efficient Code for steady state Flows in Networks, Journal of the Hydraulics Division*, ASCE, Vol. 96, No. HY1, 1970, 43–56.

[4] Adams R.W., *Distribution Analysis by Electronic Computer*, Institute of Water Engineers, Vol. 15, 1961, 415–428.

[5] Knapik K., *Dynamiczne modele w badaniach sieci wodociągowych*, Wydawnictwo Politechniki Krakowskiej, Kraków 2000.

[6] *Pipe2010 Water Utility Modeling: A Comprehensive Guide to Hydraulic and Water Quality Modeling of Drinking Water Systems Using Pipe 2010*, KyPipe, http://kypipe.com.

[7] Królikowski A.J., *Niezawodność działania systemów zaopatrzenia w wodę*, Ekologia i Technika, Vol. 1, No. 1, 1993, 7–14.

[8] Wagner J.M., Shamir U., Marks D.H., *Water distribution reliability: simulation methods*, Journal of water resources planning and management, Vol. 114, Issue 3, 1988, 276–294.

[9] Wieczysty A., *Niezawodność miejskich systemów zaopatrzenia w wodę: praca zbiorowa*, Politechnika Krakowska, Kraków 1993.

[10] Kwietniewski M., Roman M., Kloss-Trębaczkiewicz H., *Niezawodność wodociągów i kanalizacji*, Arkady, Warszawa1993.

[11] Zimoch I., *Bezpieczeństwo działania systemu zaopatrzenia w wodę w warunkach zmian jakości wody w sieci wodociągowej*. Ochrona Środowiska, Vol. 31, Issue 3, 2009, 51–55.

[12] Czapczuk A., *System ekspertowy do oceny przepływów i strat ciśnienia w układzie dystrybucji wody*, Dysertacja, Wydział Inżynierii Środowiska, Politechnika Warszawska, Warszawa 2013.

[13] Czapczuk A., Dawidowicz J., Piekarski J., *Metody sztucznej inteligencji w projektowaniu i eksploatacji systemów zaopatrzenia w wodę*, Annual Set – The Environment Protection, Vol. 17, No. 2, 2015, 1527–1544.

[14] Dawidowicz J., *Evaluation of a pressure head and pressure zones in water distribution systems by artificial neural networks*, Neural Computing & Application, 2017, doi:10.1007/s00521-017-2844-8.
[15] Dawidowicz J., *Diagnostyka procesu obliczeń systemu dystrybucji wody z zastosowaniem modelowania neuronowego*, Rozprawy Naukowe, No. 268, Oficyna Wydawnicza Politechniki Białostockiej, Białystok 2015.
[16] Dawidowicz J., *System ekspertowy do oceny układu systemu dystrybucji wody sporządzony za pomocą wnioskowania indukcyjnego*, Annual Set the Environment Protection, Vol. 14, 2012, 650–659.
[17] Gupta R.K., *Analysis and Control of Flows in Pressurized Hydraulic Networks*, PhD, UNESCO-IHE Institute, Delft 2006.
[18] Łyp B., *Wybrane problemy wodociągów i kanalizacji w przestrzennym planowaniu zagospodarowania miast*, COIB, Warszawa 1992.
[19] Bishop C.M., *Neural Networks for Pattern Recognition*, University Press, Oxford 1996.
[20] Triantaphyllou E., Felici G. (Eds.), *Data mining and knowledge discovery approaches based on rule induction techniques*, Vol. 6, Springer Science & Business Media, 2006.

TECHNICAL TRANSACTIONS 1/2018
ENVIRONMENTAL ENGINERING
DOI: 10.4467/2353737XCT.18.012.7963
SUBMISSION OF THE FINAL VERSION: 4/1/2018

Maria Elżbieta Kowalska (m.kowalska@gik.pw.edu.pl)
Janina Zaczek-Peplinska (j.zaczek-peplinska@gik.pw.edu.pl)
Faculty of Geodesy and Cartography, Warsaw University of Technology

Examples of measuring marks used in geo-reference and the connection between classic geodetic measurements and terrestrial laser scanning

Przegląd znaków pomiarowych wykorzystywanych do georeferencji i powiązania klasycznych pomiarów geodezyjnych z naziemnym skaningiem laserowym

Abstract

In the era of the development of modern measurement technologies, their interconnectedness is of high importance. This paper presents a review of the most popular, currently utilised measuring marks in tachymetric measurements and in object laser scanning. This paper presents the authors' own solutions that facilitate the linkage of data acquired through terrestrial laser scanning with tachymetric measurements. The proposed marks used to perform orientation on the scanned surfaces were successfully tested in the field with the use of laser scanners manufactured by the Z+F, Leica and Riegl companies. The document describes the consecutive steps that eliminate individual problems that arise during both tachymetric measurements and laser scanning. As a result of the work, a new kinds of marks were created allowing tachymetric measurements and laser scanning at the level of accuracy that is required for basic engineering measurements. This paper also presents a discussion on how to prepare the marks yourselves and the marks durability on the surface of the surveyed object.

Keywords: terrestrial laser scanning, marks, targets, engineering surveys

Streszczenie

W dobie dynamicznego rozwoju nowoczesnych technologii pomiarowych bardzo istotne jest ich wzajemne powiązanie. W artykule przedstawiono przegląd najpopularniejszych, aktualnie stosowanych znaków w klasycznych pomiarach tachimetrycznych oraz znaków stosowanych przy skanowaniu obiektów skanerami laserowymi. Zaprezentowano autorskie rozwiązania ułatwiające powiązanie danych z naziemnego skaningu laserowego z pomiarami tachimetrycznymi. Zaproponowane znaki do lokalizacji na skanowanych powierzchniach zostały z sukcesem przetestowane w warunkach terenowych przy wykorzystaniu skanerów laserowych firm Z+F, Leica i Riegl. Opisano kolejne etapy postępowania eliminujące poszczególne problemy zarówno w pomiarach tachimetrycznych, jak i w przypadku skanowania laserowego. W wyniku opisanych prac powstał nowy rodzaj znaku umożliwiający pomiar tachimetryczny, jak również skanowanie laserowe z odpowiednią dokładnością wymaganą dla podstawowych pomiarów inżynierskich. W pracy przedstawiono również rozważania na temat wykonania samych znaków i ich trwałości na mierzonym obiekcie.

Słowa kluczowe: naziemny skaning laserowy, znaki pomiarowe, tarcze pomiarowe, pomiary inżynierskie

1. Introduction

Terrestrial Laser scanning is a measurement technology which is commonly used in geodetic work. In terrestrial laser scanning, the result of the measurement is presented in the form of a point cloud (X, Y, Z) along with the information on the reflected beam's intensity value. The registered point cloud contains complete information on the shape and size of the object [7] – this is quasi-continuous information not limited to individual, flagged points. Additionally, registration of the intensity value of the beam reflected from the object's surface allows the analysis of its spectral properties.

The data obtained through terrestrial laser scanning is complemented with additional information, making it easier to interpret the point cloud. Currently, the majority of the scanners are integrated with a photo camera (digital images) which, in turn, allows the 'covering' of the created models with textures and presenting it in colours similar to those in the real world.

Based on the spatial data obtained through terrestrial laser scanning, it is possible to conduct various types of surveying studies, such as: deformation and shift analysis [1, 9]; architectural inventories [4, 5, 8]; spatial and numerical models of objects and terrain [2, 10]. There have been attempts to use terrestrial laser scanning in order to create maps for design purposes and permanent monitoring of engineering works. Such dynamic development of this technology is chiefly due to its huge capabilities.

More than once, terrestrial laser scanning has been combined with classic geodetic measurements – tacheometry or levelling. The combination of these technologies requires the application of special solutions, including properly designed measurement marks. The authors of this paper focus on reviewing the issues connected with marks that make it possible to combine terrestrial laser scanning with tacheometry.

2. Marks dedicated to tacheometric measurements

In order to refer the point cloud obtained through terrestrial laser scanning with the external spatial coordinate system, it is necessary to register points with known coordinates on the scans. In classic angular and linear measurements, points of measurement are indicated using a prismatic mirror or a measurement foil (reflective – mounted on the surveyed surface).

Reflective material used in the production of foil which is good for distance measurement causes problems in the precise identification of measured point placement on the scans, both in the plane of the scanned surfaces and in a perpendicular direction – this can be observed on Illustration 1 in the form of a blurred point cloud.

Similar problems occur when analysing point placement flagged using prisms (Fig. 2).

The problem can be solved by adjusting the marks used in terrestrial laser scanning in such a way that they would serve their purpose with regard to angular and linear measurements. This mainly concerns the aspect of the precise identification of the centre of the mark (target).

Fig. 1. Blurrification of the point cloud presenting control points made from reflective foil [9]

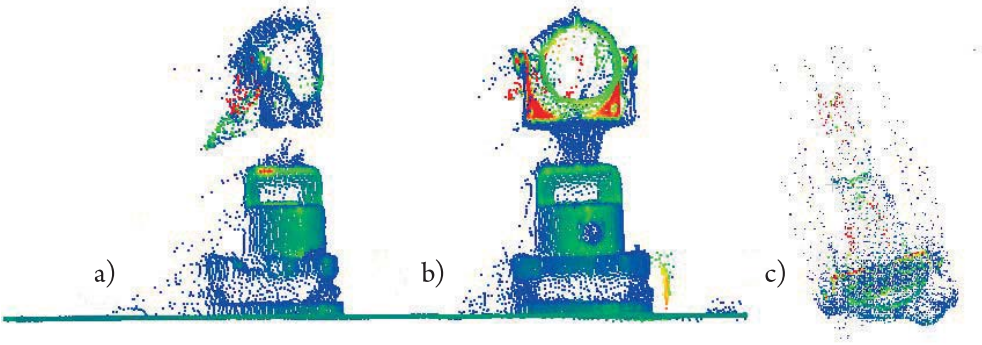

Fig. 2. View of a scanned precision reflector: a) a mirror set at an angle to the scanner b) mirror positioned in front of the scanner c) the view from the top scanned mirror

3. Measurement marks used in terrestrial laser scanning

Terrestrial laser scanning, like every measurement technology, possesses its own special measurement marks determined by the manufacturers in the form of targets, spheres or code disks. Depending on the manufacturer, they differ in colour, texture and geometry. When using the registered reflected beam's intensity value (Intensity), high-contrast fields on disks allow the precise identification of their location (Fig. 3) [6]. Disk manufacturers define the possible precision of identification if their placement even at the range of 0.2 mm.

Even though the precision with which the centre of a disk is identified is unquestionable, the use of these marks in tacheometric measurements proves problematic. One has to remember the difference between the nominal and expected precision of point placement for both measurement technologies – laser scanning 0.5–5.0 cm (depending on the precision of distance and angle measurement, accuracy of angular offset of the measuring beam and geometric properties of the scene); tacheometry – 0.2–0.5 cm.

The basic problem with using those marks in tacheometry lies in aiming, unambiguous on the scan, the dark-grey and white target blends with the crosshair in tacheometer causing the operator difficulty in judging the positioning. It is also difficult to interpret the middle of the board as in large magnification of telescope instead of clear-cut interesting lines, four adjacent monochromatic planes can be observed. The authors of this article, based on their measurement experience, suggested an improvement to those measuring marks by adding

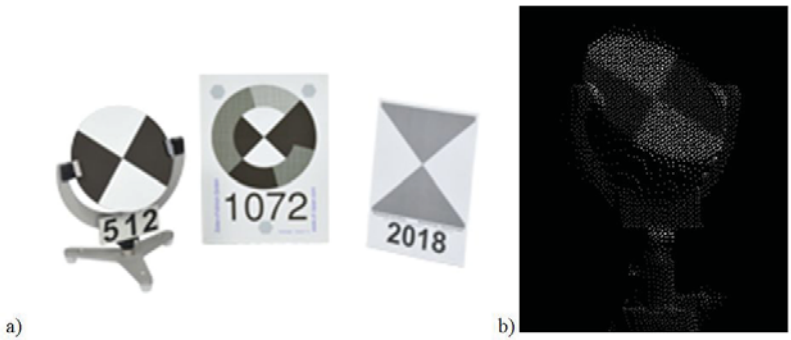

Fig. 3. Professional signal disks dedicated to terrestrial laser scanning a) mark appearance (source: http://www.zf-laser.com) b) example of visualisation of a disk using the registered reflected beam's intensity value (source: authors' archive)

a high-contrast crosshair to the target (Fig. 4). This solution facilitates and improves the aim with the telescope's crosshair and, at the same time, it avoids causing a deterioration in the quality of the mark when it is used for terrestrial laser scanning. Illustration 4 presents example targets with an integrated high-contrast crosshair.

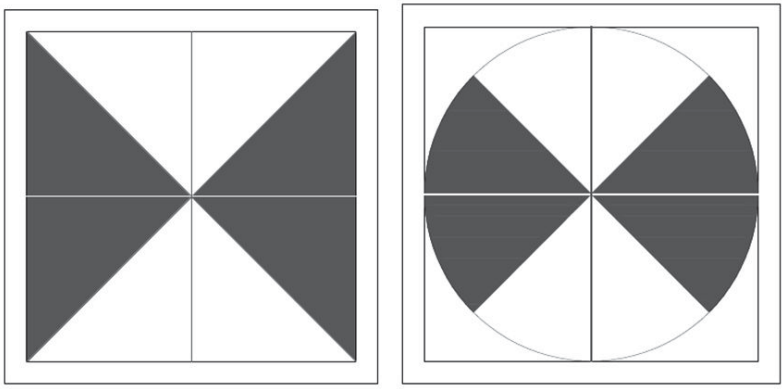

Fig. 4. Example targets with integrated contrast crosshair (source: authors archive)

The use of the above marks in angular and linear measurements requires less accurate, reflectorless measurement. In order to make use of the high accuracy of the measurement when using measurement foil, a suggestion was made to supplement terrestrial laser scanning marks with a small reflective foil. A small-sized circular (r = 12.5 mm) or square field (d = 30 mm) was designed in the middle of the mark and reflective foil was attached to it (Fig. 5, 7). This solution results in an increase in the accuracy of distance measurement and, at the same time, it makes it possible to combine it with terrestrial laser scanning. Even though the reflective foil would cause measurement noise to appear on the scan, the uncovered parts of the target would make it possible to determine its centre in the point cloud using geometric means. Due to the possibility of obtaining precise distance measurement to the mark with the attached foil and, at the same time, accurate angular and linear measurements, this mark was named the 'dual-function' mark.

Figures 6 and 7 present the proposed marks as seen through the telescope.

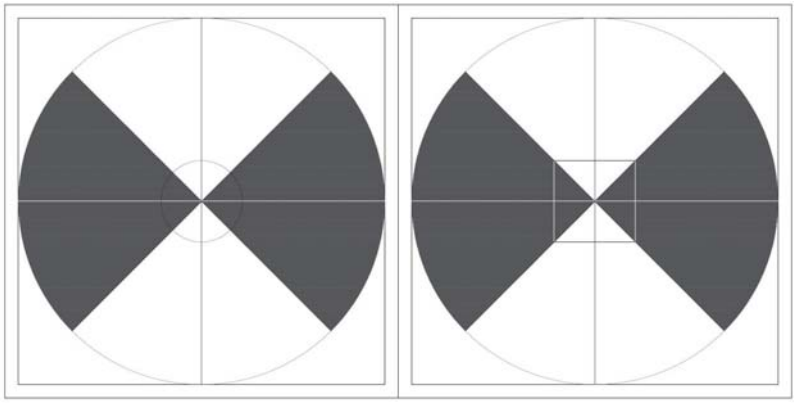

Fig. 5. Design of the terrestrial laser scanning mark with a designated field for the reflective foil

a) b)

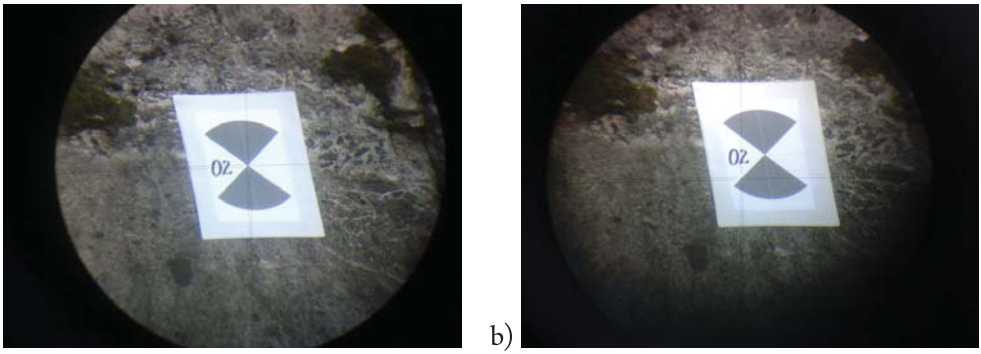

Fig. 6. View of the measurement mark in the telescope of the instrument (magnification: 30, distance: 13 m)
a) crosshair properly aimed at the measurement point, b) no aimed (source: authors' archive)

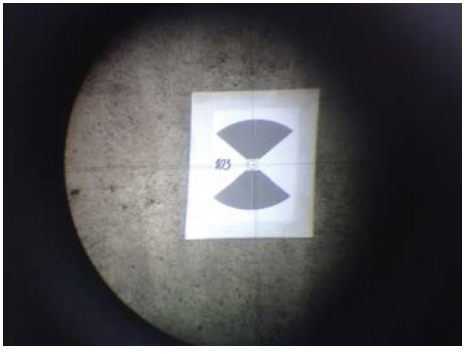

Fig. 7. Examples of aim using the mark
supplemented with reflective foil (magnification: 30, distance: 13 m)

Fig. 8 presents a scan fragment of a 'dual-function' target. A blurring of the point cloud can be clearly observed where the reflective foil was attached. Also, incomplete registration of points in the centre of the foil is visible. Similar effects were obtained for targets of different sizes and different angles of the scanned surface (different angles of incidence) (Fig. 9).

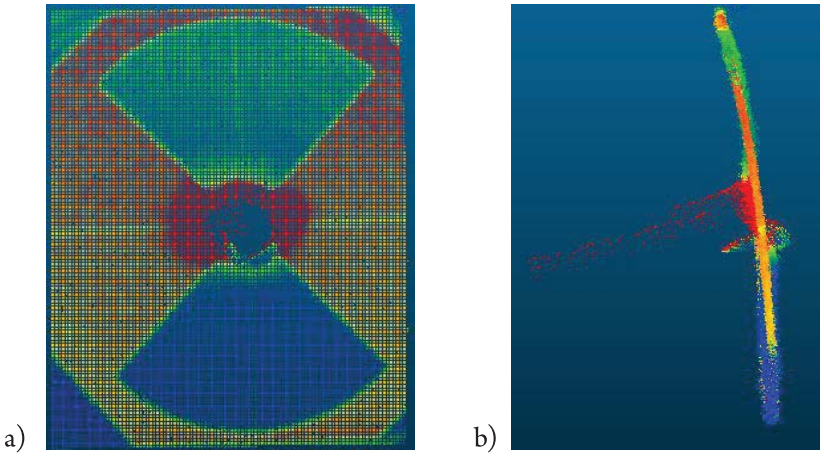

Fig. 8. View of a scanned 'dual-function' target: a) from the front and b) from the side (scans in the intensity colour range)

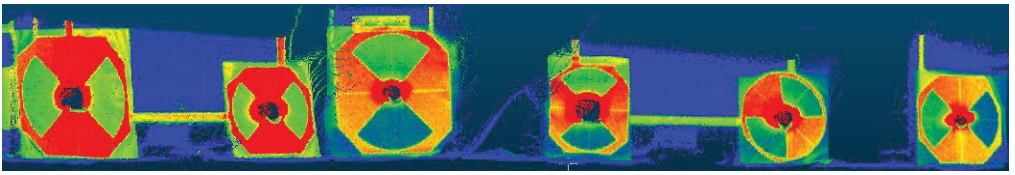

Fig. 9. An example of scans of 'dual-function' marks in different sizes and different placement. Scans in the intensity colour range

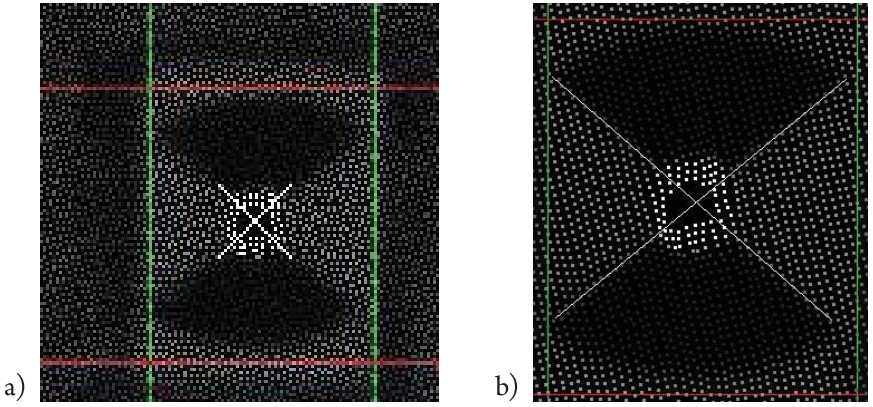

Fig. 10. Example of how the centre of a dual-function mark is identified on high-resolution scans a) using indicator of ASCAN software, b) by identifying the point of intersection of two drawn lines

As can be observed on Figures 8, 9 and 10, adding a crosshair and a small reflective foil to the marks for terrestrial laser scanning does not influence the ability to identify the disk's centre on the scan using geometric means. However, it should be emphasised that analogous to the signals dedicated to scanning, the appropriate resolution and distance should be used – the same as for signals without the added cross and reflective foil. Noise caused by the reflective measurement foil does not significantly decrease the quality of the mark. As can be observed on Table 1, the quality of marking target centres decreased by a few percent. The table below shows the results of the target centre design with cross strokes and reflective film using Z + F LaserControl software algorithms. For the purposes of the experiment, one sign with cross marks (A) was scanned from two distances (22 m and 58 m) and two signs with reflective film (B, C) were also scanned from the same two distances.

The pitch is the distance between two scan pixels. The calculation is based on the scan resolution and the distance from the scanner to the target.

The quality is due to having five different measured values. These values are standardised and calculated to be given back between 0 and 100 %. These values are: the distance to the target, the angle to the target, the fitting result, the target contrast, and the resolution.

Table 1. Summary of the quality of the centre point of the target scan

		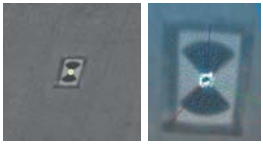	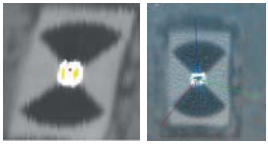
Sign	A	B	C
Distance	22.00 m	22.00 m	22.00 m
Quality	96%	91%	93%
Pitch	3.34 mm	3.54 mm	3.43 mm
	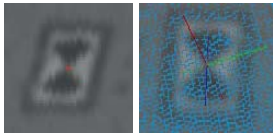	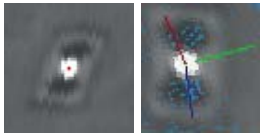	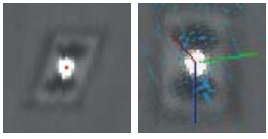
Sign	A	B	C
Distance	58.00 m	58.00 m	58.00 m
Quality	93%	93%	90%
Pitch	8.92 mm	9.08 mm	9.24 mm

4. Target multiplication problem

During measurement work, marks in the form of targets for terrestrial laser scanning were prepared multiple times. The use of such marks is essential when combining scans registered

on different spots (ex. during inventory). This requires the use of a large number of disks – at least 4 disks in order to combine two scans. For reasons of economy, paper copies of the disks are most often used; copies are made by printing or photocopying. When making disks on one's own, it is essential to pay attention to their colour. The use of black and white targets causes the appearance of distortions in the area of the black fields (Fig. 11). A much better visualisation is obtained when using dark grey and white boards.

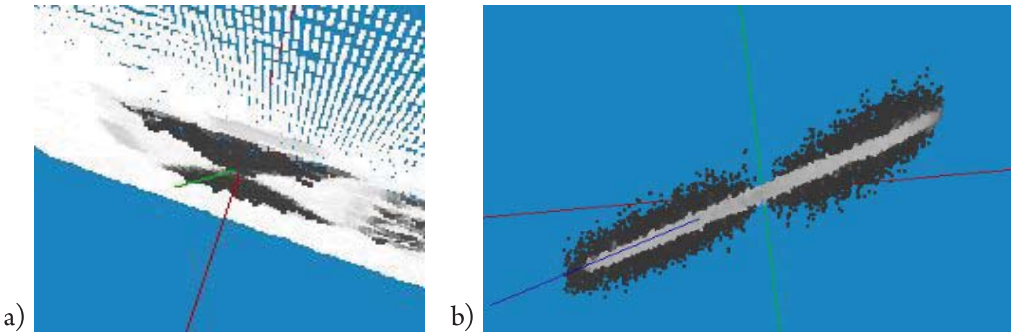

Fig. 11. View of a scan when a black and white board was used; distortions of visualisation in the black field areas are clearly visible: a) view of the point cloud, b) projection of a point cloud fragment on a horizontal plane

During the experiments, it was observed that the type of print is very important. Depending on whether it is ink-jet or laser printing, the marks visualise differently. Most probably, the mineral content present in some of the inks causes the white fields to be invisible on the scans (black fields have the same spectral values as the white fields). The same disks printed on a laser device had good visualisation on the scans. Fig. 12 presents the view of the same target printed on two different printers registered in the intensity value colour range.

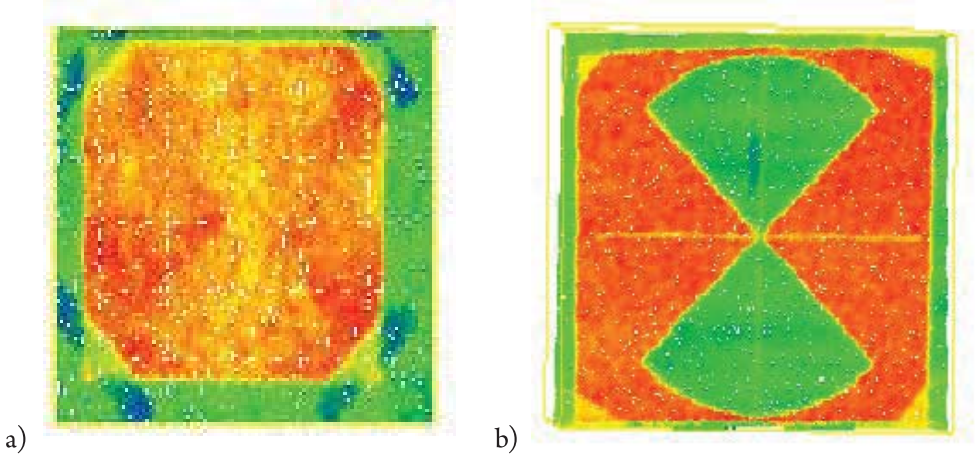

Fig. 12. View of a black and white target a) ink-jet print, b) laser print

5. Target protection

As mentioned in the introduction, terrestrial laser scanning is becoming more and more commonly used in various types of monitoring. Performing periodic measurements requires leaving the marks on the object for prolonged periods of time. Atmospheric conditions – changes in temperature, humidity, high insolation – cause the paper disks which are commonly used in terrestrial laser scanning to quickly deteriorate. The authors suggested using foil laminate in order to protect the marks. Due to the fact that too much reflectivity of the scanned surface causes shortages in data registration or noise in the point cloud, 75 μm-thick matte foil was chosen. A great advantage of a matte surface lies in the fact that when used outdoors, it does not cause sunrays to be reflected from its surface.

A laminated paper mark was tested in the field. The specially-prepared targets were attached to the downstream wall of the water dam in Rożnów, using concrete adhesive (Figs 13, 14). The changing atmospheric conditions, especially the high humidity present on the dam, served as an ideal environment for the experiment. The marks were mounted in August 2013. During control measurements in October 2015, 5 out of 25 mounted marks, that is 20% of all the mounted marks, remained intact on the wall. Most probably, the destruction of the remaining marks might have been caused by the fact that they fell off, as concrete adhesive which was not strong enough was used and the surface under the marks was not cleaned properly (a height of 6 m – this required the use of an aluminium ladder fixed to the wall, which was not conducive to thorough cleaning). The marks that remained after over two years had an excessive level of soiling; however, their structure was undamaged and they were not deformed or discoloured (Fig. 15). Some soiling could be removed by wiping the mark with a cloth.

Fig. 13. Marks mounted in August 2013, view of the whole test field

Fig. 14. Close-up on one of the marks mounted in the test field, August 2013

a)

b)

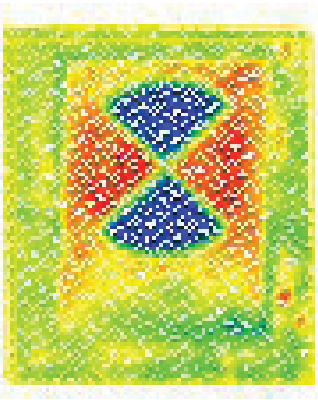

Fig. 15. Close-up on the mark that survived in the test field for over two years, October 2015
a) digital picture, b) point cloud fragment

6. Summary

In the existing works, a major emphasis was put on the decrease of the scan's reciprocal orientation connected to decreases in the ability to identify the centre of the mark as the scan's resolution decreases [3]. The decrease in the ability to orientate the scans is visible on Illustration 16, presenting images of marks created using various scanning modes.

The tests presented in the paper show that focusing on the problem of variable resolution does not cover all the needs of surveying engineering. The described results of the tests to utilise unaltered tachymetric marks in scanning as well target marks and other marks dedicated to scanning in tachymetry, unambiguously show that universal, alternate use of the marks is practically impossible or at least does not fulfil the high accuracy requirements present in surveying engineering.

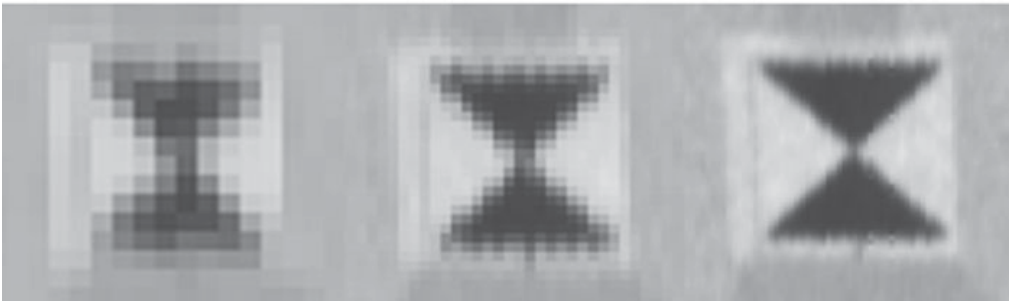

Fig. 16. Target mark images using scanning modes: high (6 mm / 10 m), super high (3.2 mm / 10 m), ultra-high (1.6 mm / 10 m), the images scaled to one size (Z+F Imager 5006 scanner) [3]

The consecutive stages of the preparatory marking process eliminating individual problems that arise both during tachymetric measurements and laser scanning presented in the paper led the authors to the creation of a new kind of mark – a high-contrast target in the form of a circle with a crosshair (Fig. 5). This mark allows accurate direction measurement and is well presented on inventory scans of objects.

The proposed method of foliating the marks with a layer of thin, matte foil appears to be a good protection measure in cases where they remain on the object for an extended period of time. Marks described in the text were fixed to an inclined concrete surface and, without any additional protective measures, remained on the object in good condition for a period of two years. After that time, they were still usable and no detriment in the ability to identify the direction or the centre of the mark on a scan was observed.

Reference

[1] Abellan A., Jaboyedoff M., Oppikofer T., Vilaplana J.M., *Detection of millimetric deformation using a terrestrial laser scanner: Experiment and application to a rockfall event*, Nat Hazards Earth Syst Sci., 03/17, 9(2), 2009, 365–372.

[2] Brasington J., Vericat D., Rychkov I., *Modeling river bed morphology, roughness, and surface sedimentology using high resolution terrestrial laser scanning*, Water Resources Research, 2012, 48(11).

[3] Markiewicz J., Kowalczyk M., Podlasiak P., Krzysztof B., Zawieska D., Bujakiewicz A., Andrzejewska E., *Analiza wpływu rozdzielczości danych źródłowych na jakość produktów fotogrametrycznych obiektu architektury*, [In:] *Measurement technologies in surveying. Geodezyjne technologie pomiarowe*, ed. Kurczyński Zdzisław, 2013, 69–84.

[4] Pu S., Vosselman G., *Knowledge based reconstruction of building models from terrestrial laser scanning data*, ISPRS Journal of Photogrammetry and Remote Sensing, 64(6), 2009, 575–584.

[5] Riveiro B., Morer P., Arias P., De Arteaga I., *Terrestrial laser scanning and limit analysis of masonry arch bridges*, Construction and building materials, 25(4), 2011, 1726–1735.

[6] Štroner M., Smítka V., Třasák P., *Evaluation of Accuracy of Control Points´ position using a Laser Scanning System Leica HDS3000*, Reports on Geodesy, Warsaw University of Technology, Warszawa 2011, Vol. 90, No. 90.
[7] Vosselman G.V., Maas, H. G., *Airborne and terrestrial laser scanning*, Whitles Publishing 2010.
[8] Zaczek-Peplinska J., Pasik M., Adamek A., Adamek A., Kołakowska M., Łapiński S., *Monitoring technical conditions of engineering structures using the terrestrial laser scanning technology*, Reports on Geodesy and Geoinformatics, 95(1), 2013, 1–10.
[9] Zaczek-Peplinska J., Popielski P., *Utilisation of terrestrial laser scanning for verification of geometry of numerical models of hydrotechnical structures using the example of a section of the concrete Besko Dam*, Czasopismo Techniczne, 10/2013, 110.
[10] Zaczek-Peplinska J., Adamek A., Kowalska M., Pasik M., Łapiński S., Adamek A., Baran M., *Inwentaryzacja stanu i monitorowanie deformacji ścian szczelinowych z wykorzystaniem technologii naziemnego skanowania laserowego*, [In:] *Teoretyczne podstawy budownictwa. Tom VI. Geodezyjne systemy pomiarowe*, eds. J. Kulesza, I. Wyczałek, Oficyna Wydawnicza Politechniki Warszawskiej, Warszawa 2014, 51–58.

TECHNICAL TRANSACTIONS 1/2018
MECHANICS
DOI: 10.4467/2353737XCT.18.013.7964
SUBMISSION OF THE FINAL VERSION: 2/1/2018

Urszula Ferdek (uferdek@mech.pk.edu.pl)
Faculty of Mechanical Engineering, Cracow University of Technology

The modelling and analysis of shock absorbers with stroke-dependent damping

Modelowanie i analiza amortyzatora z tłumieniem zależnym od amplitudy

Abstract

In order to obtain the characteristics of a damping force which depends on the amplitude and frequency of the excitation, a modification to the vehicle shock absorber is proposed in this paper. Within the range of small amplitudes, the 'soft' characteristics improve riding comfort, while within the resonance ranges, the increased damping force provides a higher level of ride safety. A nonlinear model of the system is introduced, taking into account various strategies of oil-flow control. Utilising numerical integration methods, the influence of excitation parameters and constructional parameters on the characteristics of the damper is investigated.

Keywords: hydraulic damper, vehicle suspension, nonlinear vibrations

Streszczenie

W pracy zaproponowano koncepcję amortyzatora samochodowego, którego charakterystyka zależy od amplitudy i częstotliwości wymuszenia. W zakresie małych amplitud charakterystyka miękka poprawia komfort jazdy. W zakresach rezonansowych zwiększona siła tłumienia zapewnia większe bezpieczeństwo jazdy. Opracowano nieliniowy model układu uwzględniający różne strategie sterowania przepływem oleju. Wykorzystując metody numerycznego całkowania, zbadano wpływ parametrów wymuszenia oraz parametrów konstrukcyjnych na charakterystyki tłumika.

Słowa kluczowe: tłumik hydrauliczny, zawieszenie samochodu, nieliniowe drgania

1. Introduction

The problem of the modelling and analysis of hydraulic dampers has been discussed in many papers – this is due to their wide range of applications, especially in the automotive industry. A properly designed damper should meet criteria that are partly contradictory, namely good comfort and high levels of ride safety. Within the range of small amplitudes and high excitation frequencies, a shock absorber should have 'soft' characteristics, and for higher amplitudes, the opposite – 'hard' characteristics. In order to bring together these contradictory requirements, semi-active systems [6], usually magneto-rheological [12], are often applied to adjust the damping force to the conditions of the ride. However, these have a more complicated construction and as a result, they are more expensive both in terms of production and operation. Similar properties of damping characteristics can be obtained with suitably modified passive dampers, e.g. bypass systems [10].

In order to assess the effectiveness of hydraulic dampers, analyses of various vehicle models, e.g. quarter-car or half-car [6, 7, 12] are performed. System responses to harmonic excitations of variable frequencies, impulse or random forces, are most commonly studied. The analysis of a car model requires the introduction of a hydraulic damper model which is relatively simple but properly describes its basic properties, and simultaneously allows the investigation of the influence of essential parameters. Tests of modelling twin-tube dampers [1, 5, 8, 15] and mono-tube dampers [4, 8, 10, 13, 16] are undertaken in many works. These tests mainly differ in their approach to describing the oil flow through the valves.

Alonso & Comas [1] investigated the twin-tube damper model taking into account the cavitation problem and the elasticity of the damper chambers. In order to determine the oil flow rate through the pressure valves, the shim stack blanking off an orifice in a piston is modelling by the stiff plate pressed by a spring. Talbott & Starkey [13] investigated the mono-tube damper, they also modelled the influence of the shim stack pressed by a spring. Flow through orifices covered by a shim stack is much more accurately described by Farjoud et al. [4], who investigated the influence of the shim stack properties on the characteristics of the mono-tube damper.

Benaziz et al. [2] draw attention to the acoustic comfort problem, which depends on valve vibrations. In order to describe valve vibrations, they take into account the inertial and viscoelastic properties of shims and introduce spring-supported movement limiters, which model shim strokes on the piston surface. Ventura [15] determined the frequency characteristics of a quarter-car model with a twin-tube hydraulic damper. The paper includes a comparison of theoretical and experimental pressure diagrams in two chambers of a damper. Funke & Bestle [8] performed the investigation of a mono-tube damper. They investigated the response of the system to harmonic excitations of a limited maximum velocity, assuming – for higher frequencies – appropriately lower excitation amplitudes. Titurus et al. [14] also dealt with the identification problem on the basis of system responses to excitations with a piecewise constant velocity. Witters & Swevers [16] present the black-box identification method of a semi-active mono-tube damper, by means of a neural network. Lee & Moon [10] discuss a model of a displacement-sensitive shock absorber. Depending on the piston displacement, the flow control is realised by the proper configuration of the inner surface of the cylinder.

In the present paper, a model of a hydraulic damper with characteristics dependent on the amplitude and frequency of the excitation is proposed. Numerical analysis of the model shows that the damping force depends on the amplitude and frequency of the excitation. Within the range of small amplitudes and high frequencies, the system behaves like a shock absorber of 'soft' characteristics, which improves driving comfort. Within resonance ranges, the increased damping force provides a higher level of ride safety.

2. Model of variable damping shock absorber

A model of a mono-tube hydraulic shock absorber with a construction similar to the damper presented in papers [3, 9, 11] is presented in Fig.1. There are two chambers filled with oil in the main cylinder: rebound chamber K_1 above the piston; chamber K_2 below the piston. An additional cylinder is rigidly connected to the piston rod and the resiliently attached piston divides this cylinder into two chambers, K_3 and K_4. A floating piston is placed in the main cylinder, separating chamber K_2 (which is filled with oil) from chamber K_5, which is filled with gas under high pressure (2–3 MPa).

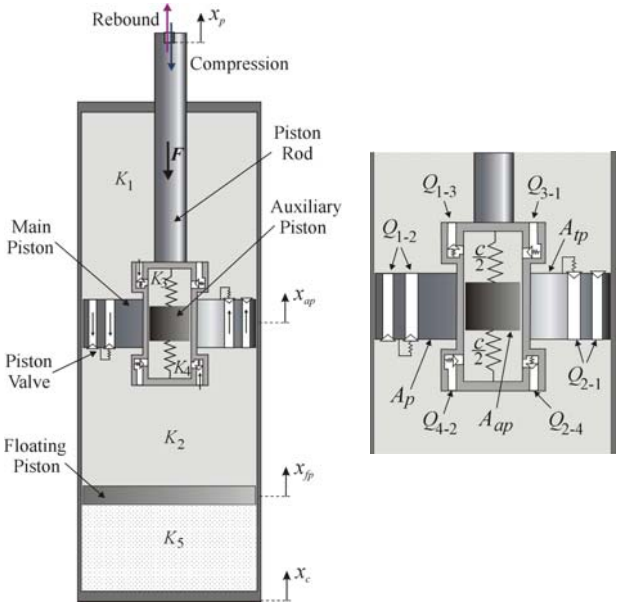

Fig. 1. Damper model

Two phases of piston rod motion are essential in damper operations, namely compression and rebound (expansion). During the compression phase, the piston rod moves down causing a pressure increase in chamber K_2 and the flow of oil into chambers K_1 and K_4. During the rebound process, the oil flows into chambers K_2 and K_3 due to the pressure increase in chamber K_1. Since the orifices in the additional cylinder can be blocked by the auxiliary

piston, the flow of oil into chambers K_3 and K_4 occurs within the limited relative displacement range of the auxiliary piston. The valves are designed so that the flow of oil in the compression and rebound phases occurs through other channels (of different cross-sectional areas), which finally causes asymmetry of the damper characteristics.

The resistance force depends on the resultant pressure force acting on the piston, therefore on the oil pressure in chambers K_1 and K_2. In order to determine these pressures, the processes taking place in the chambers should be considered with special attention directed to the proper description of the flow of oil between the chambers.

The notation used in this paper is as follows:

$p_i\,(i = 1,..,4)$ – pressures in chambers K_i;

$V_i\,(i = 1,..,4)$ – current volumes of chambers K_i;

$V_{i0}\,(i = 1,..,4)$ – initial volumes of chambers K_i (in the equilibrium state);

p_g, V_g, V_{g0} – the gas pressure and the current and initial volumes of chamber K_S;

A_{tp}, A_p – the top and the bottom area of the main piston;

A_{ap} – the area of the additional piston;

x_c – the absolute displacement of the cylinder;

x_p, $x = x_p - x_c$ – the absolute and relative displacements of main piston

x_{fp}, $y = x_{fp} - x_c$ – the absolute and relative displacements of floating piston

x_{ap}, $z = x_{ap} - x_p$. – the absolute and relative displacements of auxiliary piston.

Taking friction force F_{f1} between the main piston and the cylinder into consideration, the damping force can be described as:

$$F = (p_1 - p_0)A_{tp} - (p_2 - p_0)A_p + (p_4 - p_3)A_{ap} + F_{f1}\,\mathrm{sgn}(\dot{x}_p - \dot{x}_c) \qquad (1)$$
$$+ F_{f3}\,\mathrm{sgn}(\dot{x}_p - \dot{x}_{ap}) + c(x_p - x_{ap})$$

where p_0 is the working pressure of the gas. Pressure values p_1 and p_2 depend on all the relative displacements and on the pressures in other damper chambers. In order to determine displacements of the floating piston and the auxiliary piston, the differential equations of the following form need to be solved:

$$m_{fp}\ddot{x}_{fp} = (p_g - p_2)A_p - F_{f2}\,\mathrm{sgn}(\dot{x}_{fp} - \dot{x}_c) \qquad (2)$$

$$m_{ap}\ddot{x}_{ap} = (p_4 - p_3)A_{ap} - cz - F_{f3}\,\mathrm{sgn}(\dot{x}_{ap} - \dot{x}_p) \qquad (3)$$

where m_{fp} is the floating piston mass and m_{ap} is the auxiliary piston mass, and c is the stiffness coefficient of the spring. The friction forces between the floating piston and the cylinder, and also between the auxiliary piston and the additional cylinder, are determined by parameters F_{f2} and F_{f3}. Equations (2–3) describe the vibration of the system around the static equilibrium position. In order to determine gas pressure p_g in chamber K_S, an adiabatic process (or a polytropic process) is usually assumed: $p_g V_g^k = p_0 V_{g0}^{\ k}$, where $V_g = V_{g0} + A_p y$. The following formula is then obtained:

$$p_g = p_0 \frac{V_{g0}^{\kappa}}{(V_{g0} + A_p y)^{\kappa}} \tag{4}$$

To determine the oil pressure in chambers K_i $(i = 1, 2, 3, 4)$, the following equation can be used:

$$\dot{\rho}_i V_i + \rho_i \dot{V}_i = Q_i \tag{5}$$

where Q_i represents the mass flow rates. Volumes of chambers can be calculated as:

$$V_1 = V_{10} - A_{tp} x \tag{6}$$
$$V_2 = V_{20} + A_p (x - y) \tag{7}$$
$$V_3 = V_{30} - A_{ap} z \tag{8}$$
$$V_4 = V_{40} + A_{ap} z \tag{9}$$

After using the equation describing oil density change ρ_i in chamber K_i:

$$\frac{\mathrm{d}\rho_i}{\mathrm{d}p_i} = \frac{1}{\beta} \rho_i \tag{10}$$

where β is a bulk modulus, equation (5) can be written as:

$$\dot{p}_i = \frac{\beta}{V_i} \left[\frac{Q_i}{\rho_i} - \dot{V}_i \right] \tag{11}$$

The oil density in the corresponding chamber can be determined directly from the definition $\rho_I = m_i / V_i$ after solving the following differential equation:

$$\dot{m}_i = Q_i \tag{12}$$

3. Model of servo-valve

The operation of the hydraulic damper mainly depends on the strategies used for the control of the flow of oil, in other words on the functions describing mass flow rates Q_i in the damper model. These flow rates are the sum of the flow rates from the individual bleed orifices and are described as:

$$Q_1 = Q_{21} - Q_{12} + Q_{31} - Q_{13} \tag{13}$$

$$Q_2 = Q_{12} - Q_{21} + Q_{42} - Q_{24} \tag{14}$$

$$Q_3 = Q_{13} - Q_{31} \tag{15}$$

$$Q_4 = Q_{24} - Q_{42} \tag{16}$$

where Q_{ji} is the mass flow rate from chamber K_j to chamber K_i. In the case of flow in the reverse direction: $Q_{ji} = 0$ (then $Q_{ij} \neq 0$). In order to determine flow rate Q_{ji}, the turbulent flow is most often assumed [14]:

$$Q_{ji} = C_d A_{ji} \sqrt{2\rho_j (p_j - p_i)} \tag{17}$$

where C_d is the discharge coefficient, while A_{ji} is the effective cross-sectional area of the orifice. Equation (17) is correct for $p_j > p_i$. Area A_{ji} can have constant or variable values, depending on pressures in the respective chambers, or on the relative piston displacements. The damping force depends mainly on the ratio of the total area of the flow channels to the main piston area.

The flow through the valves located in the main piston (Q_{12}, Q_{21}), are considered first. Bleed orifices are usually covered by a stack of circular plates, which are deflecting under the influence of the resultant pressure force and gradually uncovering the orifices. The effective cross-sectional area depends on the geometrical and physical parameters of plates. For simplicity, it is assumed here that in the main piston, apart from the orifices of constantly opened, there are also orifices which are gradually uncovered when the resultant pressure force exceeds the preload force – this occurs when the pressure exceeds the certain critical value s. Let us introduce the function:

$$\theta(p_j - p_i, \sigma, k) = H(p_j - p_i - \sigma) \tanh(p_j - p_i - \sigma)/k \tag{18}$$

where $H()$ is the unit step function, and parameter k characterises the elastic properties of the valve. The maximum value of function q is equal to unity. Effective areas A_{ji} ($j = 1$, $i = 2$ or $j = 2$, $i = 1$) can be written as:

$$A_{ji} = A_p [\alpha_{ji} + \beta_{ji} \theta(p_j - p_i, \sigma_{ji}, k_{ji})] \tag{19}$$

where dimensionless parameters a_{ij} characterise the areas of orifices of constantly opened, and β_{ij} are the maximum areas of orifices covered by plates.

The oil flow into chambers K_3 and K_4 (Q_{13}, Q_{31}, Q_{24}, Q_{42}), are now considered. In the proposed damper model, the valves placed in these chambers can be covered by the auxiliary piston, in chamber K_3 for $z > h_1 - r_1$ and in chamber K_4 for $z < -h_2 + r_2$, where distances h_i and r_i, respectively, determine the location of the orifices and their radii. Let us introduce another function:

$$\vartheta(z,h,r) = \begin{cases} 0 & z \geq h + r \\ (h + r - z)/2r & h - r < z < h + r \\ 1 & z < h - r \end{cases} \tag{20}$$

where it is assumed that within the range (h–r, h+r), the areas of the cross sections are subjected to a linear change. The effective areas in chamber K_3 are described by:

$$A_{ji} = \gamma_{ji} A_p \vartheta(z, h_1, r_1)\theta(p_j - p_i, \sigma_{ji}, k_{ji}) \tag{21}$$

where $j = 1$, $i = 3$ or $j = 3$, $i = 1$, and in chamber K_4 (for $j = 2$, $i = 4$ or $j = 4$, $i = 2$) similarly:

$$A_{ji} = \gamma_{ji} A_p \vartheta(-z, h_2, r_2)\theta(p_j - p_i, \sigma_{ji}, k_{ji}) \tag{22}$$

Dimensionless parameters g_{ij} characterise the maximum cross sectional area value of the orifice. Function q, appearing in equations (21, 22), takes elastic properties of the valves in chambers K_3 and K_4 into account. For $s_{ji} = 0$ (lack of the preliminary down-pressing force) and relatively small values of k_{ji}, the effective area A_{ji} mainly depends on the relative auxiliary piston displacement.

4. Results of the numerical simulations

The basic characteristics of the shock absorber are the dependences of damping forces (1) on the piston displacements and its relative velocity. In order to determine these characteristics, the system of nonlinear differential equations (2, 3) and (11, 12) should be solved for the assumed kinematic excitation $x(t)$. In the case of a damper that is mounted in a car suspension system, the kinematic excitation results from the profile of the road. Such excitation is described by a random function in which a power spectral density is a decreasing frequency function. To determine the damping characteristics, it is more practical to use harmonic excitation, the amplitude of which decreases as frequency increases:

$$x(t) = a \sin \omega t \tag{23}$$

where $\omega a = \omega_1 a_0 = \text{const}$ (condition of constant maximum velocity), and $\omega_1 = 2\pi f_1$ is the basic frequency of the vehicle model. For many car models, the first frequency is in the range f_1=1.2-1.5 Hz, the second is in the range f_2=12–18 Hz. In the range of lower frequencies, vibrations of the so-called spring-supported mass (mainly of the motor-car body) dominate; therefore, this range is responsible for the comfort of the ride. In the second range of higher frequencies, vibrations of non-spring-supported masses are observed, (mainly in the form of wheel vibrations), so this range is important for the safety of the ride.

The values of the characteristic parameters of the shock absorber were determined in the performed simulations. The influence of the parameters determining on the flow of oil between individual chambers (α_{ij}, β_{ij}, γ_{ij}, σ_{ij}) and excitation parameters (a, f) was investigated in detail. The following values of parameters were used: $A_p = 10$ cm^2, $A_{tp} = 8$ cm^2, $A_{ap} = 3$ cm^2, $V_{10} = V_{20} = 80$ cm^3, $V_{g0} = 70$ cm^3, $V_{30} = V_{40} = 7.5$ cm^3, $p_0 = 2$ MPa, $\beta = 1.5$ GPa, $\rho_0 = 890$ kgm^{-3}, $m_{fp} = m_{ap} = 0.02$ kg, $c = 500$ Nm^{-1}, $F_{f1} = 10$ N, $F_{f2} = 1$ N, $F_{f3} = 0.1$ N, $k_{12} = k_{21} = 0.6p_0$, $h_1 = h_2 = h = 2$ cm, $r_1 = r_2 = r = 2$ mm, $C_d = 0.6$, $\kappa = 1.4$. The values of the remaining parameters were changed within certain ranges and they oscillated around the following values: $\alpha_{21} = 0.004$, $\alpha_{12} = 0.002$, $\beta_{21} = 0.016$, $\beta_{12} = 0.008$, $\gamma_{31} = 0.012$, $\gamma_{13} = 0.007$, $\gamma_{24} = \gamma_{42} = 0.012$, $\sigma_{21} = \sigma_{12} = 0.25p_0$.

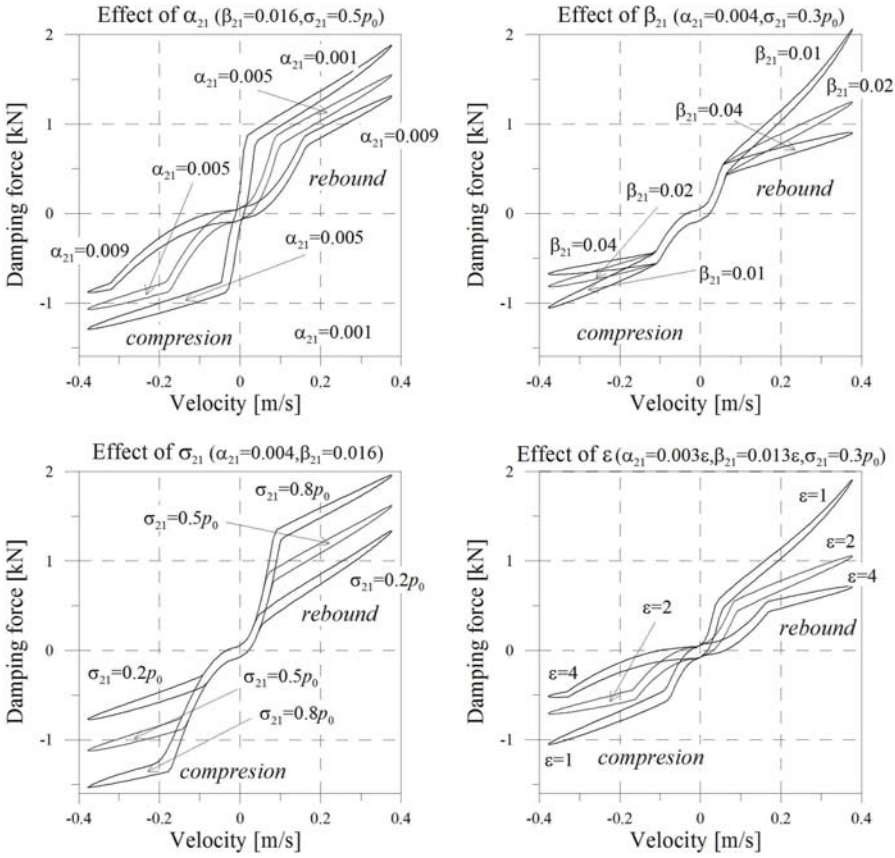

Fig. 2. Influence of valve parameters (a = 4 cm, f = 1.5 Hz)

The proposed shock absorber, within the ranges of large amplitudes, behaves in a similar fashion to the classic mono-tube damper. In these cases, the flow of oil into the K_3 or K_4 chambers is usually completely or at least partially blocked, and the influence on the damper characteristics is mainly due to the parameters: α_{ij}, β_{ij}, σ_{ij}, (i = 1,2, j = 2,1). These parameters are related to the flow of oil through valves located in the main piston.

The dependence of the damping force on the piston relative velocity for various values of parameters is shown in Fig. 2. In these calculations, it was assumed that: $\alpha_{12} = l\alpha_{21}$, $\beta_{12} = l\beta_{21}$, l = 0.5, $\sigma_{21} = \sigma_{12}$, $k_{12} = k_{21} = 0.6p_0$, γ_{31} = 0.012, γ_{13} = 0.007, $\gamma_{24} = \gamma_{42}$ = 0.012. The damping force characteristics are determined for the excitation amplitude α = 4 cm and frequency f = 1.5 Hz, this refers to the first resonance range.

The characteristics shown in Fig. 2 are asymmetrical. The resistance force of the damper during the rebound phase is greater than the force in the compression process. Such characteristics are desirable whilst driving over highly uneven surfaces (e.g. driving over a high obstacle). The ratio between the maximum and minimum values of force depends on the ratio of the effective oil flow areas during compression and rebound, that is from the parameter λ .

Parameters $\alpha_{21,}$ α_{12} influence the damping force characteristics within a range of small velocities (Fig. 2a). Within this range, along with the increasing values of parameters α_{21} and α_{12}, the inclination angle of the curve decreases – this shows the dependence of the damping force on the velocity. In turn, with increasing parameters β_{12} and β_{21}, the inclination angle of the curve decreases within the range of high velocities (Fig. 2b). Inflection points occur in diagrams, whose location significantly depends on the value of parameter σ (Fig. 2c). Parameter σ characterises the preload pressure of the shim stack. For larger values of σ, the bleed orifices open later and in effect, the shape of the characteristics changes for higher relative velocities of the piston. Simultaneously, the maximum values of the damping force increase. The damping force decreases along with increases in the effective cross-sectional area of all orifices, that is, with an increasing value of parameter ε (Fig. 2d).

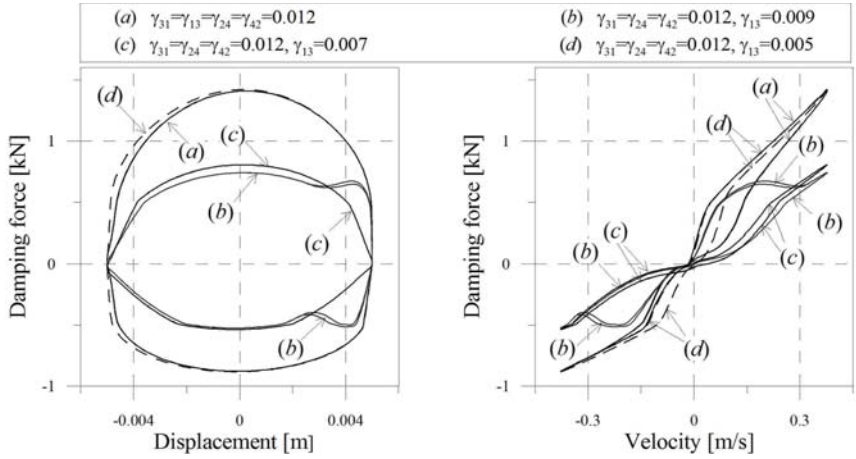

Fig. 3. Damper characteristics (a = 0.5 cm, f = 12 Hz)

In the case of high excitation amplitudes, a properly designed damper should has stiff characteristic (usually within the first resonance range) and soft characteristic for small amplitudes (within the second resonance range). Stiff characteristic is obtained when one or more holes in the inner cylinder are blocked (within K_3 or K_4). In order to obtain soft characteristic, the auxiliary piston should move between the valves without blocking them. In other cases, the characteristic change from stiff to soft or inverse. Parameters γ_{31}, γ_{13}, γ_{42} and γ_{24} have a significant influence on the behaviour of the damper. Based on the simulations, it is observed that in the case of symmetrical orifices $\gamma_{31} = \gamma_{13}$ and $\gamma_{24} = \gamma_{42}$, the damper does not work effectively. However, for $\gamma_{24} = \gamma_{42}$, the values of parameters γ_{31} and γ_{13} can be selected so that the characteristics of the damper are soft in the higher frequency range.

The characteristics of the damper in the vicinity of the second resonance (for a = 5 mm, f = 12 Hz) are shown in Fig. 3 for four parameter values. In the case of curve (a), the valve in chamber K_4 is blocked and the characteristic is stiff; in the case of curve (b), this valve is opened and closed, and the characteristic has the most complicated shape. The best solution is shown in curve (c), where the auxiliary piston moves between the valves, resulting in

a soft characteristics. Curve (d) represents a stiff characteristic, similar to curve (a), but in this case, the valve in chamber K3 is blocked. For smaller frequencies and correspondingly higher amplitudes (within the range of the first resonance, e.g. for f = 1.5 Hz, a = 4 cm), the characteristics are stiff and to a small degree, they depend on parameters γ_{ij}.

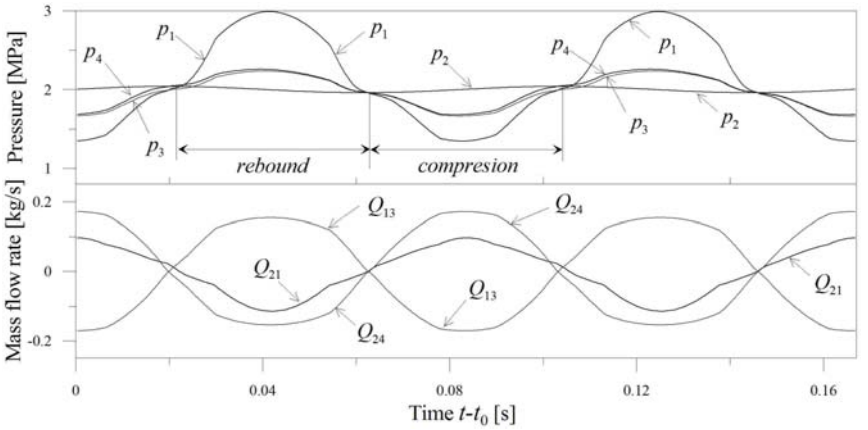

Fig. 4. Pressure time histories and mass flow rates (a = 0.5cm, f = 12Hz)

Diagrams of pressures time histories p_i in chambers K_i (i = 1,...,4) and mass flow rates Q_{21}, Q_{13} and Q_{24} corresponding to the characteristics (c) shown in Fig. 3 (for γ_{13} = 0.007), are presented in Fig. 4. The obtained results refer to the state steady of vibration, where t_0 = 2 [s] is the transition period time. Mass flow rates Q_{13} and Q_{24} are almost the same in value. The difference in the sign of these mass flow rates is also easy to explain. In the compression process: $Q_{24} > 0$ and $Q_{13} < 0$ (i.e. $Q_{31} > 0$), this means that the mass of oil flowing to chamber K_4 is approximately equal to the mass of oil flowing out of chamber K_3 (the fluid is compressible). Time histories for pressures p_3 and p_4 are very similar to each other as a result of the small impact of the spring force and the inertia of the auxiliary piston. Their character is similar to the diagram for pressure p_1. The softest is pressure p_2 – this oscillates around the working pressure. Time intervals corresponding to the compression and rebound are determined by analysing the sign of the relative piston velocity. A decisive influence on the damping force has pressure p_1 in the rebound chamber.

The characteristics of the shock absorber for the excitations satisfying the condition of the same maximum velocity value, i.e. condition fa = const, are shown in Fig. 5. When the excitation frequency increases, its amplitude decreases accordingly. Within the lower frequency range (larger amplitudes), the damping forces are significantly higher (curves (a) and (b) in Fig. 4) than within the higher frequency range. In the case of curves (c) and (d), the auxiliary piston moves in the inner cylinder between the bleed orifices.

The conclusion concerning the characteristics changing from stiff to soft in the higher frequency ranges is correct only under the assumption that the excitation amplitude decreases with increasing frequency. This is the situation which is most often encountered in practice. However, for constant excitation amplitude, the increase of frequency usually results in the

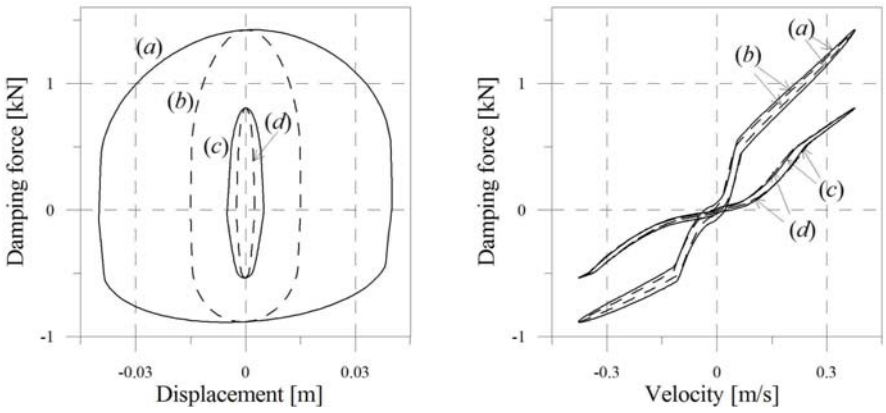

Fig. 5. Damper characteristics: (a) f = 1.5 Hz, a = 40 mm; (b) f = 4 Hz, a = 15 mm; (c) f = 12 Hz, a = 5 mm; (d) f = 24 Hz, a = 2.5 mm

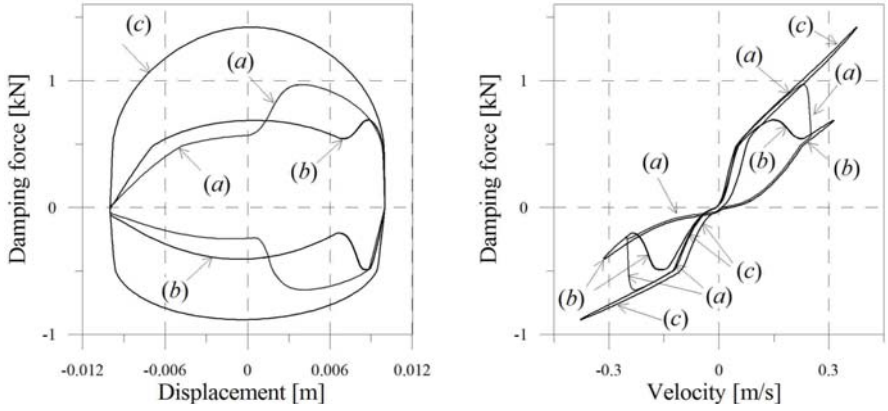

Fig. 6. Damper characteristics (a = 1 cm): (a) f = 4 Hz; (b) f = 5 Hz; (c) f = 6 Hz

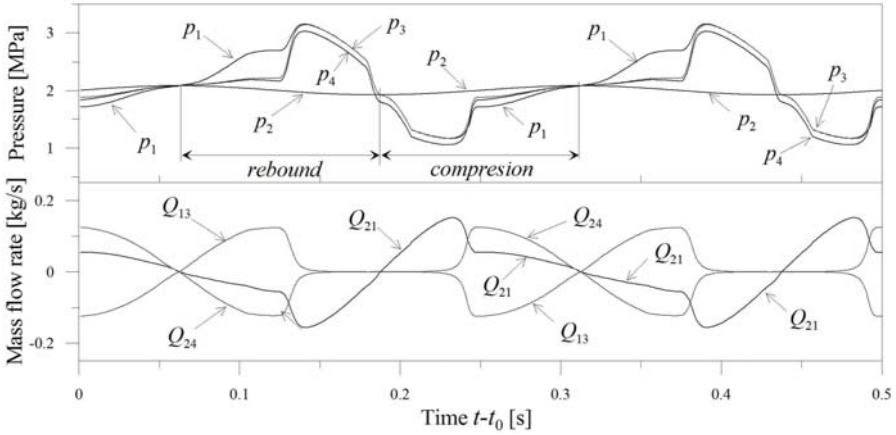

Fig. 7. Pressure time histories and mass flow rates (a = 1 cm, f = 4 Hz, $g_{24} = g_{42} = g_{31} = 0.012$, $g_{13} = 0.007$

inverse change from soft to stiff characteristics (Fig. 6). This is mainly due to the increase of the maximum values of the relative velocity of the piston.

The diagrams of pressure time histories and mass flow rates corresponding to curve (a) in Fig. 6 are presented in Fig. 7. Most of the conclusions for the analysis of the results shown in Fig. 4 remain valid. Compared Fig. 7 to the previously presented Fig. 4, more rapid changes to pressure p_1 resulting from the jump from the soft branch of characteristics to the stiff branch can be observed. Within time ranges in which $Q_{13} \approx Q_{24} \approx 0$, the valve in chamber K_3 or K_4 is closed.

5. Conclusions

A modified model of a vibration damper with characteristics dependent on the amplitude and frequency of the excitation has been proposed in the present paper. An internal cylinder with auxiliary piston to a classical mono-tube damper has been introduced. The non-linear model description has also been provided – this includes control of the flow of oil between the damper chambers, depending on both pressure and the relative displacement of the piston.

Several numerical simulations were performed and their most important results have been presented in this work. The influence of the constructional parameters of the shock absorber on the damping force characteristics was investigated in detail. The quantitative analysis indicated a significant influence of parameters depending on the geometric and physical properties of the constructional elements of valves in the main piston and in the internal cylinder.

The application of the proposed solution allows the obtaining of a satisfactorily high damping force for large relative displacements of the piston. In such a case, the shock absorber meets the requirements of a 'hard' damper, in doing so, it improves ride safety levels. On the other hand, when the relative displacements are small, the 'soft' damper characteristics provide a high level of ride comfort.

A full analysis of the effectiveness of a damper in a vehicle suspension system requires the development of a vehicle model with the tested damper and the investigation of the influence of its parameters on the indices responsible for both ride safety and ride comfort.

References

[1] Alonso M., Comas Á., *Modelling a twin tube cavitating shock absorber*, Proceedings of the Institution of Mechanical Engineers, Part D: Journal of Automobile Engineering. 220.8, 2006, 1031–1040.

[2] Benaziz M., Nacivet S., Thouverez F., *Nonlinear dynamic analysis of a shock absorber hydraulic spring valve*, Proceedings of ISMA International Conference on Noise and Vibration Engineering, 2012, 3857–3870.

[3] Deferme S., *Stroke dependent bypass*. U.S. Patent No. 6,918,473. 19 Jul. 2005.

[4] Farjoud, Ahmadian M., Craft M., Burke W., *Nonlinear modelling and experimental characterization of hydraulic dampers: effects of shim stack and orifice parameters on damper performance*, Nonlinear Dynamics. 67.2, 2012, 1437–1456.
[5] Ferdek U., Łuczko J., *Modelling and analysis of a twin-tube hydraulic shock absorber*, Journal of Theoretical and Applied Mechanics. 50.2, 2012, 627–638.
[6] Ferdek U., Łuczko J., *Performance comparison of active and semi-active SMC and LQR regulators in a quarter-car model*, Journal of Theoretical and Applied Mechanics. 53.4, 2015, 811–822.
[7] Ferdek U., Łuczko J., *Vibration analysis of a half-car model with semi-active damping*, Journal of Theoretical and Applied Mechanics, 54.2, 2016, 321–332.
[8] Funke T., Bestle D., *Physics-based model of a stroke-dependent shock absorber*, Multibody System Dynamics. 30.2, 2013, 221–232.
[9] Götz O. et al., *Dashpot with amplitude-dependent shock absorption*, U.S. Patent No. 7,441,639. 28 Oct. 2008.
[10] Lee C.T., Moon B.Y., *Simulation and experimental validation of vehicle dynamic characteristics for displacement-sensitive shock absorber using fluid-flow modelling*, Mechanical Systems and Signal Processing. 20.2, 2006, 373–388.
[11] Nowaczyk M., Vochten J.: *Shock absorber with frequency dependent passive valve*, U.S. Patent No. 9,441,700. 13 Sep. 2016.
[12] Prabakar R.S., Sujatha C., Narayanan S., *Optimal semi-active preview control response of a half car vehicle model with magnetorheological damper*, Journal of Sound and Vibration, 326.3, 2009, 400–420.
[13] Talbott M.S., Starkey J., *An experimentally validated physical model of a high-performance mono-tube damper*, SAE Technical Paper, 2002.
[14] Titurus B., Du Bois J., Lieven N., Hansford R., *A method for the identification of hydraulic damper characteristics from steady velocity inputs*, Mechanical Systems and Signal Processing. 24.8, 2010, 2868–2887.
[15] Ventura P., Ferreira C., Neves C., Morais R., Valente A., Reis M.J., *An embedded system to assess the automotive shock absorber condition under vehicle operation*, Sensors, 2008 IEEE. IEEE, 2008, 1210–1213.
[16] Witters M., Swevers J., *Black-box model identification for a continuously variable, electro-hydraulic semi-active damper*, Mechanical Systems and Signal Processing, 24.1, 2010, 4–18.

TECHNICAL TRANSACTIONS 1/2018
MECHANICS
DOI: 10.4467/2353737XCT.18.014.7965
SUBMISSION OF THE FINAL VERSION: 20/12/2017

Marcin Jasiewicz (marcin.jasiewicz@zut.edu.pl)
Institute of Mechanical Technology, Faculty of Mechanical Engineering and Mechatronics, West Pomeranian University of Technology, Szczecin

The dynamic repeatability of a machine tool–holder–workpiece system

Powtarzalność wyznaczania właściwości dynamicznych układu obrabiarka–uchwyt–przedmiot obrabiany

Abstract

Knowledge of the dynamic properties of a machine tool–holder–workpiece system is crucial for the appropriate selection of machining parameters based on stability lobes. One of the most convenient methods allowing for the experimental identification of these properties is impact testing. However, the repeatability of such measurements may be different depending on the machine–workpiece setup and can lead to incorrect cutting parameter calculations. The article presents this issue on the example of a lathe-workpiece system. The experimental setup and obtained measurement results are presented and discussed.

Keywords: machining stability, turning, impact testing, dynamic repeatability

Streszczenie

Znajomość właściwości dynamicznych układu obrabiarka–uchwyt–przedmiot obrabiany jest kluczowa przy doborze odpowiednich parametrów technologicznych obróbki przy wykorzystaniu krzywych workowych. Jedną z podstawowych eksperymentalnych metod wyznaczania tych właściwości są testy impulsowe. Jednakże, w ramach rozpatrywanego układu obrabiarka–przedmiot wyniki uzyskane w ramach przeprowadzania takich pomiarów mogą się różnić, co jednocześnie prowadzić może do doboru niewłaściwych parametrów obróbki. W pracy przedstawiono niniejsze zagadnienie na przykładzie tokarki. Zaprezentowano badany układ, wyniki przeprowadzonych pomiarów oraz interpretację wyników.

Słowa kluczowe: stabilność obróbki, toczenie, testy impulsowe, powtarzalność

1. Introduction

In addition to ensuring appropriate dimensional accuracy and surface quality of machined parts, contemporary machining also needs to be highly efficient. The achievement of these requirements is possible only when the machining is carried out in stable cutting conditions i.e. where there are no chatter vibrations, leading to the surface damage on the workpiece (chatter marks), reduction of tool-life and faster wear of machine tool subassemblies [1–3]. Chatter vibrations may be avoided by proper selection of cutting parameters such as feed rate, cutting depth and rotational speed (of the workpiece for turning or the tool for milling). The selection of these parameters can be carried out using the so-called stability lobes presented as a border cutting depth at which chatter vibration develops as a function of rotational speed [2, 4]. In order to calculate the stability lobes, a model of the cutting process (determined by cutting force coefficients for specific machining operations) and the dynamic properties of the machine tool–holder–workpiece system need to be identified. These dynamic properties as a frequency response function (FRF) can be determined using a number of methods, these can be analytical, numerical (e.g. Finite Element Method models) or experimental (e.g. impact testing). It is the experimental methods that provide the most complete information about the dynamic properties of the real system; however, these are troublesome due to them typically being particularly laborious, requiring specialised equipment and the measurement uncertainty arising from the variability of the impact test results.

The problem of the repeatability of FRFs was raised by Medicus and Schmitz [5], where tool point dynamics for tool and holder changes were investigated. They proposed a number of methods of frequency based data presentation. A similar problem was examined in [6] by Lee and Donmez, where the authors presented tool point dynamic variability in milling and its influence on stability lobes. As a result, they highlighted the necessity for continuous updates to dynamic properties to minimalise uncertainty of stability lobes evaluation. In [7], the authors worked on the natural variability of the frequencies and mode shapes of the Alamosa Canyon bridge and proposed another approach for dynamic variability analysis. Kim and Schmitz in [8] widely discussed uncertainty contributors for FRF measurement obtained through

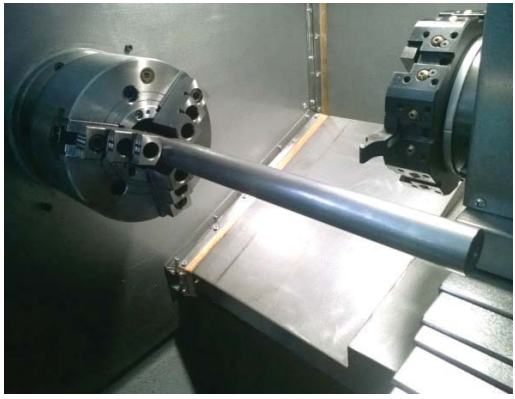

Fig. 1. Test setup: workpiece mounted in a 3-jaw lathe chuck

impact testing. They indicated four main contributors: statistical uncertainty, modal hammer and accelerometers' calibration coefficient uncertainty, cosine errors (due to misalignment between the hammer impact direction and the transducers axis) and accelerometer mass loading. As the authors pointed out, the cosine and mass loading uncertainty are negligible.

In this paper, the issues of repeatability of FRFs measurements for the machine-holder-workpiece system shown in Fig. 1, consisting of a rod-workpiece mounted in 3-jaw lathe chuck are presented. This setup is typical for rope thread machining.

In most cases relating to turning, to calculate the stability lobes, only the tool-tip impact test is preformed, assuming that the workpiece is a rigid body and that its dynamics are negligible. However, in the presented system, the workpiece is the source of significant dynamic compliance that cannot be disregarded.

For the considered system, variability in the experimentally determined FRF may be caused by a number of factors, such as:

- Machine tool issues – the degree of wear of bearings and chuck jaws, type of mounting, the rotational position of the spindle (arrangement of chuck jaws and rolling element of bearings)
- Workpiece issues – for objects of different geometrical and material properties, variability may be different
- Testing setup errors – e.g. variable length of the workpiece in the jaws of the holder, inaccuracies in the location of the accelerometers and the force impact points.

Knowledge of the variability of FRFs obtained experimentally appear to be important as it affects the location of stability lobes, which consequently, may indicate the selection of inappropriate cutting parameters.

The purpose of this study is to investigate the repeatability of the experimentally obtained FRFs of the machine-holder-workpiece system and the determination of their level of variability depending on the above factors and their influence on the calculated stability lobes.

2. Testing setups

The object of the research was the mid-size AFM TAE 35N 'Hanka' CNC lathe presented in Fig. 2 with a spindle equipped with a hydraulically clamped 3-jaw chuck Bison-Bial 2405-200-66K. The fact that the considered lathe was brand new enables the elimination of factors arising from wear of its assemblies (such as chuck jaws or spindle bearings), thus allowing the focus to be on factors independent of a particular machine.

In order to investigate the variability of the FRFs, a series of impact tests of the machine tool–holder–workpiece system presented in Fig. 3 was performed. Measurements on a workpiece of diameter D and length L are carried out at four equidistant points. Only the x-direction was considered for further analyses, since the other directions have a minor effect on the machining stability.

Fig. 2. Testing lathe – AFM TAE 35N

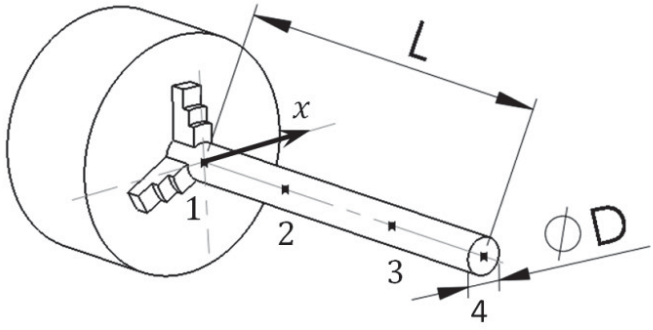

Fig. 3. Distribution of the measurement points on the workpiece

The measurements were carried out for four geometrical and material setups of the workpiece – these are presented in Table 1 below.

Used as workpiece material, A10X is a steel grade especially suitable for high-speed machining and thread cutting because the presence of a large number of non-metallic inclusions facilitates the breaking of the chip during cutting. C45 is a non-alloy quality steel for general engineering purposes.

Apart from workpiece issues, the experiment was designed to investigate the influence of spindle rotational position and testing setup errors (described in paragraph 1) on FRF

Table 3. Workpiece setups

No.	Diameter [mm]	Length [mm]	Material
1	35	350	A10X
2	31	300	C45
3	40	360	C45
4	35	200	C45

repeatability. Therefore, for each workpiece setup presented in Table 1, it was necessary to repeat the measurement cycle, which consisted of:

1) Adjusting the rotational position of the spindle (summary in Fig. 4)
2) Chucking the workpiece in the holder
3) Distribution of the measuring points
4) Impulse test at all four measuring points
5) Removal of the accelerometers
6) Unchucking the workpiece and removal from the holder

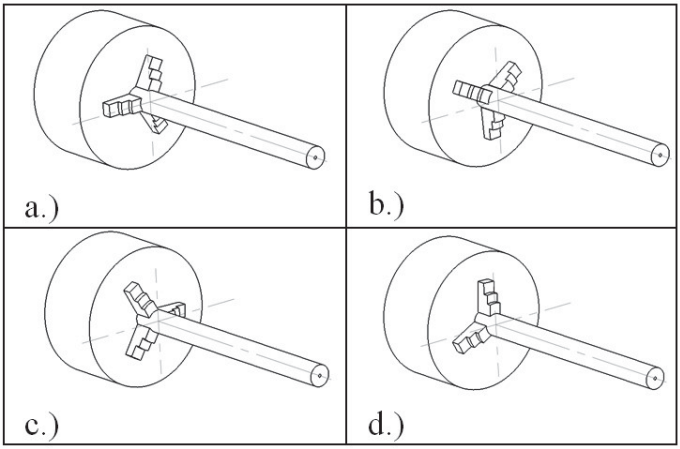

Fig. 4. Rotational positions of the spindle

The above measurement cycle was repeated 12 times for each workpiece configuration (three for each rotational position of the spindle presented in Fig. 4).

3. Experimental tests

In this section, the results of impact tests carried out according to the measurement cycle are presented. The impact tests were carried out using the LMS Scadas III data acquisition system, working with LMS Test Lab software (module Impact Testing). Vibration responses were measured using four PCB 356A01 3 – axial accelerometers, while the structure was

excited with Kistler 9726A20000 modal hammer. A single measurement of FRF consisted of eleven averages (hits). The measurement frequency bandwidth was set at 2048 Hz.

The measurements were carried out at four points – this enabled the identification of the vibration mode shapes. However, the analyses of the repeatability are presented only in two characteristic points – the least compliant, at the spindle (point '1' – FRF H11), and the most flexible, at end of the workpiece (point '4' – FRF H44).

3.1. Mode Shapes analysis

In the considered frequency range, for setups 1-3, three major mode shapes are presented in Fig. 5. Due to it having the highest stiffness, the third mode shape of setup '4' occurred at a frequency above the bandwidth. The first and third modes are characteristic for lateral vibration *of fixed-free continuous beam* and the second, is associated with the vibration mode of the spindle.

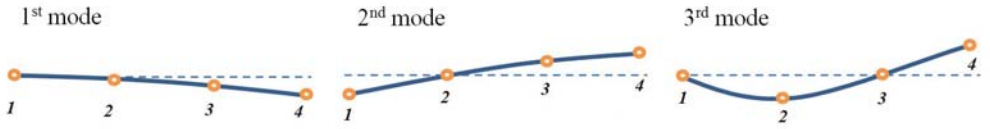

Fig. 5. Mode shapes

3.2. FRFs analysis

The experimentally obtained FRFs of all considered workpiece setups are presented as raw data, i.e. each Fig. contains twelve FRFs measured according to the cycle submitted in Section 2, without distinction between the rotational position of the spindle and other issues. The natural frequencies are summarised in Table 2.

Table 2. Measurement results – frequencies

Setup no.	Mode frequency range	Mean frequency	Standard deviation
1	139 – 149 Hz	144.2 Hz	3.13 Hz
	411 – 413 Hz	412.6 Hz	0.79 Hz
	988 – 1015 Hz	992.2 Hz	10.7 Hz
2	183 – 192 Hz	187.3 Hz	4.4 Hz
	419 – 420 Hz	419.6 Hz	0.51 Hz
	1184 – 1239 Hz	1216.8 Hz	22.3 Hz
3	119 – 142 Hz	131.1 Hz	9.44 Hz
	408 – 413 Hz	412.4 Hz	1.24 Hz
	930 – 1039 Hz	985.9 Hz	43.73 Hz
4	324 – 335 Hz	329.4 Hz	3.53 Hz
	464 – 488 Hz	473.77 Hz	9.66 Hz

The measured FRFs of setup '1' are presented below in Fig. 6.

For rotational spindle positions ‘a’ and ‘c’ (Fig. 4), the best repeatability for all three modes

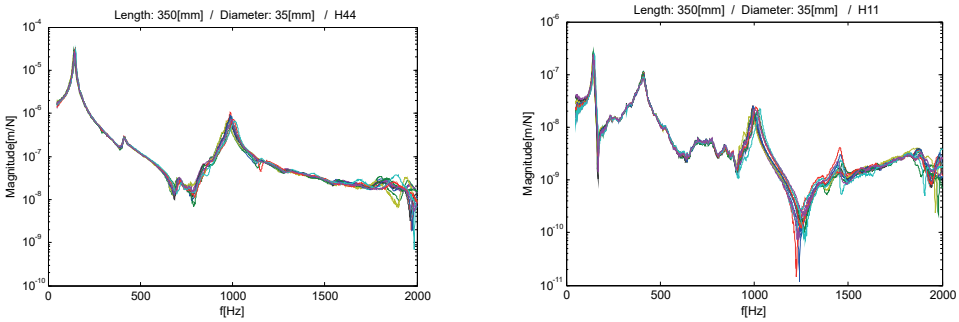

Fig. 6. Workpiece setup ‘1’ – FRFs in points ‘1’ and ‘4’

has been observed. Identified mode frequencies in these cases ranged 142–145 Hz for the first mode (first beam mode), 411–412 Hz for the second (spindle mode), and between 992–998 Hz for the third mode (second beam mode). For rotational positions ‘b’ and ‘d’, more divergence of the results has been observed, particularly for beam modes – the repeatability of the second mode (spindle) remained at a similar level. Apart from the type of rotational position presented in Fig. 4, the exact repetition of the position (one of the chuck jaws was marked) turned out to be significant.

The results of the impact tests for setup ‘2’ are presented below in Fig. 7.

Similarly to the setup ‘1’ three modes have been observed and the highest repeatability was

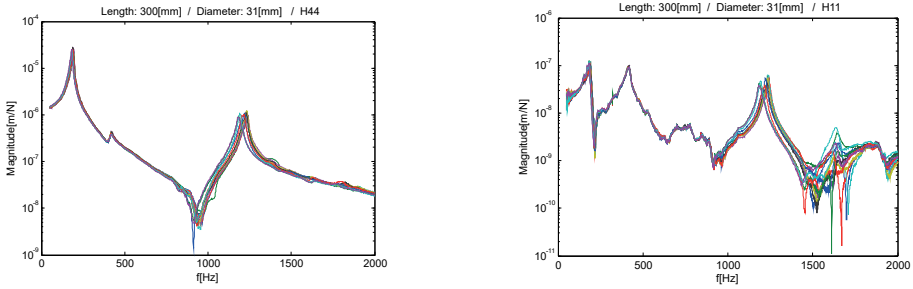

Fig. 7. Workpiece setup ‘2’ – FRFs in points ‘1’ and ‘4’

reached for the second mode (spindle mode) at 420 Hz which is a higher frequency than in other cases. For this setup, there was no noticeable influence of the rotational position of the spindle on the discrepancies of particular FRFs.

The repeatability of the experimental FRFs for setup ‘3’ presented above, taking into consideration all performed measurements, appears to be the lowest. However, out of all

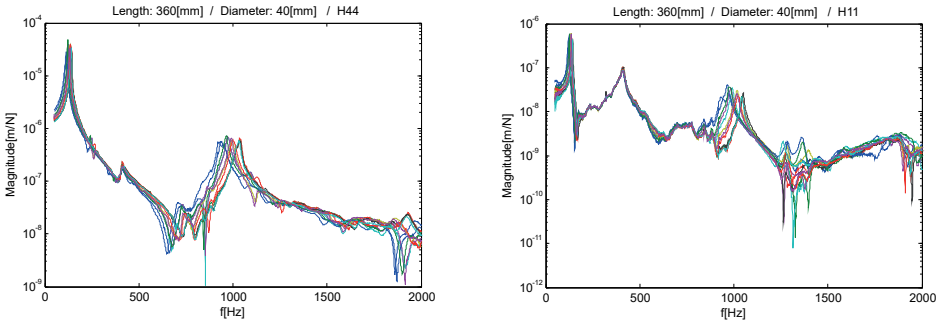

Fig. 8. Workpiece setup '3' – FRFs in points '1' and '4'

examined setups, it was for this case that the impact of the spindle rotational position turned out to be the most influential. The first mode ranged 136–137 Hz for the 'a' position, 119–121 Hz for the 'b' position, 126–129 Hz for 'c' and 139–142 Hz for position 'd'. In all cases, as with setups 1–2, the second mode has the highest repeatability, irrespective of rotational position. Discrepancies for the third mode were significant for all rotational positions.

The results of the impact tests for the last considered setup are presented in Fig. 9.

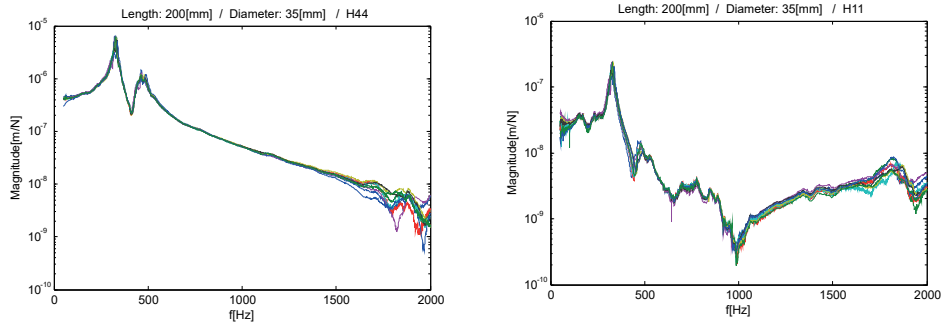

Fig. 9. Workpiece setup '4' - FRFs in points '1' and '4'

The structure of the FRFs of setup '4' is different from the other three setups due to observed dynamic absorber effect [5] that occurs when the natural frequency of the workpiece approaches the natural frequency of the spindle (410–420 Hz), splitting it into two resonant frequencies. Moreover, due to the highest stiffness, in the considered frequency range only two modes have been observed. There was also no effect of the rotational position of the spindle to the variability of the FRFs.

4. Conclusions

In this paper, the issues of repeatability of experimentally obtained FRFs of the machine tool–holder–workpiece for the turning operation are presented. The experimental tests were carried out for four configurations of the workpiece mounted in the 3-jaw chuck of the same, new lathe. For all considered configurations, the variability of results has been observed; however, this has been within different ranges. In setups 1 and 3, the angular position revealed its influence on the obtained FRFs, but not for all positions. Moreover, in configurations 2 and 4, this influence was not observed, and therefore this factor cannot be considered as the main cause of the discrepancies. The results may indicate the need for variability analysis of FRFs depending on the particular workpiece. Only such analysis would allow the reliable identification of the areas of stable machining by applying stability lobes uncertainties.

The researches were carried out within the project INNOTECH – K3/IN3/18/226861/NCBR/14 financed by The National Centre for Research and Development (NCBiR).

References

[1] Altintas Y., Weck M., *Chatter Stability in Metal Cutting and Grinding*, Annals of the CIRP, Key Note, Paper of STC-M, Vol. 53/2 2004, 619–642.

[2] Schmitz T. L., Smith K.S., *Machining dynamics: frequency response to improved productivity*, Springer Science & Business Media, New York 2008.

[3] Pajor M., Marchelek K., Powałka B., *Method of reducing the number of DOF in the machine tool-cutting process system from the point of view of vibrostability analysis*, Modal Analysis 8(4) 2002, 481–492.

[4] Altintas Y., Budak E., *Analytical prediction of stability lobes in milling*, CIRP Annals-Manufacturing Technology, 44(1) 1995, 357–362.

[5] Medicus K., Schmitz T.L., *Evaluating the tool point dynamic repeatability for high-speed machining applications*, Proceedings of the 16th Annual ASPE Meeting, Vol. 19, 2001, 357–360.

[6] Lee K.J., Donmez M.A., *Repeatability analysis on the tool point dynamics for investigation on uncertainty in milling stability*, ASME 2007 International Mechanical Engineering Congress and Exposition American Society of Mechanical Engineers 2007, 477–483.

[7] Farrar C.R., Doebling S.W., Cornwell P.J., Straser E.G., *Variability of modal parameters measured on the Alamosa Canyon Bridge*, Proceedings-SPIE The International Society for Optical Engineering 1997, 257–263.

[8] Kim H.S., Schmitz T.L., *Bivariate uncertainty analysis for impact testing*, Measurement Science and Technology 18.11 2007, 3565–3571.

TECHNICAL TRANSACTIONS 1/2018
MECHANICS
DOI: 10.4467/2353737XCT.18.015.7966
SUBMISSION OF THE FINAL VERSION: 20/12/2017

Patryk Różyło (p.rozylo@pollub.pl)
Machine Design and Mechatronics, Mechanical Faculty, Lublin University of Technology

Numerical analysis of crack initiation and propagation in an aluminium sample

Analiza numeryczna procesu inicjacji i propagacji pękania próbki aluminiowej

Abstract

This paper reports an analysis of simulated crack propagation in an aluminium sample depending on the direction of external loads. The objective of the study was to perform a numerical analysis of crack propagation as well as to determine regions which are most susceptible to failure. The object of study was created from numerical analysis of material failure due to fibre separation using Abaqus 6.14. The modelling of crack propagation was performed using the numerical xFEM method for separating material fibres irrespective of the finite element mesh.

Keywords: Abaqus, xFEM, numerical analysis, crack initiation and propagation

Streszczenie

W ramach pracy przeprowadzono symulację numeryczną procesu propagacji pękania aluminiowej próbki, w zależności od kierunku obciążeń zewnętrznych. Celem pracy było wykonanie badania numerycznego propagacji pękania materiału oraz wykazanie obszarów najbardziej newralgicznych. Przedmiot badań przygotowano w ramach analizy numerycznej zniszczenia materiału na skutek rozdzielenia włókien w oparciu o środowisko Abaqus 6.14. Propagacja procesu pękania materiału została przeprowadzona na podstawie metody badań numerycznych xFEM, stanowiącej metodę rozdzielania włókien materiału niezależnie przebiegającego od siatki elementów skończonych.

Słowa kluczowe: Abaqus, xFEM, Analizy numeryczne, Inicjacja i propagacja pękania

1. Introduction

Nowadays, the phenomenon of the permanent separation of fibres in structures is a significant problem related to the long-term and proper operation of machinery. It is desirable to design solutions which offer immediate ways of preventing undesired phenomena such as fibre cracking due to excessive loads [6–8].

Previous numerical methods for investigating material failure enable the prediction of crack initiation regions – their results are highly compatible with experimental results. The popular methods for predicting material failure regions are connected with different calculation algorithms. One of the most popular methods for fibre separation in the Abaqus system is the cohesive zone method (CZM). Over the years, other methods for failure visualisation have been developed, for instance, the virtual crack closure technique (VCCT) for interlayer delamination. One more widely used method for investigating failure is the extended finite element method (xFEM) for determining crack propagation irrespective of the generated finite element mesh. There are also other methods for describing material failure; however, the above three methods are the most widely used ways of visualising material failure due to external loads.

Structures containing indentations are much more susceptible to damage during long-term operation. The process of permanent fibre separation in samples with indentations often begins in the regions above or below the indentation, and not, as it would seem, on the edge of the indentation. When designing structures, it is important that undesirable phenomena of material failure caused by loads are prevented, and if they occur, it is crucial to predict areas where failure propagation begins. There are numerous studies [4, 5, 11–16] on crack propagation processes and the use of the xFEM method. The innovative character of this method stems from the fact that the simulation of crack initiation and propagation processes runs independently of the applied FEM mesh type and density. The research works [4, 14, 16, 17] related only to the determination of crack progression for different types of material depending on one specific type of boundary condition. Regarding the current problems of machinery operation, it is necessary to adopt an approach which results in the improvement of the operational conditions of machines. As far as material strength is concerned, it is valuable to have the knowledge to predict failure initiation regions. These processes can be computer simulated without the necessity of conducting expensive strength tests or cyclic loading tests. The application of numerical tools such as ABAQUS enables the effective determination of critical regions of structures depending on the defined physical processes that are consistent with real phenomena leading to the loss of initial mechanical properties [2, 3, 9, 10].

2. Materials and research methods

The study was conducted on square samples with symmetrical incisions in the central region. The samples were made from aluminium 6082. The numerical model was designed using Abaqus 6.14. The structure was described by a selection of material properties – these are listed in table below [1].

Table 1. Characteristics of the aluminium

Material: Aluminium	
Young's Modulus [MPa]	70,000
Poisson's Ratio	0.3
Max Principal Stress [MPa]	300

The numerical model was designed only for the elastic range in order to determine the region of crack initiation and propagation due to applied loads. The geometrical parameters of the element are given in millimetres. The thickness of the sample was only 1 mm. The prepared model is shown below.

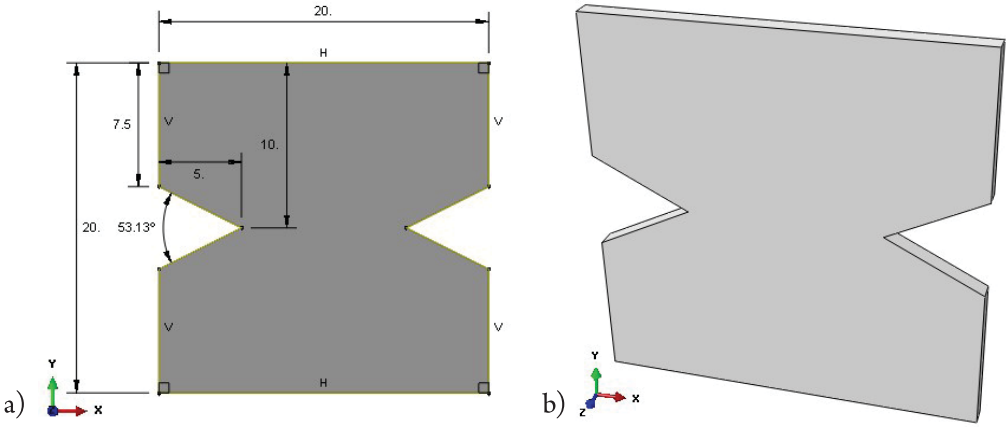

Fig. 1. Test sample: a) geometrical parameters, b) CAD model (source: own study)

The numerical model was defined by boundary conditions and external loads in the form of forced displacements causing tension and bending of the sample. The upper surface of the profile was fully fixed in each of three tested variants of load. In the first case, axial tension was defined by the application of forced displacement of the lower surface by 0.5 mm. The second variant involved the displacement of the bottom right surface towards the material (opposite to the X-axis) and downwards by 0.75 mm. The final variant corresponded to the second variant and involved the displacement of the bottom left surface relative to the X-axis and downwards by 0.75 mm. The objective of each case was to simulate failure of the FEM model under varying loads. The figures below illustrate the three variants of the applied boundary conditions.

The discretisation of the numerical model was performed using the best possible type of finite elements, i.e. C3D8R, with 550 mesh elements and 1224 nodes. The number of mesh elements is relatively small, yet the investigation of crack propagation by the xFEM method does not require increasing mesh density owing to the fact that the process does not depend on the FEM mesh. Eight-node elements with three degrees of freedom and reduced integration (C3D8R) are characterised by a very high degree of accuracy of the results. Its obtained due to removing false modes of deformation of numerical elements (by the application of higher-order polynomial equations to describe this process) [18]. Basically, the static measurements

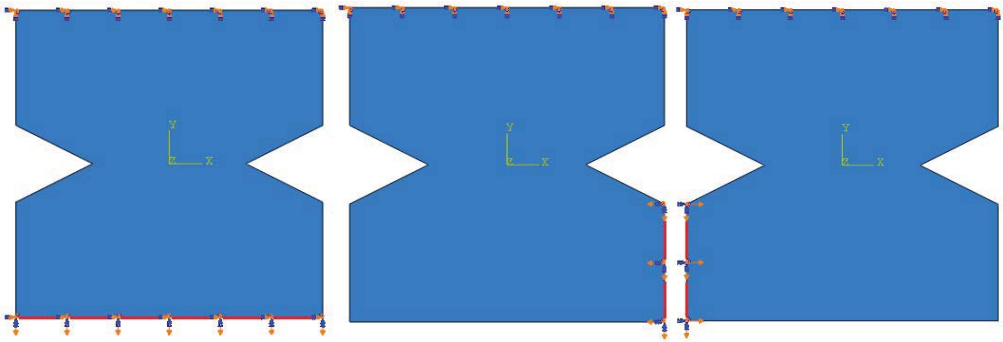

Fig. 2. Numerical model for three cases of boundary conditions (source: own study)

only involved the definition of mesh type and mesh density. The numerical model with the implemented mesh for the entire structure is shown in the figure below.

The objective of the study was to perform a complex analysis of structure effort until crack initiation. It then involved the modelling of the propagation of the crack in order to obtain the shapes of separated fibres under varying loads. The numerical results were constantly compared with the material properties of the sample to examine material effort.

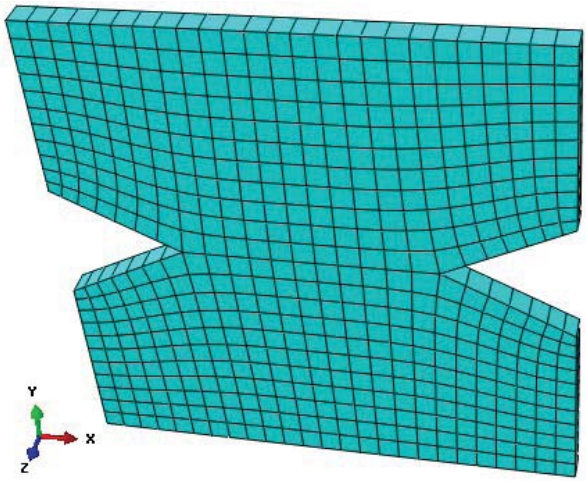

Fig. 3. Numerical model after discretisation (source: own study)

3. Results

The analysis of crack initiation and propagation performed by the innovative xFEM method enabled the identification of the region of crack initiation and the direction of shape of the propagating crack. Micro-failures of the element can occur when the element reaches the state of tensile strength. The moment when the material undergoes considerable elongation and loss of fibre cohesion due to the impact of tensile and bending forces, the irreversible failure of the element's structure begins to take place. Crack propagation is totally

independent of a finite element mesh, and it is possible to investigate structures with the aim of predicting potential regions of failure initiation until their complete failure. The FEM analysis enabled the determination of the regions of crack initiation as well as the shape of the crack. The study investigated the regions of structure failure using three different variants of boundary conditions in order to compare fibre separation depending on applied external loads. All three cases of failure are illustrated in the figures below.

A solid model was used to map the crack propagation process with respect to the 3D solid structure; this model had eight-node finite elements with three translational degrees of freedom in each of the eight nodes per one finite element. The crack initiation occurred precisely in the spot of sample necking, right next to its incision. FEM analysis enabled showing research results dependent upon applied boundary conditions. The first result of structural failure results from the axial tension of the sample by 0.5 mm. The effect of tension was symmetrical crack propagation until the complete separation of fibres of the tested material. Following the complete failure of the sample, the stresses were concentrated in the

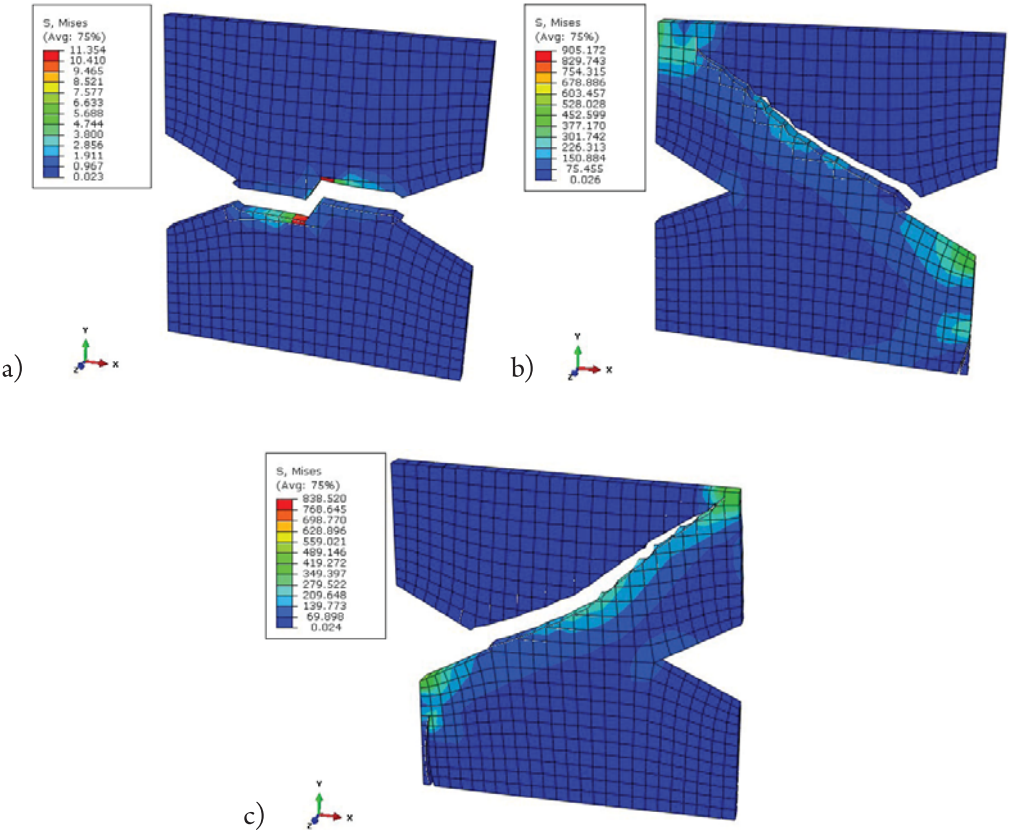

Fig. 4. Visualisation of failure: a) axial tension failure, b) failure under second load, c) failure under third load (source: own study)

central region of the crack, and the value of stress after total failure was slightly over 11 MPa. The stresses of 11 MPa were the residual stresses resulting from the elastic unloading. The second result is concerned with a partially bending and tensile force acting on the bottom right surface of the sample. It can be observed here that the cracking was initiated on the right side of the central incision of the sample. Regarding crack propagation in the upper left part of the sample, the stresses amounted to over 905 MPa (three times more than the max principal stress – value of crack initiation). The results of the third variant of the applied boundary conditions reveal that the crack propagation here was symmetrical to that in the previous case. Crack initiation also occurred in the region of the sample incision on the left. Due to the impact of tensile-bending loads, the crack propagated towards the right upper edge of the sample. The visualisation of structure failure additionally shows the regions of complete failure of selected finite elements depending on the applied variant of boundary conditions. When the value was 1, and thus met the xFEM criterion, specific regions of the structure underwent failure. The visualisation of the results below illustrates the numerically determined regions of complete failure of the structure.

Based on material data and crack propagation coefficients, the XFEM method enables simulation of complex failure processes for popular materials depending on external loads. The STATUSXFEM variable (i.e. the percentage of structure failure) describes regions of structure failure, where a value of 1 defines the region of complete failure of selected elements of the FEM mesh. In the first variant of the boundary conditions, the structure underwent total failure only in the region of central necking. The results of the second variant of boundary conditions reveal that the structure undergoes failure from the right side of central necking to the top left corner of the sample. The results of the last variant of boundary conditions demonstrate that the structure's failure is almost symmetrically identical to that observed in Variant 2.

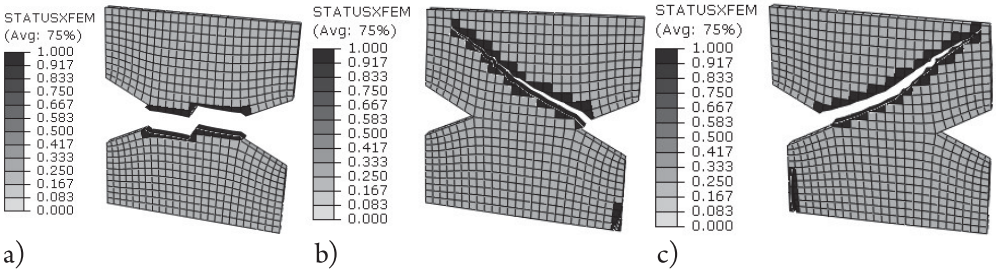

Fig. 5. Damage criterion determined by xFEM method: a) failure in case 1, b) failure in case 2, c) failure in case 3 (source: own study)

4. Conclusions

The investigation of structural failure based on numerical simulations enabled the identification of crucial regions of the structure. Nowadays, it is important to have information about regions that are problematic regarding the operation of these structures. The possibility of predicting regions that are critical for a given element by numerical simulation greatly

facilitates the design and production processes. The simulation of complex physical processes enables the reduction of production costs and the time for manufacturing prototypes and their validation. Predictions of the potential areas of fracture of structures subjected to external loads can reduce the cost of part production by removing structural defects during design processes and advanced computer simulations. The results of the investigation of structural failure due to crack propagation depending on the applied boundary conditions demonstrate that further studies can be conducted in order to re-design this element such as to prevent its failure. The numerical results lead to the following conclusions:

- numerical analysis of the effort of structures enables the precise prediction of failure initiation regions in these structures;
- xFEM method for simulating structural failure enables the visualisation of crack initiation and propagation irrespective of the applied finite element mesh;
- FEM simulations of material cracking enable the determination of both the direction of crack propagation due to load and the degree of failure of mesh elements;
- it is possible to determine the relationship between the mode of structural failure and varying boundary conditions.

The above conclusions confirm the significance of FEM modelling in effort analysis. Systems for strength analysis offer wide opportunities for structural examination and further design optimisation.

References

[1] Banaszek J., *Examples of calculations within machines constructions basics Part II*. The University Publishing House, 1996, 196–197.

[2] Dębski H., Koszałka G., Ferdynus M., *Application of FEM in the analysis of the structure of a trailer supporting frame with variable operation parameters*. Eksploatacja i Niezawodnosc – Maintenance and Reliability, 2012, 14 (2), 107–114.

[3] Dębski H., Rudawska A., *Experimental and numerical analysis of adhesively bonded aluminium alloy sheets joints*. Eksploatacja i Niezawodnosc – Maintenance and Reliability, 2011, 1, 4–10.

[4] Gajewski J., Nowakowski P., Różyło P., *Prognozowanie występowania pęknięć w oparciu o system FEM-MLP*, Logistyka 2015, 3, 1381–1386.

[5] Gill P., Davey K., *Analysis of thermo-mechanical behaviour of a crack using XFEM for Leak-before-Break assessments*, International Journal of Solids and Structures, 2014, Vol. 51, 2062–2072.

[6] Jonak J., *Zagadnienia mechaniki pękania i skrawania materiałów*, Politechnika Lubelska, Lublin 2010, 90–95.

[7] Kąkol W., Łodygowski T., *Metoda elementów skończonych w wybranych zagadnieniach mechaniki konstrukcji inżynierskich*. Politechnika Poznańska, Poznań 2003.

[8] Kleiber M., *Wprowadzenie do metody elementów skończonych*, Biblioteka Mechaniki Stosowanej IPPT PAN, PWN, Warszawa-Poznań 1985.

[9] Lonkwic P., Różyło P., *Theoretical and experimental analysis of loading impact from the progressive gear on the lift braking distance with the use of the free fall method*. Advances in Science and Technology Research Journal, 2016, 10(30), 103–109.
[10] Lonkwic P., Różyło P., Dębski H., *Numerical and experimental analysis of the progressive gear body with the use of finite-element method*. Eksploatacja i Niezawodność – Maintenance and Reliability, 2015, Vol. 17, No. 4, 544–550.
[11] Moes N., Belytschko T., *Extended finite element method for cohesive crack growth*. Northwestern University, USA 2001.
[12] Nasirmanesh A., Mohammadi S., *XFEM buckling analysis of cracked composite plates*, Composite Structures, 2015, Vol. 131, 333–343.
[13] Naderi M., Iyyer N., *Fatigue life prediction of cracked attachment lugs using XFEM*, International Journal of Fatigue, 2015, Vol. 77, 186–193.
[14] Różyło P., *Numerical analysis of crack propagation in a steel specimen under bending*, Applied Computer Science 2015, Vol. 11, No. 4, 20–29.
[15] Różyło P., *Optimization of I-section profile design by the finite element method*, Advances in Science and Technology Research Journal, 2016, 10(29), 52–56.
[16] Różyło P., Gajewski J., Nowakowski P., Machrowska A., *Zastosowanie sieci RBF w analizie pękania elementów maszyn*, Logistyka 2015, No. 3, 4172–4186.
[17] Różyło P., Wójcik Ł., *Comparison of numerical and experimental analysis of the crack propagation process*, Applied Computer Science 2015, Vol. 11, No. 2, 60–67.
[18] Zienkiewicz O.C., Taylor R.L., *Finite Element Method (5th Edition)* Vol. 2, Solid Mechanics, Elsevier, 2000.

TECHNICAL TRANSACTIONS 1/2018
MECHANICS
DOI: 10.4467/2353737XCT.18.016.7967
SUBMISSION OF THE FINAL VERSION: 20/12/2017

Lena Krawczyk
Marlena Sołek (marlena.solek@pk.edu.pl)
Institute of Thermal and Process Engineering, Faculty of Mechanical Engineering, Krakow University of Technology

Łukasz Mika
Department of Thermal and Fluid Flow Machines, Faculty of Energy and Fuels, AGH University of Science and Technology.

Ice slurry flow in ball valves

Przepływ zawiesiny lodowej przez zawory kulowe

Abstract

This paper presents the results of experimental studies of the flow resistance of slurry ice flowing through ball valves. Loss coefficients in ball valves were determined from experimental investigations. The study focused on 1/2", 3/4" and 1" ball valves at two valve positions (20° and 30°). The ice mass fraction in the studied ice slurry ranged between 5% and 30%.

Keywords: ice slurry, ball valve, Bingham model, laminar flow

Streszczenie

W pracy przedstawiono wyniki badań doświadczalnych oporów przepływu zawiesiny lodowej w zaworach kulowych. Na podstawie wyników badań doświadczalnych wyznaczono wartości współczynników strat miejscowych w badanych zaworach. W badaniach wykorzystano przelotowe zawory kulowe o średnicach 1/2", 3/4" oraz 1" przy dwóch pozycjach zamknięcia (20° i 30°). Udziały masowe drobinek lodu w zawiesinie w badaniach wynosiły od 5 do 30%.

Słowa kluczowe: zawiesina lodowa, zawór kulowy, model Binghama, przepływ laminarny

1. Introduction

Ice slurry, also known as binary ice, is a mixture containing a liquid and small ice particles which are usually less than 0.5 mm in size. Water, which may contain a freezing-point depressant, is most often the base fluid. Frequently used freezing-point depressants include, for example, ethyl alcohol. Other possible additives include: methanol, ethylene glycol, propylene glycol and sodium chloride [1, 6, 10]. Ice slurry is mainly used as a refrigerant in intermediate refrigeration systems. It is also used in applications where its excellent 'cold' storage properties can be taken advantage of [1, 2].

The mass fraction of ice particles in ice slurries may vary – this determines their rheological properties [1, 2, 6, 10]. Most researchers believe that ice slurry with mass fraction of ice (by mass) of up to 15% exhibits the properties of a Newtonian fluid (similar to those of water), while at higher mass fractions of ice, its properties resemble those of a non-Newtonian fluid [6, 10]. One of several rheological models must be used to describe the rheological properties of ice slurries. The most frequently used models include those proposed by: Bingham [6, 10], Casson [4] and Ostwald-de Waele [3]. In this paper, Bingham's model will be used to describe the rheological properties of the ice slurry. This model has been selected because, taking into consideration an analysis of pipe flow curves, it best describes the rheological properties of ice slurry with an aquatic solution of ethyl alcohol as the base fluid [6, 10].

The authors of papers concerning this topic have presented results of experimental studies of ice slurry flow resistances in most basic pipeline elements, such as straight sections [11, 12], bends and elbows [10], expansion and contraction joints [7, 9] as well as poppet and ball valves (mainly in the turbulent flow range) [6, 8]. Paper [6] presents sample values of local loss coefficients for ice slurry with ice fractions ranging between 5% and 30% during its flow through a straight DN20 ball valve for aperture angles of 25° and 35°. In the turbulent flow area, the authors reported high levels of consistency between the calculated values of the local loss coefficients and the theoretical values given in [13]. However, the local loss coefficients in the valves referred to the velocity of the ice slurry in the pipeline downstream of the valve. Therefore, it is impossible to analyze any phenomena characteristic of ice slurry flow directly in the valve itself. Most experimental studies which focus on flow resistance in the ball valves described in [6] concern the turbulent flow range.

The main conclusion to be drawn from a review of the available literature on ice slurry flow in all pipeline fittings is the fact that the values of local loss coefficients for the turbulent flow area approximate the theoretical values given in literature for Newtonian fluids [6, 7, 9, 10]. In ball valves, local loss coefficients for the flow of ice slurry with different ice fractions in the turbulent range are consistent with the theoretical values given in [13] for Newtonian fluids with regard to most valve aperture angles. Another conclusion to be drawn from the analysis of literature is that the ice slurry flow resistance increases in a valve when the ice particles cumulate in the almost fully closed ball valve (right before the valve is fully closed). This is probably due to the presence of ice particles which might hamper ice slurry flow through the valve at high valve closure angles [9].

In literature, there are no reports on comprehensive studies of ice slurry resistances in ball valves in the laminar flow range of various ice fractions. Furthermore, the measured ice slurry flow resistances in valves have not referred to the actual velocity of ice slurry flow in the valve itself.

2. Experimental setup

In order to measure the flow resistance of the ice slurry in ball valves, an experimental stand was used which enabled the flow resistance of the mixture to be investigated in various pipeline fittings (e.g. Y-pipes, distributors, contractions, expansions and valves). The set-up was quite advanced. Only part of the entire experimental set-up was used to measure ice slurry flow resistances in a ball valve (Fig. 1). Pumps installed in the pipeline drive the flow of ice slurry through the system (1). Refrigerant is generated in the ice slurry generator (2) and collected in the buffer tank (3), from where it is pumped towards the investigated valve (8). The tank is fitted with mixers (3) which are designed to maintain a homogenous composition of the ice slurry. Before the ice slurry is generated, it is necessary to prepare the essential, exchangeable elements of the test stand, such as the investigated ball valve (8) and the necessary measurement equipment.

Among the measurement devices used in the experimental setup were PT100 temperature sensors (7) used to measure the temperature of the ice slurry flowing through the system. In order for the measurements to be accurate, the sensors were previously calibrated using a Beamex MC2 calibrator. The PT100 sensors were placed in thermometric sleeves. Other measurement devices used at the stand were Fuji Electric pressure difference sensors (9) with measurement ranges of 0-1 kPa, 0-6 kPa and 0-32 kPa. 4 mm pressure impulse nozzles were used in the studies due to the presence of ice particles. Non-insulated, transparent impulse ducts (10) were used for measurements using the nozzles. The transparent duct made it possible to verify that no air bubbles formed in the slurry – it is essential to detect any air bubbles to ensure that the measurement results are accurate, as the presence of air bubbles often causes measurement errors. The measurement of the mass flux of the ice slurry and its density was possible with the use of the MASSFLO MASS 6000 mass flow meter (5).

The ice slurry studied in the paper was produced using a 10.6% aquatic solution of ethyl alcohol.

When studying ice slurry flow, it is essential to determine the mass fraction of ice in the slurry. Several methods can be used to determine the content of ice particles, including calorimetric measurements, the use of the freezing curve of an aquatic solution of ethyl alcohol [5] and measurements of the density of the slurry using a mass flow meter [6, 10]. All three methods were used in this paper. The freezing curve and measurements of slurry density were used for continuous measurements, whereas the calorimetric method, which is more accurate but more problematic for continuous measurements, was used to verify the results of the primary method.

Ice slurry consists of a solid phase, with lower density, and a liquid phase. It is necessary to ensure that its composition is homogeneous. Due to the content of ice particles in the

ice slurry, it is essential to keep stirring it. The stirring may, however, have the undesirable effect of aeration. As a result, a three-phase mixture is created – this may distort flow resistance measurement results. In order to avoid the aeration of the ice slurry, a special method was used whereby the surface of the liquid in the tank was stabilised using a large float. During the stirring process, the float was located on the surface of the ice slurry in the tank, stabilising it and thus minimising aeration. This method does not fully resolve the problem, hence the need to use rotating speed adjusters to control the speed of the mixers. The correct mixing speed was chosen by means of experimentation, whilst at the same time, controlling the content or air in the slurry on a continual basis. The use of the float and the adjustment of the rotation speed of the mixers made it possible to eliminate the aeration of the ice slurry [6, 10].

The problem of maintaining a homogenous composition of the ice slurry also applies to distribution pipelines. It is necessary to ensure that the flow velocity is never lower than the velocity necessary to ensure the homogeneity of slurry composition. The results presented in [2] suggest that – regardless of the mass fraction of ice – below the velocity of 0.15 m/s, the flow of the ice slurry corresponds to the structure of moving sludge.

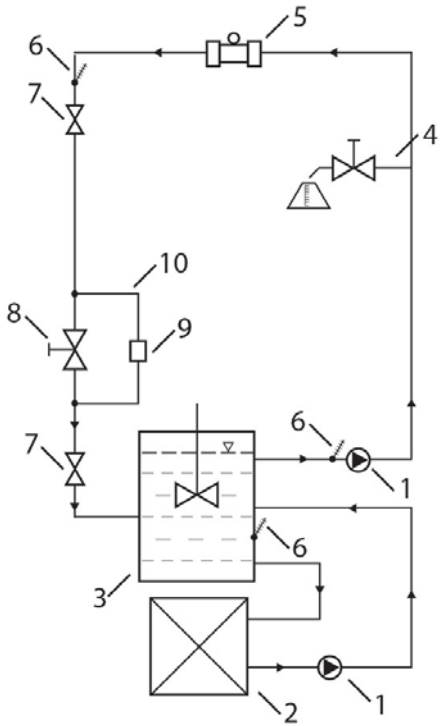

Fig. 1. Outline of the experimental setup 1 – pump, 2 – ice slurry generator, 3 – ice slurry buffer tank with mixers, 4 – ice fraction control, 5 – MASSFLO MASS 6000 mass flow meter, 6 – PT100 temperature sensor with a digital display, 7 – cut-off valve, 8 – the investigated ball value, 9 – Fuji pressure difference transducer, 10 – transparent impulse ducts

3. Results of experimental studies

The experimental studies on the ice slurry flow velocity relied on three ball valves with diameters of 1/2", 3/4" and 1", which were fitted in a copper pipeline with inner diameters of 16 mm, 20 mm and 26 mm, respectively. A series of measurements of flow resistances for ice slurry with the ice fractions of 5%, 10%, 15%, 20%, 25% and 30% were conducted for each ball valve at a closure angle of 20° and 30°. The actual opening position was controlled using a handle with an angle scale. The ball valve closure angles of 20° and 30° enabled the generation of laminar flows through the valve. Figure 2 shows the actual position of the ball against the valve body at a certain rotation angle adjustment.

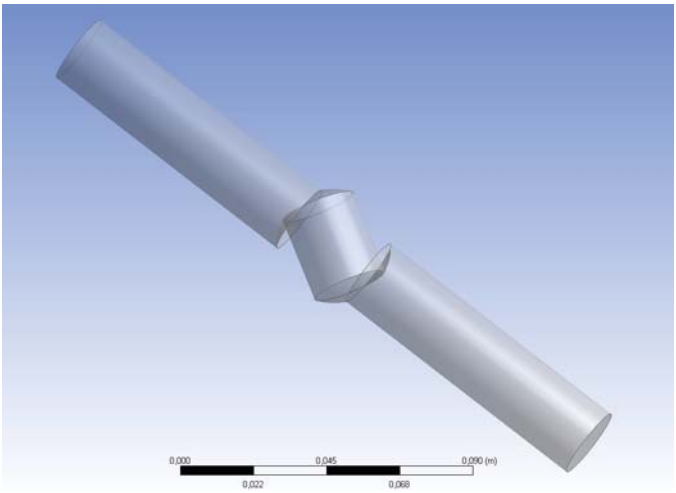

Fig. 2. Model of 1" ball valve at an angle of 30°

The experimental studies also focused on measuring the flow resistances in the ball valve Δp_{meas} as the sum of local resistances along with friction resistances in straight-line sections with distances L_1 and L_2 (downstream and upstream of the valve), as well as friction resistances Δp_L within a straight-line section with length L. Later, local resistances at the ball valve were determined on the basis of formula (1):

$$\Delta p = \Delta p_{meas} - \Delta p_L \frac{L_1 + L_2}{L} \tag{1}$$

The local loss coefficients for ball valves for both valve closure angles were determined using equation (2):

$$k = \frac{2\Delta p}{\rho_{zl} w^2} \tag{2}$$

where w is the velocity of the ice slurry [m/s], and ρ_{zl} is the measured density of the slurry [kg/m^3].

The Reynolds number for Bingham fluids was used in the graphs to present the results of experimental studies and of the calculations of local loss coefficients for the ice slurry in the ball valves. It was represented with equation (3):

$$\mathrm{Re}_B = \frac{\rho_{zl} w D}{\mu_p} \tag{3}$$

The dynamic coefficient of plastic viscosity in equation (3) for an ice slurry prepared on the basis of a 10.6% solution of ethyl alcohol and mid-sized 0.125mm ice particles was determined experimentally on the basis of pipe flow curves and is represented with equation (4) [6, 10]:

$$\mu_p = 0.0035 + 0.0644(x_S) - 0.7394(x_S)^2 + 5.6963(x_S)^3 - 19.759(x_S)^4 + 26.732(x_S)^5 \tag{4}$$

where x_S represents the content of ice particles in the slurry [-].

The hydraulic diameter D in correlation (3) was determined for all three ball valves and two closure angles (20° and 30°) from equation (5), taking into consideration the curve of the free surface area of the flow of ice slurry through valve A [m^2] and the circumference of that surface *Circ* [m]:

$$D = \frac{4A}{Circ} \tag{5}$$

The dimensions of all the valve elements were represented in the Ansys software program – this made it possible to determine both values from equation (5) necessary to calculate the hydraulic diameter for the two valve positions. Table 1 presents the values of A and *Circ* for two valve closure angles (20° and 30°) for 1/2", 3/4" and 1" valves obtained from Ansys.

Table 1. Values of ***A*** and ***Circ*** for two closure angles of 1/2", 3/4" and 1" valves

Valve/position	A [m^2]	Circ [m]
1/2"/20°	$112.9 \cdot 10^{-6}$	$36.8 \cdot 10^{-3}$
1/2"/30°	$88.3 \cdot 10^{-6}$	$33.6 \cdot 10^{-3}$
3/4"/20°	$177.3 \cdot 10^{-6}$	$46.0 \cdot 10^{-3}$
3/4"/30°	$139.5 \cdot 10^{-6}$	$42.1 \cdot 10^{-3}$
1"/20°	$325.5 \cdot 10^{-6}$	$62.2 \cdot 10^{-3}$
1"/30°	$257.9 \cdot 10^{-6}$	$57.1 \cdot 10^{-3}$

Figs 3, 4, 7, 8, 11 and 12 present the relationship between the pressure drops in the 1/2", 3/4" and 1" ball valves (at closure angles of 20° and 30°) and the velocity in the valve of ice slurry with mass fractions of ice of 5%, 10%, 15%, 20%, 25% and 30%. Figs 5, 6, 9, 10, 13 and 14 present the relationship between local loss coefficients in the 1/2", 3/4" and 1" ball valves

(at closure angles 20° and 30°) and the Reynolds number from the Bingham model for ice slurry with a mass fraction of ice of 5%, 10%, 15%, 20%, 25% and 30%. In the turbulent flow range, the local loss coefficients for the flow of ice slurry through the ball valves was compared to the values of those coefficients found in literature [13] for Newtonian fluids.

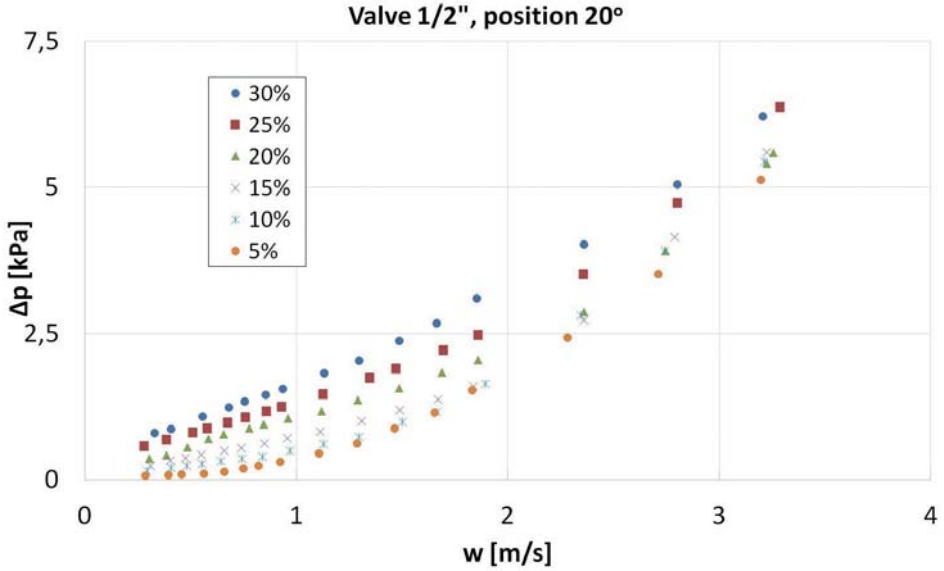

Fig. 3. Relationship between the pressure drop in the 1/2" valve at an angle of 20° and the velocity of the ice slurry in the valve for various ice fractions

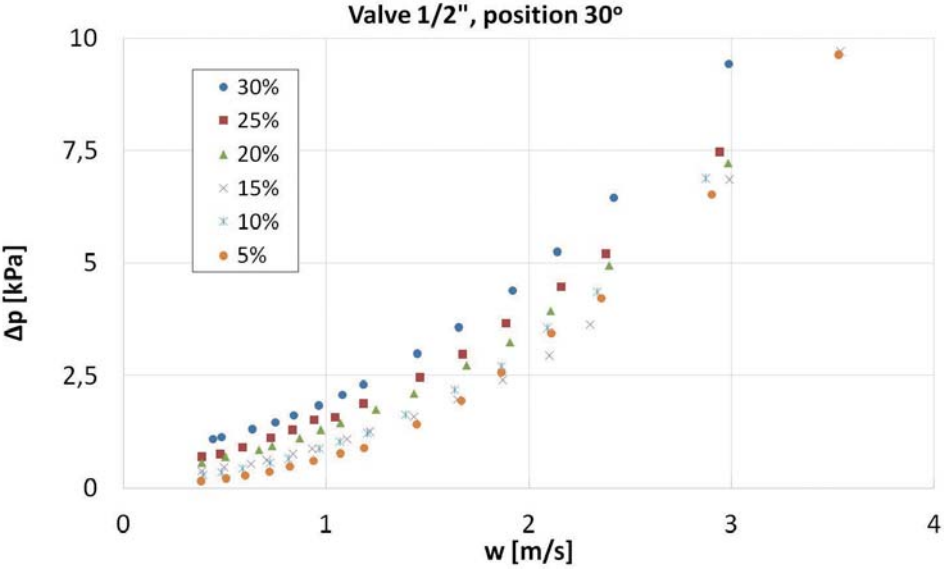

Fig. 4. Relationship between the pressure drop in the 1/2" valve at an angle of 30° and the velocity of the ice slurry in the valve for various ice fractions

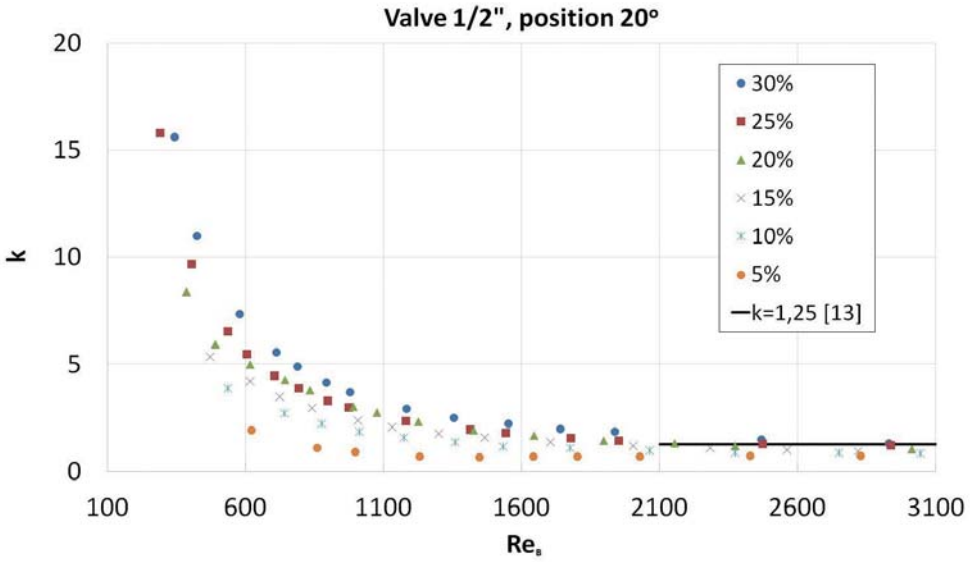

Fig. 5. Relationship between the local loss coefficients in the 1/2" valve at an angle of 20° and the Reynolds number from the Bingham model for various ice fractions

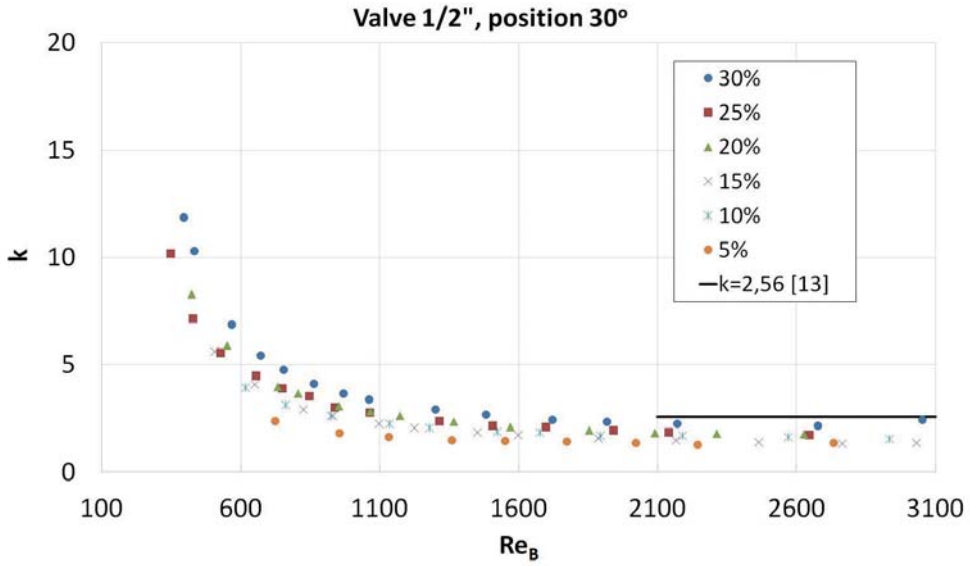

Fig. 6. Relationship between the local loss coefficients in the 1/2" valve at an angle of 30° and the Reynolds number from the Bingham model for various ice fractions

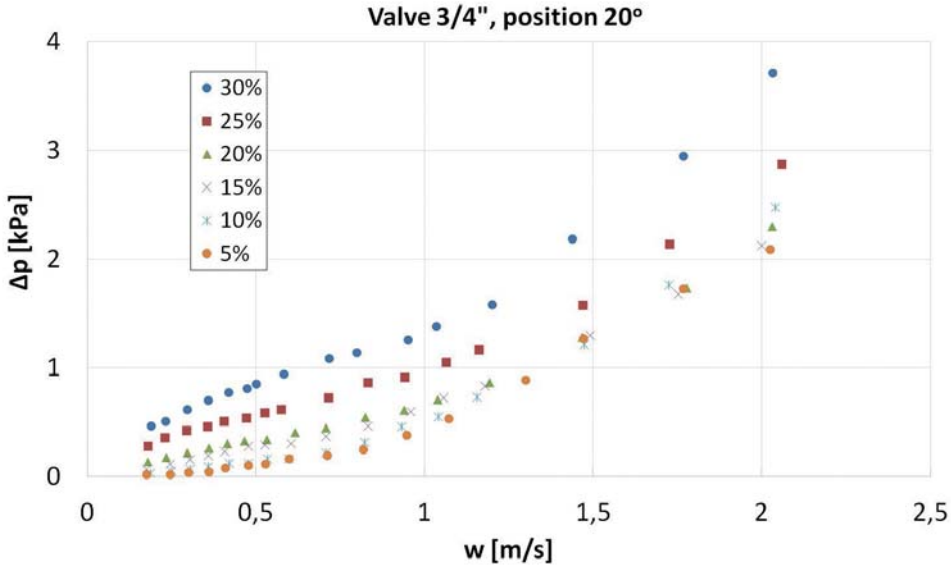

Fig. 7. Relationship between pressure drop in the 3/4" valve at an angle of 20° and the velocity of the ice slurry in the valve for various ice fractions

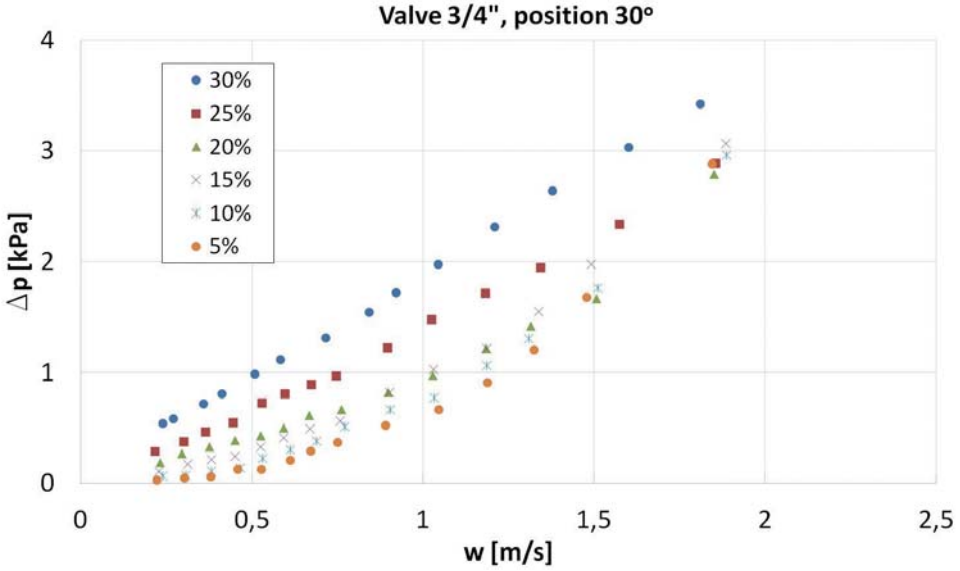

Fig. 8. Relationship between pressure drop in the 3/4" valve at an angle of 30° and the velocity of the ice slurry in the valve for various ice fractions

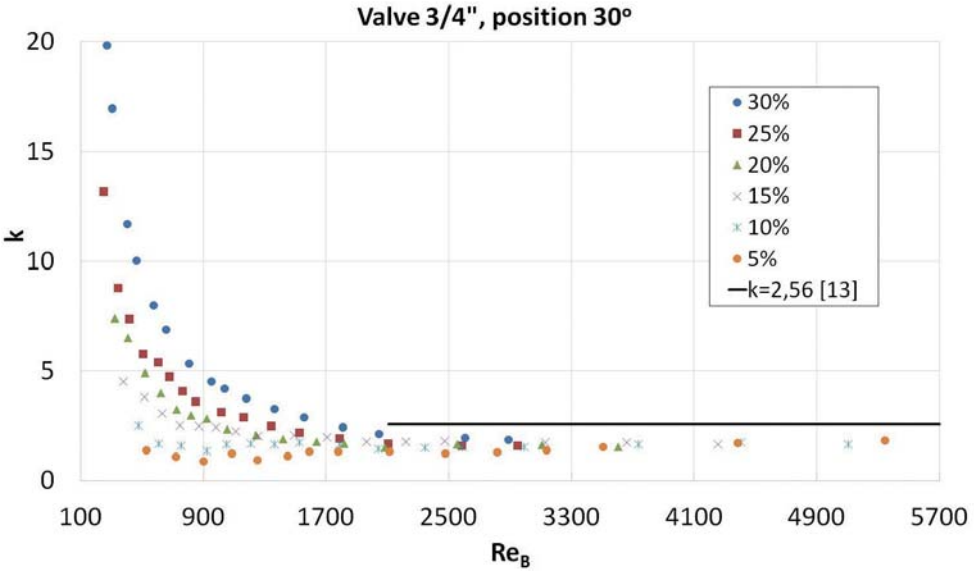

Fig. 9. Relationship between the local loss coefficient in the 3/4" valve at an angle of 20° and the Reynolds number from the Bingham model for various ice fractions

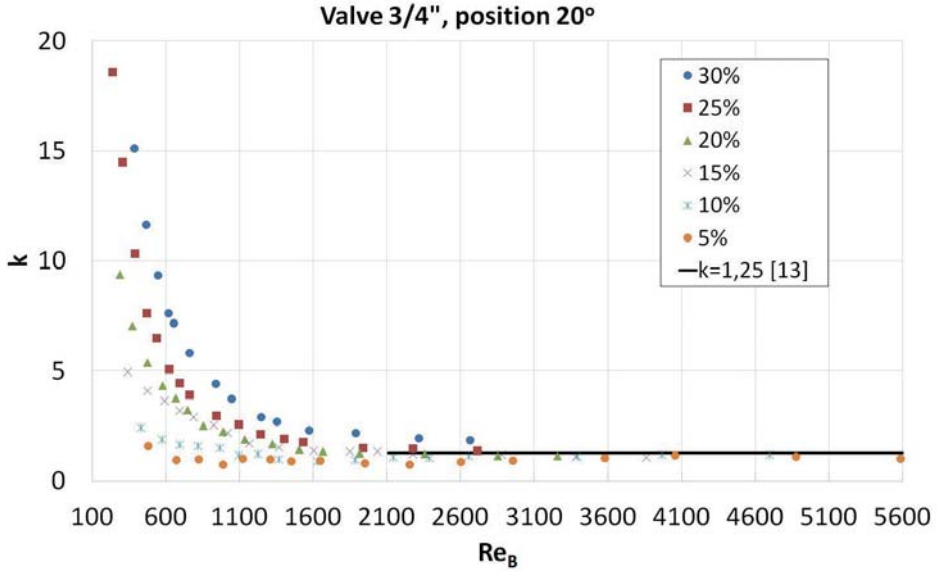

Fig. 10. Relationship between the local loss coefficient in the 3/4" valve at an angle of 30° and the Reynolds number from the Bingham model for various ice fractions

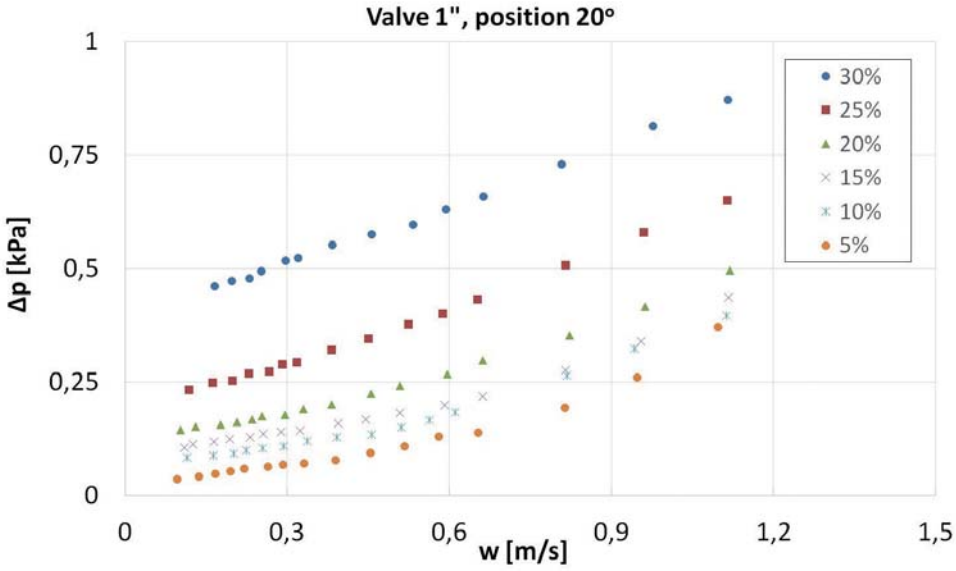

Fig. 11. Relationship between pressure drop in the 1" valve at an angle of 20° and the velocity of the ice slurry in the valve for various ice fractions

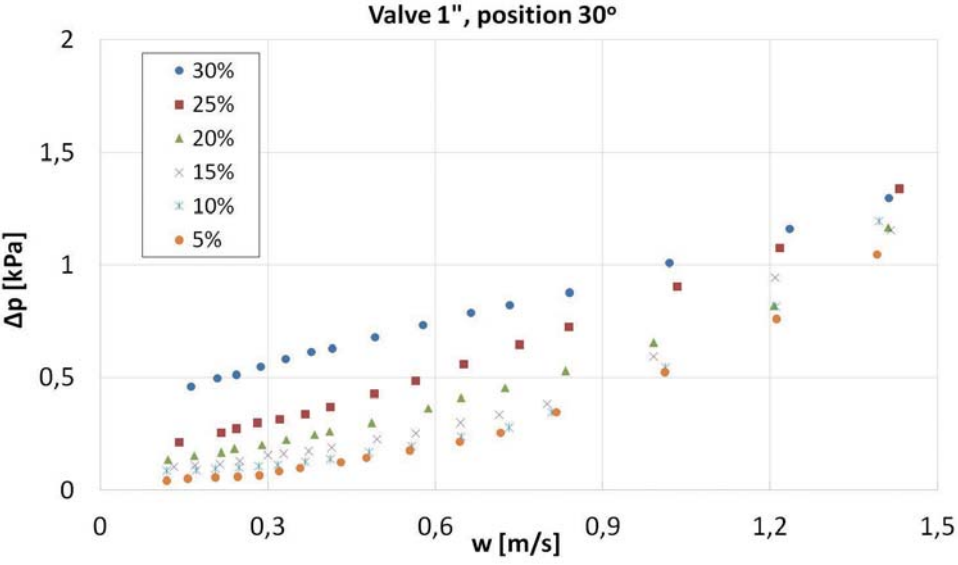

Fig. 12. Relationship between pressure drop in the 1" valve at an angle of 30° and the velocity of the ice slurry in the valve for various ice fractions

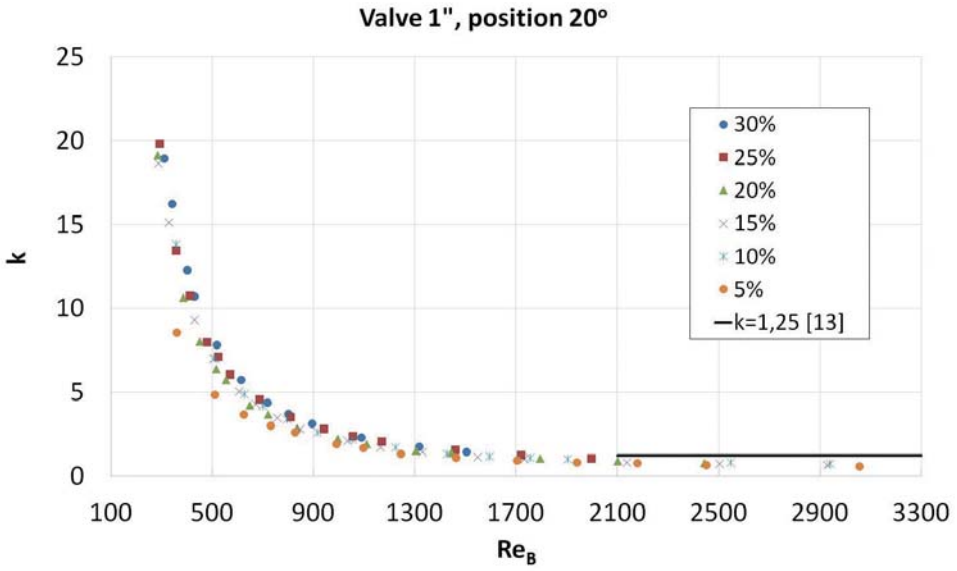

Fig. 13. Relationship between the local loss coefficient in the 1'' valve at an angle of 20° and the Reynolds number from the Bingham model for various ice fractions

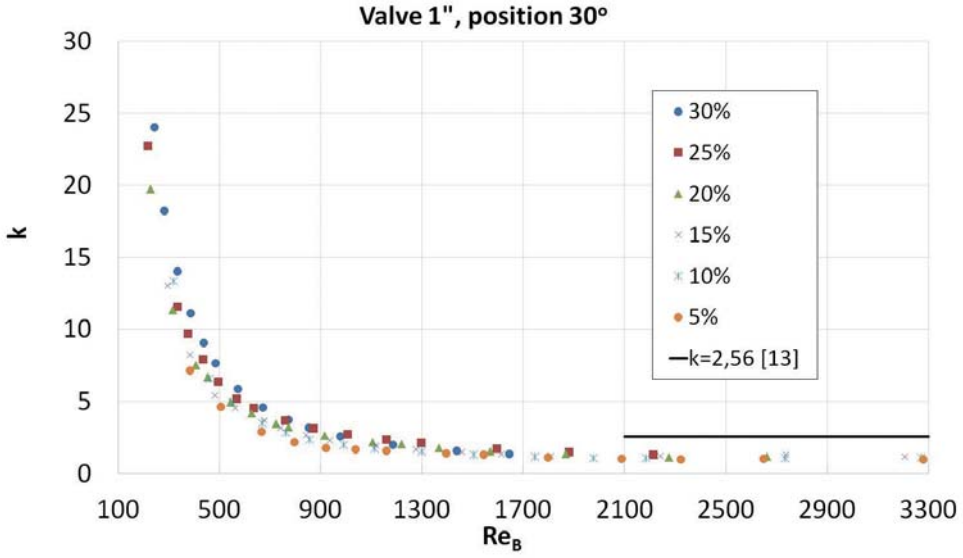

Fig. 14. Relationship between the local loss coefficient in the 1'' valve at an angle of 30° and the Reynolds number from the Bingham model for various ice fractions

4. Conclusions

The analysis of the relationship between pressure drops in the 1/2", 3/4" and 1" ball valves and the flow velocity in the valve for ice slurry with a mass fraction of ice of 5%, 10%, 15%, 20%, 25% and 30% presented in Figs 3, 4, 7, 8, 11 and 12 reveals a similar nature of the obtained measurement points for the three valves and the two positions (20° and 30°). In each graph, the highest pressure drops were detected for the ice slurry with the greatest proportion of ice particles (30%) and the lowest for the ice slurry with the smallest proportion of ice particles (5%). Moreover, in all cases, it is clear that the higher the pressure drop at the valve the higher the content of ice particles in the ice slurry. The relationships between the measurement points presented in Figs 3, 4, 7, 8, 11 and 12 are of a linear nature up to a certain boundary velocity, as the smaller ice mass fraction in the slurry the lower velocity of the studied mixture. Therefore, it is possible to claim that the presence of ice particles in the slurry influences the laminar nature of the flow. Once a certain boundary value of flow velocity (different for each valve and position of choking element) is exceeded, the course of pressure drops changes into a parabolic nature.

Analysis of Figs 5, 6, 9, 10, 13 and 14, which present the relationship between local loss coefficients in the 1/2", 3/4" and 1" ball valves (at closure angles 20° and 30°) and the Reynolds number from the Bingham model, reveals that in the turbulent flow range, the values of the coefficients are consistent with the values given in literature for Newtonian fluids. In the laminar flow range, the values of local loss coefficients are higher than in the turbulent flow range. The higher value of the local loss coefficient the greater content of ice particles and closure angle of the valve (30°). The greatest differences in the values of the local loss coefficients are seen in valves with smaller diameters, whereas in the 1" valve, the values are quite similar. This is probably related to the value of the quotient of the medium diameter of an ice particle and the hydraulic diameter, which is identified in literature as an important parameter which has a significant impact on the flow of ice slurries [6, 10].

References

[1] Egolf P.W., Kauffeld M., *From physical properties of ice slurries to industrial ice slurry applications*, International Journal of Refrigeration, 28, 2005, 4–12.

[2] Hansen T.M., Kauffeld M., *Viscosity of ice slurry,* Second Workshop on Ice-Slurries of the International Institute of Refrigeration, Paris, France 2000.

[3] Kawashima T., Sasaki M., Takahashi H., *Dynamics of snow – water flow in pipelines, slurry handing and pipeline transport*, Hydrotransport 12, 1993, 533–613.

[4] Kumano H., Yamanada Y., Makino Y., Asaoka T., *Effect of initial aqueous solution concentration on rheological behavior of ice slurry*, International Journal of Refrigeration, 68, 2016, 218–225.

[5] Melinder A., *Thermopysical properties of liquid secondary refrigerants. Tables and diagrams for the refrigerants industry*, IIF/IIR, Paris 1997.

[6] Mika Ł., *Opory przepływu zawiesiny lodowej w elementach instalacji chłodniczej*, Monografia No. 339, wyd. Politechniki Krakowskiej, Kraków 2011.
[7] Mika Ł., *Flow resist of the slurry ice in contractions*, Technical Transactions, 2-M/2012, 273–282.
[8] Mika Ł., Górski B., Kantor R., *Flow modelling of slurry ice in a control valve,* Technical Transactions, 1-M/2015, 59–66.
[9] Mika Ł., Zalewski W., *Local pressure loss coefficient during the flow of slurry ice trough sudden pipe expansions*, Technical Transactions, 1-M/2015, 67–74.
[10] Niezgoda-Żelasko B., *Wymiana ciepła i opory przepływu zawiesiny lodowej w przewodach*, Monografia No. 334, wyd. Politechniki Krakowskiej, Kraków 2006.
[11] Niezgoda-Żelasko B., Zalewski W., *Momentum transfer of ice slurry flows in tubes, experimental investigation*, International Journal of Refrigeration 29, 2006, 418–428.
[12] Niezgoda-Żelasko B., Zalewski W., *Momentum transfer of ice slurry flows in tubes, modeling*, International Journal of Refrigeration 29, 2006, 429–436.
[13] Polska Norma M-34034, Rurociągi. Zasady obliczeń strat ciśnienia, 1976.